

CE767 HIGHWAY AND RAILROAD INFRASTRUCTURE

Spring 2013-2014

Alp Caner, Ph.D, P.E.

“The design of a bridge begins in the mind” – Fritz Leonhardt

Section 1:.....	7
Introduction	7
Who is a designer?	7
Engineering Aspects.....	8
Importance of Infrastructures	8
Bridge Types and Span Lengths.....	8
Bridge Aesthetics.....	9
Bridge Type Selection.....	10
Bridge Failures.....	11
Section 2:	14
Uncertainties in Design	14
Reliability Index and Calibration of LRFD.....	15
<i>Resistance Components</i>	19
<i>Demand Components</i>	19
<i>Load Factor Computation</i>	19
Live Load	20
Fatigue Live Load	23
Live Load Impact Factor	24
Multiple Presence	24
Girder Distribution Factors	25
Section 3	28
Typical Precast Prestressed Girder Cross-Sections.....	28
Selection of Girder Type	29
Material Properties.....	29
Production Cycle (2-3 days).....	30
Gravity Design Load Combinations.....	31
Limiting Stresses	32
Computing Cross-Sectional Stresses.....	32
Stresses due to M_{DC}	33
Stresses due to Prestressing.....	34
The moment due to pre-stressing at the neutral axis can be computed as	34

Stresses due to Superimposed Dead Load	34
Stresses due to Live Load Plus Impact.....	37
Required Prestress	37
Section 4	39
Pre-stress Losses.....	39
Elastic Shortening	39
Long term pre-stress loss due to creep, shrinkage and relaxation-approximate method	39
The advanced methods are described in the AASHTO-LRFD (2010).....	39
Evaluation of End Zones at Transfer of Prestress	40
Evaluation of Mid Span at Transfer of Prestress	41
Service I & III Mid-Span Stress Evaluations	41
Optional Deflection Check	41
The optional truck deflection check can be evaluated for the following truck loads	41
Fatigue Limit Check	41
Strength I Flexural Evaluation	42
Flexural Reinforcement Requirements.....	43
Maximum Reinforcement.....	43
Minimum Reinforcement.....	43
Strength Shear Design.....	44
Minimum Transverse Reinforcement.....	45
Maximum Spacing of Transverse Reinforcement	45
Transverse Design (Deck)	45
Computer Modeling	46
Spliced Precast Prestressed/Postensioned Multiple I-Girder/Slab Bridge	48
High Speed Railroad Bridge Passenger Comfort	51
Section 5	53
Balanced Cantilever Bridge Design.....	53
Post-tensioning Operation (FHWA 2004)	53
The post-tensioning operation will be based on the following schedule	53
Post-tensioning losses (Lucko and Garza 2003)	54
Construction Cycle (Lucko and Garza, 2003)	55
Overall Section Dimensions (AASHTO LRFD 2010).....	55
Efficiency Index	55

Depth of Section:.....	56
Construction Loads	58
Required Post-tensioning	58
Closed Position	59
Shear Lag	60
Principal Tension Stress Check.....	61
Transverse Design	62
Design Detailing of Superstructure Connections	63
Taken from PTI Design Handbook – Monolithic.....	63
Bearing System – In service.....	63
Bearing System – In temporary construction phase.....	63
Computer Modeling	64
Section 6	64
Preliminary Sizing of Steel Girder Slab Bridges	64
Depth	64
Cross-Section Proportion Limits	64
Compactness check.....	64
Compression Flange Local Buckling.....	66
Cross-Braces	66
The limiting unbraced length, L_p , to achieve nominal flexural resistance is	66
Strength Limit States.....	67
Flexural Resistance Composite Section – Positive Moment Compact Sections.....	67
Flexural Resistance Composite Section – Positive Moment Non-Compact Sections ..	69
Flexural Resistance Composite Section – Negative Moment Region.....	70
Shear Resistance	71
Shear Connectors	72
Spliced Bolted Connections	72
Preliminary Design of Cables of Cable Stayed Bridges.....	74
Section 7	76
Pier Design Load Combinations.....	76
Pier Design Resistance.....	76
Factored axial resistance can be determined from the following equation	76
<i>P-Δ Requirements</i>	77

Biaxial Flexure – Non Circular Members	78
Longitudinal Reinforcement Limits.....	78
<i>Tie and Spiral Reinforcement – (Section 5.10.6)</i>	79
Seismic Analysis.....	79
Time History Analysis – Ground Motion Selection	81
Column Design	81
Overstrength Resistance in Columns – AASHTO LRFD Definition	82
Single Columns (Piers).....	83
Multiple Column Piers	83
Abutments	83
Section 8	84
Nonlinearites in Bridge Modelling.....	84
The nonlinear analysis of the bridge can involve the following non-linearity's	84
Plastic Hinge Models	84
Mander's Concrete Compression Model.....	85
Concrete Under Tension Model.....	85
Reinforcement Tension Model.....	86
Column Plastic Hinge Length	86
Converting Moment-Curvature to Moment Rotation Element.....	86
Effective Inertia of the Column.....	88
Hysteretic Elements with Degradation Properties.....	89
Yield Surface Element.....	90
Reinforcement Slip Model	90
Shear Keys and Abutment	91
Shear Key Response Model.....	92
Structural Modeling of Gap Elements.....	93
Damper Element	94
Soil Structure Interaction Models	95
Group Effects	98
Elastomeric Bearings	99
Section 9	101
Tunnel Types	101
Tunnel Cross-Sections	101

Groundwater Control	103
Tunnel Portal Structures.....	104
Cut And Cover Structures	105
Initial Support of Excavation.....	107
Flexible Support	108
Rigid Support	108
Slurry Wall.....	108
Tangent Pile Wall	108
Secant Pile Wall	109
Design Procedure for Cut and Cover Structures	109
New Austrian Tunneling Method (NATM).....	112
TBM Tunnels	114
Analysis Types	114
Elastic Equation Method.....	115
Schulze and Duddeck Method.....	117
Muir Wood Method	118
Finite Element Method	121
Theoretical Approaches on Beam – Spring Method.....	122
2D and 3D Analysis of TBM Segmental Linings.....	128
Section 10	130
Review Of Seismic Design Procedures For Cut And Cover Structures	130
Review of Seismic Analysis Procedures for Rectangular Tunnels	131
Pseudo-static Methods	132
Free-Field Racking Deformation Method	133
Simplified Tunnel-Ground Interaction Analysis	134
Structural Fire Resistance of Cut and Cover Tunnels.....	137
Introduction	137
Test Segments	137
Fire Tests	140
Material Tests.....	141
Static Load Test	144
Structural Fire Safety Evaluation.....	146
Blast Design Philosophy	151

Reflected pressure due to an explosive that can be carried by a luggage	151
Incident pressure due to an explosive that can be carried by a luggage.....	152
Blast Pressure due to a small incident is taken as design value ($p=100 \text{ kN/m}^2$).....	152
References:.....	153
APPENDIX A. BALANCED CANTILEVER BRIDGE COMPUTER MODEL	158
Definition of the Bridge	158
Defining Section Properties	160
Pier.....	160
Click at the f of the bt and type the following equation $1200 + x^*-950$	162
Drawing Members	163
Tendons	167
Enter the following info found at input data- geometry- tendon by adding a row	167
Adding Loads and Construction Stages.....	168
Load Combo: DC+CLL+DIFF+CE+IE+CR+SH.....	168

Section 1:

Introduction

Bridges and tunnels must be planned and engineered before they can be constructed. In this document, the design of bridges and tunnels that are main components of the transportation system are covered using the modern design methods principles.

Who is a designer?

It is important to define the duties or functions of a designer. A designer may be able to perform one or all of the tasks listed below.

- Creativity and aesthetics
- Analytic
- Technical and practical

Engineering Aspects

Use of technical knowledge should not ignore the human factor. In a typical bridge design engineering aspects can be:

- selection of the bridge type
- analysis of load effects
- resistance of cross-sections
- conformance with related specifications

Importance of Infrastructures

Infrastructures such as bridges and tunnels are critical parts of the highway network due to the following facts

- controls capacity of the traffic system
- highest cost per kilometer of the network
- if infrastructure fails, detour is required

Table 1.1. Estimated average costs of infrastructure (for two lanes of traffic)

Type	Cost /m
Standard Highway Bridge w/piles (Turkey)	20000 USD/m
Special Highway Bridge (Turkey)	40000 USD/m
Standard Railroad Bridge (Turkey)	30000 USD/m
Tunnel (US)	120000 USD/m
Tunnel (Turkey)	30000 USD/m

Bridge Types and Span Lengths

Bridges can span from 2 meters to 2000 meters with one single main span, if desired. The maximum span lengths were given in Table 1.2.

Table 1.2. Bridge Types and Span Lengths

Bridge Type	Max Span Length
Wood Slab	5 – 10 m
R/C Slab	5 – 10 m
R/C Beam/Slab	15 – 20 m
Precast Prestressed I-Girder Slab	20 – 40 m
Steel Composite	30 - 100 m

Movable Bridge	< 170 m
Segmental Post-tensioned Bridge	40 - 300 m
Steel Box Section	30 – 300 m
Extradose Bridge	< 275 m
Truss Bridge	< 550 m
Arch Bridge	< 550 m
Cable Stayed Bridge	< 1100 m
Suspension Bridge	< 2000 m
Floating Bridge	< 2000 m

Bridge Aesthetics

Bridge aesthetics is one of the important parts of the design. There are couple of simple rules to improve the aesthetics of a bridge.

- Proportions with golden number (1.61803). The negative space framed with the piers and superstructure of the bridge can be proportioned to reflect the golden number proportions.

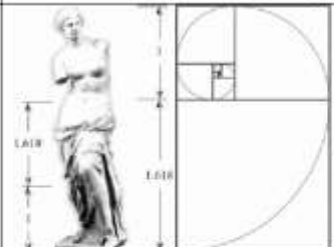
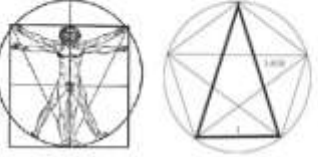
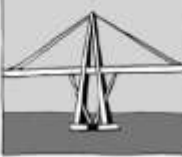
Proportion	Masterpieces	Bridge Piers
Golden Ratio $X^2 = X+1$ that is 1:1.618	 <p>La Venus De Milo</p>	
	 <p>Vitruvian man by Leonardo da Vinci (1492)</p>	

Figure 1.1 Golden Number – Bridges (Moon 2009)

- Deep valley bridges can be designed to have odd number of spans.
- Width of pier walls can be limited not to exceed 1/8 of the span length
- Distance measured between exterior columns of a multiple column bent can be limited not to exceed 1/3 of the span length
- Slenderness of the superstructure defined by the span length/beam depth ratio is one of the important aspects of the aesthetics and can be improved by creating shadows. Shadows can be developed by use of cantilevering decks.
- Tall piers can be tapered at their high point not only for aesthetics reasons but also for improving the strength and stability in resisting lateral loads.

Bridge Type Selection

Bridges can be categorized based on materials, function, span or structural form. Main structure can be in three forms as presented in Table 1.3.

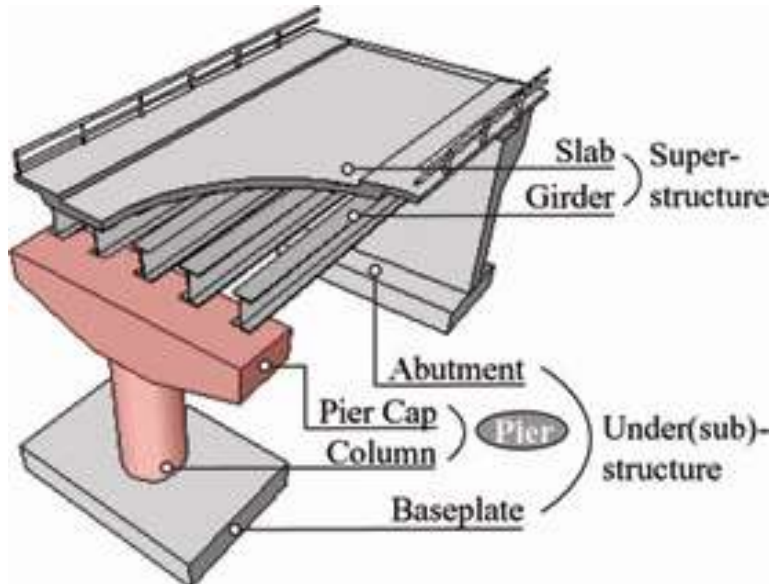


Fig. 1.2 Components of a Standard Highway Bridge (Moon 2009)

Table 1.3. Main Structure

Type	Example
Below Decking	Arch , Truss
Above Decking	Arch, truss, Cable-Stayed, Suspension, Extradosed
Along the Deck Line	Girder or Box Type, Floating

The selection of the bridge can be developed based on the type, size and location report (TLS) that shall include the cost study and preliminary bridge drawings. Function, economy, safety, construction experience, traffic control, soil conditions, seismicity and aesthetics are the main factor considered in selection of the type of the bridge.

Foundation soils can govern the selection type of the foundation such as spread footings, driven piles or drilled shafts.

Initial cost, maintenance cost, minimum number of spans, few deck joints and wide spacing of girders typically result in economical solutions. It shall also be noted that steel girders have higher maintenance cost compared to concrete bridges.

Bridge Failures

Wardhana and Hadipiriono (2003) and Imam and Chyrssanthopoulos (2012) studied the bridge failures in detail. The top five types of bridges failed out of 500 bridges between 1989 and 2000 is given in the below table.

Table 1.4. Most Common Failed Bridge Types – (Wardhana and Hadipiriono – 2003)

Type	Material	Number of Failures	% of Failure in the Set
Beam-Girder	Steel	145	28.83
Truss	Steel	107	21.27
Beam Girder	Concrete	29	5.77
Arch	-	17	3.38
Culvert	Steel	17	3.38
Others (more than 20 types)		188	37.37



Construction Failure – India



Fire – USA



Construction Failure – China



High Speed Train Accident – China



Construction Failure – USA



Figure 1.3

Wardhana and Hadipiriono (2003) have also investigated principal causes of failure for the collapsed bridges as presented in Table 1.5.

Table 1.5. Types of Failures

Types of Failures	% in Total
Hydraulic : Scour, Flood	52.88
Collision: Auto, ship	11.73
Overload	8.75
Deterioration	8.55
Earthquake	3.38
Fire	3.18
Construction	2.58
Fatigue-Steel	0.99
Design	0.60
Others (More than 10 items)	7.36

In a more recent study in UK prepared by Imam and Chryssanthopoulos (2012), the failure sources were identified for the metallic bridges for the investigated 164 collapses. Majority of these bridges were highway bridges (53%) and railway bridges (34%). The rest of collapse belongs to pedestrian bridges. They have categorized the collapses into seven categories as presented in Table 1.6.

Table 1.6. Failure Categories for Metallic Bridges

Categories	% in Total
Limited Knowledge	22
Design Error	22
Human Error	13
Natural Hazards (except earthquake)	21
Accidents	14
Overloading	5
Deterioration	3

The bridge failure can result in four different type of consequences categorized as human, economic, environmental and social as presented in Table 1.7.

Table 1.7. Categorized consequences

Consequences	Examples
Human	Fatalities, injuries and physical damage
Economic	Replacement/repair cost, traffic delays and detours, rescue cost, clean up cost,
Environmental	CO ₂ emission, energy use
Social	Loss of reputation, erosion of public confidence

Imam and Chryssanthopoulos (2012) have referenced an estimation equation for number of people on or under the bridge.

NBRGD = CDF x Commuter Population

Where CDF is the commuter distribution factor and can be taken as 0.02 for peak hours and 0.01 for off-peak hours. Expected number of causalities can be assumed as 7% of the NBRGD.

The closure cost of a bridge can be estimate from the unit prices defined below. These unit prices represent the average estimations for European value of time.

Table 1.8. Average European value of time for travel (2011)

Mode	Type	Definition	Value per Hour (in Euros)
Passenger Transport	Car	Business/person	32.9
		Commuting/private	9.4
		Vacation	6.3

	Train	Business/person	32.9
		Commuting/private	10.0
		Vacation	5.0
Freight Transport	Car	Light goods	62.6
		Heavy goods	67.3
	Train	Full Train (per 1 ton)	1.2
		Wagon (per 1 ton)	1.2

Section 2:

Uncertainties in Design

The design is typically based on a certain set of selected geometry, material, construction, loads and other factors while all these factors may be totally different than what has been assumed. For instance, the design drawings may specify a certain dimension on the drawings for cross-sections but the construction may not be fully in accordance with the drawing dimensions. The selection of design materials typically specified in terms of minimum strength but in reality the material may be more stronger than its assumed min value.

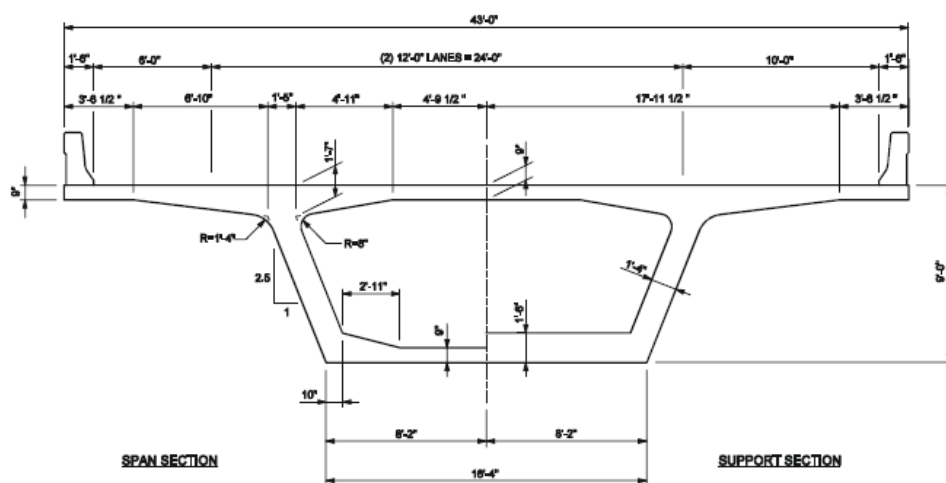




Figure 2.1 Design drawing (taken from AASHTO-LRFD Example) and Manufactured Section (taken from www.activeinfo.ca)

Reliability Index and Calibration of LRFD

Reliability index is an advanced version of factor of safety defined by statistical approaches and is basis for the development of the Load Resistance Factor Design (LRFD). In this approach, typically a limit state function $g(X)$ is defined to represent the vector of random variables (X) (Wisniewski et al 2009 and Barker and Puckett 2007) to consider related uncertainties for the given problem. The uncertainties can be in terms of geometry, material, structural analysis and construction technique. Failure or loss of function is defined by the following equation.

$$g(X) = R - D < 0 \quad (2.1)$$

The limit state function $g(x)$ is usually defined by the difference between the structural resistance (R), and demand (D) as shown in below figure.

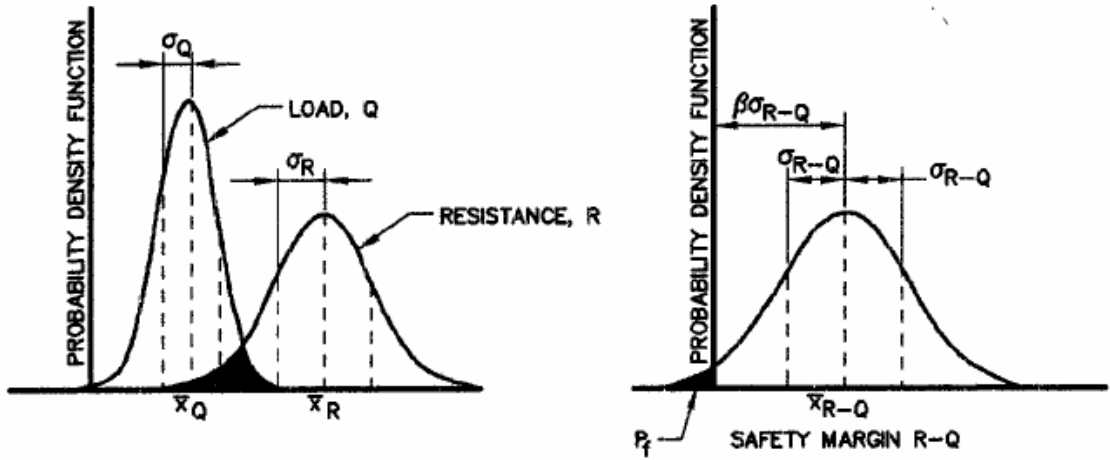


Figure 2.2 Reliability Index (FHWA 2001)

The probability of failure can be expressed as:

$$p_f = \Pr(g(X) < 0) \quad (2.2)$$

In many engineering applications including the bridge structures, the inverse standard normal probability distribution function ($\beta = \text{NORMSINV}(\text{probability})$ in MS Excel) is defined for the structural reliability index, β . The values of the inverse standard normal distribution can be found in any standard text book or in the MS Excel spreadsheet functions.

$$\beta = -\phi^{-1}(p_f) \quad (2.3)$$

The relationship between probability of failure and reliability index is tabulated below for normal distribution.

Table 2.1 Probability of Failure and Reliability Index (Normal Distribution)

β	P_f
2.0	0.022739
2.5	0.006215
3.0	0.001350
3.5	0.000233
4.0	0.000032

For normally distributed \bar{R} and \bar{D} (or Q) the reliability index can be computed from the following equation.

$$\beta = \frac{\bar{R} - \bar{D}}{\sqrt{\sigma_R^2 + \sigma_D^2}}$$

(2.4)

where \bar{R} and \bar{D} are the mean values of the generalized resistance and demand, σ_R and σ_D are the standard deviations of the generalized resistance and action.

$$\bar{R} = \lambda_d R \quad (2.5)$$

$$\bar{D} = \lambda_d D \quad (2.6)$$

where λ is the bias factor. The bias factor can be computed from the following equation. In the above equation the R and D are specified values. To give a better example the mean value for compressive concrete strength tests is determined to be 28 MPa and the min specified concrete compressive strength used in design is 25 MPa. In this case, the bias factor will be $28/25 = 1.12$.

As it can be recalled from the standard probability theory, the standard deviation is equal to the mean value multiplied by the coefficient of variation (COV).

$$V_r = \sigma / \bar{R} \quad (2.7)$$

$$V_d = \sigma / \bar{D} \quad (2.8)$$

For concrete structures, bias factors and coefficient of variation for various parameters can be found in the work of Argınhan (2010), Barker and Puckett (2007), FHWA (2001), NCHRP489(2003) and Wisniekski et al (2009). For steel structures, bias factors and coefficient of variation can be found in the work of Barker and Puckett (2007), Kun and Qilin (2012) and Liu (2002).

In case, the resistance or the demand part has sub parameters in the computation, an equivalent coefficient of variation can be computed using the following equation.

$$V_R = \sqrt{V_{R1}^2 + V_{R2}^2 + V_{R3}^2 \dots + V_{Rn}^2} \quad (2.9)$$

$$V_D = \sqrt{V_{D1}^2 + V_{D2}^2 + V_{D3}^2 \dots + V_{Dn}^2} \quad (2.10)$$

The bias factor, λ , is usually applied to the mean resistance and demand values. For log-normally distributed R and D the reliability index can be computed from the following equation.

$$\beta = \frac{\ln(\bar{R}/\bar{D})}{\sqrt{V_R^2 + V_D^2}} \quad (2.11)$$

Barker and Puckett (2007) suggested a formal process to define load and resistance factors using reliability index as follows.

- Data collection: Determining statistical parameters for load and resistance.
- Determine the inherent reliability index of the current bridge design.
- Study reliability levels for different span lengths, dead load to live load ratios, load combinations, types of bridges
- Select a target reliability index for design
- Compute load and resistance factors consistent with the selected reliability index.

The following equation need to be satisfied for the load combinations and resistance in design where the resistance needs to be larger than the load effects.

$$\sum \eta_i \cdot \gamma_i \cdot D_i \leq \phi \cdot R_n = R_r \quad (2.12)$$

where η_i is the load modifier, γ_i is the load factor and ϕ is the resistance factor.

The LRFD method is still under research in Turkey and the early results of the research indicate that the following reliability indices can be targeted in design.

Table 2.2 Target Reliability Index

Load Combination	Target Reliability Index
Live Load	4.0
Wind	3.0
Scour	2.0
Ship collision	3.0
Earthquake	2.5

As shown below, switching from LFD method to LRFD method minimize the discrepancies in safety index of reliability.

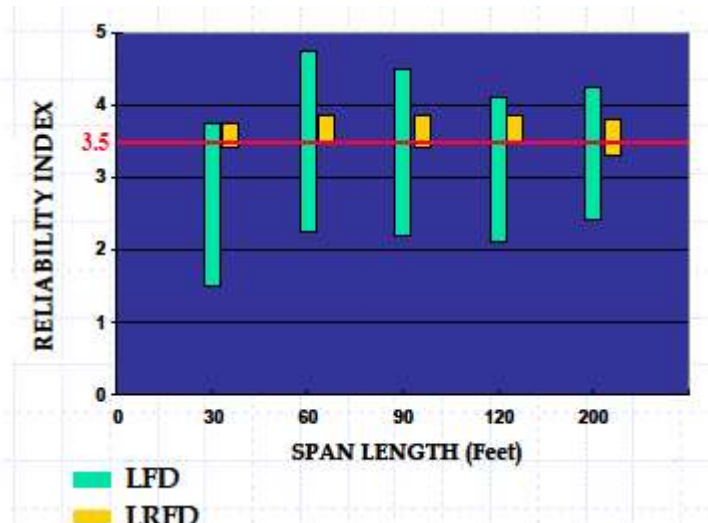


Figure 2.2 Difference in LFD and LRFD Method (taken from
http://www.inti.gob.ar/cirsoc/pdf/puentes_hormigon/24-bridge-INTRO_to_LRFD_rev.pdf)

Example :

A prestressed concrete bridge with a simple span of 30 meters and girder spacing of 2 meters has the following mean bending moments (normal distribution).

M_{DC} : 2103 kN-m (dead load of girders, slabs) - (COV = 0.10)

M_{DW} : 336 kN-m (superimposed dead load such as barriers and wearing surfaces) (COV=0.25)

M_{LL+IM} : 2354 kN-m (live load plus impact) – (COV = 0.18)

The resistance moment (lognormally distributed) is determined to be from the cross-section analysis

$$M_r = \phi M_n > M_u \quad (\phi = 1.0 \text{ given}) \quad (\text{COV} = 0.075 \text{ and bias factor} = 1.05) \quad (2.13)$$

Determine the load factor for the live load component to have a minimum reliability index of 4.0 (use normal distribution in reliability index comps).

$$M_u = 1.25 (M_{DC}) + 1.25 (M_{DW}) + ??? (M_{LL+IM}) \quad (2.14)$$

Answer:

Resistance Components

The mean resistance moment = $\overline{M_r} = \lambda M_r = 1.05 \times M_u$ kN-m (assume demand is almost equal to resistance)

The corresponding standard deviation for resistance component = $0.075 \times 1.05 \times M_u$ (kN-m)

Demand Components

The mean demand moment is = $2103 + 336 + 2354 = 4793$ kN-m

Demand standard deviation= $[(0.10 \times 2103)^2 + (0.25 \times 336)^2 + (0.18 \times 2354)^2]^{0.5} = 480.4$ kN-m

Load Factor Computation

Solving for reliability index = 4 to determine the M_u is determined to be 7950 kN-m as presented below.

$$4 = (1.05 M_u - 4793) / (480.4^2 + (0.07875 M_u)^2)^{0.5}$$

If $M_u = 7950$ kN-m then the load factor in front of the live load can be determined from

$$7950 = 1.25(2103) + 1.25(336) + \gamma_{LL}(2354)$$

Solving the unknown load factor yields to 2.08 as the load factor for live load and a minimum moment resistance of 7950 kN-m.

Live Load

The development of design truck load in Turkey is based on modification of a HS20-44 truck specified in AASHTO specifications (1996). In the AASHTO (1996), design either the truck or the lane load is selected in the analysis to achieve the maximum force effect.

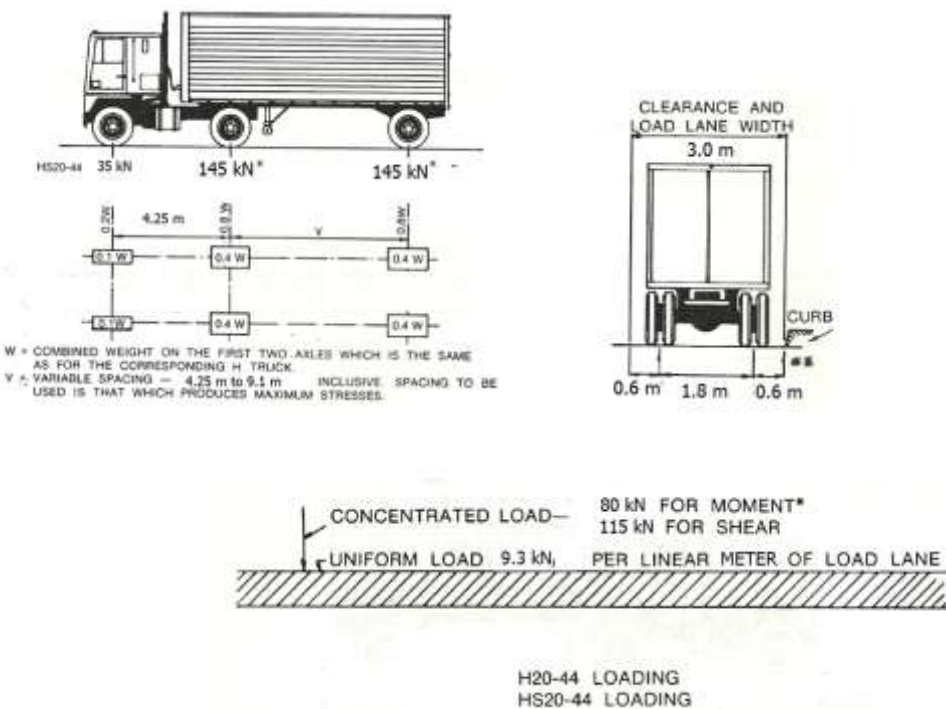
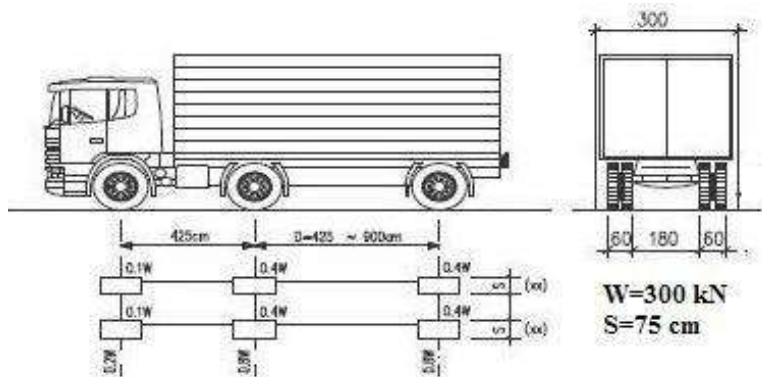


Figure 2.3.

The Turkish design truck used in design of highway bridges is very similar to the AASHTO HS20-44 truck and named as H30-S24 truck (KGM 1982).



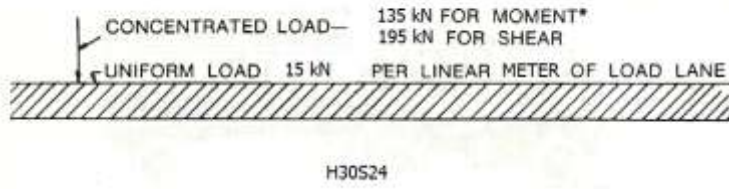


Figure 2.4.

The new LRFD design truck, HL93 is much heavier than the HS20-44 truck presented in the earlier versions of the AASHTO. The lane load is combined with the heavy truck load in this configuration to represent a more realistic loading condition.

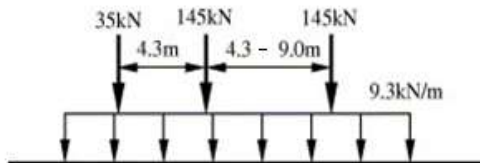
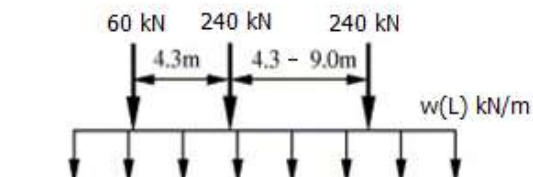


Fig 2.5 HL 93 Truck

It is still under research but the following truck system, H30S24Y is proposed to be used in bridge designs in Turkey similar to the HL93 design truck philosophy as follows.



$L < 40 \text{ m}$	$w(L) = 0 \text{ kN/m}$
$41 \text{ m} < L < 65 \text{ m}$	$w(L) = 7 \text{ kN/m}$
$66 \text{ m} < L < 90 \text{ m}$	$w(L) = 8 \text{ kN/m}$
$91 \text{ m} < L < 135 \text{ m}$	$w(L) = 9 \text{ kN/m}$
$L > 136 \text{ m}$	$w(L) = 10 \text{ kN/m}$

H30S34Y

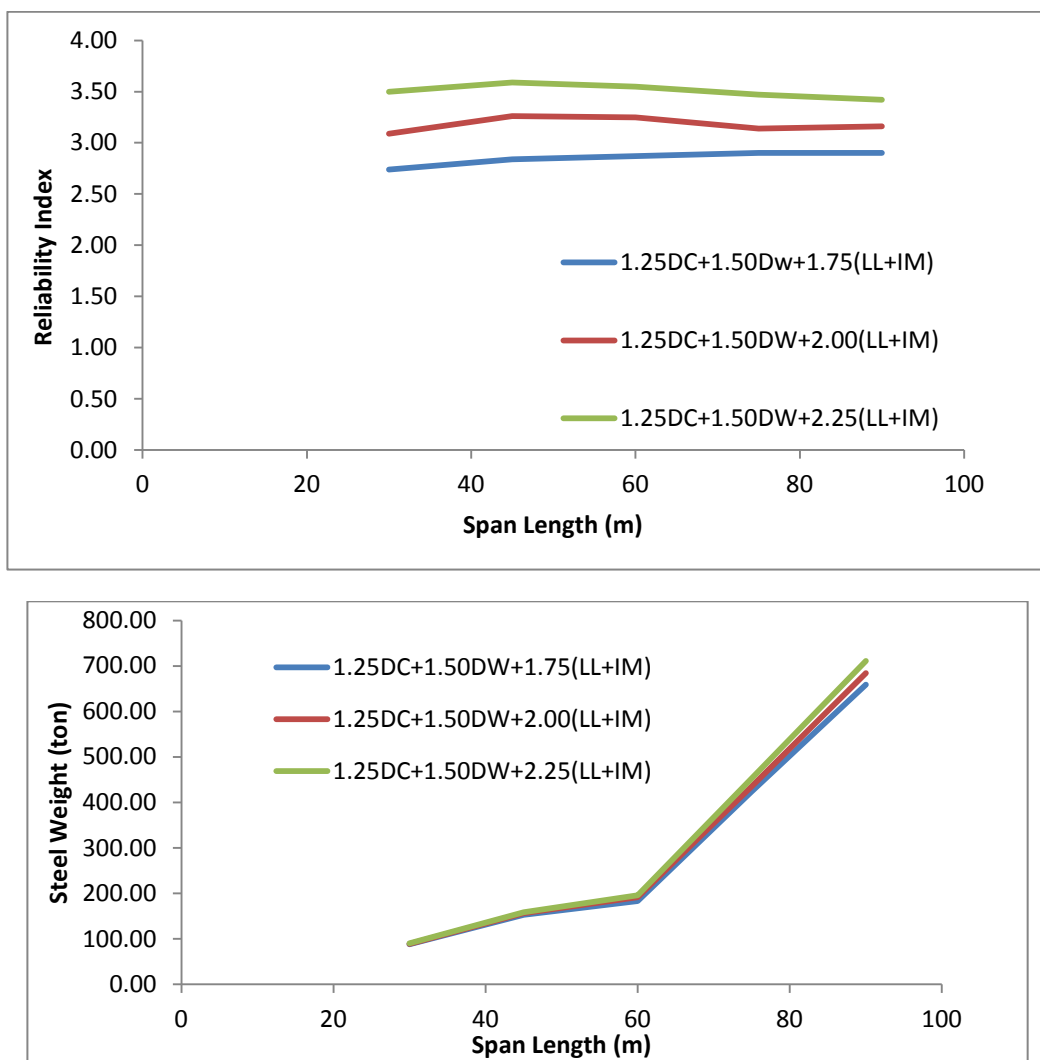


Figure 2.6

The design tandem load (AASHTO 2007) is presented below representing two close axle loads.

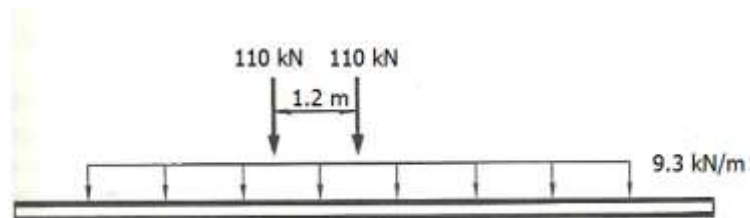


Figure 2.7

For negative moment design of continuous bridges the trucks can be placed on the bridge as shown below (AASHTO 2007).

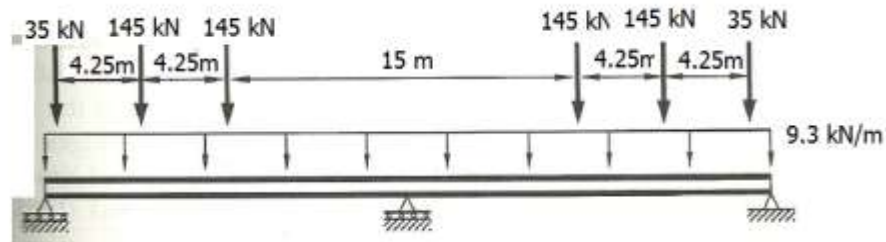


Figure 2.8

It has also been known that the overload truck usage in Turkey is frequent, and the axle and weight configurations are different than the standard design trucks (KGM 1982).

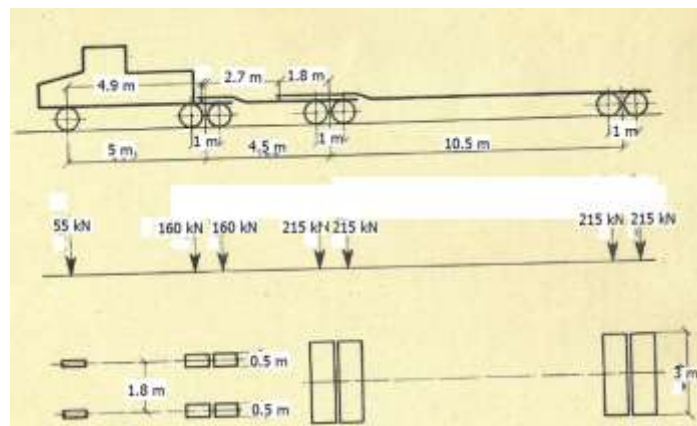


Figure 2.9

Other than the above design trucks, another truck with lane load is proposed as AYK45.

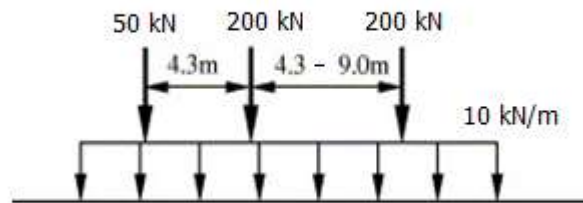


Figure 2.10

Fatigue Live Load

Under repetitive loading, the elements of bridge can fracture significantly below the yield strength. The design truck is usually a rare truck load on bridges and for fatigue

evaluations the design truck load can be reduced by 25% to represent a more realistic case of repetitive loads. The lane load shall not be included in the structural analysis. Only one single lane shall be loaded with the moving truck load. The live load impact factor described in the following section shall be included in the analysis. The weights of surveyed trucks are much less than the weight of design trucks as shown below.

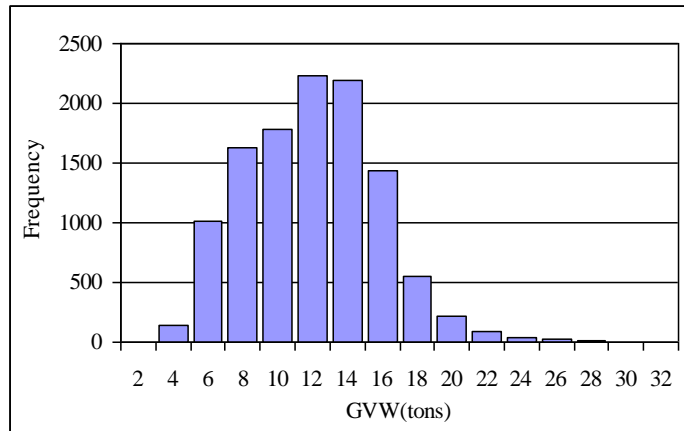


Figure 2.11

Live Load Impact Factor

The roadway surface of the bridge is not smooth and the vehicle suspension system compresses and extends during the travel time. This action develops larger forces than static load cases on the bridges. Usually, it is only applied to the design truck but not to the lane load.

The dynamic factor applied to the live load is defined by the following equation in the KGM (1982) document.

$$\varphi = 15 / (L + 37) < 30\% \quad (2.15)$$

Where L is the span length (m). In the new AASHTO-LRFD, the dynamic factor is modified for a constant value of 1.33.

Multiple Presence

The probability of having multiple heavy trucks traveling at the same speed of a multi-lane bridge is rare event. Therefore, a typical design considers reducing the truck loads for multiple lane bridges.

Table 2.2. Multiple Presence Factors (AASHTO 2007)

Number of Design Lanes	Multiple Presence Factor
1	1.2
2	1.0

3	0.85
More than 3	0.65

Girder Distribution Factors

The most common type of bridges is slab-girder type in Turkey.

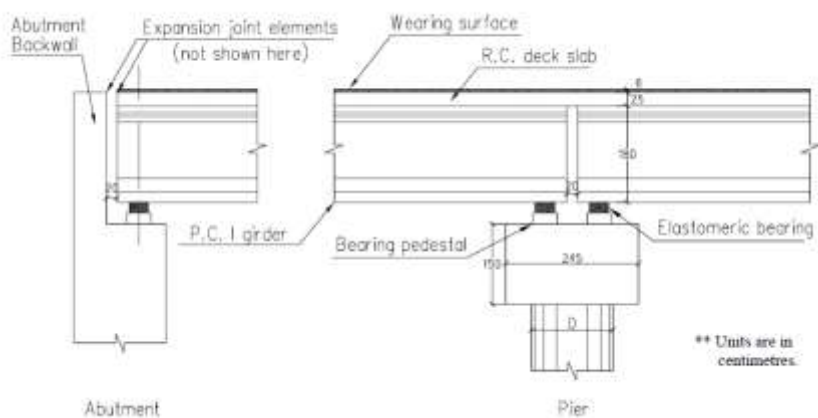
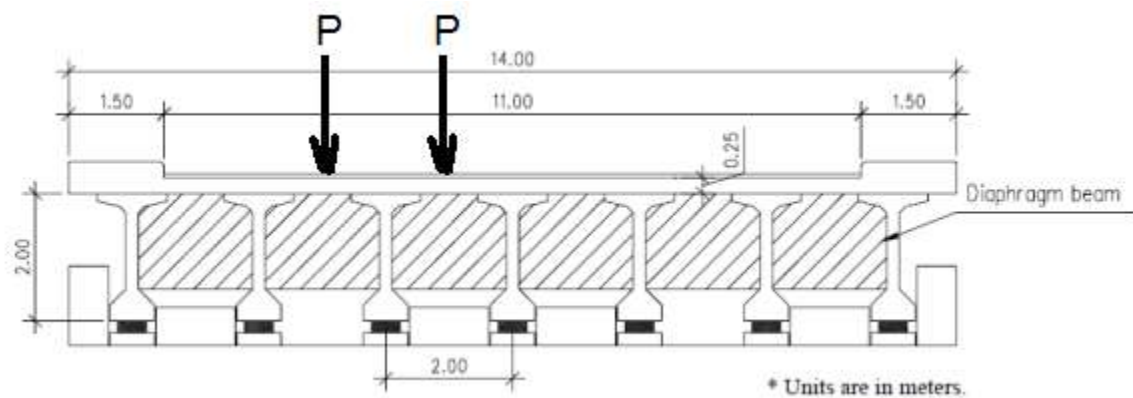


Figure 2.12

The loads acting near to a girder is shared with the group of the girders. To quantify the distribution of loads in multiple girder system AASHTO suggests using distribution factors for practical reasons.

In the AASHTO LFD (1996) or KGM (1982), the moment determined based on the wheel loads are distributed to the girders using the following equations.

$GDF = S/2000$ if one lane is loaded

$GDF = S/1800$ if two or more lanes are loaded

Different than AASHTO LFD (1996) wheel load distribution factor, in the AASHTO-LRFD (2010) the design moment per lane (axle loads) is distributed to each interior girder by the following expression given in AASHTO LRFD (2010)

$$GDF = 0.06 + \left(\frac{S}{4300}\right)^{0.4} \left(\frac{S}{L}\right)^{0.3} \left(\frac{K_g}{Lt_s^3}\right)^{0.1} \text{ if one lane is loaded}$$

$$GDF = 0.075 + \left(\frac{S}{2900}\right)^{0.6} \left(\frac{S}{L}\right)^{0.2} \left(\frac{K_g}{Lt_s^3}\right)^{0.1}, \text{ if two or more lanes are loaded}$$

where, GDF is the girder distribution factor, S is the spacing of beams (mm.), L span length of beam (mm.), K_g is the longitudinal stiffness parameter(mm^4) and t_s is the depth of concrete slab (mm.). The longitudinal stiffness can be expressed by (AASHTO LRFD 4.6.2.2.1-1)

$$K_g = n(I + Ae_g^2) \text{ and } n = \frac{E_B}{E_D} \quad (2.16)$$

where, E_B is the modulus of elasticity of beam material, E_D is the modulus of elasticity of deck material, I is the moment of inertia of beam (mm^4) and e_g is the distance between the centers of gravity of the basic beam and deck (mm). Note that, n is a non-dimensional coefficient.

Similar equations are available for exterior girder moment, shear interior girder and shear exterior girder in the AASHTO-LRFD code (2010). In the calibrations of AASHTO LRFD by Nowak, the bias factor for girder distribution function is taken as 1.0 and coefficient of variation as 0.12.

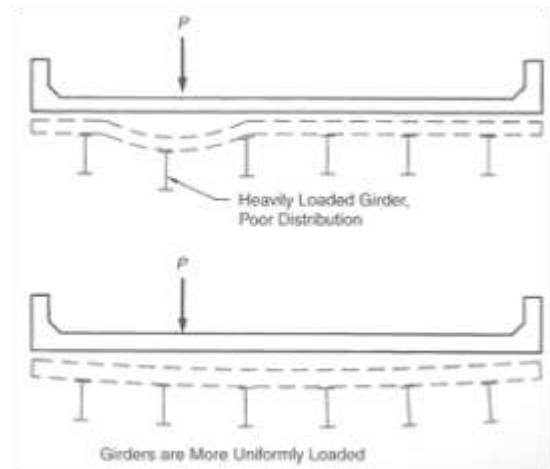


Fig 2.10 Taken from Barker and Puckett (2007)

Section 3

Typical Precast Prestressed Girder Cross-Sections

The most common sections used for the multi-girder slab type bridges and span lengths are given below.

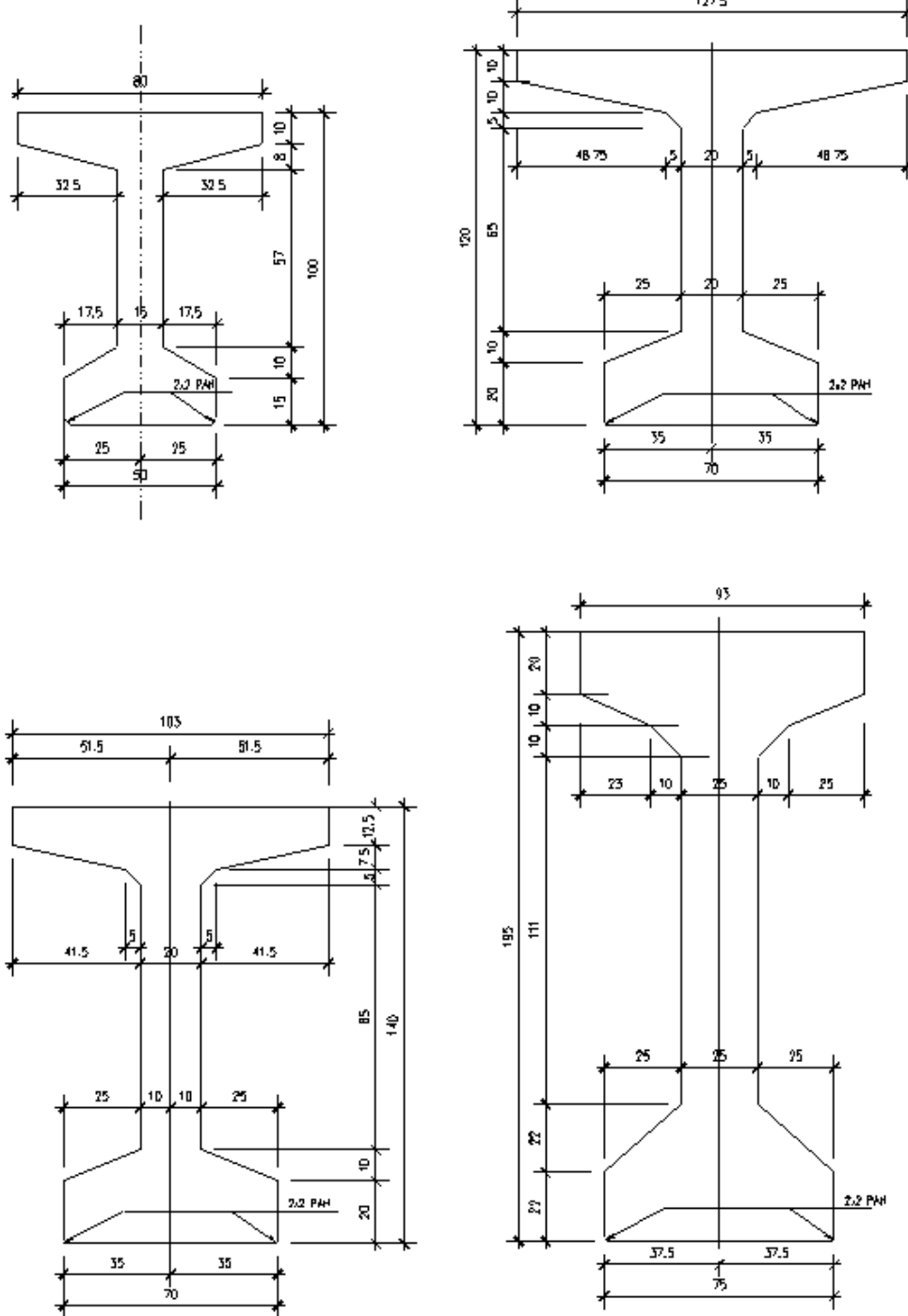


Figure 3.1.

Selection of Girder Type

In the preliminary design stage of the precast-prestressed I or T girders, the recommended minimum depth of girder is given as $0.045L$ in the AASHTO-LRFD (2010). The thickness of reinforced concrete deck slab is around 20 to 25 cm in most of the applications. A recent study for these types of bridges on spacing and span depth ratio is given below.

Table 3.1. Spacing versus Span Depth Ratio

Spacing (m)	Span/Depth Ratio
1.0	27
1.5	25
2.0	22
2.5	19
3.0	17

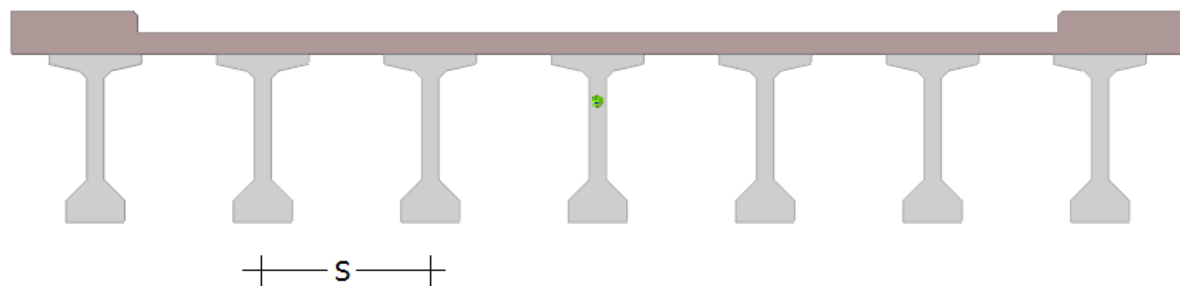


Figure 3.2.

Material Properties

In a typical precast prestressed girder design low-relaxation 7-wire strands are used.

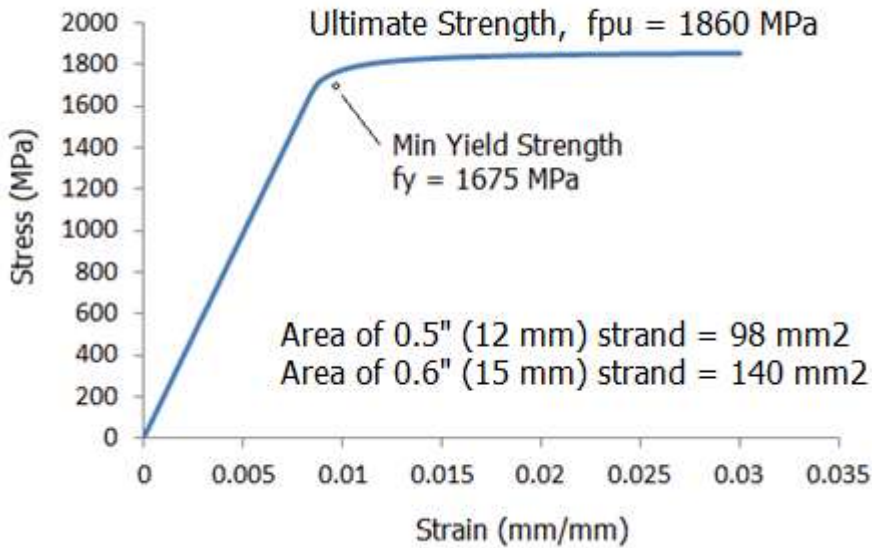


Figure 3.3.



Typical design values used in Turkey for precast prestressed girder design are given below.

Figure 3.4.

For Concrete:

At transfer of prestressing: C30

28 day Strength : C40

For Tendons:

Jacking Stress : 0.75 fpu = 1395 MPa

After Losses: 0.80 fpy = 1340 MPa

Production Cycle (2-3 days)

The tendons will be laid out a fabrication bed between two anchor heads. The mild reinforcement will be placed along the bed per the design drawings. Once the mild

reinforcement is placed steel forms will be placed over the fabrication bed and the concrete will be poured into the forms. The fabrication pieces will be moist cured over the night. In the morning, if the test cylinders reach the specified concrete strength of tendon transfer, the tendon between the series of girders will be cut to apply pre-stressing. The girders will be stored at the site before the shipment.

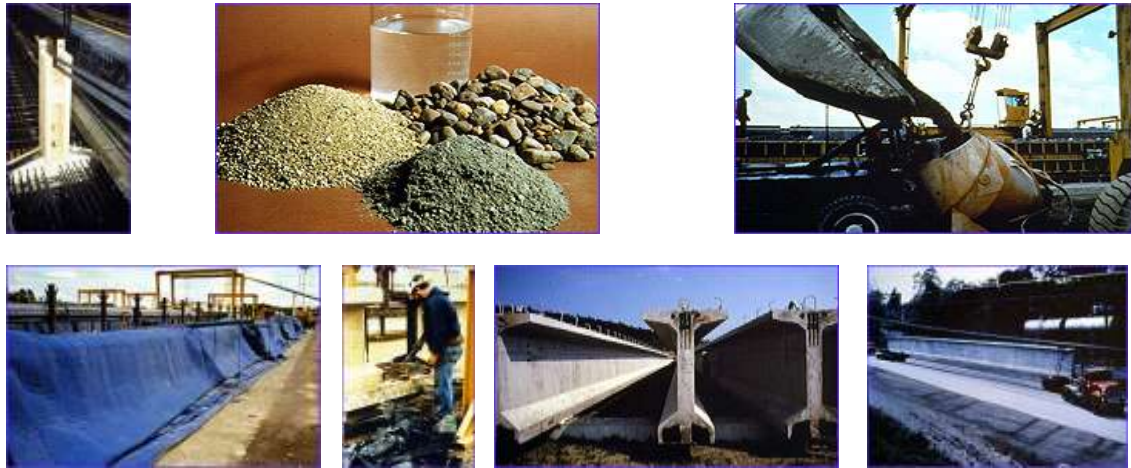


Figure 3.5.

Gravity Design Load Combinations

The factored load shall be based on the following formulation.

$$D = \eta \sum \gamma_i D_i \quad (3.1)$$

where the factor, η , relating to ductility, redundancy and operational importance can be taken equal to 1.0 unless otherwise noted.

The limiting compression stress for the girder can be checked through using the following load combination (Service I).

$$D=1.0 \text{ (DC+DW)} + 1.0 \text{ (LL+IM)} \quad (3.2)$$

The limiting tension stress for the girder can be checked through using the following load combination (Service III).

$$D=1.0 \text{ (DC+DW)} + 0.8 \text{ (LL+IM)} \quad (3.3)$$

The load combination for capacity can be evaluated through Strength I load combination

$$D= 1.25 \text{ DC} + 1.50 \text{ DW} + 1.75 \text{ (LL+IM)} - \text{maximum effects}$$

$$D= 0.90 \text{ DC} + 0.65 \text{ DW} + 1.75 \text{ (LL+IM)} - \text{minimum effects} \quad (3.4)$$

Fatigue Load Combination:

$$0.75(LL+IM) \quad (3.5)$$

Limiting Stresses

The compression stresses are limited to $0.45 f_c'$ (MPa) for this type of girder design. The limiting tensile stresses are given in the below tables (AASHTO LRFD 2010). (f_c' – design strength, f_{ci} – strength at initial pre-stressing)

Table 3.2. Temporary Tensile Stress Limits Before Losses

Item	Stress Check Location	Limiting Stress (MPa)
1	Pre-compressed tensile zone without mild reinforcement (typically bottom of the girder)	0.00
2	At locations other than the ones described in item 1	$0.24\sqrt{f_{ci}} < 1.38$
3	In locations with mild reinforcement in which mild reinforcement stresses do not exceed 50% of the yield stress	$0.60\sqrt{f_{ci}}$

Table 3.3. Tensile Stress Limits After Losses at Pre-compressed Tensile Zones

Item	Stress Check Location	Limiting Stress (MPa)
1	Bonded steel and potential moderate corrosion	$0.48\sqrt{f_c'}$
2	Bonded steel and potential severe corrosion	$0.24\sqrt{f_c'}$
3	Unbonded steel	0.00

Computing Cross-Sectional Stresses

The stresses due to self weight of the girder, haunch and the fresh concrete weight of the deck, prestressing forces will develop on the girder section itself only. The superimposed dead load and live load plus impact stresses are computed on the transformed composite section.



Used in Stress Comp due to M_{DC}
and Prestressing

Used in Stress Comp due to M_{DW} and
 M_{LL+IM}

Figure 3.6.

Stresses due to M_{DC}

The girders will have a tendency to displace downwards under its self weight. The maximum moment, M_{DC} can be computed from the following equation for a simply supported girder.

$$M_{DC} = w_{DC}L^2/8 \quad (\text{N-mm}) \quad (3.6)$$

The stresses at top and bottom can be computed using the following equations. (-) is compression and (+) is tension.

$$\sigma_{top} = -\frac{M_{DC}}{S_{top}} \quad (3.7)$$

$$\sigma_{bot} = \frac{M_{DC}}{S_{bot}} \quad (3.8)$$

where

$$S_{top} = I_{girder}/y_{top} \quad (\text{mm}^3)$$

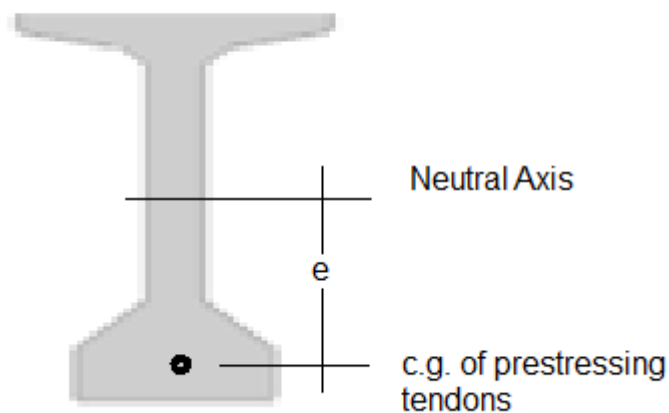
$$S_{bot} = I_{girder}/y_{bot} \quad (\text{mm}^3).$$

y_{top} (mm) is the distance measured between the neutral axis and top of the girder

y_{bot} (mm) is the distance measured between the neutral axis and bottom of the girder.

Stresses due to Prestressing

The pre-stressing tendons are typically located at the bottom of the girder for simply supported spans. The pre-stressing force will pre-compress the bottom flange and will develop a compressive axial load and moment about the neutral axis. This action of force effects can result in cambering up of the girder.



The moment due to pre-stressing at the neutral axis can be computed as

$$M_p = P \cdot e \quad (3.6)$$

Where P is the pre-stressing force in (N) and e is the distance measured from c.g of the tendons to the neutral axis of the beam. Stresses at the top and bottom of the section can be computed from the following relationship.

$$\sigma_{top} = -\frac{P}{A} + \frac{M_p}{S_{top}} \quad (3.7)$$

$$\sigma_{bot} = -\frac{P}{A} - \frac{M_p}{S_{bot}} \quad (3.8)$$

Stresses due to Superimposed Dead Load

Once the concrete deck hardens, additional dead load can be placed on top of the deck. These items are typically wearing surface (asphalt), side walk, diaphragm beams and barriers for highway bridges. For railway bridges instead of wearing surface, direct fixation or ballast and tracks can be defined as the superimposed dead load.

A typical barrier weighs around 4.4 kN/m and a 5 cm thick wearing surface develops a pressure of 1.1 kN/m². These loads effects can be equally distributed for each girder.

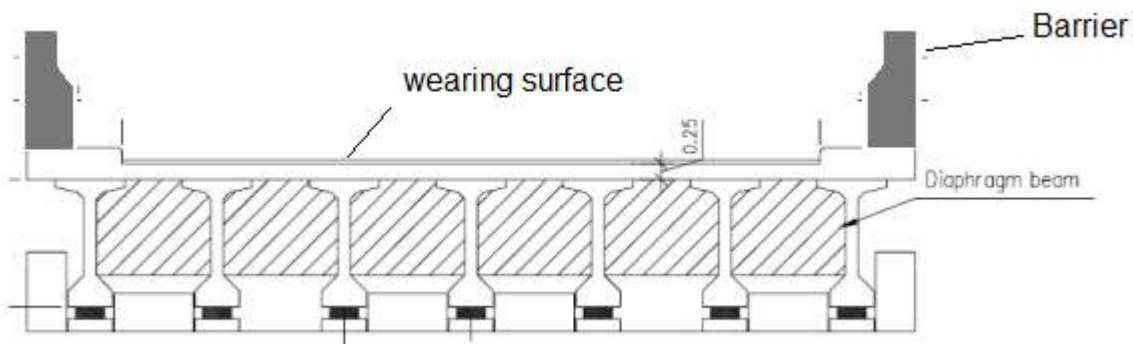


Figure 3.8.

The applied superimposed uniform load on any girder can be computed from the following equation.

$$W_{\text{sdl}} = n_b W_b / N_g + W_w \cdot S + W_{\text{side}} / N_g \quad (3.12)$$

Where

n_b is the number of barriers,

W_b is the weight of the barrier (N/mm),

N_g is the number of girders

W_w is the weight of the wearing surface (N/mm²)

S is the spacing of the girders (mm)

W_{side} is the total weight of the side walk (N/mm)

At the location of the transverse beam diaphragms used to balance the load distribution between the girders, point loads can be computed

$$P_{\text{sdl}} = W_{\text{db}} \cdot S \quad (3.13)$$

Where

W_{db} is the weight of the diaphragm beam (N/mm)

The following loading can be solved to determine the maximum moments due to superimposed dead load

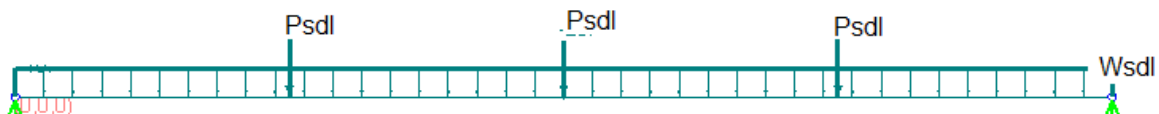


Figure 3.9.

It shall be noted that the P_{sdl} point force only exists if there is a beam diaphragm.

In stress computations the cross-sectional properties shall account for the composite action.

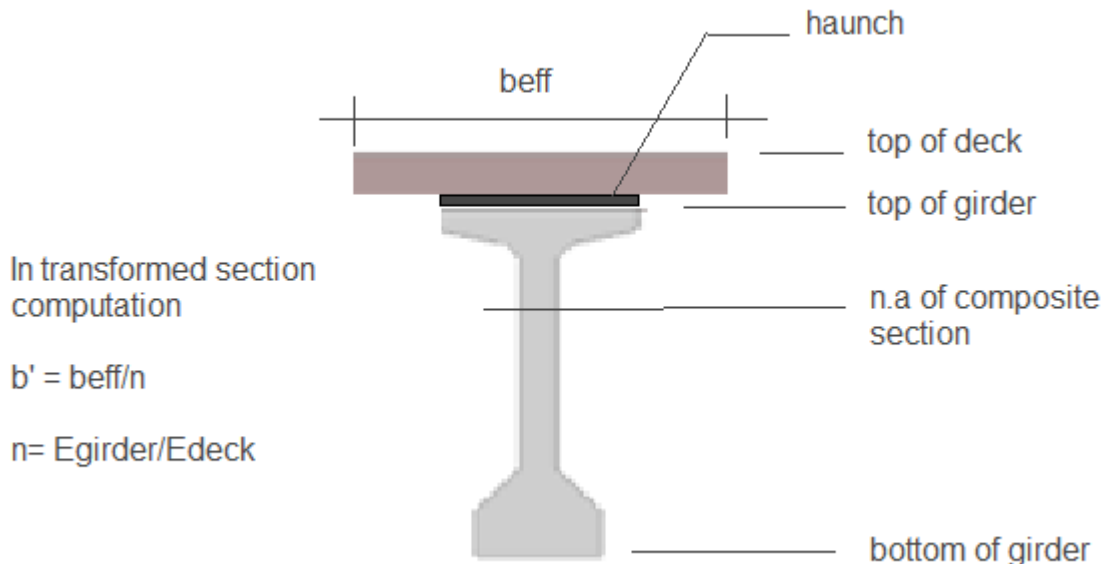


Figure 3.10.

As shown in the above figure, transformed section need to be computed for the stress analysis. The effective flange width of the section can be taken as minimum of the three listed conditions.

$$b_{eff} = \min \left(\frac{L/4}{12t_d}, S \right) \quad (3.14)$$

Where t_d is the thickness of the deck (mm). The transformed width of the deck can be computed from the below equation that has to be used in the stress computations.

$$b' = b_{eff}/n \quad (3.15)$$

The stresses can be computed as follows:

$$\sigma_{topdeck} = -\frac{M_{SDL}}{nS_{ctopdeck}} \quad (3.16)$$

If neutral axis is below the top deck the stress at the top of girder will be compression otherwise it will be tension.

$$\sigma_{top} = -\frac{M_{SDL}}{S_{ctop}} \quad (3.17)$$

$$\sigma_{bot} = \frac{M_{SDL}}{S_{cbot}} \quad (3.18)$$

$$S_{ctopdeck} = I_{composite}/y_{topdeck} (\text{mm}^3)$$

$$S_{ctop} = I_{composite}/y_{topg} (\text{mm}^3)$$

$$S_{cbot} = I_{composite}/y_{botg} (\text{mm}^3)$$

Stresses due to Live Load Plus Impact

Similar to the superimposed dead load stress computations, stresses due to live load plus impact can be computed using the same set of equations. A moving load or influence line analysis can be conducted to determine the maximum effects of live load. For a simply supported girder, the location of the c.g of the truck can be matched to mid-span length of the girder develop the maximum effects.

The stresses can be computed as follows:

$$\sigma_{topdeck} = -\frac{GDF.M_{LL+IM}}{nS_{ctopdeck}} \quad (3.19)$$

If neutral axis is below the top deck the stress at the top of girder will be compression otherwise it will be tension.

$$\sigma_{top} = -\frac{GDF.M_{LL+IM}}{S_{ctop}} \quad (3.20)$$

$$\sigma_{bot} = \frac{GDF.M_{LL+IM}}{S_{cbot}} \quad (3.21)$$

The GDF term, girder distribution function is defined in the previous sections.

Required Prestress

The concrete tensile stress computations (Service III case) are the governing set of equations in determination of the required number of strands in a girder. At the first stage compute the stresses at the bottom of the girder without the prestressing effect from the below equation.

$$\sigma_{bot} = \frac{M_{DC}}{S_{bot}} + \frac{(M_{DW} + 0.8.GDF.M_{LL+IM})}{S_{cbot}} \quad (3.22)$$

A correction for tensile stress can be applied by subtracting the allowed tensile stress limit defined in Table 3.2.

$$\sigma_{bottens} = \sigma_{bot} - \sigma_{tenslimit} \quad (3.23)$$

The pre-stressing shall develop compressive stresses at the bottom of the girder to overcome the tensile stresses computed at the above equation.

$$\sigma_{prestbot} = -\sigma_{bottens} = -\frac{P_p}{A_{girder}} - \frac{M_p}{S_{bot}} = -\frac{P_p}{A_{girder}} - \frac{P_p e}{S_{bot}} \quad (3.24)$$

The required pre-stressing to develop such compressive stress at the bottom of the girder can be computed from the above equation as follows.

$$P_p = \left(\frac{A_{girder} S_{bot}}{S_{bot} + A_{girder} e} \right) \sigma_{bottens} \quad (3.25)$$

The required number of strands can be computed using the pre-stressing forces after losses as follows.

$$n_{prestress} = \frac{P_p}{f_{pi} A_{strand} (1 - loss\%)} \quad (3.26)$$

The f_{pi} , jacking stress ($0.75 f_{pu}$) will have approximately about 15% to 20% loss in the long-term due to creep, shrinkage and relaxation. The A_{strand} can be found in the materials section with the other parameters.

Section 4

Pre-stress Losses

Pre-stress losses can develop due to elastic shortening of the girder, creep, shrinkage and relaxation.

Elastic Shortening

The prestress loss due to the elastic shortening can be computed from the below equation.

$$\Delta f_{pes} = \frac{E_p}{E_c} f_{cgp} \quad (4.1)$$

Where

E_p = elastic modulus of the pre-stressing strands, 196500 MPa

f_{cgp} = compressive stress at the concrete layer matching the c.g of the tendons that results in shortening of the stressed tendon length (MPa)

$$f_{cgp} = -\frac{P_i}{A_{girder}} - \frac{P_i e^2}{I_{girder}} + \frac{M_{girder} e}{I_{girder}} \quad (4.2)$$

Where

P_i = $n_{prestress} \cdot A_{strand} \cdot f_{pi} \cdot (1\% \text{loss})$, the loss can be assumed to be around 8% in the first trial (N)

M_{girder} = moment due to selfweight of the girder (N-mm)

Long term pre-stress loss due to creep, shrinkage and relaxation-approximate method

The long term prestress loss due to creep and shrinkage and relaxation can be computed using the following equation.

$$f_{plt} = 10.0 \frac{f_{pi} A_{ps}}{A_{girder}} \gamma_h \gamma_{st} + 83.0 \gamma_h \gamma_{st} + \Delta f_{pr} \quad (4.3)$$

where

f_{pi} = jacking stress (MPa)

A_{ps} = total area of prestressing steel (mm^2)

$\gamma_h = 1.7 - 0.01H$, where H is the % of relative humidity

34.475

$$\gamma_{st} = \frac{34.475}{(6.895 + f_{ci})}$$

γ_{st} is the correction factor for the compressive concrete strength at the time of transfer

Δf_{pr} is the relaxation of the prestressing steel and can be taken as 16.6 MPa for the low-relaxation one.

The advanced methods are described in the AASHTO-LRFD (2010).

Evaluation of End Zones at Transfer of Prestress

At the end zones of the girder, the prestressing forces are not needed too much since the positive moment due to self weight of the girder is very low at the end zones. Therefore, the prestressing tendons can be debonded to reduce the adverse effects of the prestressing force at the end zones.

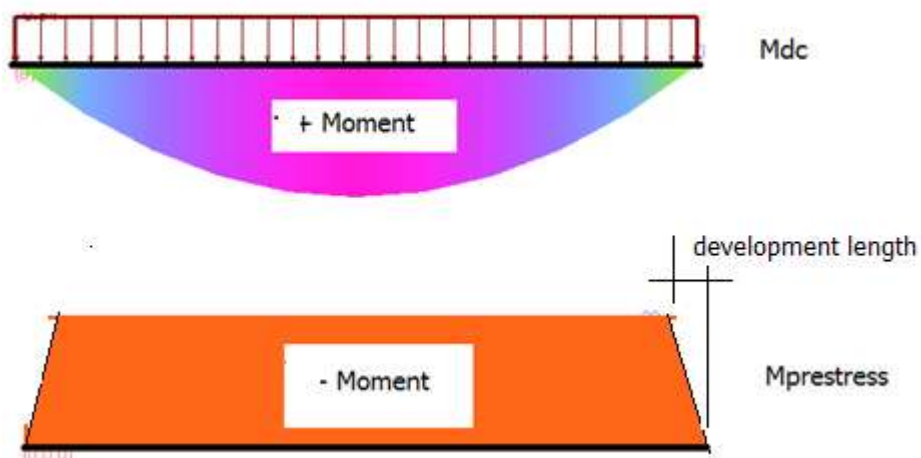


Figure 4.1

The temporary limiting stresses shown in Table 3.2 need to be satisfied. The typical development length of the prestressing tendons is equal to the $60 \times$ diameter of the prestressing tendon per AASHTO-LRFD. At the end zones, the prestressing tendons can be debonded based on the following suggestions.

- Only 25% of the tendons required at the max positive moment region can be debonded at the end zones.
- In a row of tendons only 40% can be debonded
- Debonding can be done in a symmetric wave. Pipes and sleeves can be used for this purpose.

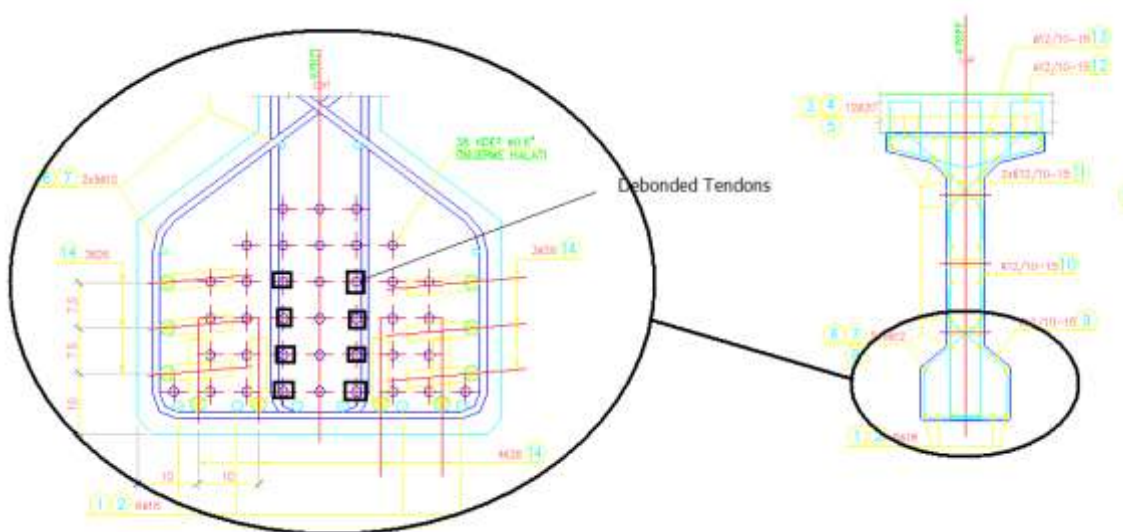


Figure 4.2

Evaluation of Mid Span at Transfer of Prestress

The temporary stress limits for the bottom and top of the girder need to be checked at the mid-span using the total number of tendons.

Service I & III Mid-Span Stress Evaluations

Service I load combination shall only be used to evaluate the compression stress limit of $0.45f_c'$. Service III load combination shall only be used to determine the tension stresses.

Optional Deflection Check

The optional truck deflection check can be evaluated for the following truck loads

- Deflection resulting from the truck load only
- Deflection resulting from 25% of the design truck load plus lane load.

The optional deflection limit can be taken as 1/800 of the span length. The evaluated deflections shall be less than this limiting value.

Fatigue Limit Check

Fatigue can be checked for regions where initial compressive stress is less than the tensile stresses induced by the live load Fatigue I combination. The fatigue need to be checked if the tensile stresses due to combined effects of permanent load, prestress load and fatigue load combination exceeds $0.24\sqrt{f_c'}$.

For straight prestressing tendons the threshold stress is determined to be around 120 MPa. For prestressing tendons with curved path the threshold stress is usually taken as 70 MPa.

For mild reinforcement the fatigue limit can be computed from the following equation.

$$165 - 2.3f_{min}$$

where f_{min} is the minimum stress due to combined effects of fatigue live load combination with permanent loads.

Strength I Flexural Evaluation

The flexural capacity of the section can be computed using the following equation.

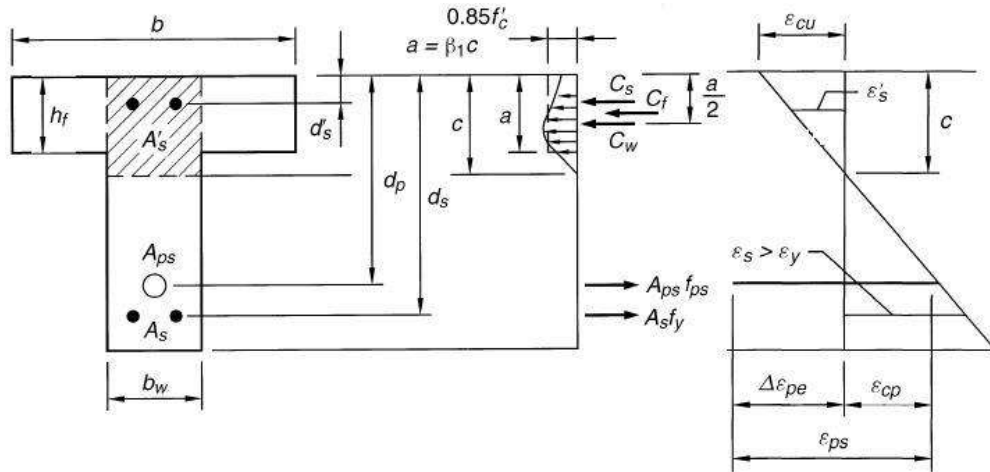


Figure 4.3

Barker and Puckett (2007).

$$M_r = \phi M_n$$

$$\begin{aligned} M_n = & A_{ps} f_{ps} \left(d_p - \frac{a}{2} \right) + A_s f_s \left(d_s - \frac{a}{2} \right) - A'_s f'_s \left(d'_s - \frac{a}{2} \right) \\ & + 0.85 f'_c (b - b_w) h_f \left(\frac{a}{2} - \frac{h_f}{2} \right) \end{aligned} \quad (4.4)$$

Where

A_{ps} = area of prestressing steel (mm^2)

f_{ps} = average prestress at the prestressing steel (MPa)

d_p = distance from extreme compression fiber to the center of prestressing tendon (mm)

f'_c = 28 day compressive strength (MPa)

b = width of the compression face of member (mm)

b_w = width of web (mm)

h_f = compression flange for T-Beam (mm)

$a = \beta c$ – depth of equivalent stress below (mm)

β = stress block factor ($\beta = 0.85$ for $f'_c < 30$ MPa, $0.85 > \beta > 0.65$ for $30 < f'_c < 55$ MPa respectively)

If the computed "c" stays with in the deck, b_w and h_f can be taken as "0".

$$f_{ps} = f_{pu}(1 - k \frac{c}{d_p}) \quad (4.5)$$

where $k = 0.28$ for low relaxation steel.

$$c = \frac{A_{ps}f_{pu} - A_s f_s - A_s' f_{s'} - 0.85 f'_c (b - b_w) h_f}{0.85 f'_c \beta b_w + k A_{ps} \frac{f_{pu}}{d_p}} \quad (4.6)$$

Flexural Reinforcement Requirements

Maximum Reinforcement

The amount of maximum reinforcement is indirectly controlled in the LRFD method. As tension reinforcement increases, the factored resistance of prestressed and non-prestressed reinforcement is reduced. For these sections, most of the time the failure mechanism is compression controlled. (AASHTO-LRFD 2010)

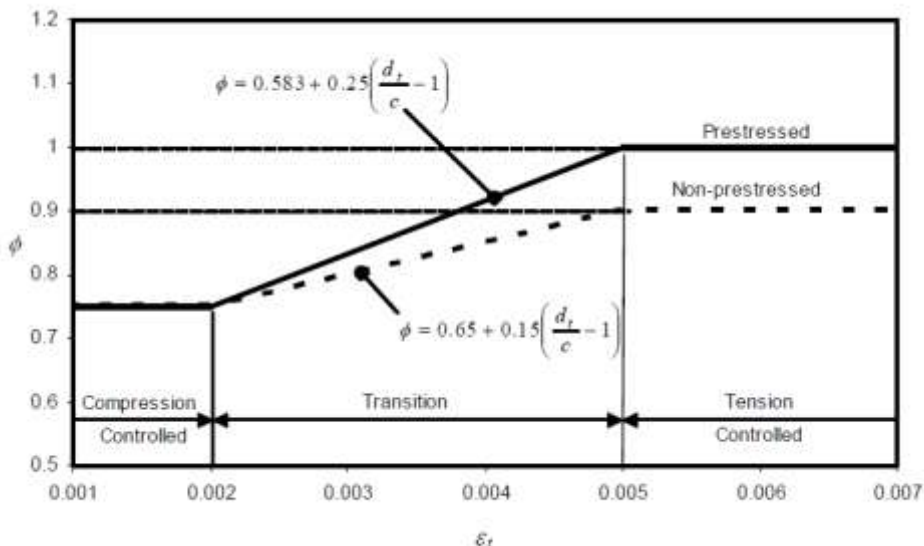


Figure 4.4.

Where

d_t = distance measured between the extreme compression fiber and tension steel (mm)
 c = distance between the extreme compression fiber and the neutral axis (mm)

Minimum Reinforcement

The selected mild or prestressing steel shall develop at least a minimum amount of flexural moment resistance defined below.

- a) 1.2 times the M_{cr} (cracking moment)

$$M_{cr} = S_{cbot} (f_r + f_{cpe}) - M_{dnc} \left(\frac{S_{cbot}}{S_{bot}} - 1 \right) \geq S_{cbot} f_r \quad (4.7)$$

where

S_{cbot} = section modulus of the composite section at the tension side (mm^3)

f_r = modulus of rupture = $0.6\sqrt{f_c'}$ (MPa)

f_{cpe} = compressive stress in concrete due to effective prestress (after losses) at extreme fiber where tensile stresses are developed by external loads (MPa).

M_{dnc} = total unfactored dead load moment acting on the girder section (N-mm)

- b) 1.33 times the factored moment determined from the load combinations.

Strength Shear Design

The shear resistance is related to the nominal shear resistance as follows.

$$V_r = \phi V_n \quad (4.8)$$

Where $\phi=0.9$

The minimum nominal shear resistance can be computed from the following equations.

$$V_n = V_c + V_s + V_p \quad (4.9)$$

$$V_n = 0.25f_c'b_v d_v \quad (4.10)$$

where

$$V_c = 0.08\beta\sqrt{f_c'}b_v d_v \quad (4.11)$$

$$V_s = \frac{A_v f_y d_v (\cot\theta + \cot\alpha) \sin\alpha}{s} \quad (4.12)$$

where

d_v : effective depth (mm)

b_v : effective web (mm)

s : spacing of the transverse reinforcement (mm)

β : a factor defined for diagonally cracked concrete to transfer tension and shear

$$\beta = \frac{4.8}{1 + 750\varepsilon_s}$$

θ : angle of inclination of compression stresses

$$\theta = 29 + 3500\varepsilon_s$$

α : angle of inclination of transverse reinforcement to longitudinal reinforcement

A_v : area of shear reinforcement (mm)

V_p : component of prestressing force in the direction of applied shear load (N)

ε_s : is the net tension strain along the centroid of the tension reinforcement and can be computed using the following equation

$$\varepsilon_s = \frac{\left(\frac{|M_u|}{d_v} + 0.5N_u + |V_u - V_p| - A_{ps}f_{po}\right)}{E_s A_s + E_p A_{ps}} \quad (4.13)$$

where

f_{po} : locked in stress ($0.7f_{pu}$)

N_u : factored axial load (N) (+tension)(- compression)

M_u : factored moment and can not be less than $IV_u - V_p Id_v$
 V_u : factored shear force (N)

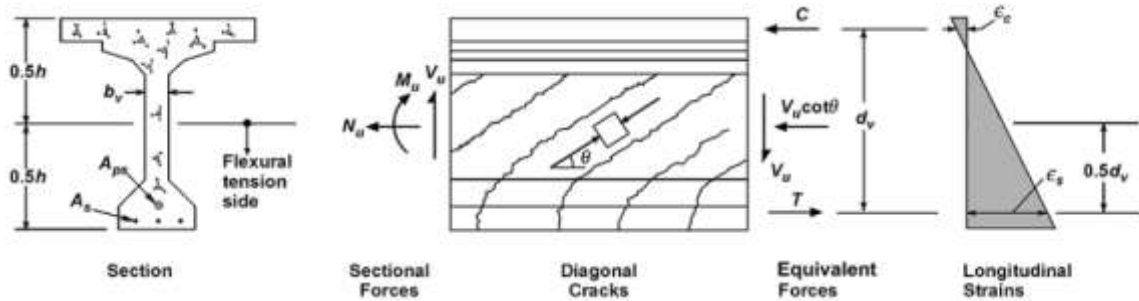


Figure 4.5.

There is also one other method to determine the shear resistance of the concrete that requires trial and error method defined in AASHTO LRFD but not covered in this course.

Minimum Transverse Reinforcement

Transverse reinforcement shall be provided if the following equation is valid.

$$V_u > 0.5\phi(V_c + V_p) \quad (4.14)$$

The minimum transverse reinforcement can be determined from the following equation.

$$A_v = 0.08\sqrt{f'_c} \frac{b_v s}{f_y} \quad (4.15)$$

Maximum Spacing of Transverse Reinforcement

The maximum spacing of the transverse reinforcement can be computed from the following equation.

If $v_u < 0.125f'_c$, then $s_{max}=0.8d_v < 600$ mm

If $v_u > 0.125f'_c$, then $s_{max}=0.4d_v < 300$ mm

$$v_u = \frac{|V_u - \phi V_p|}{\phi b_v d_v} \quad (4.16)$$

Transverse Design (Deck)

In transverse deck design of the bridge, typically following sections has been checked using the worst case of loading.

- Maximum negative bending moment at the root of the deck overhang
- Maximum positive and bending moments at the centerline between two girders
- Maximum negative bending moment in the top deck at the interior face of the girder
- Check for shear at face of girder top flange

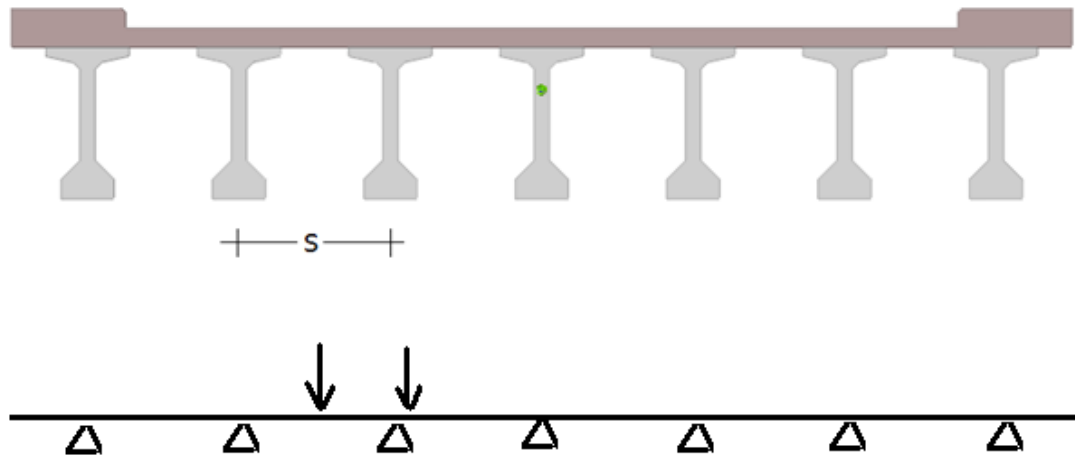


Figure 4.6.

A 1 meter strip of the deck can be analyzed for the given structural idealization. The footprint of the wheels can be distributed by an 45° angle at the depth of the deck. The typical tire foot print is about 500 mm in width and 250 mm in length.

Computer Modeling

In computer modeling, simple stick elements and stick and shell elements can be used together to model the superstructure. Barr et al (2001) suggested the following modeling technique for the live load distribution factor analysis.

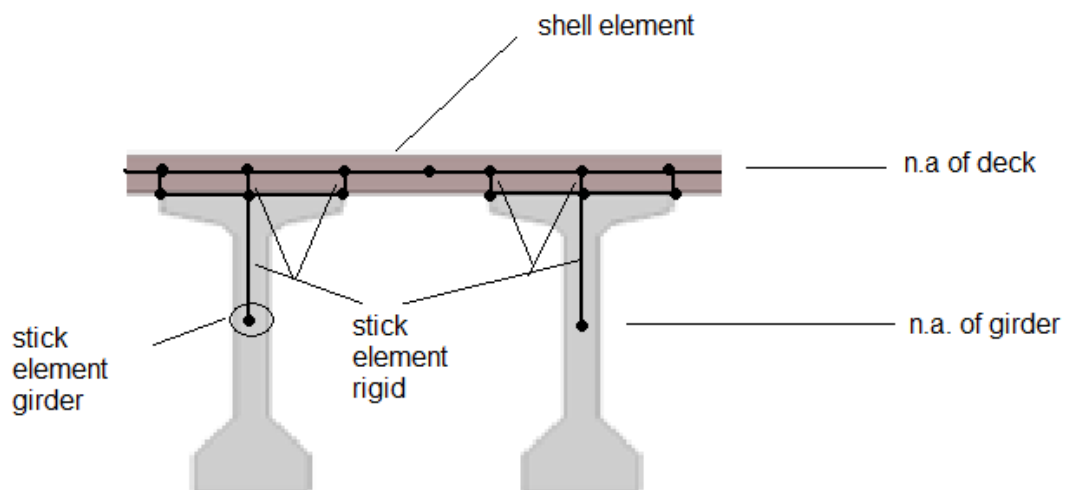


Figure 4.7.

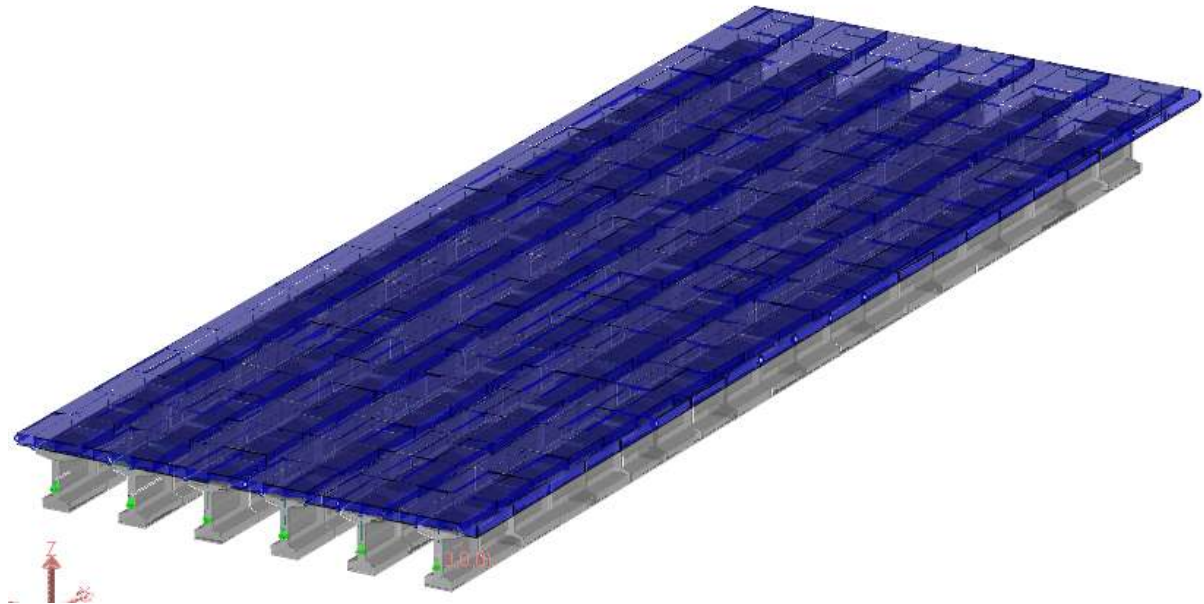


Figure 4.8.

L=32 m, Girder Spacing = 2 m, Deck Thickness = 0.25m

(LARSA 4D Model: week4compmode.lar)

To determine the forces at the neutral axis of the section, a transformation of forces is needed as follows

$$M_{comp} = N_{deck} \cdot a + N_{girder} \cdot b + M_{deck} + M_{girder}$$

$$N_{comp} = N_{deck} + N_{girder}$$

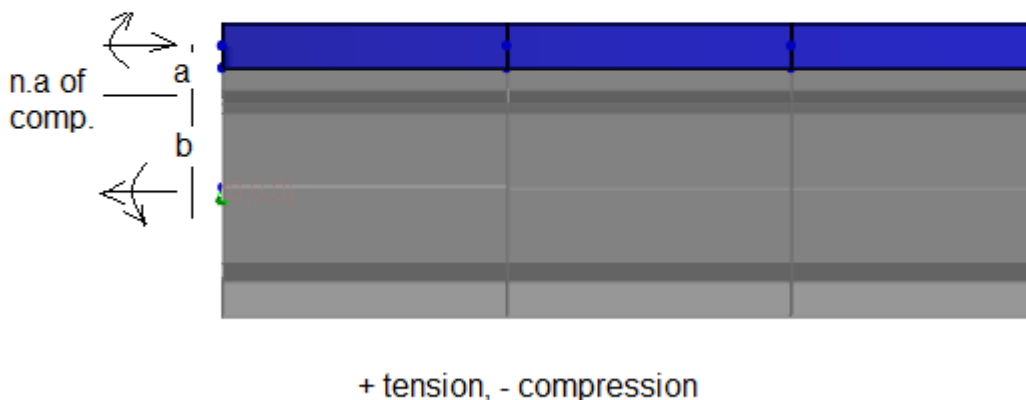


Figure 4.9.

Spliced Precast Prestressed/Posttensioned Multiple I-Girder/Slab Bridge

The span lengths can be increased by having intermediate splices along the girders. The spans can be made continuous up to 85 meters by use of post-tensioning the precast girders.

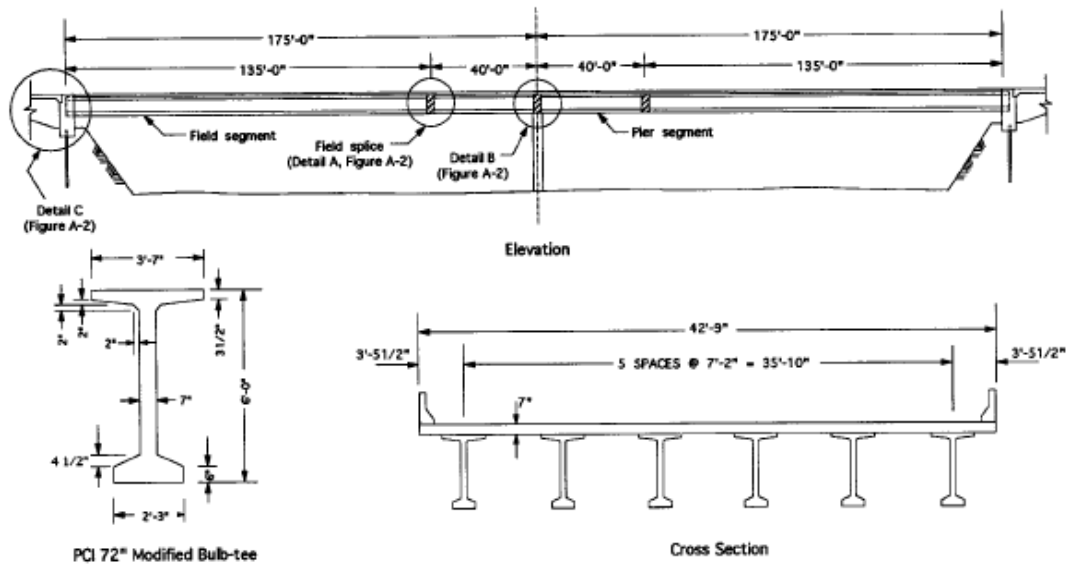


Figure 4.10.

The details of the construction are given below. (Abdel Karim 1995)

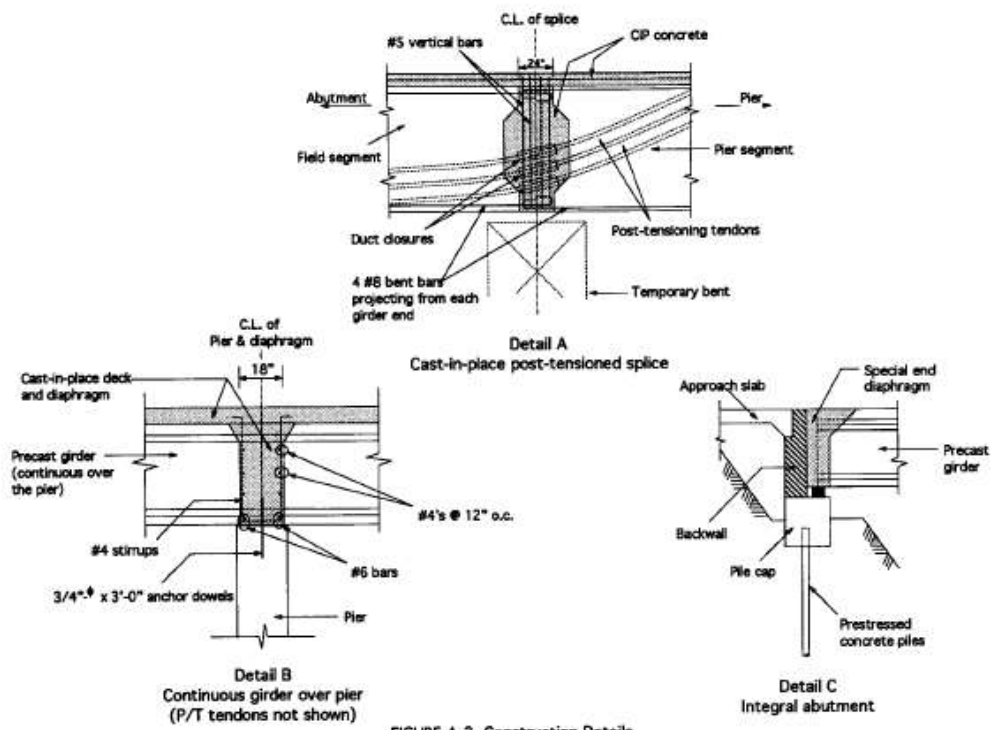


FIGURE A-2 Construction Details.

Figure 4.11.

The construction sequence of the spliced beam slab bridge design can follow the below schedule.

Table 4.1. Construction Stages

Stage	Days since precasting	Event
0	0	Pretension and pour concrete
1	1	Release of pretensioning force
2	28	Erection of precast beams
3	35	CIP deck & joints
4	42	Post-tensioning & supp. Removal
5	60	Application of SIDL
6	70	Application of LL (open to traffic)
7	10000	After final prestress losses

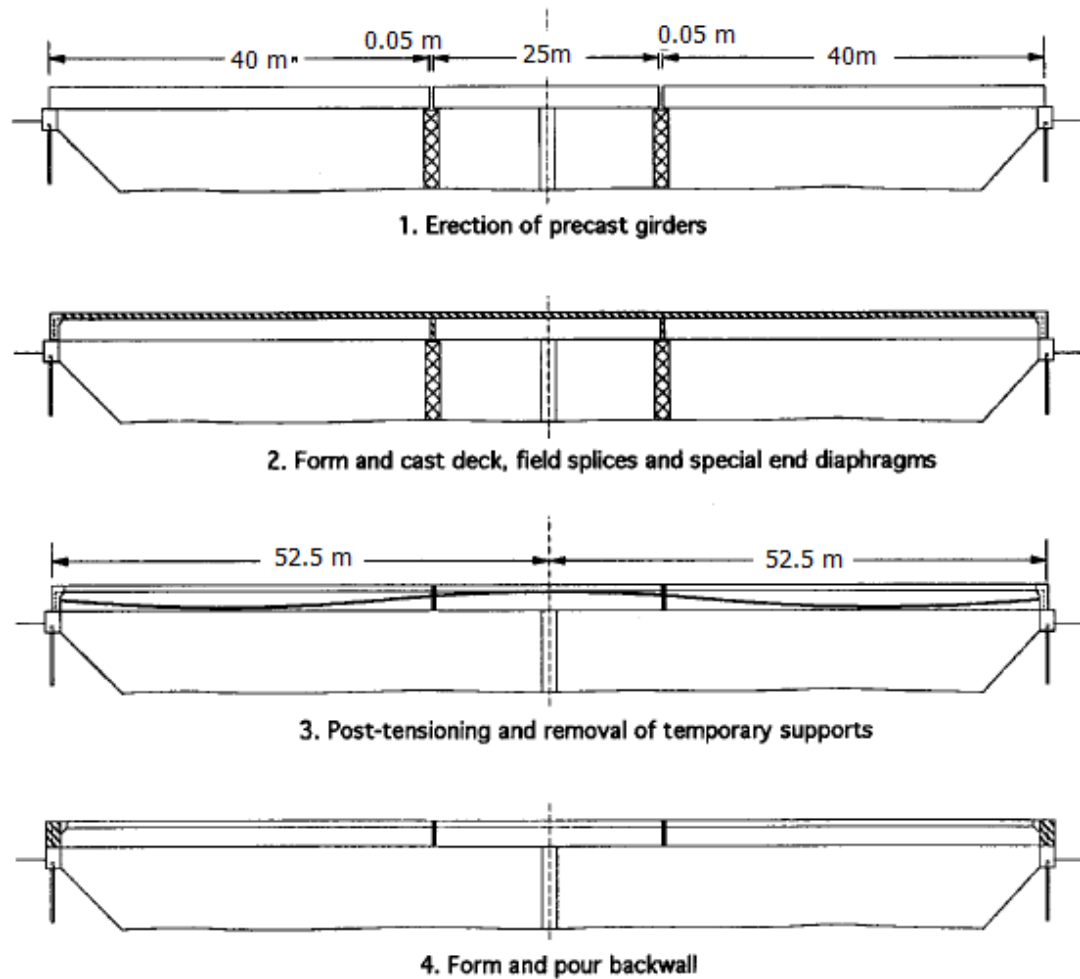


Figure 4.12.

The cost comparisons indicate this type of bridge can be 30% cheaper than the steel girder slab bridge type.

High Speed Railroad Bridge Passenger Comfort

The resonance or excessive vibrations of the bridge may develop at the time of the train pass. Such vibrations may yield to ballast instability and excessive stress over the deck.

The dynamic analysis is not required if the speed of the train is less than 200 km/hr, bridge is a continuous one and the first bending natural frequency is within the given limit as shown in the below figure (EN:1991 (2003)). In this case, the static equivalent amplification factor can be used (impact factor for with standard maintained bridge given below).

$$\emptyset_3 = \frac{2,16}{\sqrt{L_0} - 0,2} + 0,73 \quad (4.17)$$

Where L is the length of the bridge (m)

For a simply supported bridge the vertical frequency of the bridge can be computed using the following equation

$$\eta_o = \frac{17,75}{\sqrt{\delta_o}} \quad (4.18)$$

Where δ_o is the deflection due to permanent loads (mm)

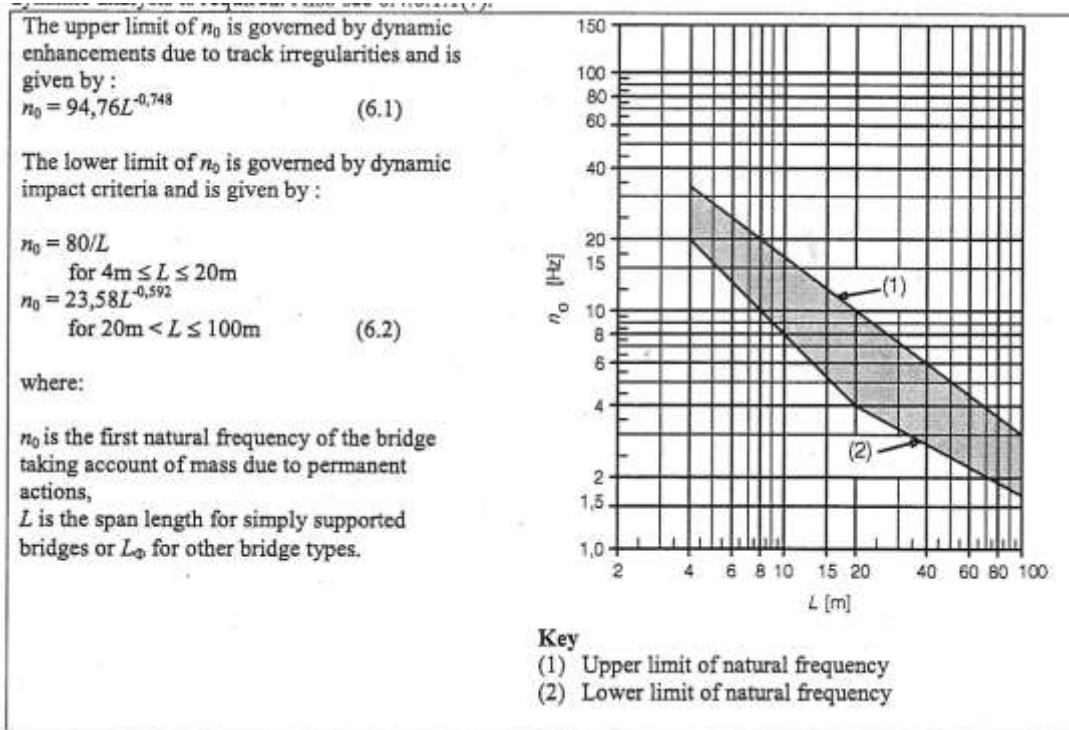
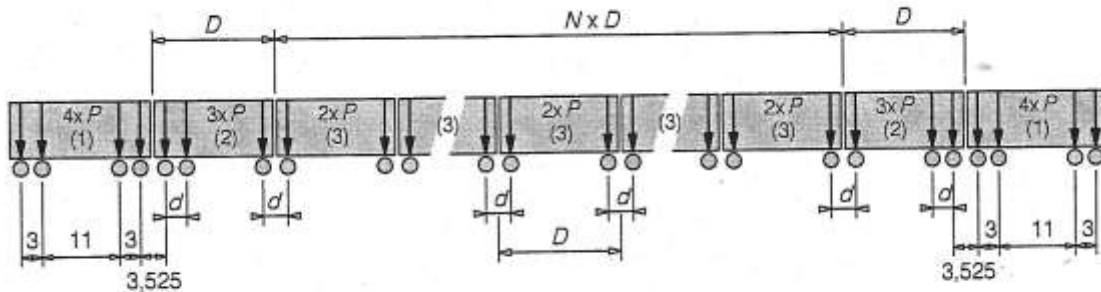


Figure 4.13.

For the dynamic analysis of the bridge, the following train layouts can be used unless otherwise noted.



Key

- (1) Power car (leading and trailing power cars identical)
- (2) End coach (leading and trailing end coaches identical)
- (3) Intermediate coach

Universal Train	Number of intermediate coaches N	Coach length D [m]	Bogie axle spacing d [m]	Point force P [kN]
A1	18	18	2,0	170
A2	17	19	3,5	200
A3	16	20	2,0	180
A4	15	21	3,0	190
A5	14	22	2,0	170
A6	13	23	2,0	180
A7	13	24	2,0	190
A8	12	25	2,5	190
A9	11	26	2,0	210
A10	11	27	2,0	210

(5) HSLSM-B comprises of N number point forces of 170 kN at uniform spacing d [m]

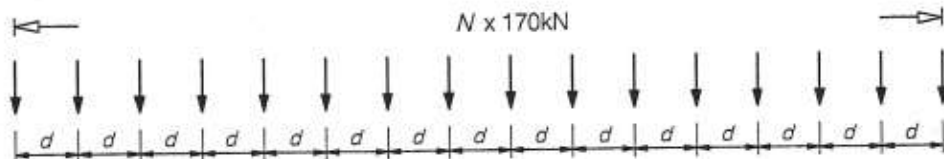


Figure 4.14.

The motion equation can be used to determine the passenger comfort without including the vehicle mass interaction (conservative approach) while the axle forces and variations in spacing of individual axles shall be included.

$$m\ddot{u} + c\dot{u} + ku = F(t) \quad (4.19)$$

The damping of the bridge is around 1% and the lower bound shall be used for the stiffness of the superstructure. In any case, only one track shall be loaded. The limiting vertical deck acceleration is 5m/s^2 for direct fixation and 3.5m/s^2 for ballasted track.

Section 5

Balanced Cantilever Bridge Design

Post-tensioning Operation (FHWA 2004)

The post-tensioning operation will be based on the following schedule

- Tendons are installed after the concrete hardens to a prescribed initial compressive strength
- A hydraulic jack is attached to one or both ends of the tendon and pressurized to a target value with bearing against the end of concrete element. Tendon usually elastically elongates
- At the end of jacking, the force in tendon is transferred from the jack to end anchorage
- Protruding strands are cut by an abrasive disc saw instead of flame cut.
- Tendons are grouted using a cementitious based grout.

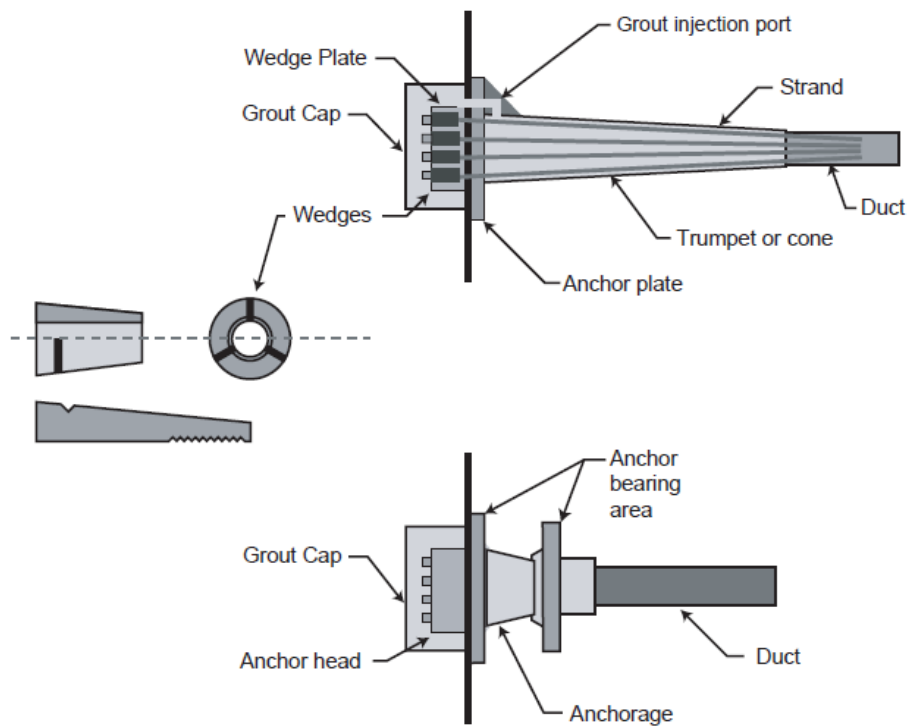


Figure 5.1.

Post-tensioning losses (Lucko and Garza 2003)

Post-tensioning loss can be grouped as follows:

- Anchor set: Initial loss of prestressing force occurs due to incremental slippage of the tendon strands at the anchorages prior to the wedges or nuts that provide a firm seat for the strands grip. (typically equal to 9 mm)
- applying a prestressing force on a newly cast segment and its predecessors will partially relieve tendons that have been stressed earlier because of the elastic shortening of the previously cast segments.
- Friction between the tendons and the ducts in which they are encased reduces the overall pre-stressing force, as tendons in curved ducts will contact the interior surface of the ducts ~“wobble effect” .
- Long-term losses: creep, shrinkage, relaxation

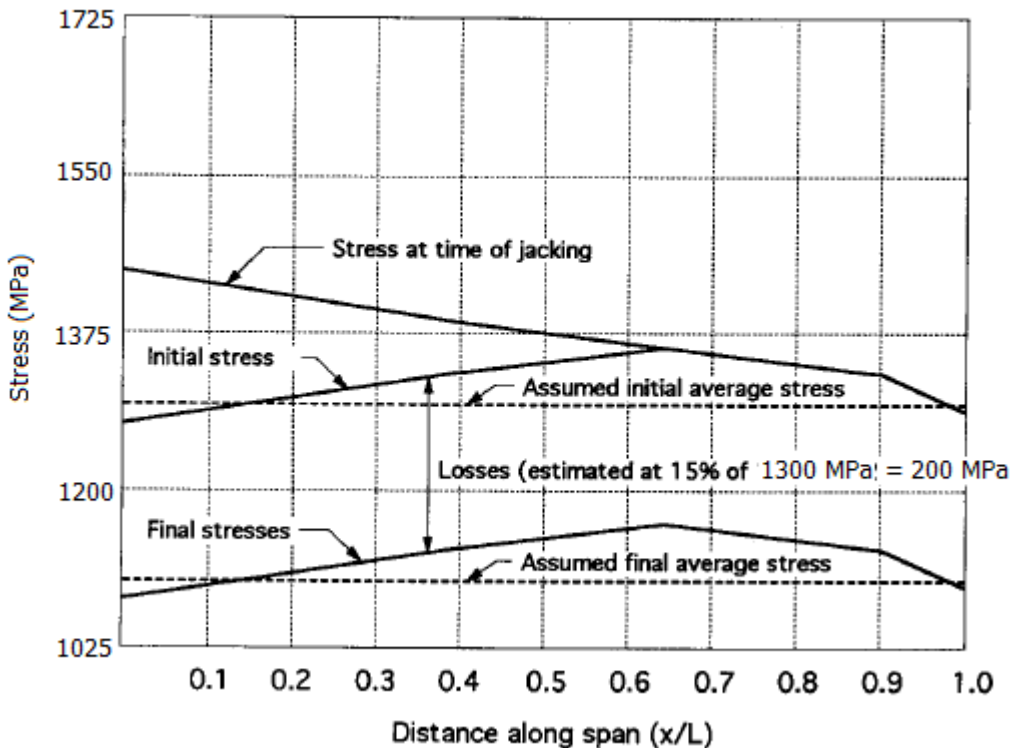


Figure 5.2.

Friction result in loss between the internal prestressing tendons and the duct and can be computed from

$$\Delta f_{PF} = \Delta f_{pj} (1 - e^{-(Kx + \mu\alpha)}) \quad (5.1)$$

Where Δf_{pj} is the stress due to jacking, K is 6.6×10^{-7} (1/mm), x is the length of tendon starting from the jacking point to the end of point under consideration, μ is coefficient of friction (0.25) and α is the sum of angular change.

Construction Cycle (Lucko and Garza, 2003)

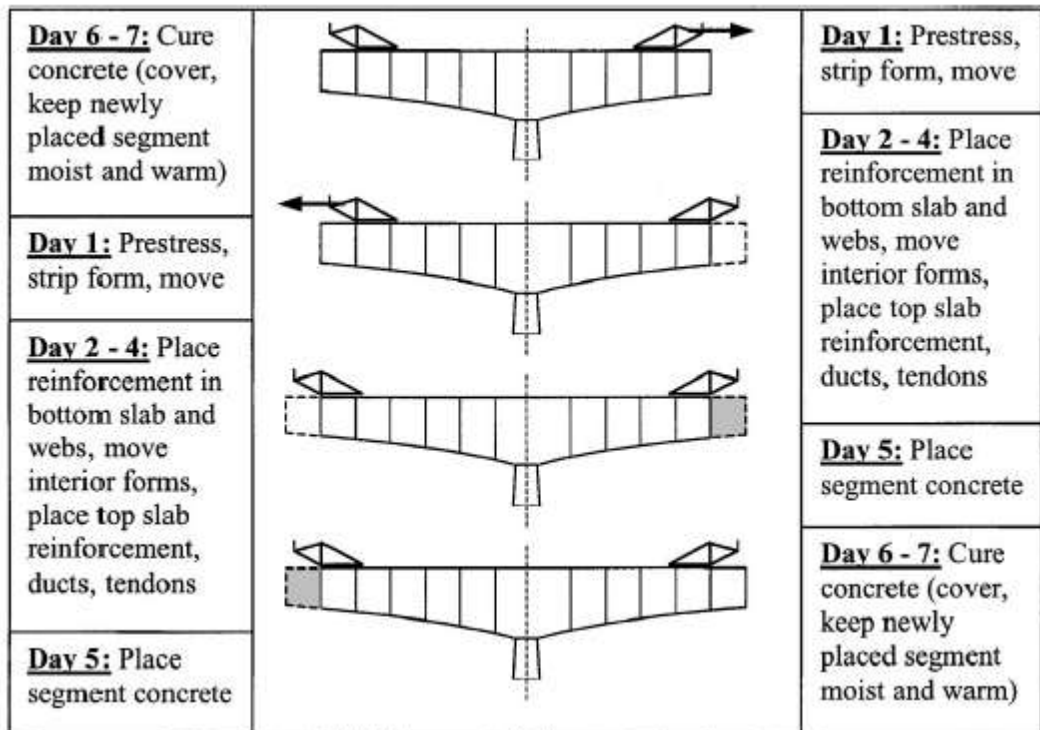


Figure 5.3.

Overall Section Dimensions (AASHTO LRFD 2010)

Efficiency Index

Efficiency index is defined in terms of geometric properties of the section and represents bending resistance in terms of amount of concrete used. Typically, the efficiency index is 0.6.

$$\rho = \frac{I}{A z_{top} z_{bot}} \quad (5.2)$$

Minimum Flange Thickness : 1/30 the clear span between webs or haunches and top flange thickness shall not be less than 225 mm if transverse post-tensioning is used. Transverse post-tensioning is required if the clear distance between the webs or haunches is more than 4600 mm. Application of transverse post-tensioning can minimize cracking in the top flange and can result in a thinner slab that helps to reduce the weight. In the long-run, by minimizing the cracking on the top flange, the durability of the longitudinal post-tensioning can be improved significantly.

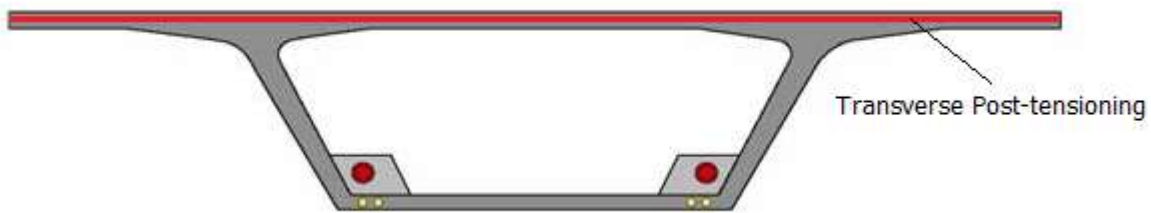


Figure 5.4.

Minimum Web Thickness: Webs with no longitudinal and vertical post-tensioning can be set to a minimum of 200mm. In case of webs with either longitudinal or vertical post-tensioning, the minimum thickness shall be around 300 mm. If tendons exist in both directions, minimum web thickness will be set to 400 mm. Application of post-tensioning in vertical direction improves the shear resistance and can result in a more economical web thickness.



Figure 5.5.

Length of Top Flange Cantilever : The cantilever measured from the tip to the centerline of web shall not exceed 45% of the span measured between centerlines of the two webs.

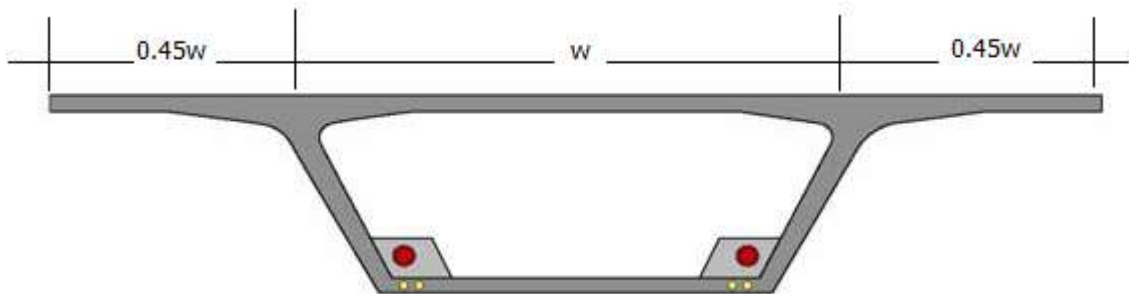


Figure 5.6.

Depth of Section:

Constant depth girder, $1/5 > do/L > 1/30$ (optimum 1/18 to 1/20)

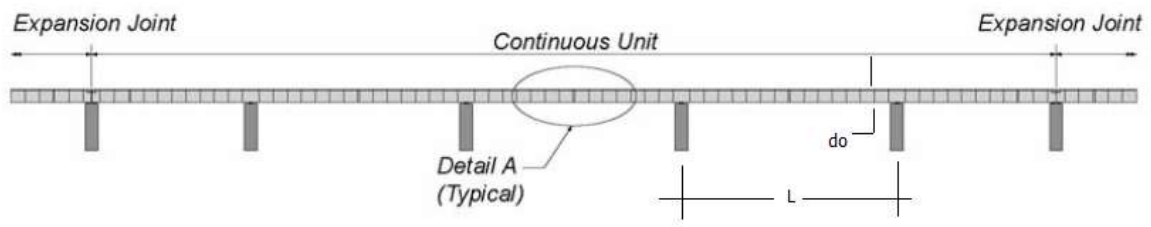


Figure 5.7.

Incrementally launched girders,

$$L = 30 \text{ m} \quad 1/15 < do/L < 1/12$$

$$L = 60 \text{ m} \quad 1/13.5 < do/L < 1/11.5$$

$$L = 90 \text{ m} \quad 1/12 < do/L < 1/11$$

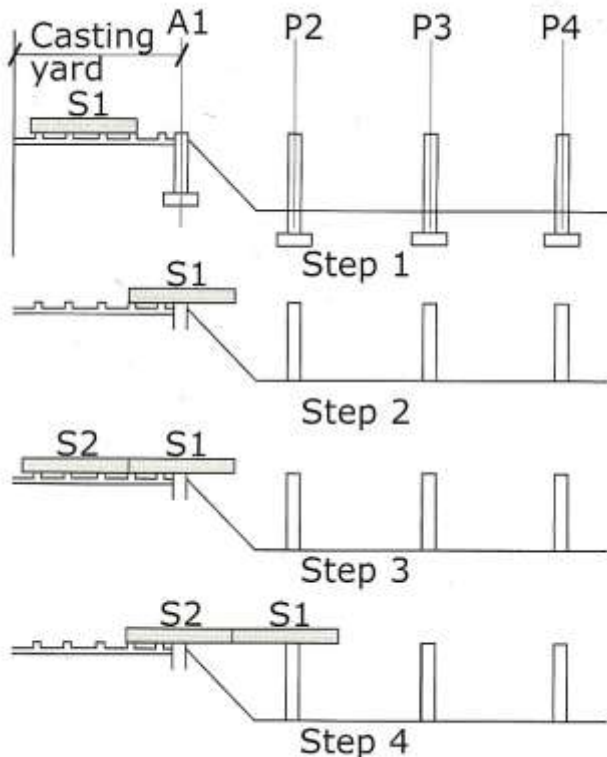


Figure 5.8.

For variable depth girder with straight haunches:

$$\text{Over Pier} : 1/16 > do/L > 1/20$$

$$\text{At Mid-Span: } 1/22 > do/L > 1/28$$

For variable depth girder with parabolic or circular haunches:

$$\text{Over Pier} : 1/16 > do/L > 1/20$$

At Mid-Span: $1/30 > do/L > 1/50$

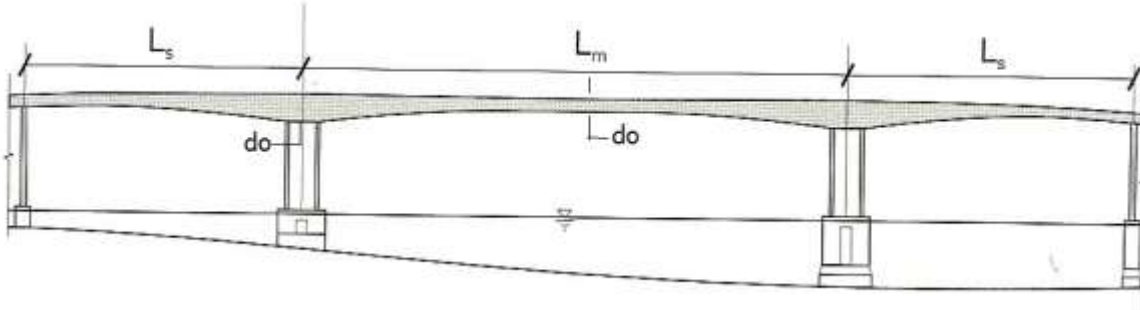


Figure 5.9.

If $do/b > 1/6$ use single cell box. Otherwise use double cell box.

Live load Deflection Limit: When the bridge is fully loaded with live loads, the deflection ratio to span length shall be less than 1/1000.

Construction Loads

AASHTO-LRFD has listed many load combinations for the construction. The primary load combination (allowable tensile limit $0.50\sqrt{f_c'}$):

$$DC + DIFF + CLL + CR + SH + (CE+IE) \quad (5.3)$$

DC : selfweight of segments

DIFF : 2% increase in DC applied only to one cantilever

CLE : construction live load on deck surface : 0.5 kN/m^2 on one cantilever and 0.25 kN/m^2 on the other one

CR & SH: Use default for CEB-FIP 90 models

CE : construction equipment (80 tons- traveler forms)

IE : impact force on construction equipment is 10% weight of the traveler form.

The bridge need to be checked at the open position for a low level earthquake and wind force as well.

Required Post-tensioning

The required number of tendons can be determined as described in the prestressed I-girder sections of this document. The negative moment over the pier can be used to determine the number of strands. Nineteen (19) strands can be collected in a duct for this purpose. The duct diameter is typically 100 mm and the center to center spacing is typically two duct diameter (2D). The moment diagram under its own dead load is shown below.

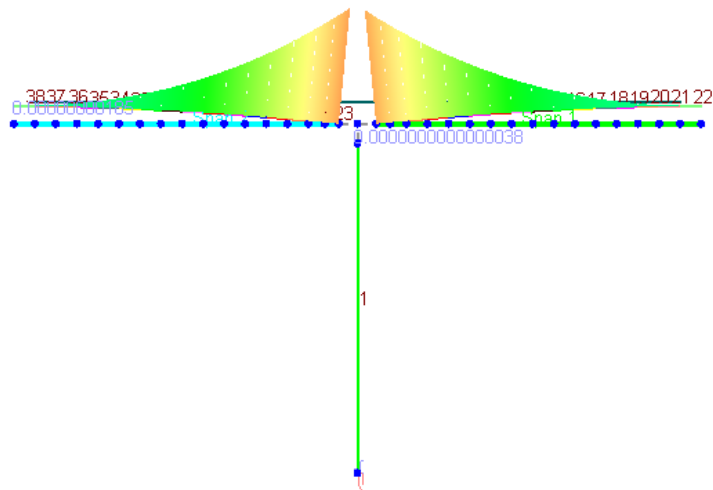


Figure 5.10.

The typical segment length is around 3 to 5 meters. Close to the pier short lengths can be selected. The typical tendon layout is given below. The longitudinal post-tensioning is applied from intersection of web and flange in order not to damage the concrete since this region is reinforced in two directions.

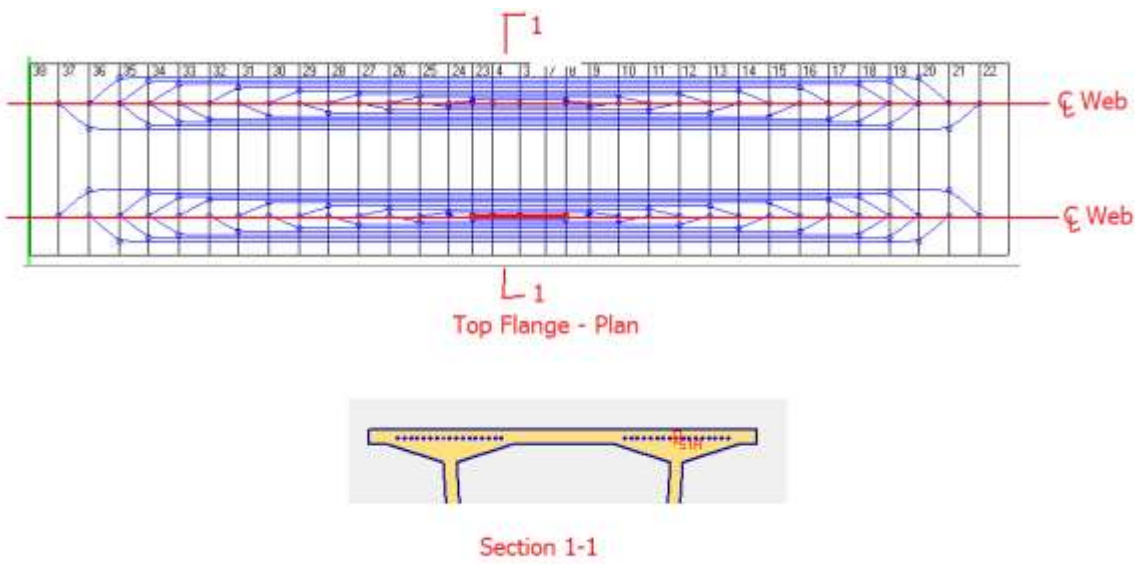


Figure 5.11.

Closed Position

The cantilever construction will be closed at the abutment and main span. The abutment segments can consist of couple of segments to act as a counter weight and can be closed before the main span. In this approach, potential sagging of the main span can be minimized. The main span closure is typically around 2 meters length.

After the closure, the bridge can continue to sag at the mid-span due to time-dependent deformations. In the preliminary design stage the required amount of post-tensioning at the bottom slab can be determined based on the modified positive moment using the following equation (PTI 2006).

$$M_{D,final} = M_{D,cant} + 0.8(M_{D,CONT} - M_{D,cant}) \quad (5.4)$$

The LRFD equations defined for the prestressed I-girder sections can be used to evaluate the nominal moment and shear to check the adequacy of the design under load factored combinations defined in the AASHTO LRFD.

Shear Lag

Shear lag can be defined as the nonlinear distribution of normal stress across a component due to shear distortions. In plane shear stresses are the governing factor in distribution of longitudinal stresses across the deck of composite and monolithic flexural members. The plane sections do not remain plane due to the shear deformations, Therefore, the longitudinal stresses across the deck are not uniform.

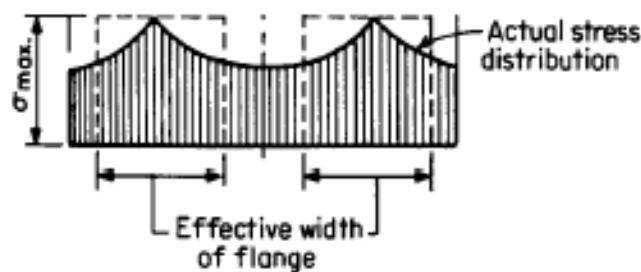
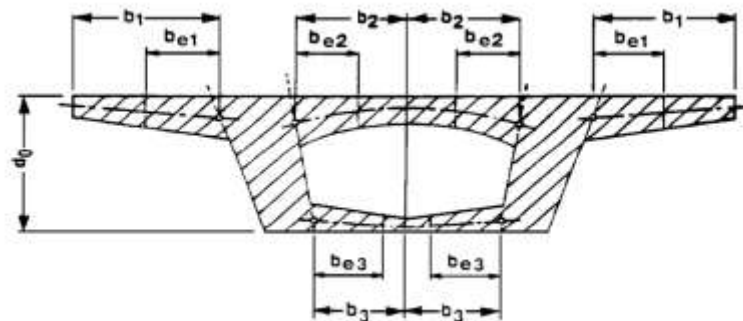


Figure 5.12.

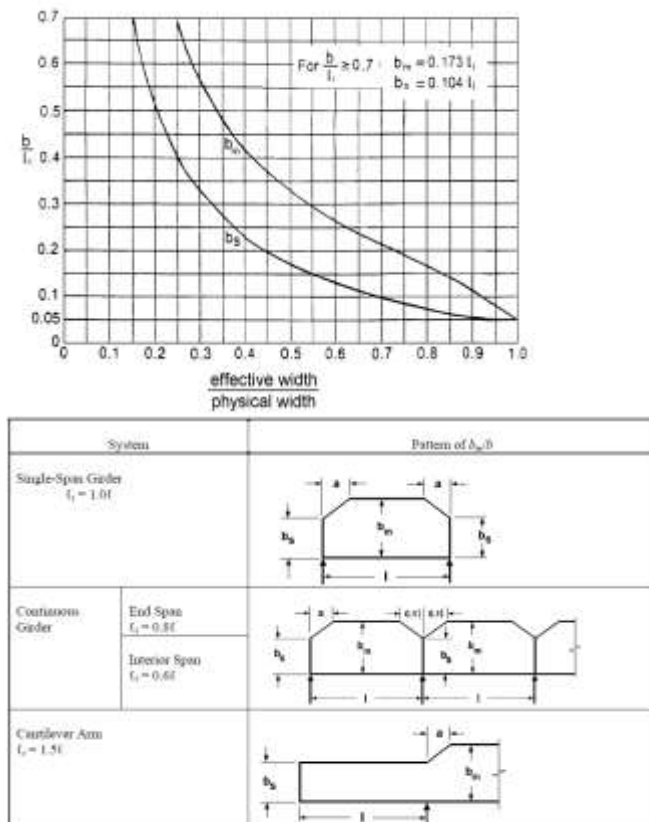


Figure 5.13.

The shear lag effect can be ignored for the following conditions.

$$b < 0.1 l_i$$

$$b < 0.3 d_o$$

where b is the physical flange width on each side of the web and b_e is the computed effective flange width. Within the effective width, linear stress distribution can be determined from the constant stress distribution.

Principal Tension Stress Check

The principal tension stress check is typically used to identify the potential web cracking, especially at the segments close to the pier where shear forces are higher. In evaluation of the webs close to the piers one single truck can be used instead of two trucks used in evaluation of the negative bending moment. The live load can have a load factor of 0.8. The principal tension stress can be limited to $0.28\sqrt{f_c'}$ per AASHTO-LRFD. In the study of Okeil (2006), suggested an alternative limiting stress based on a more refined analysis.

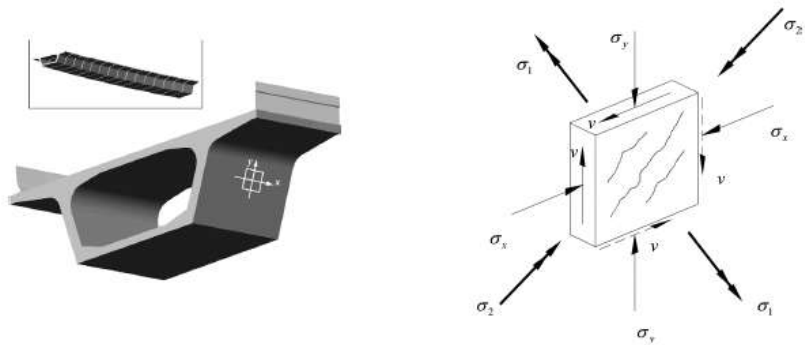


Figure 5.14.

$$v = \frac{VQ}{Ib} \quad (5.4)$$

where V= vertical shear force, Q = first moment of an area with respect to c.g of section, I = moment of inertia with respect to c.g of section, b = perpendicular web thickness.

$$f_1 = \frac{\sigma_x + \sigma_y}{2} - \frac{1}{2} \sqrt{4v^2 + (\sigma_x - \sigma_y)^2} \quad (5.5)$$

Where, compression stress is positive in the above equation. In case of there is no vertical post-tensioning ($\sigma_y = 0$) the allowable shear stress can be computed from the following equation using a different form of Mohr circle.

$$v_a = \sqrt{f_a x (f_a + f)} \quad (5.6)$$

Where, f_a = allowable principal tension stress and f compressive stress at level on web under investigation.

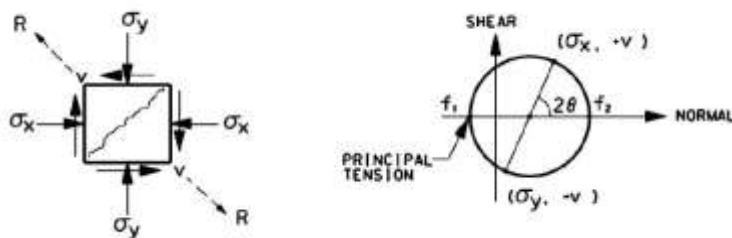


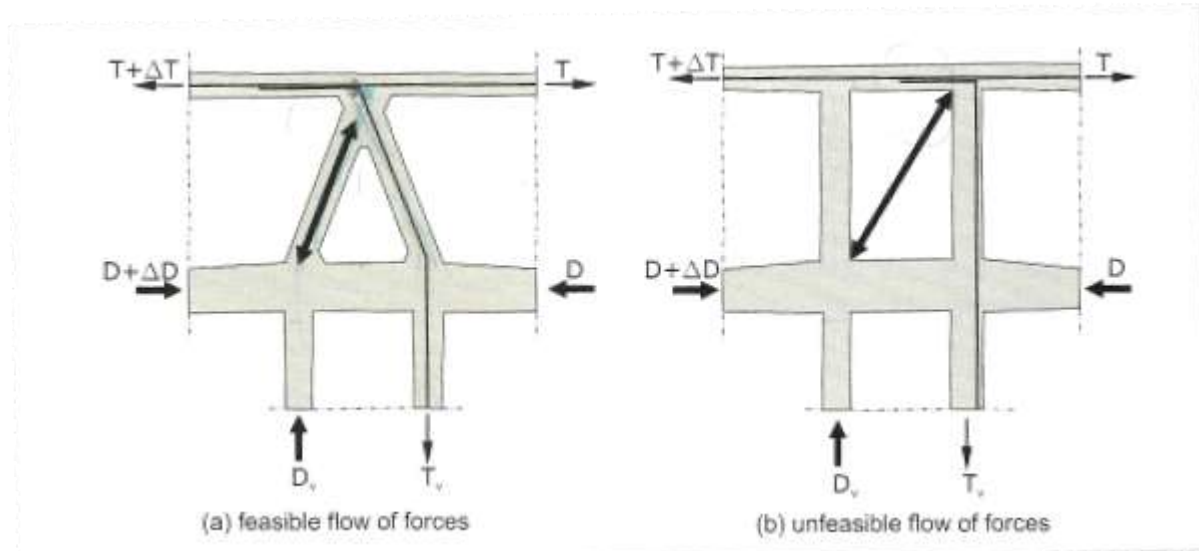
Figure 5.15.

Transverse Design

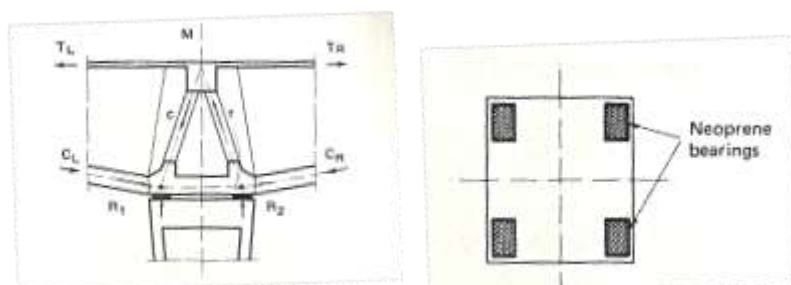
Transverse design of the bridge shall be performed to check the adequacy of the cantilever portions and flange section that remains between the webs. If excessive cracking develops in this region, provide transverse post-tensioning. The cracking shall be computed for service load combinations. The slab reinforcement design can be based on the LRFD equations.

Design Detailing of Superstructure Connections

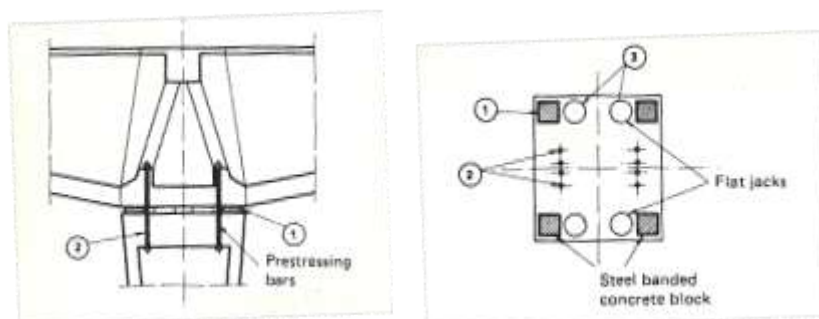
The connection of pier to the superstructure can be monolithic or bearings can be placed if needed.



Taken from PTI Design Handbook – Monolithic



Bearing System – In service



Bearing System – In temporary construction phase

Computer Modeling

The computer modeling can be developed using stick and tendon elements. The analysis shall include the construction staging with time-dependent effects. An example model is given in Appendix A.

Section 6

Preliminary Sizing of Steel Girder Slab Bridges

Depth

The optional minimum depth requirement of the AASHTO-LRFD (2010) is

=0.027L for the steel

=0.032L for the composite section

Cross-Section Proportion Limits

The web shall be proportioned to be $D/t_w < 150$, flanges shall satisfy $b_f/2t_f < 12$ and $bf > D/6$, and $t_f > 1.1t_w$. (b_f is the width of the flange, t_f is the thickness of the flange, t_w is the thickness of the web and D is the height of the web)

Compactness check

The cross-section can be defined as compact if the following proportions are satisfied

For the web (without longitudinal stiffeners):

$$\frac{D}{t_w} \leq 150 \quad (6.1)$$

Web slenderness limit (positive moment region):

$$\frac{2D_{cp}}{t_w} \leq 3.76 \sqrt{\frac{E}{F_{yc}}} \quad (6.2)$$

Web slenderness limit (negative moment region):

$$\frac{2D_{cp}}{t_w} \leq 5.7 \sqrt{\frac{E}{F_{yc}}} \quad (6.3)$$

where D_{cp} is the depth of the web in compression at the plastic moment region.

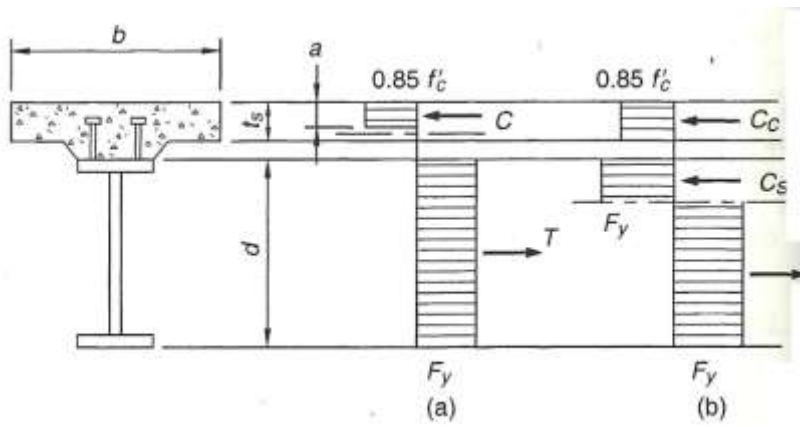
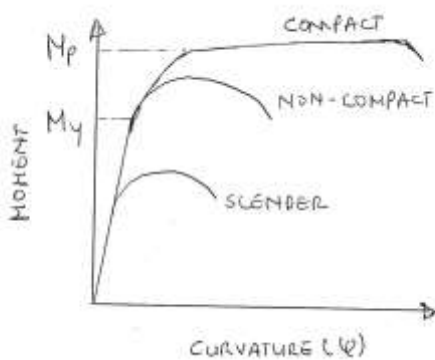


Figure 6.1.

a) Plastic state neutral axis in the slab, b) Plastic neutral axis in steel

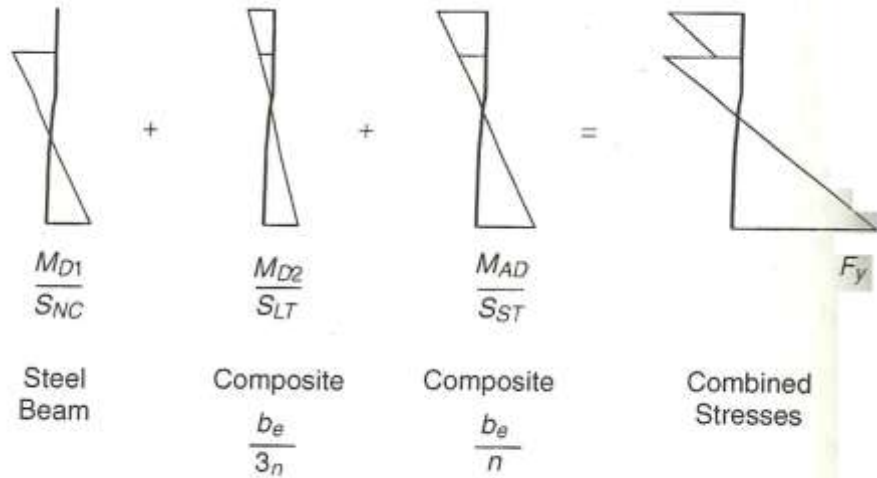


Figure 6.2.

Stresses at First Yield.

For the negative moment region, the D_{cp} can be calculated from the below equation if the neutral axis is within the steel web. Otherwise D_{cp} can be taken equal to D.

$$D_{cp} = \frac{D}{2A_w F_{yw}} [F_{yt} A_t + F_{yw} A_w + F_{yrs} A_{rs} - F_{yc} A_c] \quad (6.4)$$

For the positive moment region, the D_{cp} can be calculated from the below equation if the neutral axis is within the steel web. Otherwise D_{cp} can be taken equal to 0 (zero).

$$D_{cp} = \frac{D}{2} \left(\frac{F_{yt} A_t - F_{yc} A_c - 0.85 f'_c A_s - F_{yrs} A_{rs}}{F_{yw} A_w} + 1 \right) \quad (6.5)$$

where

F_{yt} = min. yield strength of tension flange

F_{ysr} = min. yield strength of longitudinal reinforcement

F_{yw} = min. yield strength of web

F_{yc} = min. yield strength of compression flange

A_s = area of concrete deck

Compression Flange Local Buckling

The limiting slenderness ratio for a compact flange, $\lambda_{pf} = 0.38 \sqrt{\frac{E}{F_{yc}}}$

The limiting slenderness ratio for a noncompact flange, $\lambda_{rf} = 0.56 \sqrt{\frac{E}{F_{yr}}}$

Where F_{yr} is the smallest of F_{yw} or $0.7 F_{yc}$.

The existing slenderness ratio can be computed from ($\lambda_f = \frac{b_{fc}}{2t_{fc}}$)

Cross-Braces

The cross-braces can be located based on the investigation of the lateral torsional buckling of compression flanges. In a composite section, the deck will provide a continuous bracing for the compression flange in the positive moment region (only true for live load case if not braced).

The limiting unbraced length, L_p , to achieve nominal flexural resistance is

$$= 1.0 r_t \sqrt{\frac{E}{F_{yc}}} \quad (6.6)$$

The limiting unbraced length, L_r , to achieve the onset of nominal yielding in either flange under uniform bending with inclusion of residual stresses at compression flange

$$= \pi r_t \sqrt{\frac{E}{F_{yr}}} \quad (6.6)$$

where r_t is the effective radius of gyration for lateral torsional buckling

$$r_t = \frac{b_{fc}}{\sqrt{12\left(1 + \frac{1}{3} \frac{D_{ctw}}{b_{fc} t_{fc}}\right)}} \quad (6.7)$$

Strength Limit States

The flexural and shear resistance is usually checked at the strength limit state. The flexural resistance and shear resistances are defined by the following equations respectively

$$M_r = \phi_f M_n \quad (6.8)$$

$$V_r = \phi_v V_n \quad (6.9)$$

Flexural Resistance Composite Section – Positive Moment Compact Sections

The following equation need to be checked at the strength limit state for compact sections.

$$M_u + \frac{1}{3} f_l S_{xt} \leq \phi_f M_n \quad (6.10)$$

where $\phi_f = 1.0$, f_l flange lateral bending stress, M_u bending moment about the major axis, M_n nominal moment resistance, S_{xt} is the elastic section modulus with respect to tension flange

In continuously braced flanges (such as the ones with composite deck) the lateral flange bending can be taken equal to zero (0).

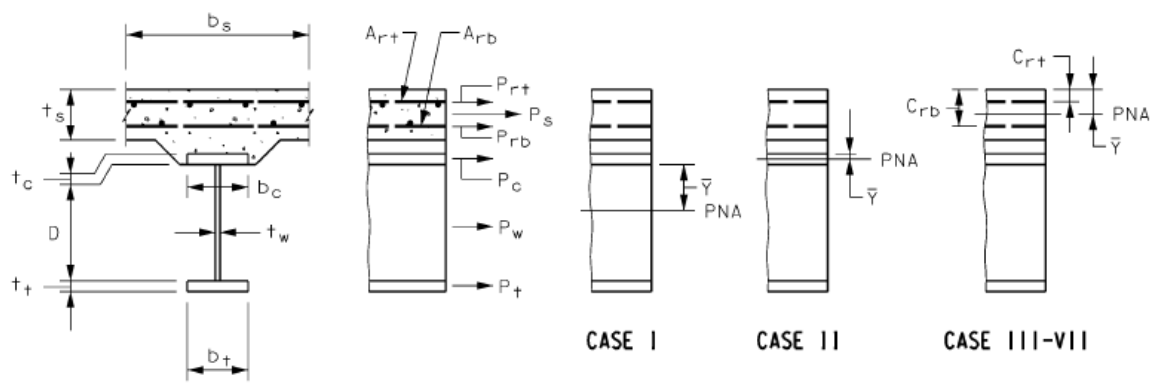
If the distance measured from top of deck to plastic neutral axis, D_p , is less than 10% of the depth, D_t , of the composite section the nominal moment capacity can be computed from the following equation.

$$M_n = M_p \quad (6.11)$$

Otherwise

$$M_n = M_p \left(1.07 - 0.7 \frac{D_p}{D_t}\right) \quad (6.12)$$

The plastic moment shall be computed as the moment about the plastic neutral axis. The plastic neutral axis shall be determined based on the axial force equilibrium to develop no net axial force at the section.



$$P_n = F_{yt} A_n$$

$$P_s = 0.85 f'_c b_s t_s$$

$$P_{rb} = F_{ytb} A_{rb}$$

$$P_c = F_{yc} b_c t_c$$

$$P_w = F_{yw} D t_w$$

$$P_t = F_{yt} b_t t_t$$

Figure 6.3.

Table 6.1.

Case	PNA	Condition	\bar{Y} and M_p
I	In Web	$P_t + P_w \geq P_c + P_s + P_{rb} + P_\pi$	$\bar{Y} = \left(\frac{D}{2} \right) \left[\frac{P_t - P_c - P_s - P_\pi - P_{rb}}{P_w} + 1 \right]$ $M_p = \frac{P_w}{2D} \left[\bar{Y}^2 + (D - \bar{Y})^2 \right] + [P_s d_s + P_\pi d_\pi + P_{rb} d_{rb} + P_c d_c + P_t d_t]$
II	In Top Flange	$P_t + P_w + P_c \geq P_s + P_{rb} + P_\pi$	$\bar{Y} = \left(\frac{t_c}{2} \right) \left[\frac{P_w + P_t - P_s - P_\pi - P_{rb}}{P_c} + 1 \right]$ $M_p = \frac{P_c}{2t_c} \left[\bar{Y}^2 + (t_c - \bar{Y})^2 \right] + [P_s d_s + P_\pi d_\pi + P_{rb} d_{rb} + P_w d_w + P_t d_t]$
III	Concrete Deck, Below P_{rb}	$P_t + P_w + P_c \geq \left(\frac{c_{rb}}{t_s} \right) P_s + P_{rb} + P_\pi$	$\bar{Y} = (t_s) \left[\frac{P_c + P_w + P_t - P_\pi - P_{rb}}{P_s} \right]$ $M_p = \left(\frac{\bar{Y}^2 P_s}{2t_s} \right) + [P_\pi d_\pi + P_{rb} d_{rb} + P_c d_c + P_w d_w + P_t d_t]$
IV	Concrete Deck, at P_{rb}	$P_t + P_w + P_c + P_{rb} \geq \left(\frac{c_{rb}}{t_s} \right) P_s + P_\pi$	$\bar{Y} = c_{rb}$ $M_p = \left(\frac{\bar{Y}^2 P_s}{2t_s} \right) + [P_\pi d_\pi + P_c d_c + P_w d_w + P_t d_t]$
V	Concrete Deck, Above P_{rb} Below P_π	$P_t + P_w + P_c + P_{rb} \geq \left(\frac{c_\pi}{t_s} \right) P_s + P_\pi$	$\bar{Y} = (t_s) \left[\frac{P_{rb} + P_c + P_w + P_t - P_\pi}{P_s} \right]$ $M_p = \left(\frac{\bar{Y}^2 P_s}{2t_s} \right) + [P_\pi d_\pi + P_{rb} d_{rb} + P_c d_c + P_w d_w + P_t d_t]$
VI	Concrete Deck, at P_π	$P_t + P_w + P_c + P_{rb} + P_\pi \geq \left(\frac{c_\pi}{t_s} \right) P_s$	$\bar{Y} = c_\pi$ $M_p = \left(\frac{\bar{Y}^2 P_s}{2t_s} \right) + [P_{rb} d_{rb} + P_c d_c + P_w d_w + P_t d_t]$
VII	Concrete Deck, Above P_π	$P_t + P_w + P_c + P_{rb} + P_\pi < \left(\frac{c_\pi}{t_s} \right) P_s$	$\bar{Y} = (t_s) \left[\frac{P_{rb} + P_c + P_w + P_t + P_\pi}{P_s} \right]$ $M_p = \left(\frac{\bar{Y}^2 P_s}{2t_s} \right) + [P_\pi d_\pi + P_{rb} d_{rb} + P_c d_c + P_w d_w + P_t d_t]$

Flexural Resistance Composite Section – Positive Moment Non-Compact Sections

In non-compact section design, the flexural resistance is based on the lateral torsional buckling limit and/or local buckling resistance. The stresses at the top and bottom of the girder shall satisfy the following stress limits. For compression flange, the following equation needs to be satisfied.

$$f_{bu} \leq \phi_f F_{nc} \quad (6.13)$$

where f_{bu} is the maximum compressive stress along the unbraced length of the flange without including the flange lateral bending. The moment at first yield usually defines the nominal flexural resistance of non-compact composite section subjected to positive moment. The compression flange resistance is also function of the brace spacing.

For $L_b < L_p$ and $\lambda_f \leq \lambda_{pf}$:

$$F_{nc} = R_b R_h F_{yc} \quad (6.14)$$

where, R_h is the hybrid factor (=1.0 if flanges and webs are of the same grade), R_b , web load shedding factor. If the web of the section is slender, stress in compression flange increase due to shedding of compressive stresses in web that results in reduction of flexural resistance. R_b is usually taken equal to 1.0 in positive moment composite section computations if cross-section proportion limits are satisfied for webs (defined in earlier section). Otherwise, the R_b can be computed from the following equation.

$$R_b = 1 - \left(\frac{a_{wc}}{1200 + 300a_{wc}} \right) \left(\frac{2D_c}{t_w} - \lambda_{rw} \right) \quad (6.15)$$

where $\lambda_{rw} = 5.7\sqrt{E/F_{yc}}$ is the limiting slenderness ratio for a noncompact web and a_{wc} is a constant that can be computed from

$$a_{wc} = \frac{2D_c t_w}{b_{fc} t_{fc}} \quad (6.16)$$

Flexural Resistance Composite Section – Negative Moment Region

Negative moment regions can develop at the continuous spans. Typically, the composite section is composed of the steel girder and the longitudinal steel reinforcement. The concrete deck is ignored in the computations. The top and bottom stresses at the girder and the stresses at the deck level reinforcement are usually evaluated.

The compression flange shall satisfy the following equation at the strength limit state.

$$f_{bu} + \frac{1}{3}f_l \leq \phi_f F_{nc} \quad (6.17)$$

All other cases

$$f_{bu} \leq \phi_f F_y \quad (6.18)$$

The negative plastic moment capacities of the section can be determined using the following table and figure.

Case	PNA	Condition	\bar{Y} and M_p
I	In Web	$P_c + P_w \geq P_t + P_{rb} + P_\pi$	$\bar{Y} = \left(\frac{D}{2} \right) \left[\frac{P_c - P_t - P_\pi - P_{rb}}{P_w} + 1 \right]$ $M_p = \frac{P_w}{2D} \left[\bar{Y}^2 + (D - \bar{Y})^2 \right] + [P_\pi d_{rt} + P_{rb} d_{rb} + P_t d_t + P_c d_c]$
II	In Top Flange	$P_c + P_w + P_t \geq P_{rb} + P_\pi$	$\bar{Y} = \left(\frac{t_i}{2} \right) \left[\frac{P_w + P_c - P_\pi - P_{rb}}{P_t} + 1 \right]$ $M_p = \frac{P_t}{2t_i} \left[\bar{Y}^2 + (t_i - \bar{Y})^2 \right] + [P_\pi d_{rt} + P_{rb} d_{rb} + P_w d_w + P_c d_c]$

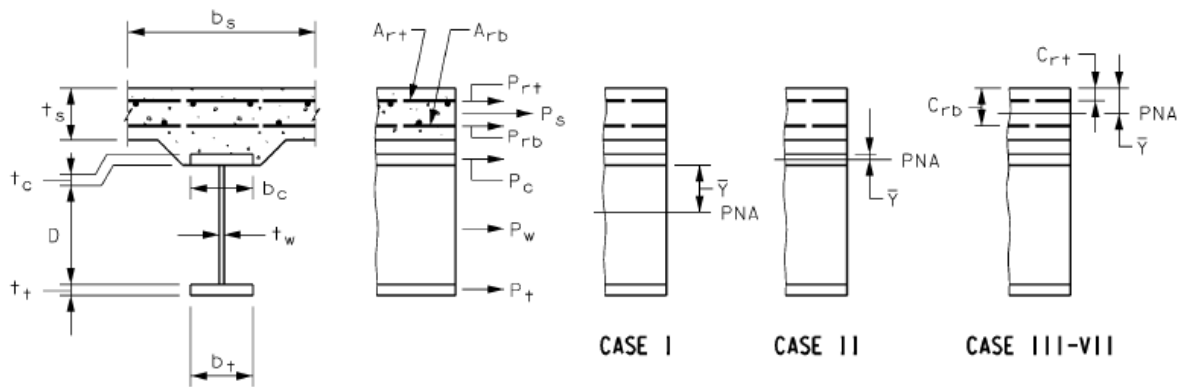


Figure 6.4.

Shear Resistance

For unstiffened webs and end panels the resistance can be computed from the following equation.

$$V_n = CV_p \quad (6.19)$$

where C is the ratio of shear buckling resistance to shear yield strength and

$$V_p = 0.58F_{yw}Dt_w \quad (6.20)$$

In the below computations, k (shear buckling coefficient) can be taken as 5.0 (conservative approach)

$$\text{If } D/t_w \leq 1.12\sqrt{Ek/F_{yw}} \text{ then } C=1.0 \quad (6.21)$$

$$\text{If } 1.12\sqrt{Ek/F_{yw}} < D/t_w \leq 1.40\sqrt{Ek/F_{yw}} \text{ then } C = \frac{1.12}{\frac{D}{t_w}} \sqrt{\frac{Ek}{F_{yw}}} \quad (6.22)$$

$$\text{If } \frac{D}{t_w} > 1.40\sqrt{Ek/F_{yw}} \text{ then } C = \frac{1.57}{\left(\frac{D}{t_w}\right)^2} \frac{Ek}{F_{yw}} \quad (6.23)$$

For stiffened internal panel webs if the below equation is satisfied the shear resistance can be computed using the same set of equations with a different k value.

$$\frac{2Dt_w}{(b_{fc}t_{fc} + b_{ft}t_{ft})} \leq 2.5 \quad (6.24)$$

In computation of C, the k value shall be taken as

$$k = 5 + \frac{5}{\left(\frac{d_o}{D}\right)^2} \quad (6.25)$$

Where d_o is the spacing of the stiffeners. If the geometric check is not satisfied for the internal panels, the nominal resistance can be computed from the below equation.

$$V_n = V_p \left[C + \frac{0.87(1-C)}{\left(\sqrt{1+\left(\frac{d_o}{D}\right)^2} + \frac{d_o}{D}\right)} \right] \quad (6.26)$$

Shear Connectors

The shear connectors are the part that provides the composite action between the reinforced concrete deck and the steel. The ratio of the height to diameter of the stud shall not be less than 4.0. In transverse spacing the studs shall not be placed more than 4 diameter center to center spacing.

The pitch of the shear connectors shall be determined based on the fatigue limit states defined in the AASHTO-LRFD.

Spliced Bolted Connections

Webs and flanges of the section can be spliced by use of bolts.

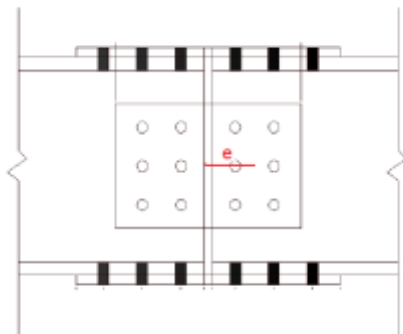


Figure 6.5.

Web splice connection including the plates and bolts shall be designed for shear, moment due to eccentricity of the shear at point of the splice and portion of the flexural moment that will be resisted by the web.

The connection design shear force, V_{uw} , shall be selected for the matching condition:

If $V_u < 0.5\phi_v V_n$ then $V_{uw} = 1.5V_u$

Otherwise, $V_{uw} = 0.5 (V_u + \phi_v V_n)$

The moment due to eccentricity of the connection center to the center of splice can be determined from

$$M_{ue} = V_{uw} e \quad (6.27)$$

Portion of the flexural moment carried by the web and corresponding horizontal load can be computed from the below equations.

$$M_{uw} = \frac{t_w D^2}{12} |R_h F_{cf} - R_{cf} f_{ncf}| \quad (6.28)$$

where F_{cf} is the design stress for the controlling flange (+ tension, - compression), R_{cf} is the ratio of the absolute value of F_{cf} to the maximum stress at the controlling flange, f_{cf} , computed due to the factored loads at the splice, f_{ncf} is the maximum flange stress at the non-controlling flange.

$$F_{cf} = \frac{\left(\left|\frac{f_{cf}}{R_h}\right| + \alpha \phi_f F_{yf}\right)}{2} \geq 0.75 \alpha \phi_f F_{yf} \quad (6.29)$$

where α is 1.0 except $F_n/F_{yf} < 1.0$, F_n is the nominal flexural resistance of flange. The total moment will be equal to

$$M_u = M_{uw} + M_{ue} \quad (6.30)$$

The horizontal load will be equal to

$$H_{uw} = \frac{t_w D}{2} (R_h F_{cf} + R_{cf} f_{ncf}) \quad (6.31)$$

The shear force at the i^{th} bolt is:

$$V_{vertbolt_i} = \frac{V_{uw}}{N} + \frac{Mx_i}{I_p} \quad (6.32)$$

$$V_{longbolt_i} = \frac{H_{uw}}{N} + \frac{My_i}{I_p} \quad (6.33)$$

The total shear force and resistance can be computed from

$$V_{cu} = \sqrt{V_{vertbolt_i}^2 + V_{longbolt_i}^2} < R_n = 0.58A_gF_y \quad (6.34)$$

The design of web thickness and, design of top and bottom flange connection details can be found at the AASHTO-LRFD.

Preliminary Design of Cables of Cable Stayed Bridges

The cable stayed bridges and suspension bridges are used to span longer lengths. Cable stayed bridges are more advantageous to suspension bridges in terms of cable weight. Furthermore cable stayed bridges are more rigid compared to the suspension one.

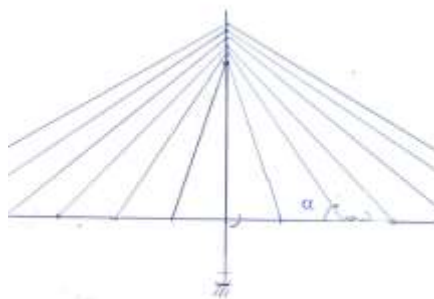


Figure 6.6.

The preliminary design of cables can be executed by ignoring the cable weight at the first stage. The design loads can be determined from the unfactored load combination of

Preliminary Design Load Combination: 1.0 DL+1.0 LL

The allowable stresses in the cables shall be less than 0.45 fs, where fs is the ultimate tensile strength of cables. In case of parallel strands are used the fs will be 1860 MPa. The required number of strands can be computed from the below equation

$$A_{cable} = \frac{w.s}{0.45f_s \sin\alpha} \quad (6.35)$$

where w is the uniform unfactored load determined from the above load combination, The adjacent cables can have similar vertical rigidities by adjusting the area of the cable. Typically the main span is longer than the back spans of the structure and the unbalanced force at the tower can be balanced by the anchor pier stays.

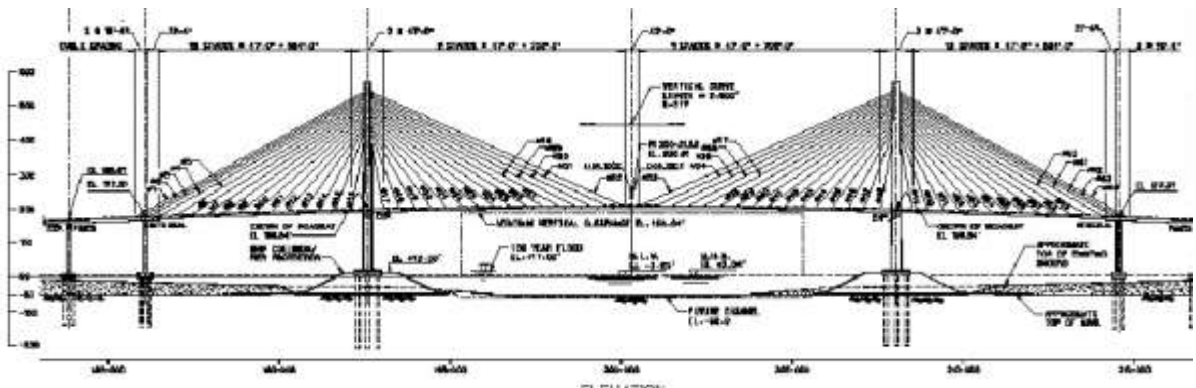


Figure 6.7.

Section 7

Pier Design Load Combinations

Pier design is generally performed under gravity loads and checked for seismic events. The typical load combinations are given in AASHTO-LRFD 2010 (Table 3.4.1-1).

The main gravity load combination is:

$$\gamma_{p1}(DC) + \gamma_{p2} (DW) + 1.75(LL+IM) \quad (7.1)$$

where $\gamma_{p1} = 1.25$ and $\gamma_{p2} = 1.50$ for maximum effects, and $\gamma_{p1} = 0.90$ and $\gamma_{p2} = 0.65$ for minimum effects

Seismic events are defined as extreme events in the specification and can be computed using the following load combination.

$$\gamma_{p1}(DC) + \gamma_{p2} (DW) + \gamma(LL) + 1.00(EQ) \quad (7.2)$$

where γ for live load shall be project specific. The recent research indicates that the live load effect can reduce the seismic forces of the substructure due to mass damping of trucks. Therefore γ defined for live load can be taken as 0.0.

Pier Design Resistance

Slenderness effects can be ignored for columns with slenderness ratio $kL/r < 22$. If the slenderness ratio is higher than 22 and less than 100 an approximate method can be used in design. k = effective length factor, L = unbraced length and r = radius of gyration.

Factored axial resistance can be determined from the following equation

$$P_r = \phi P_n \quad (7.3)$$

For members with spiral reinforcement the following equation can be utilized to determine the nominal axial load capacity.

$$P_n = 0.85(0.85f'_c(A_g - A_{st} - A_{ps}) + f_yA_{st} - A_{ps}(f_{pe} - E_p\varepsilon_{cu})) \quad (7.4)$$

For members with tie reinforcement the following equation can be utilized to determine the nominal axial load capacity.

$$P_n = 0.80(0.85f'_c(A_g - A_{st} - A_{ps}) + f_yA_{st} - A_{ps}(f_{pe} - E_p\varepsilon_{cu})) \quad (7.5)$$

P_r = factored axial resistance

P_n = nominal axial resistance

f'_c = specified strength of concrete at 28 days

A_g = gross area of section

A_{st} = total area of longitudinal steel

f_y = specified yield strength of reinforcement

ϕ = resistance factor (5.5.4.2) = 0.75 for gravity loads, 0.90 for extreme event

A_{ps} = area of prestressing steel

E_p = modulus elasticity of prestressing steel

f_{pe} = effective stress in prestressing steel after losses

ε_{cu} = failure strain of concrete

P-Δ Requirements

The response spectrum curve has been modified from being proportional to $1/T^{2/3}$ to $1/T$. The $1/T^{2/3}$ version (AASHTO 2007) was giving conservative estimates of force and displacement in bridges with longer periods (>1.0 secs) which, in an indirect way, provided for such effects as $P\Delta$. With the shift of the spectrum to being proportional to $1/T$, a check for $P\Delta$ is needed.

$$\Delta P_u < 0.25\phi M_n \quad (7.6)$$

where $\Delta = R_d \Delta_e$ and Δ_e is the pier displacement between point of contraflexure and foundation level.

if $T < 1.25T_s$ (T_s is the corner period)

$$R_d = (1-1/R)1.25T_s/T + 1/R$$

If not $R_d=1$

R = R-factor.

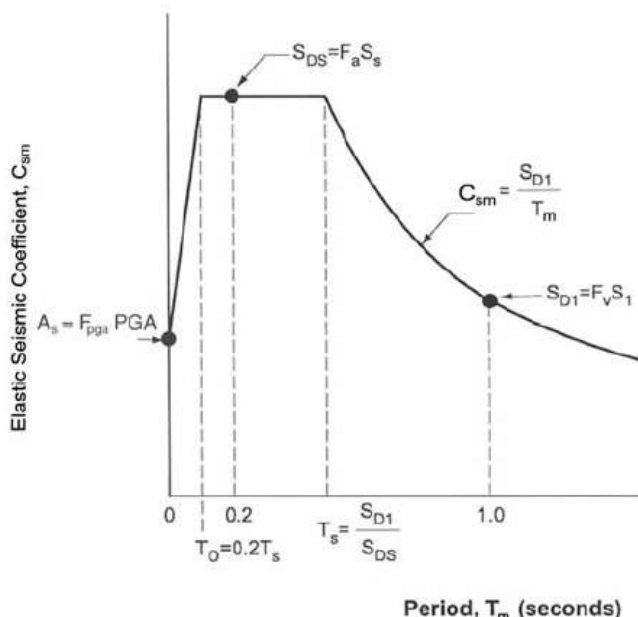


Figure 7.1.

(taken from AASHTO-LRFD 2010)

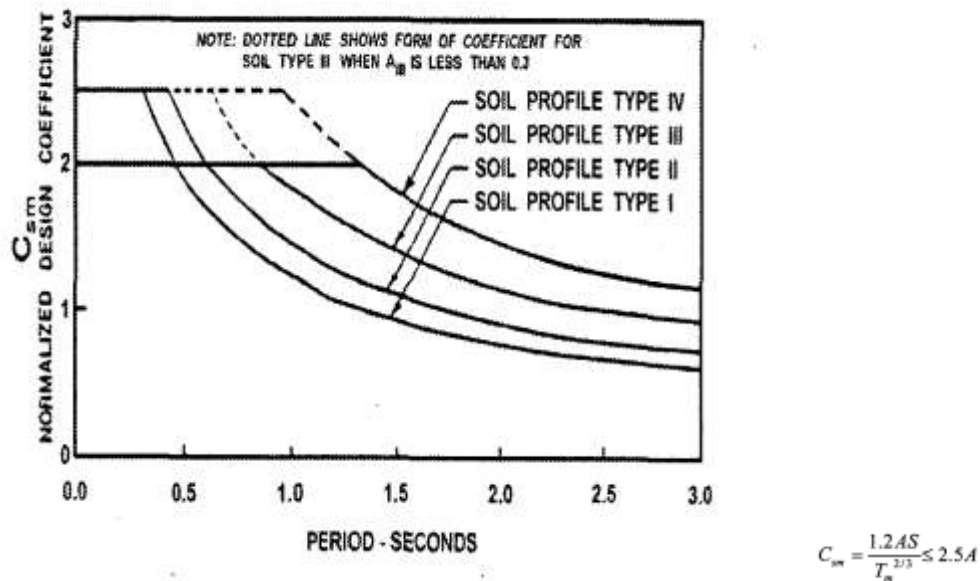


Figure 7.2.

(AASHTO 2007)

Biaxial Flexure – Non Circular Members

If the factored axial load > 0.10 $\phi f'_c A_g$ than the following equation can be used.

$$1/P_{xy} = 1/P_{rx} + 1/P_{ry} - 1/\phi P_o \quad (7.6)$$

$$P_o = (0.85f'_c(A_g - A_{st} - A_{ps}) + f_y A_{st} - A_{ps}(f_{pe} - E_p \epsilon_{cu})) \quad (7.7)$$

If the factored axial load < 0.10 $\phi f'_c A_g$

$$M_{ux}/M_{rx} + M_{uy}/M_{ry} < 1.0 \quad (7.8)$$

where

P_{xy} = factored axial resistance in biaxial flexure

P_{rx} = factored axial resistance based on the eccentricity of $e_y = M_{ux}/P_u$

P_{ry} = factored axial resistance based on the eccentricity of $e_x = M_{uy}/P_u$

Longitudinal Reinforcement Limits

Maximum area of reinforcement

$$A_s/A_g + A_{ps}f_{pu}/A_gf_y < 0.08 \text{ - gravity load combination}$$

$$A_s/A_g < 0.06 \text{ - Seismic Zone 2 (reverse system used in Turkey) (Section 5.10.11.3)}$$

$$A_s/A_g < 0.04 \text{ - Seismic Zone 3 & 4}$$

Minimum area of reinforcement (controlled by bending)

$$A_s f_y / A_g f_c + A_{ps} f_{pu} / A_g f_c > 0.135 \text{ - gravity load combination}$$

$$A_s/A_g > 0.01 \text{ Seismic Zone 2,3 and 4. (Section 5.10.11.4.1a)}$$

Tie and Spiral Reinforcement – (Section 5.10.6)

The minimum bar diameter for the spiral is set to $\phi 10$. Min spacing can not be less than 25 mm and the maximum spacing can not exceed 150 mm. For tie reinforcement the maximum spacing can not be larger than 300 mm and if bundled can not be larger than 150 mm.

The minimum spiral reinforcement – gravity loads

$$\rho_s > 0.45 (A_g/A_c - 1) f_c'/f_{yh} \text{ - gravity}$$

$$\rho_s > 0.12 f_c'/f_y \text{ - seismic zone 3 or 4}$$

Spiral pitch can be computed from

$$s = 4 A_{sp} / \rho_s D_c \text{ where } D_c \text{ is the core diameter for circular columns.}$$

For rectangular columns

$$A_{sh} > 0.30 s h_c f_c'/f_y (A_g/A_c - 1) \text{ - seismic requirement}$$

$$A_{sh} > 0.12 s h_c f_c'/f_y$$

Where h_c is the core dimension of tied column in the direction under consideration

Seismic Analysis

Bridges can have significant damage after an earthquake with seven percent probability of exceedance in 75 years (1000 year return period) while having a low probability of collapse.

Site specific procedure can be used if one of the condition exists.

- The site is within 10 km away from the fault line.
- The site is classified as F (very soft soil conditions)
- Long duration EQ's are expected
- Importance of the bridge is high and requires a low probability of exceedance than the standard.

A response spectrum can be constructed by knowing the peak ground acceleration, short and long spectral accelerations (S_s and S_1 respectively). PGA's for a 1000 year return period earthquake can be determined from the study of Gulkan et al (1993).

Table 7.1.

**UFC 3-310-01
25 May 2005**

TABLE D-2

		Seismic Loading (Site Class B)				
Continent / Region	Country	Base / City	MCE S_s (%g)	MCE S_1 (%g)	10/50 S_s (%g)	10/50 S_1 (%g)
Asia	South Korea	Taegu	29	11	14	6
		Uijongbu	17	7	8	3
		Yongsan / Seoul	17	7	9	3
Vietnam		Da Nang	18	7	9	4
		Ho Chi Minh City	14	6	7	3
		Nha Trang	13	5	6	3
Taiwan		Tainan	239	96	120	48
		Taipei	325	130	162	65
		Tsoying	251	100	125	50
Thailand		Bangkok	28	11	14	6
		Chiang Mai	27	11	14	5
		Sattahip	21	9	11	4
Turkey		Udonthani	24	10	12	5
		Ankara	99	40	49	20
		Incirlik AB / Adana	105	42	52	21
		Izmir AS	242	97	121	48

US Army Corps have studied the seismicity of different regions around the world. MCE stands for the maximum credible earthquake in the above table. MCE typically represents an earthquake with a 2500 year return period. 10/50 typically represents an earthquake with 500 year return period.

For the 5/50 event 1000 year return period $\frac{3}{4}$ MCE values can be used per
<http://www.hnd.usace.army.mil/techinfo/ti/809-04/chapter%203.pdf>

The design load combinations need to be used in design of column connections or foundation if column plastic hinging forces are used. Shear and moment shall be based on the column hinging forces. The axial load can be taken from the corresponding load combination that is used to compute the plastic hinging state.

The analysis methods for earthquake can be determined from AASHTO-LRFD 4.7.4.3

- Single Mode Spectral Method (4.7.4.3.2b)
- Uniform Load Method (4.7.4.3.2c)
- Multi Mode Spectral Method (4.7.4.3.3)
- Time History Method (4.7.4.3.4)
- Push over Analysis – performance

Time History Analysis – Ground Motion Selection

If site specific earthquake records do not exist, one can use response spectrum compatible earthquake records. Apply the acceleration-time records in three orthogonal directions at the same time for the main body. Or apply displacement-time at foundation level. Displacement-time records are usually used for multiple support excitation. If three earthquake records were used in the analysis, use the maximum values for design check, and if seven earthquake records were used, use the average of seven earthquake records in the analysis.

Column Design

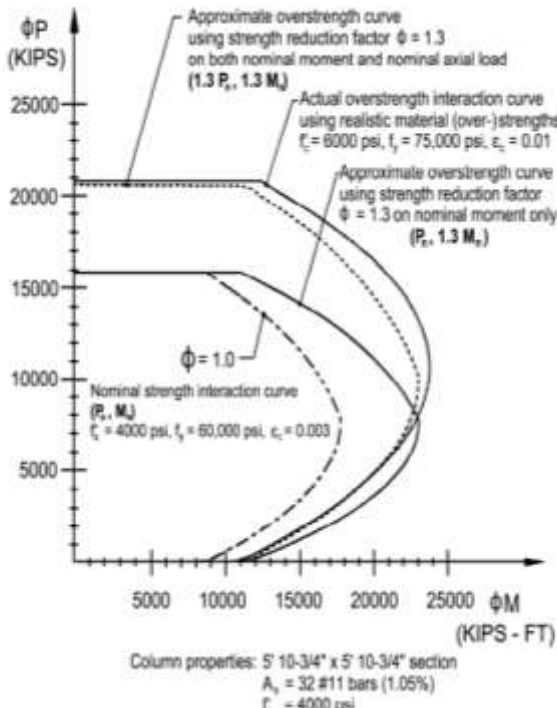
In seismic analysis, the full earthquake effects are applied to the structure. Only column moments obtained thru elastic dynamic analysis are reduced by response modification factors. The column shear design and foundation design is based on the plastic hinging capacity of the columns.

Substructure	Importance Category		
	Critical	Essential	Other
Wall-type piers-larger dimension	1.5	1.5	2
Reinforced concrete pile bents			
- Vertical piles only	1.5	2	3
- With batter piles	1.5	1.5	2
Single columns	1.5	2	3
Steel or composite steel and concrete pile bents			
- Vertical piles only	1.5	3.5	5
- With batter piles	1.5	2	3
Multiple column bent	1.5	3.5	5

Overstrength Resistance in Columns – AASHTO LRFD Definition

The overstrength resistance develops due to the fact that actual properties being greater than the minimum specified values and is implemented by specifying resistance factors greater than unity.

- The effect of an increased steel strength over the specified minimum f_y and for strain hardening effects. Increased $f_y = 1.25 \text{ min } f_y$
- The effect of an increased concrete strength over the specified f'_c and confinement provided by the transverse steel. Also, with time, concrete will gradually increase in strength. Increased $f_c' = 1.5 \text{ min } f'_c$
- The effect of an actual concrete ultimate compressive strain above 0.003. Increased strain = 0.01



Single Columns (Piers)

1. The column over strength resistance can be computed by using a ϕ of 1.3 for reinforced concrete columns in determination of interaction diagrams.
2. Determine the shear force corresponding to column over strength resistance
3. Axial forces can be determined from Extreme Event Load Combination I with the unreduced maximum and minimum seismic axial load.

Multiple Column Piers

1. The column over strength resistance can be computed by using a ϕ of 1.3 for reinforced concrete columns in determination of interaction diagrams. Use the initial axial load at Extreme Event Load Combo 1 with Faxial_EQ = 0.
2. Determine the corresponding shear force at columns.
3. Apply the total shear force at center of mass of the bent to determine the axial load distribution for the bents.
4. Use these axial loads to revise the over strength column force. Recompute the shear forces and check if they are within 10% of the ones determined in Step 2. If not rerun the analysis with the new shear forces in Step 3.

Abutments

Abutment structures shall be designed to have stability against bearing capacity failure, overturning, and sliding. Safety against deep-seated foundation failure can also be investigated. The overall stability of the structure need to be checked. The seismic analysis can be performed using Mononobe – Okabe method.

Section 8

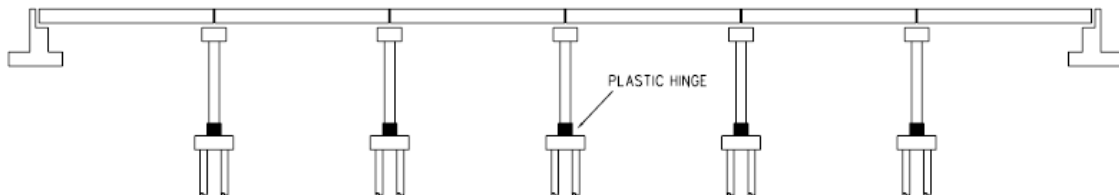
Nonlinearities in Bridge Modelling

The nonlinear analysis of the bridge can involve the following non-linearity's

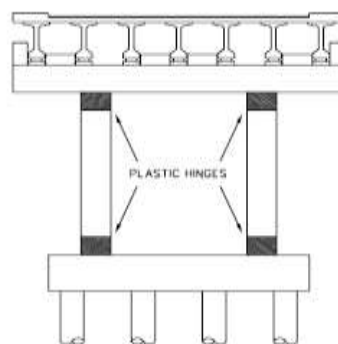
- Plastic Hinging
- Shear Key
- Abutment
- Bearing
- Pounding Between Adjacent Spans
- Soil-Structure Interaction
- Geometric Non-Linearity
- Gap

Plastic Hinge Models

Plastic hinge models require knowledge on material non-linearities of concrete and rebars for columns of the bridge. In a typical capacity protection design, the plastic hinges are allowed to develop at the column tops or bottoms as targeted. The foundation and the cap beams are targeted to remain in essentially elastic state.



(a) In Longitudinal Direction



(b) In Transverse Direction

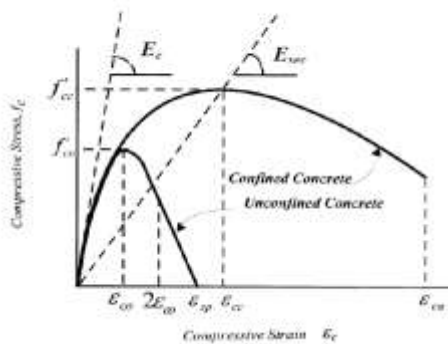
Figure 8.1.

In plastic hinge models, moment-curvature elements with axial force interaction, lump sum plastic moment-rotation elements or fiber elements can be used. In case of lump-plasticity elements, it is required to compute the plastic hinge lengths. These elements can include the strength degradation of the seismic performance of the element.

Mander's Concrete Compression Model

The confined and unconfined concrete have a different stress-strain relationship as shown below. The most common concrete model used by bridge engineers is Mander's model.

Concrete under Compression, Mander's Model



$$\varepsilon_{co} = 0.002 \left[1 + 5 \left(\frac{f'_c}{f'_{co}} - 1 \right) \right]$$

$$\varepsilon_{cc} = 0.004 + \frac{1.4 \rho_i f_{sh} \varepsilon_{co}}{f'_c}$$

$$r = \frac{E_c}{E_c - E_{uc}}$$

$$E_{uc} = \frac{f'_{uc}}{\varepsilon_{uc}}$$

$$f'_c = \frac{1}{2} K_s \rho_i f_{sh} \quad (\text{For circular sections})$$

$$\rho_i = \frac{4 A_g}{d_i t}$$

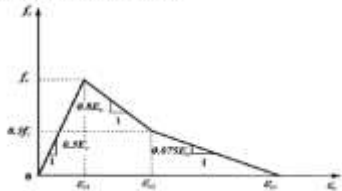
$$f_c = \frac{f'_{cc} (\varepsilon_c / \varepsilon_{cc}) r}{r - 1 + x}$$

$$f'_{co} = f'_{cc} \left(2.254 \sqrt{1 + \frac{7.94 f'_c}{f'_{co}}} - \frac{2 f'_c}{f'_{co}} - 1.254 \right)$$

Figure 8.2.

Concrete Under Tension Model

Concrete Under Tension, Yabe's Model



$$f_t = \begin{cases} 0.5 E_t \varepsilon_t & \varepsilon_t \leq \varepsilon_{t1} = 2 f_r / E_t \\ f_r [1 - 0.8 E_t (\varepsilon_t - \varepsilon_{t1})] & \varepsilon_{t1} < \varepsilon_t \leq \varepsilon_{t2} = 2.625 f_r / E_t \\ f_r [0.5 - 0.075 E_t (\varepsilon_t - \varepsilon_{t2})] & \varepsilon_{t2} < \varepsilon_t \leq \varepsilon_{t3} = 9.292 f_r / E_t \end{cases}$$

Figure 8.3.

Reinforcement Tension Model

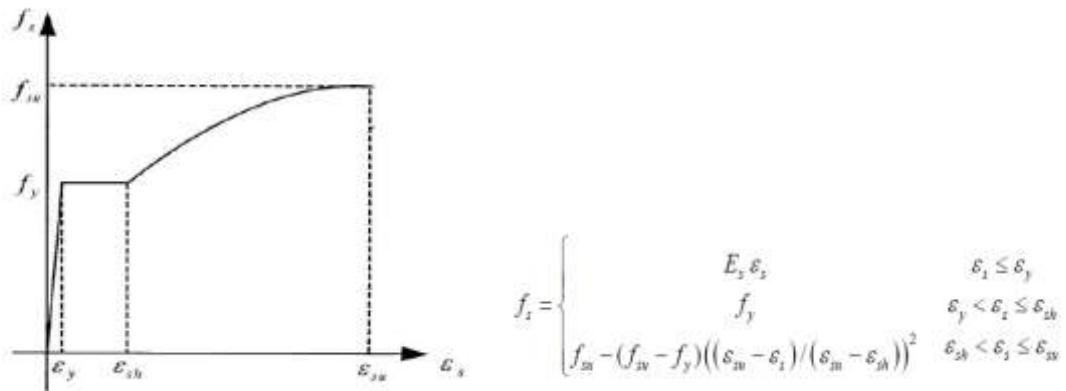


Figure 8.4.

Column Plastic Hinge Length

Plastic hinge length can be computed using the following equation.

$$L_p = 0.08 L + 0.022 f_{ye} d_{bl} \geq 0.044 f_{ye} d_{bl} \quad (8.1)$$

L: length of column from the point of maximum moment to the point of contra-flexure

f_{ye}: expected yield strength of column longitudinal reinforcing steel

d_{bl}: nominal diameter of column longitudinal reinforcing steel bars

Converting Moment-Curvature to Moment Rotation Element

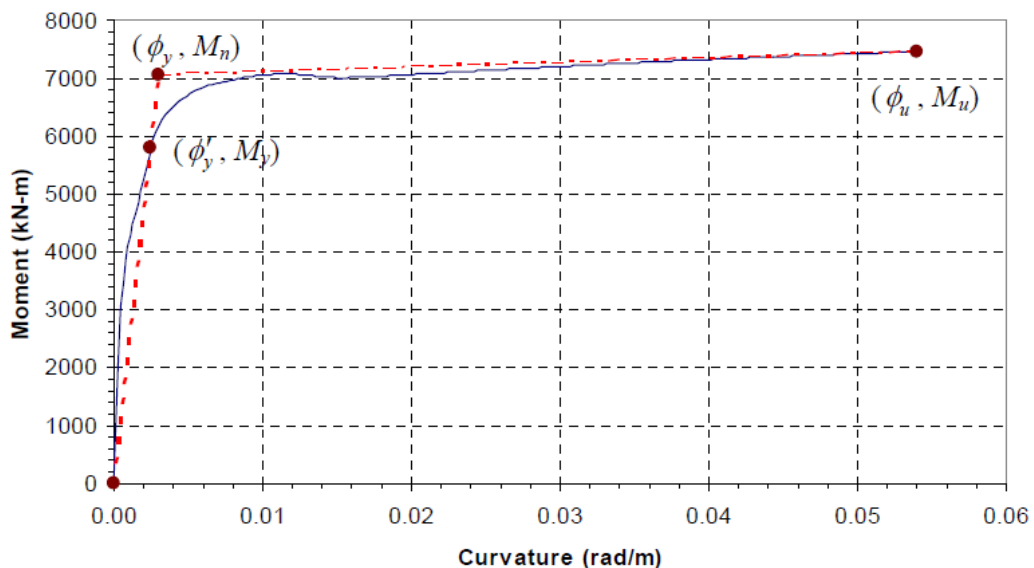


Figure 8.5

Chord yield rotation: (note that for a pure cantilever position the denominator will be 2)

$$\theta_y = \frac{\phi_y L}{3} \quad (8.2)$$

Ultimate rotation

$$\theta_u = \phi_y + (\phi_u - \phi_y)L_p \quad (8.3)$$

It shall be noted that the moment-curvature of the member is depend on the level of axial force and amount of reinforcing steel as shown below.

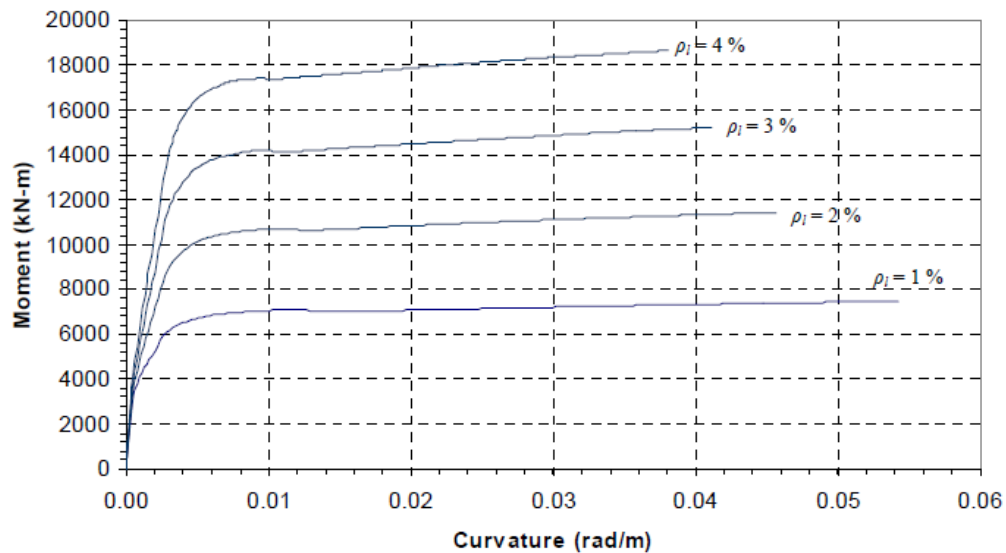
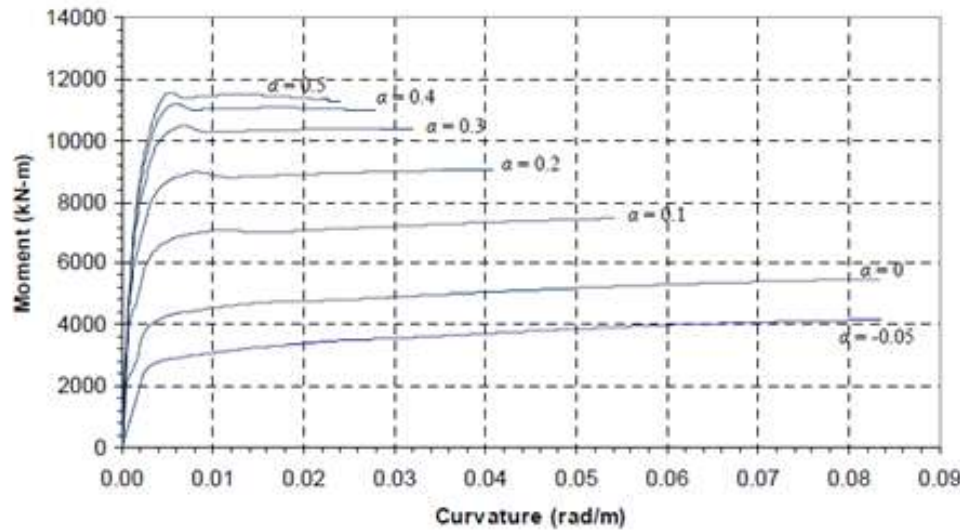


Figure 8.6



$$\alpha = \frac{P}{f'_c A_c}$$

where;

P : Axial load acting on the section (compression is taken as positive)

A_c : Area of the section

f'_c : Compressive strength of concrete

Figure 8.7.

Effective Inertia of the Column

The effective inertia to be used in column modeling can be computed from the slope of the moment curvature between the point of (0,0) and moment curvature correspond to first yield of the longitudinal rebars.

$$EI_{eff} = \frac{M_y}{\phi_y} \quad (8.5)$$

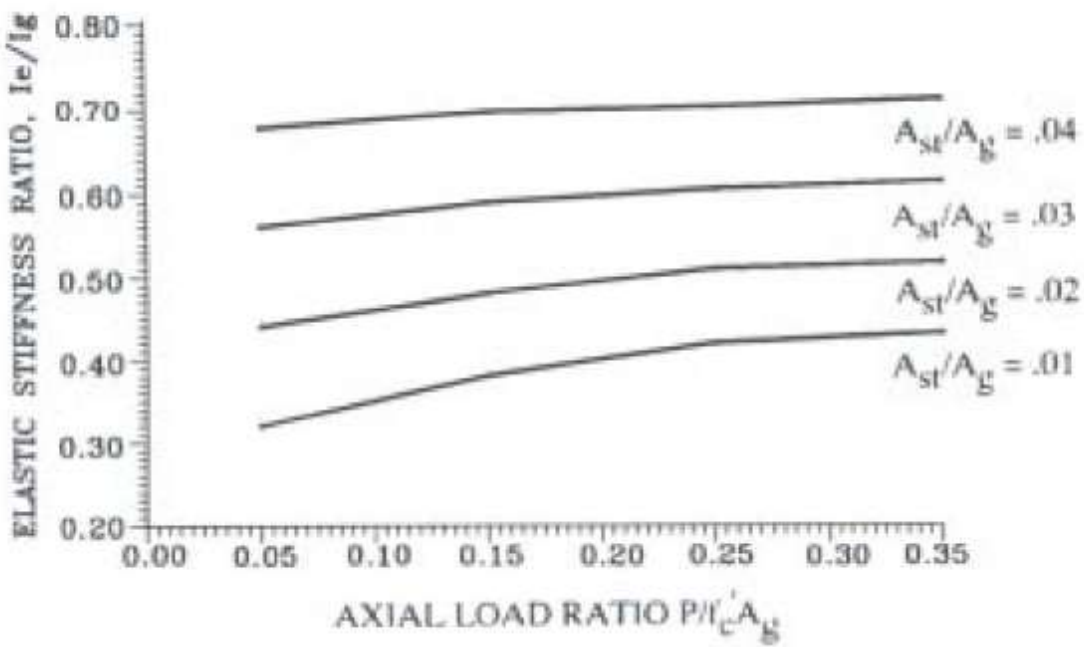


Figure 8.8.

Hysteretic Elements with Degradation Properties

- *Backbone*: Either bilinear or trilinear curves are defined.
- *Polygonal hysteretic model*: The type of cyclic behavior can be bilinear, vertex-oriented, or yield oriented
- *Alpha*: Stiffness degradation parameter
- *Beta1*: Ductility-based strength degradation parameter
- *Beta2*: Energy-based strength degradation parameter
- *Gamma*: Slip parameter



Figure 8.9.

Yield Surface Element

These elements are defined to envelope the yield surface for an element taking into account the axial force and moment interaction.

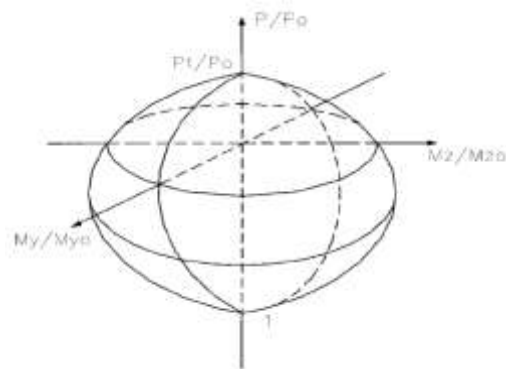


Figure 8.10.

Reinforcement Slip Model

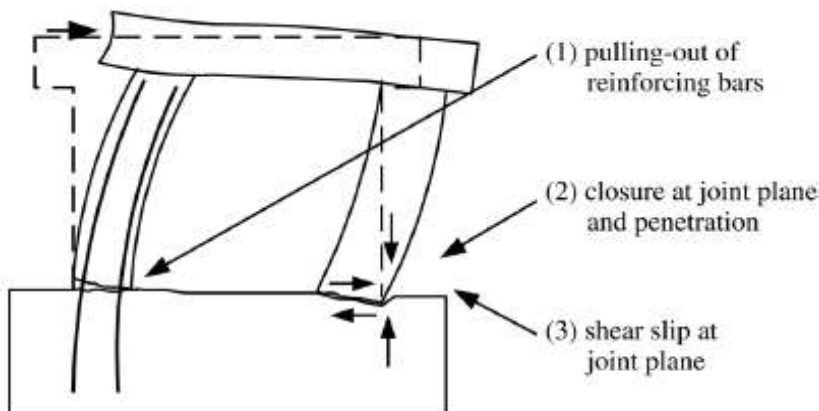


Figure 8.11.

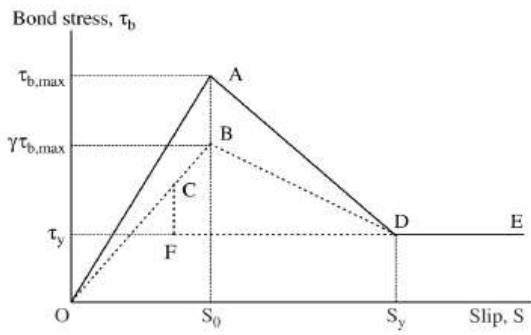


Fig. 6. Idealized bond stress–slip relationship [19].

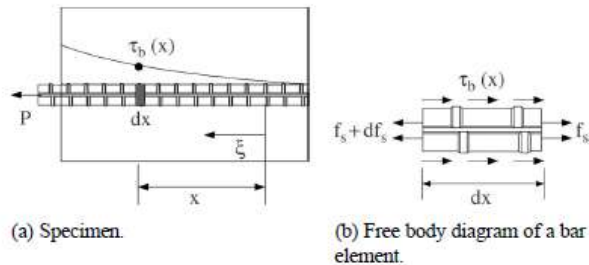


Figure 8.12.

Shear Keys and Abutment

Shear keys are usually assumed to be sacrificial elements to stop the seismic movement of the superstructure in transverse direction. The gap model between the girder and the shear key can be modeled by a hysteretic spring-gap element.

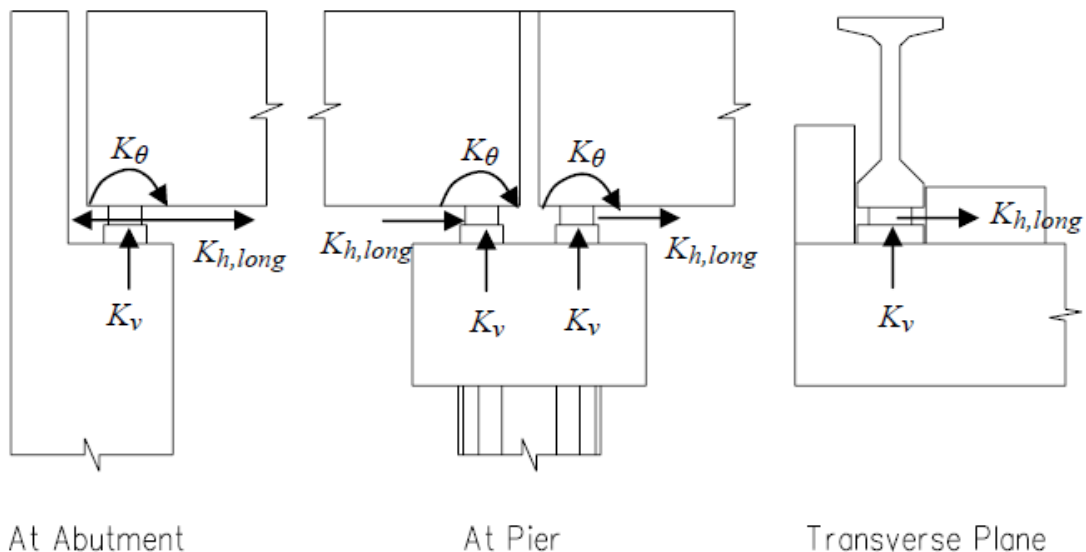


Figure 8.13.

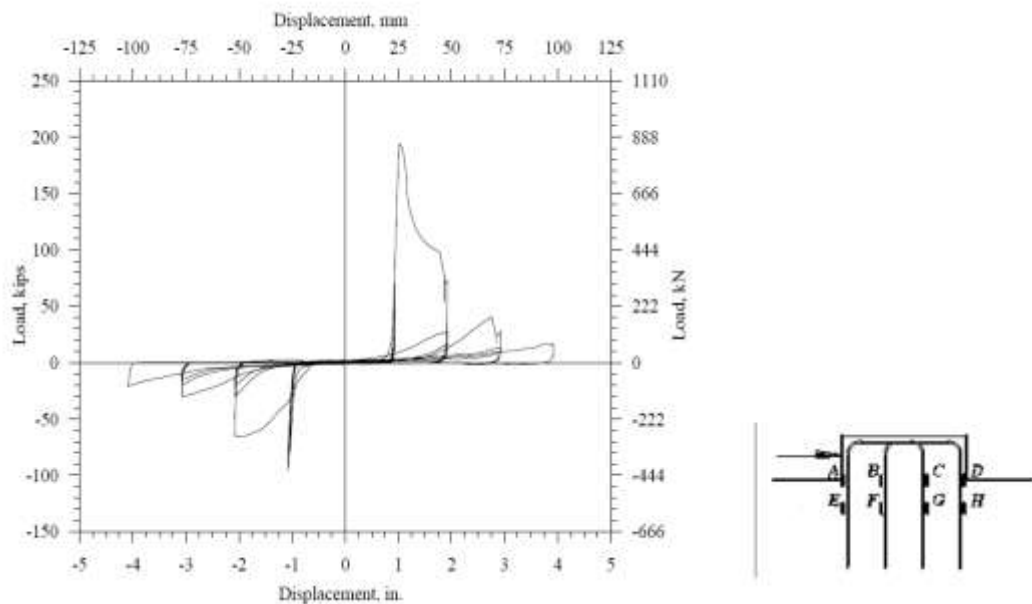


Figure 8.14.

Shear Key Response Model

Abutments and the soil at the back can stop the longitudinal seismic movement of the bridge and can be modeled with a gap spring element.

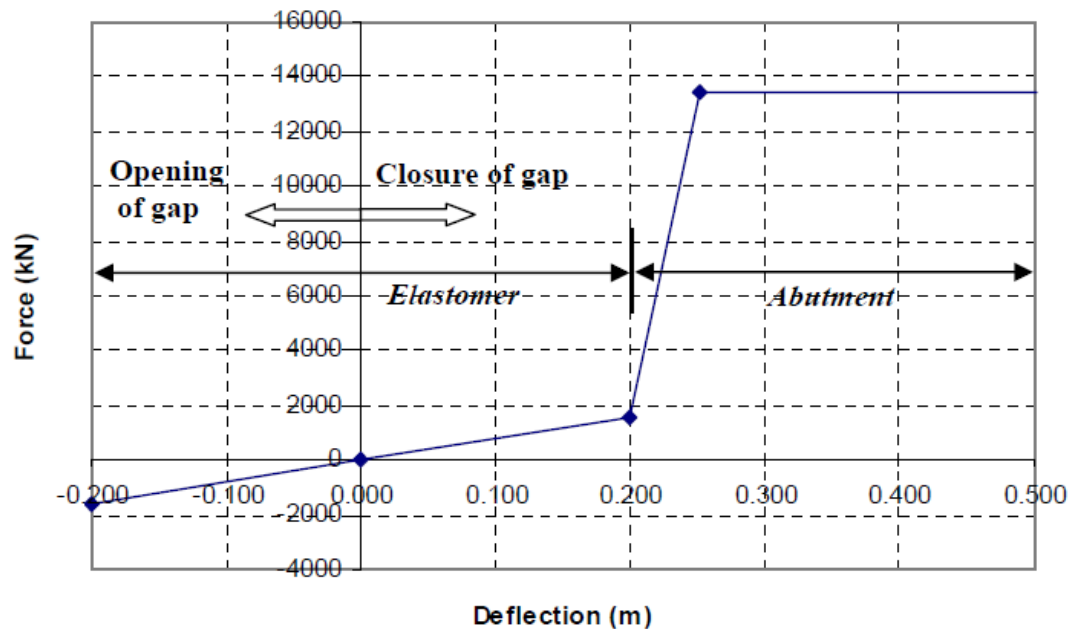


Figure 8.15.

Structural Modeling of Gap Elements

The following model can be used in a standard non-linear analysis of a bridge.

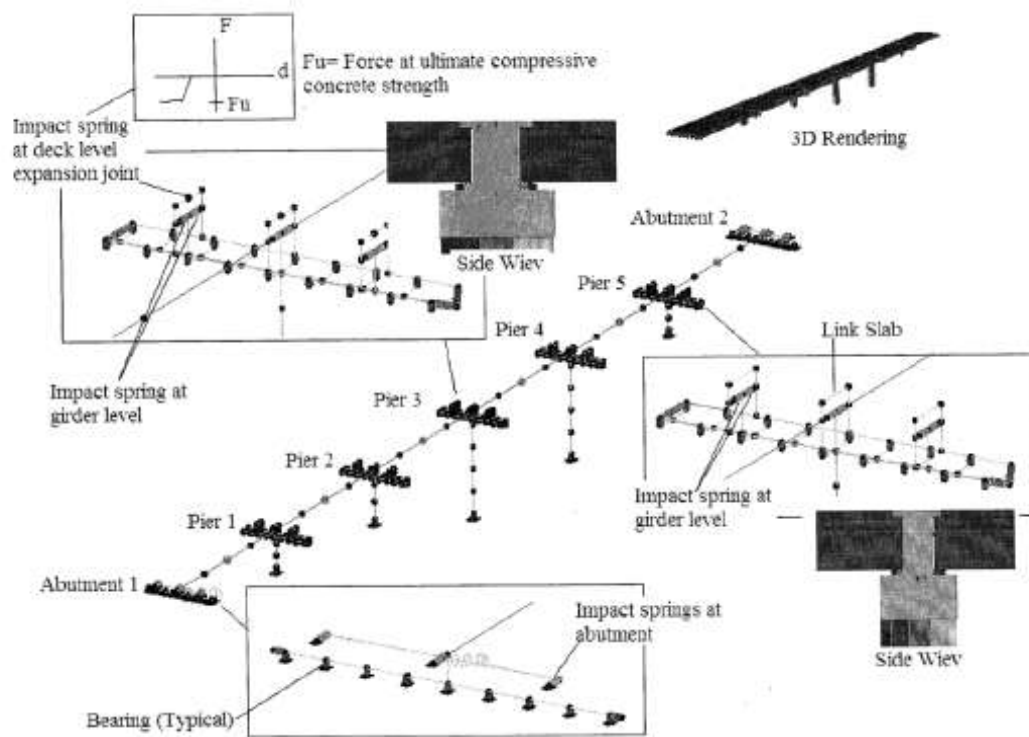


Figure 8.16.

Expansion joint pounding model is shown below.

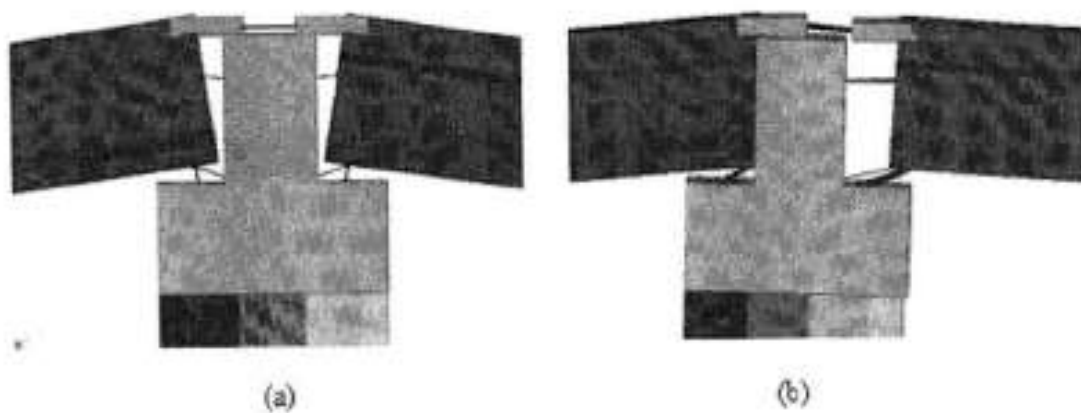


Figure 8.17.

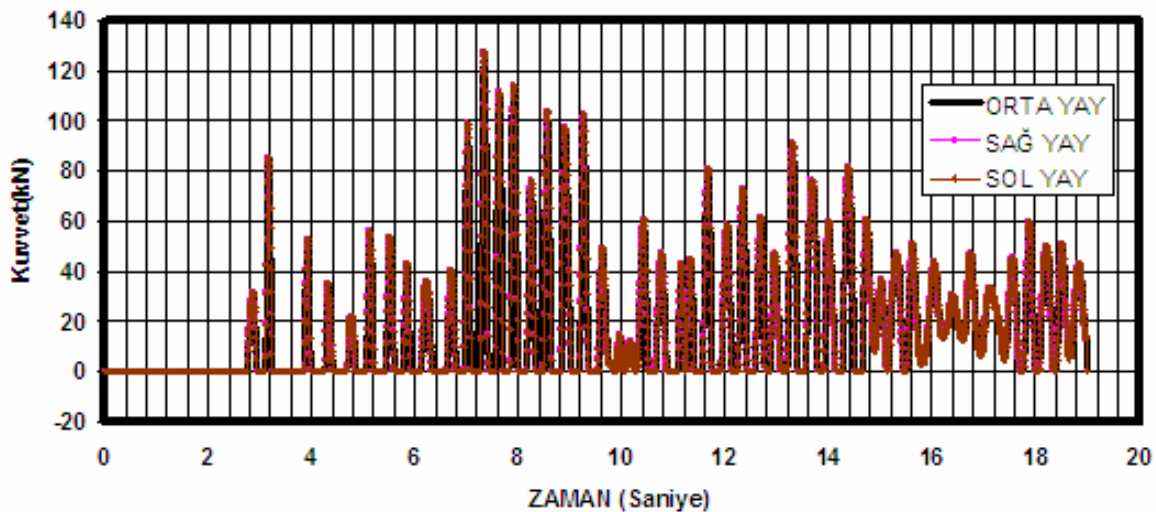


Figure 8.18.

Damper Element

$$F = C V^a$$

This element is suitable for modeling the behavior of fluid viscous dampers or other devices displaying viscous behavior. This element can only be used in the time history analysis because the response of the element is velocity-dependent.

Fluid dampers which operate on the principle of fluid orificing produce an output force which is proportional to the power of the velocity. That power can take values in the range of 0.5 to 2.0.

This element can be either linear or nonlinear. For the linear element, the power of the velocity is assumed one. Only a single viscous constant is needed.

For the nonlinear element, the nonlinear damping force of these devices is proportional to the power of the relative velocity across the damper. The nonlinear element can be single-range (type 1) or two-range (type 2). These elements are used to model Coulomb damping, viscous damping, orifice damping, and velocity-raised-to-power-p damping. One or two sets of viscous constants, power ranges, and force offsets are needed.

The Viscous Constant, Velocity Power, and Force Offset fields are entered for nonlinear Type I and II dampers. They are not applicable for dampers with the sub-type linear. For Type I Nonlinear dampers, the fields are entered for Range 1 only. For Type II dampers, they are entered for both Range 1 and Range 2.

Viscous Constant (Range 1/2)

The damping coefficient.

Velocity Power (Range 1/2)

The power that the velocity is raised to. The usual range is 0.5 to 1.2. If the value is 1.0, then the element is a linear viscous element.

Force Offset (Range 1/2)

The initial force value at rest. This value is determined from the operation data of the damper.

The remaining two fields are entered for all viscous dampers.

Max Damper Force

The maximum force that can be applied by the damper.

Soil Structure Interaction Models

AASHTO LRFD allows to use the API specs for soil-structure interaction. At a certain depth the soil-structure can be defined by hysteretic springs to account for stiffness and damping of the soil.

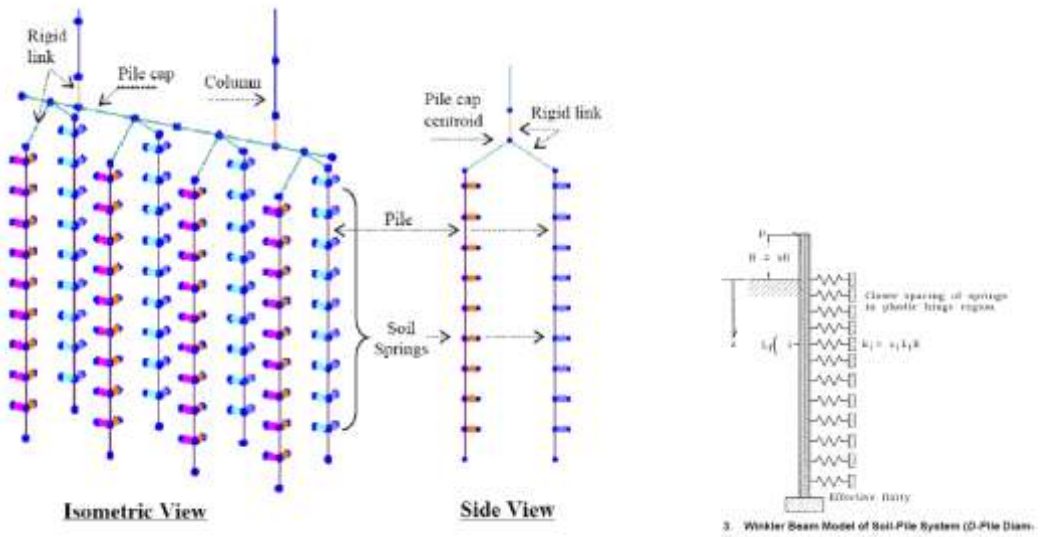


Figure 8.19.

The lateral soil resistance-deflection (p - y) relationships for sand are nonlinear and can be approximated at any specific depth H , by the following expression [6]:

$$P = A \cdot p_u \cdot \tanh \left[\frac{k \cdot H}{A \cdot p_u} \cdot y \right] \quad (\text{C.1})$$

where;

A = Factor to account for cyclic or static loading condition. Evaluated by:

$$A = 0.9 \quad \text{for cyclic loading.}$$

$$A = \left(3.0 - 0.8 \frac{H}{D} \right) \geq 0.9 \quad \text{for static loading}$$

k = Initial modulus of subgrade reaction, lb/in.³ (kN/m³). Determine from Figure C.1 as function of angle of internal friction, ϕ'

y = Lateral deflection, in. (m)

H = Depth, in. (m)

D = Average pile diameter from surface to depth, in. (m)

p_u = Ultimate bearing capacity at depth H , lbs/in. (kN/m)

The smaller value of the following p_u should be used as the ultimate bearing capacity:

$$p_u \text{ for shallow depths; } p_{us} = (C_1 \cdot H + C_2 \cdot D) \cdot \gamma \cdot H \quad (\text{C.2})$$

$$p_u \text{ for deep depths; } p_{ud} = C_3 \cdot D \cdot \gamma \cdot H \quad (\text{C.3})$$

C_1, C_2, C_3 = Coefficients determined from Figure C.2
 γ = Effective soil weight, lb/in.³ (kN/m³)

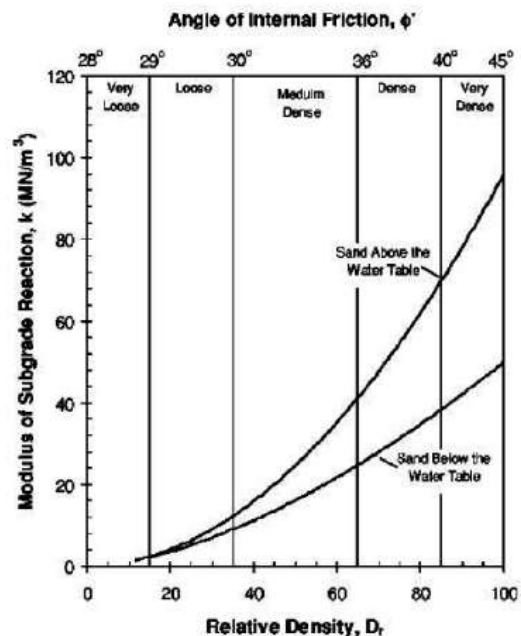


Figure C.1: Modulus of Subgrade Reaction for Sands [6]

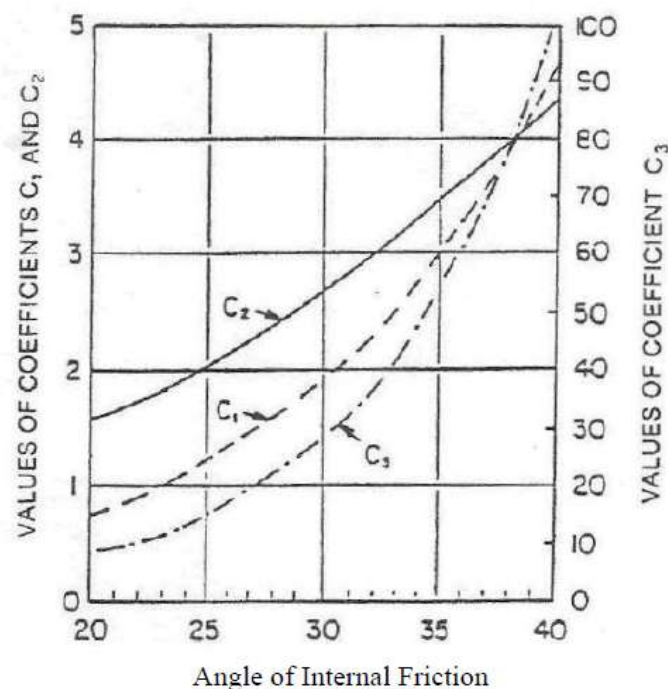
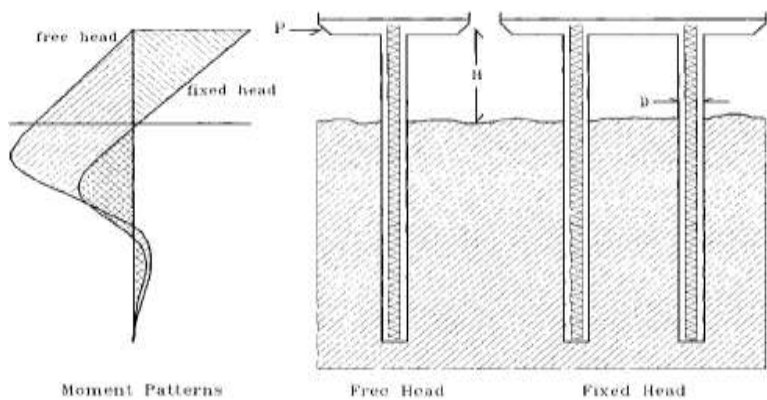
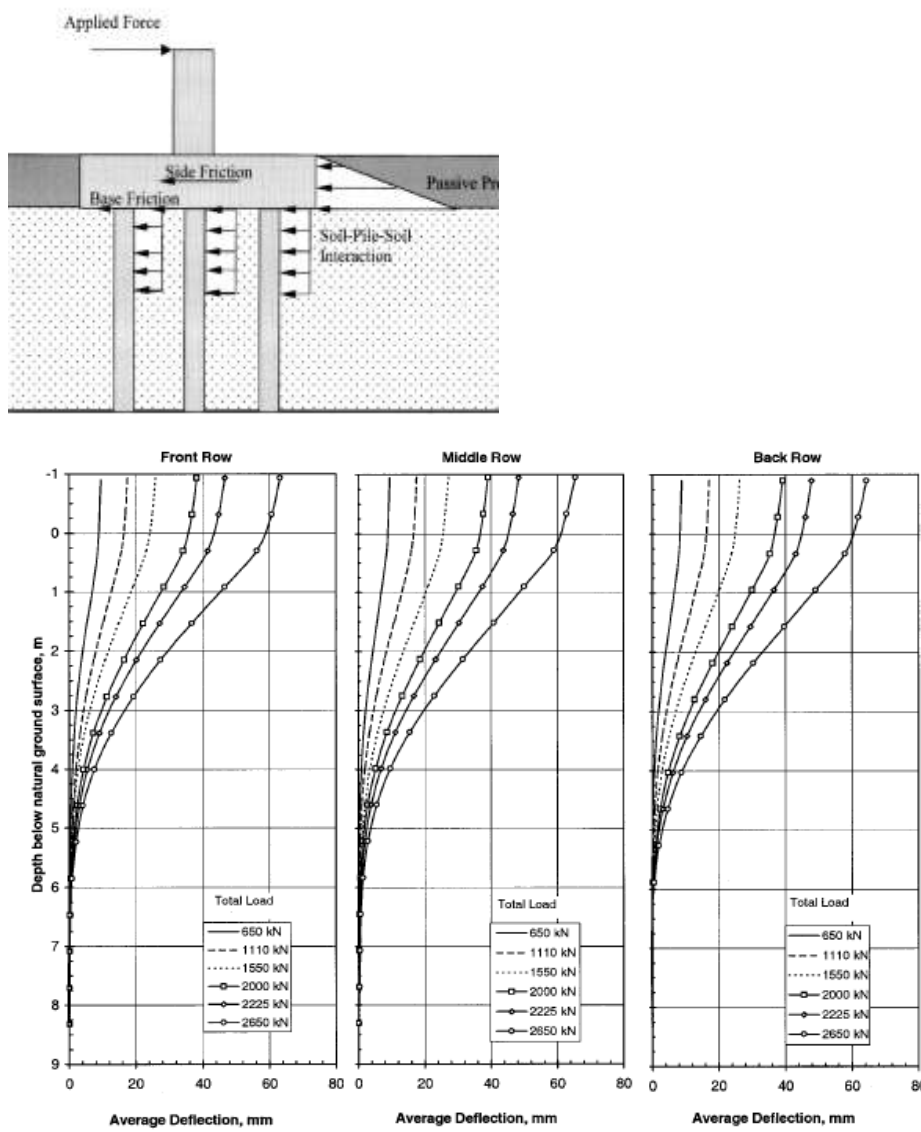


Figure C.2: Coefficients for Computation of Ultimate Bearing Capacity [6]



Group Effects

Group effects may be ignored if pile spacing is equal or more than 3D per CALTRANS. Some other references state that the group effect can be ignored around 5D pile spacing.



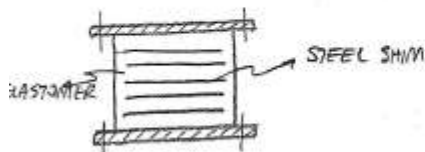
Elastomeric Bearings

ELASTOMERIC BEARINGS

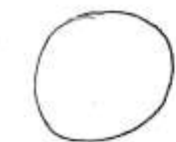
METHOD A

METHOD B

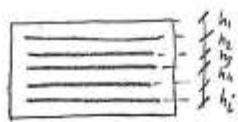
WE JUST CONCENTRATE ON METHOD B



THIS TYPE OF BEARINGS ALLOW
MOMENT BY A CERTAIN RIGIDITY



CROSS-SECTION



$$h_{rt} = h_1 + h_2 + \dots + h_i$$

$$S = \frac{D}{4h_{rt}} - \text{CIRCULAR BEARINGS}$$

(EQ 14.7.5.1-2)

ONCE THE HARDNESS IS ASSIGNED IN DESIGN SHEAR MODULUS "G"
(TABLE 14.7.6.2-1) CAN BE DETERMINED TYPICAL HARDNESS ≈ 60

$$\text{ELASTIC MODULUS} = 6GS^2 \quad (\text{EQ C14.6.3.2.1})$$



$$k_{\text{LATERAL}} = \frac{GA}{h_{rt}} \quad (\text{EQ 14.6.3.1-2})$$

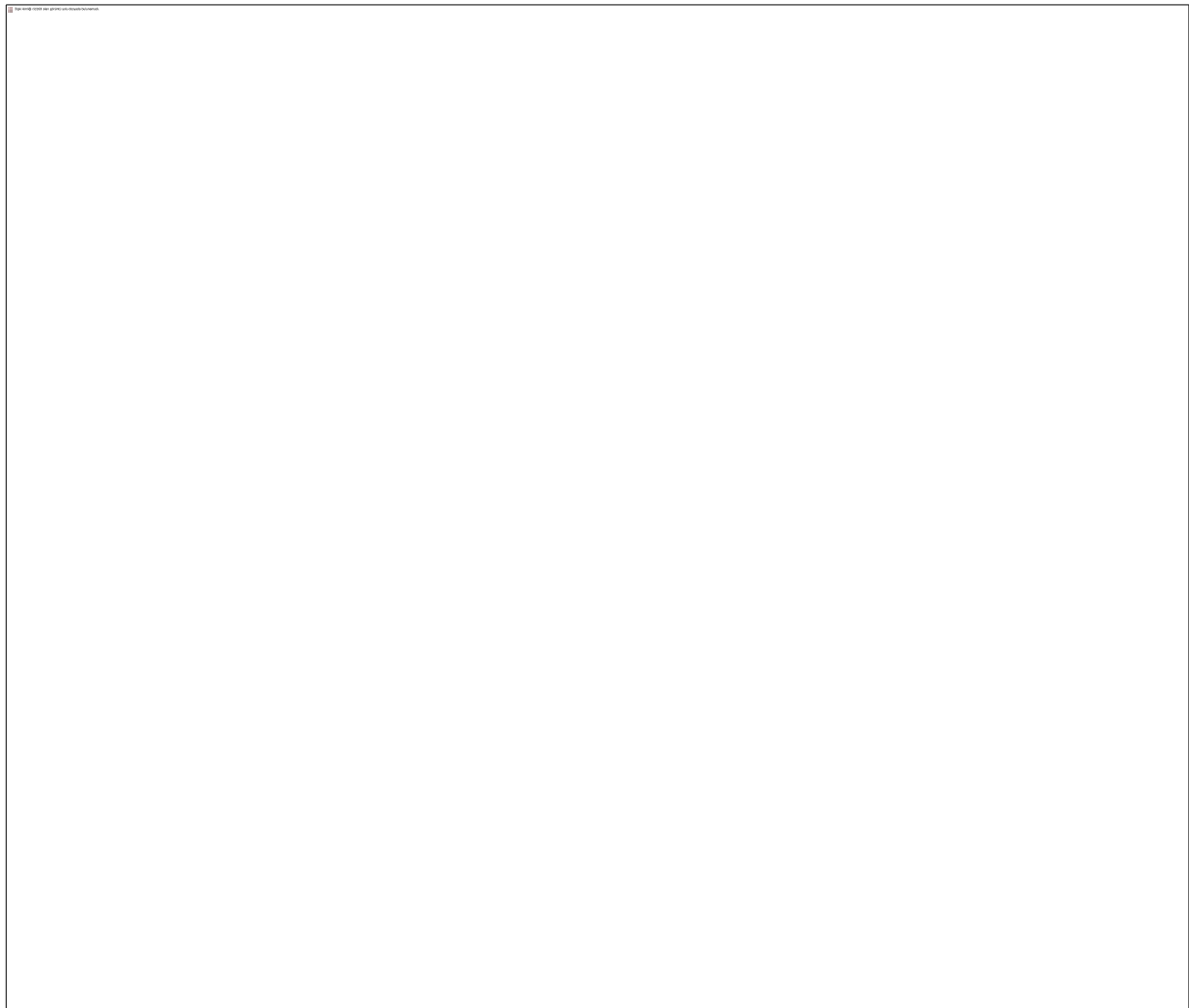
$$k_{\text{VERTICAL}} = \frac{EA}{h_{rt}} \quad A = \text{AREA OF BEARING}$$

$$k_{\text{ROTATIONAL}} = 0.8 \frac{EI}{h_{rt}} \quad (\text{EQ 14.6.3.2-3})$$

FOR COMPRESSION CHECK - STATIC LOADS. (SECTION 14.7.5.3.2)

$$\sigma_{\text{SERVICE}} < 1.66 GS$$

$$\sigma_{LL} < 0.66 GS \quad (\text{LIVE LOAD ONLY})$$

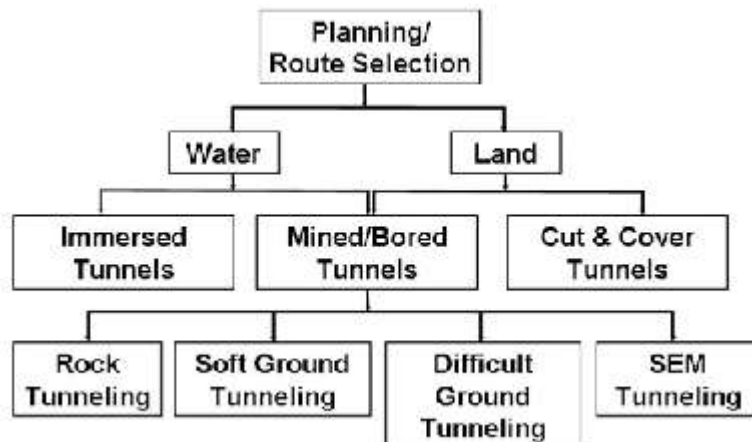


Section 9

Tunnel Types

Tunnel types can be classified based on the construction methodology that has been selected.

- Cut and Cover type
- Tunnel Boring Machine type (TBM)
- Rock Tunnels
- Sequential Excavation Method (SEM)/ New Austrian Tunneling Method type (NATM)
- Immersed Tube Tunnels



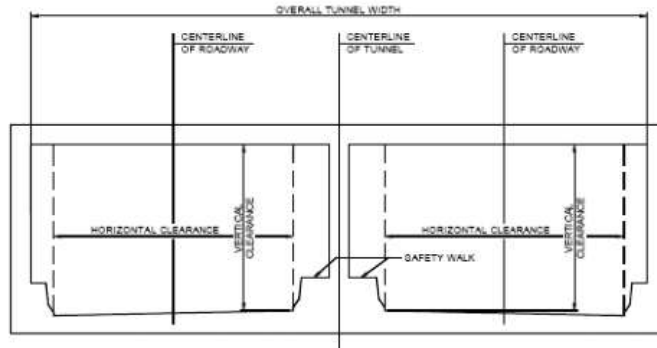
Hung et al (2009)

The most common types used in Turkey are cut and cover, NATM and TBM types. Before deciding on the type of the tunnel, geotechnical investigations need to be completed. The challenges in design of underground structures can be listed as

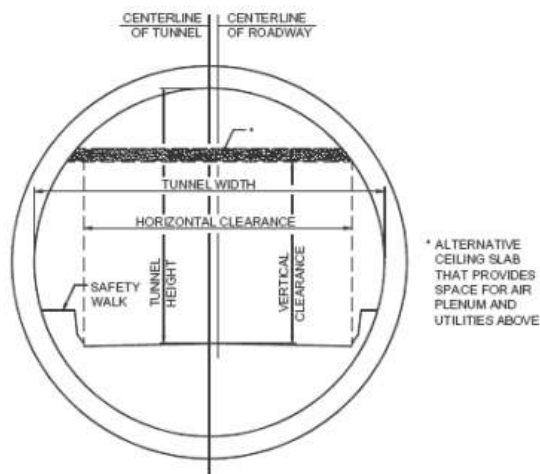
- Vast uncertainties
- Cost and feasibility is very much dependent on the geology
- Groundwater level

Tunnel Cross-Sections

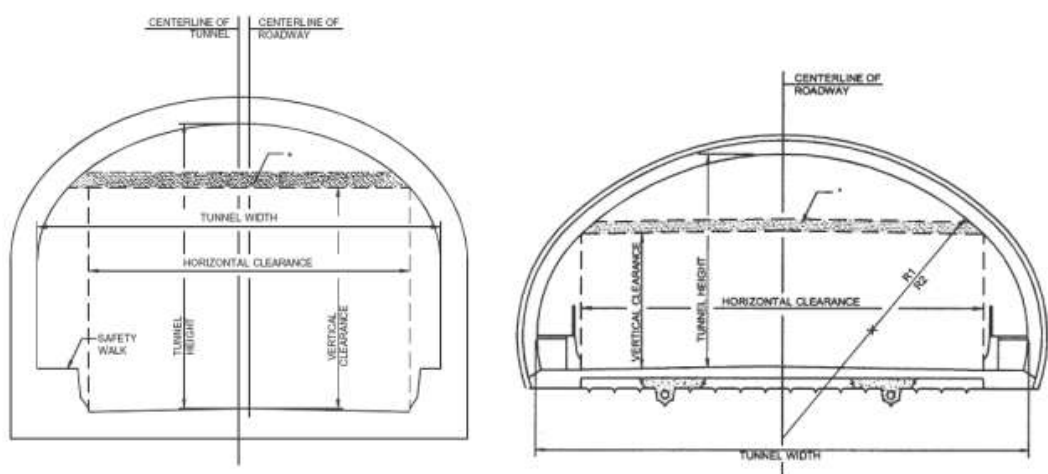
Tunnel cross-sections can be rectangular, circular or horse shoe shape.



Rectangular shapes used for Cut and Cover or Immersed Types (Hung et al 2009)



Circular cross-sections are used in TBM or Rock (Hung et al 2009)



Horse-shoe cross-sections are used in NATM or SEM (Hung et al 2009)

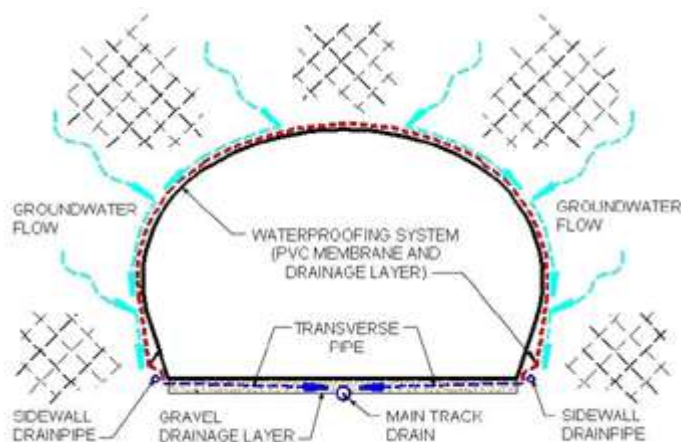
Groundwater Control

The tunnels need to be constructed to be in almost dry condition (Hung et al 2009). The allowed water leakage per day is

Tunnels – 0.075 lt/m²/day

Public space – 0.038 lt/m²/day

The ground water can be controlled by proper water proofing. Two basic types exist as drained (open) or undrained (closed) ones. In the open system, the ground water is collected at the footing level of the tunnel and drained out of the tunnel system where ground water leakage through the rock or soil is very low. The hydraulic pressure built around the walls can be significantly minimized by draining the water. The open system is sometimes called as the umbrella system. In closed ground water control, the entire cross-section of the tunnel is water proofed. In the later case, the structure shall be designed to resist the full hydraulic pressure.



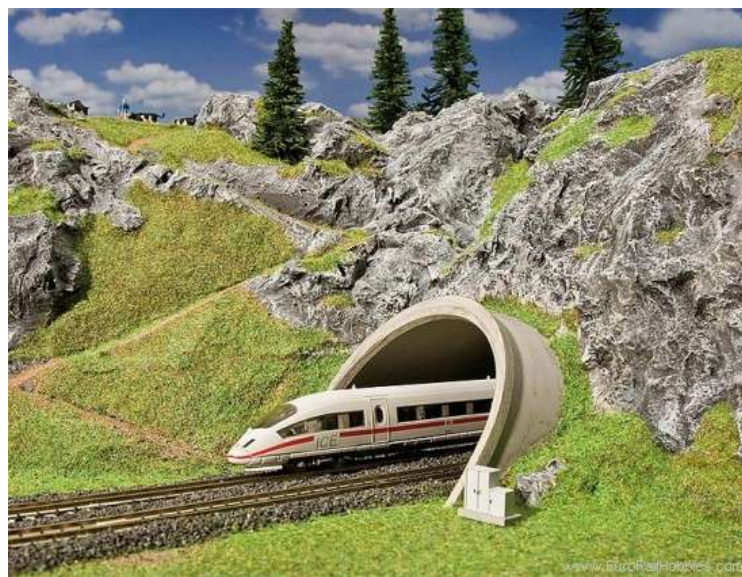
Open water proofing (www.fhwa.dot.gov)



Closed Water Proofing System (www.fhwa.dot.gov)

Tunnel Portal Structures

Tunnel portal structures are the entrance and exit structures of the tunnel that provides a protection against irregular water flows and soil accumulation at the entrances.



(www.eurorailhobbies.com)

Cut And Cover Structures

Cut and cover is a simple method of construction that is generally used for shallow tunnels, subway stations, and some underground facilities. This method is preferred if the underground facility or tunnel is near the grade and the geometry is rectangular. Construction usually starts with excavation of a trench slightly larger than the final structure. Then the structure is constructed (final liner) in the trench, and finally covered with soil. Figure shows a typical construction site of cut and cover tunnel.



Figure 9.1. Cut and cover Tunnels (C. Jeremy Hung et al 2009)

There are two basic construction techniques for constructing cut and cover structures:

- Bottom-up method
- Top-down method

In the bottom-up method, after providing the initial support of excavation system, a trench is fully excavated and the tunnel is constructed by casting the invert (floor slab), walls, and finally the tunnel roof. The tunnel may be of cast in place concrete, precast concrete, or steel bents filled with concrete infill between each bent. The trench is then backfilled compacted, and the surface is prepared according to its final use. Figure shows the construction sequence of a cut and cover tunnel using bottom-up method.

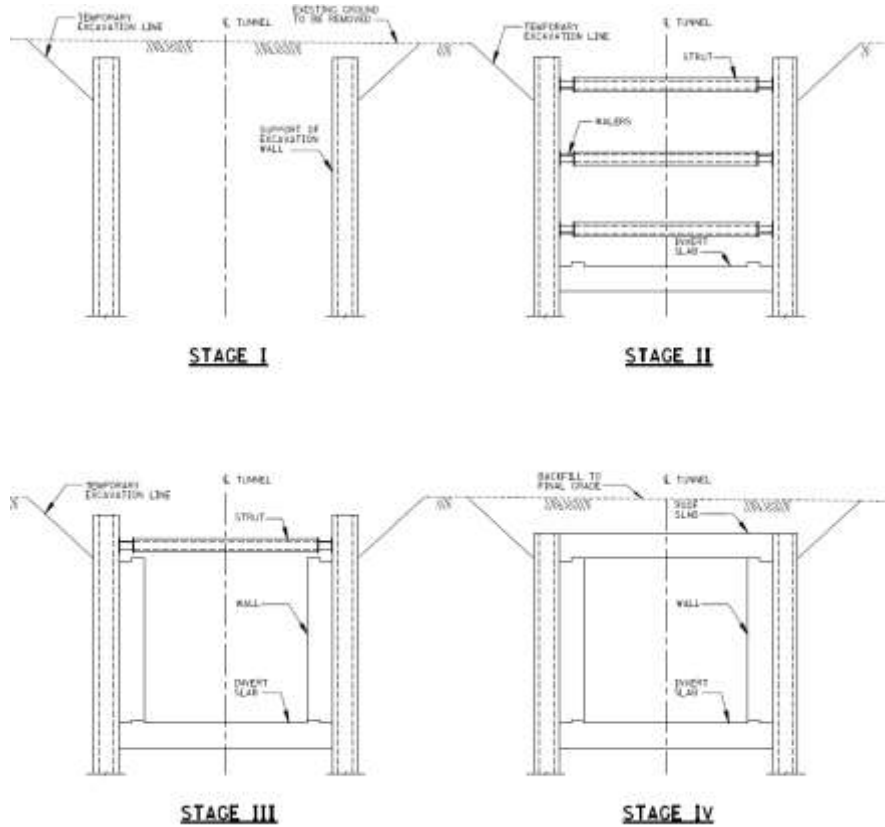


Figure 9.2. Bottom-up method construction sequence

In the top-down method, side support walls and capping beams are constructed from ground level, using slurry wall, bored piles, or secant piles. A shallow excavation is made to allow the tunnel roof to be constructed using precast beams or cast in place concrete. The surface work is then completed to serve its final function. This allows early restoration of roadways, and services. Excavation machinery is lowered into the excavation area, and the main excavation is carried out under the permanent tunnel roof, followed by constructing the base slab and internal walls as planned. Figure shows this method schematically.

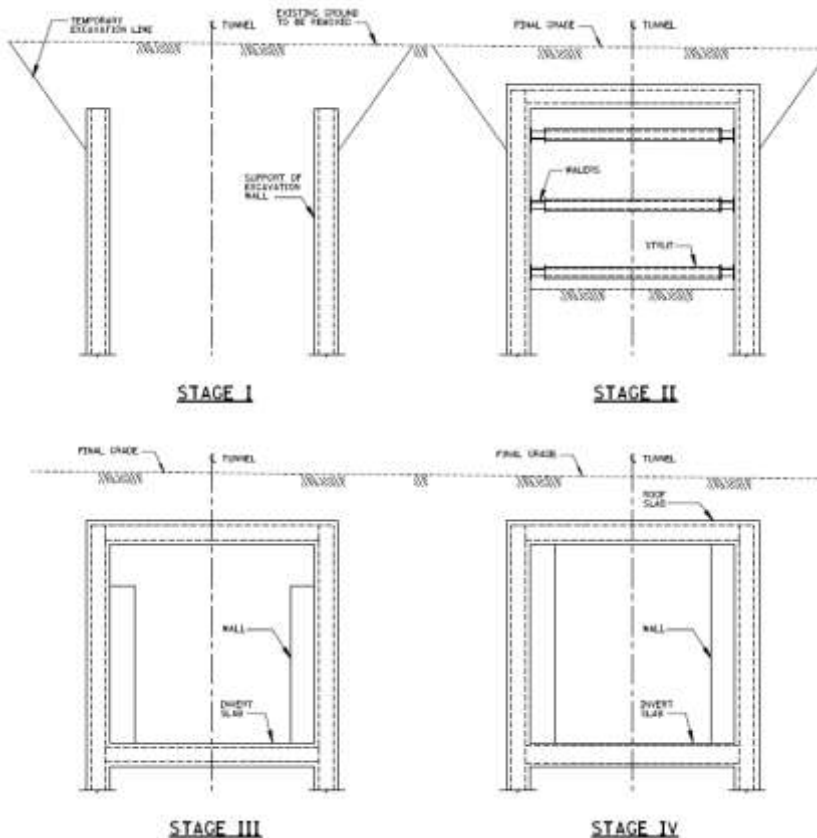


Figure 9.3. Top-down method construction sequence

Initial Support of Excavation

The support of excavation systems as defined in the Technical Manual for Design and Construction of Road Tunnels (C. Jeremy Hung et al 2009) are:

- **Open cut slope:** This method is used in areas where sufficient room is available to excavate a wide area, then the final structure will be constructed in segments and open cut area will be backfilled to the required elevation
- **Temporary:** This is a structure designed to support the excavation area as a vertical wall against soil lateral pressure and protects adjacent structures' foundation against any movement. It will either be left in place or will be removed after construction is complete. Sheet pile walls and soldier pile and laggings are mostly used for this type of support system.
- Permanent: This structure is designed and constructed to support vertical faces of the excavation. Initial support of the excavation walls will be part of the permanent tunnel structure. Slurry walls, secant pile walls, or tangent pile walls are mostly used as permanent support system.

Furthermore, the initial support of excavation systems can be classified as flexible and rigid.

Flexible Support

Flexible supports of excavation examples are sheet piling, and soldier pile and lagging walls. These types of supports have many limitations in application and are not suitable for relatively deep excavation or construction in areas that are close to structures that cannot tolerate large settlements or deflections. They are also not rigid and durable enough to be part of load resisting system for final structure. Therefore, in practice these types of support are mostly ignored in the final design of structures.

Rigid Support

Rigid supports of excavation, such as slurry walls, secant piles, or tangent piles are very stiff, and they could be used as final structure for resisting lateral loads. In most cases, construction of an initial support system to protect structures that are in the vicinity of the excavation and to minimize the obstruction in the excavation area requires a rigid type of initial support system.

Next section will explain different types of rigid initial support system and their construction methods in detail.

Slurry Wall

Slurry wall is constructed by excavating a trench usually 80 cm to 150 cm thick, as it is required by the design. As excavation of the trench is progressing, it is stabilized by placement of bentonite slurry in place of the soil that is excavated. This excavation has to be extended as deep as it is required by the design for stability of the wall or if the bedrock elevation is high enough it will penetrate into it, until it can be assumed fixed at the bottom. Reinforcement steel or in most cases wide flange steel beams will be placed in the trench and the slurry is replaced by placing concrete from bottom to the top of the trench and removing the bentonite slurry as concrete is added. During the excavation, additional bracing such as struts or tiebacks will be used as required.

Tangent Pile Wall

Tangent pile walls are constructed by drilling circular shafts next (tangent) to each other along the excavation area. These shafts are 60 cm to 120 cm in diameter. Like slurry wall system, these piles have to extend below the invert level or lock into the rock, if it is possible. Steel casing will be used to keep the drilled shaft area open, during the soil removal. After drilling is complete, steel beams or reinforcement bars are placed in, and the shaft is filled with concrete. Steel casing can be removed as the concrete is placed in the shaft. Again, during the excavation additional support might be required for stability of the wall. Figure shows the construction sequence of a tangent pile system.

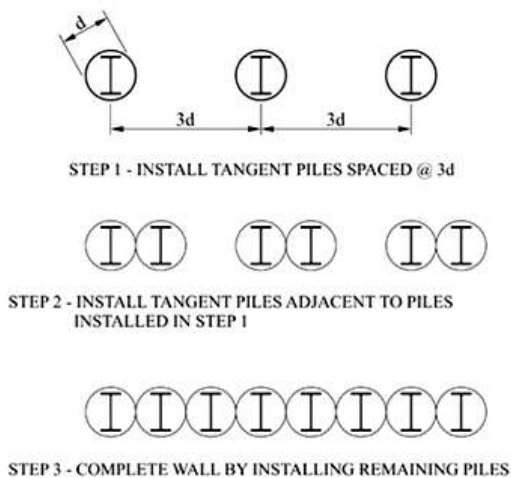


Figure 9.3. Tangent pile wall construction sequence (C. Jeremy Hung et al 2009)

Secant Pile Wall

Secant pile walls are constructed in a similar way that tangent pile walls are constructed. The only difference is that the drilled shafts have some overlap. This provides some more stiffness and water tightness for areas with high ground water elevation. Figure shows a completed secant pile wall.

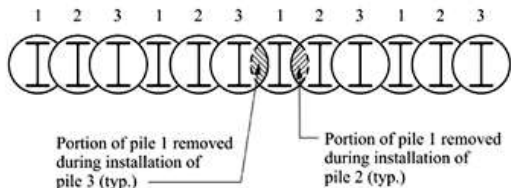


Figure 9.5. Completed secant pile wall (C. Jeremy Hung et al 2009)

Design Procedure for Cut and Cover Structures

All components of cut and cover structures shall be designed to sustain the most severe combination of service loads, such as, dead and live loads, surcharge, hydrostatic, earth pressure, shrinkage, thermal, differential settlement, impact loads due to train derailment, and seismic loads to which they may be expected to be subjected at any time. Based on an assumed construction sequence the effect of erection and other temporary loads occurring during construction shall be considered as well.

All design loads shall be combined according to applicable codes and specifications. Symmetrical and asymmetrical loadings are two major loading types that will create primary load combination for cut and cover structures.

Figures depict schematic presentation of the loads acting on a typical cut and cover tunnel for top-down and bottom-up construction in soil respectively.

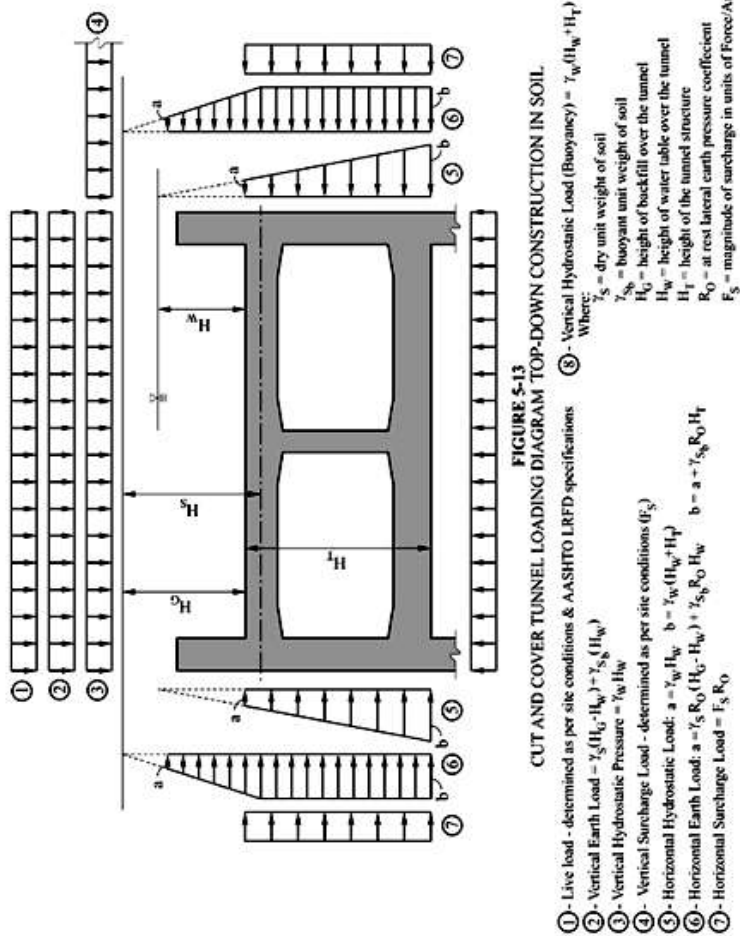
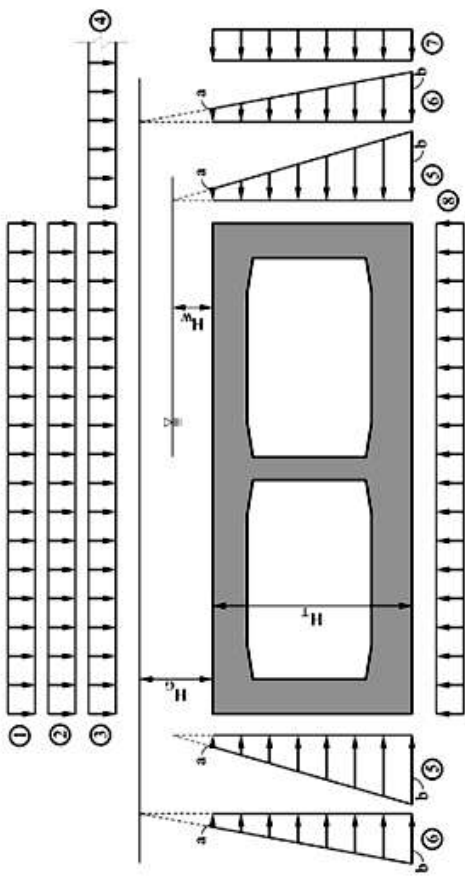


Figure 9.6. Typical loads acting on cut and cover tunnel Top - down construction (C. Jeremy Hung et al 2009)



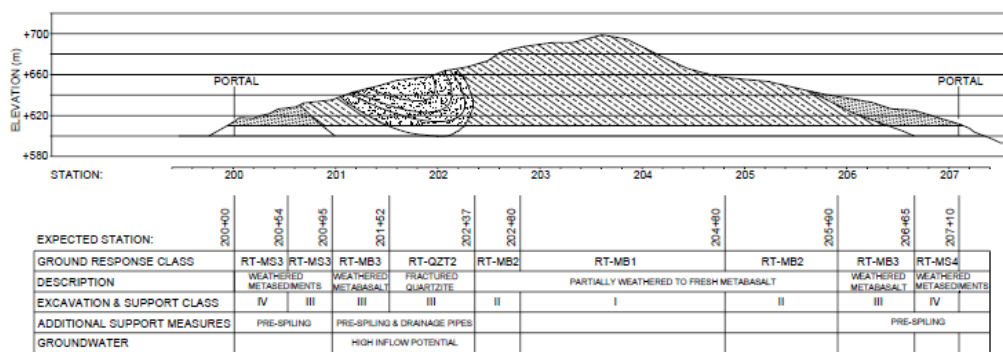
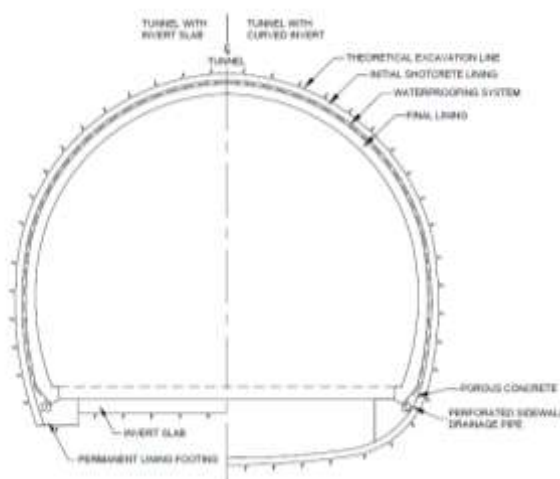
CUT AND COVER TUNNEL LOADING DIAGRAM - BOTTOM UP CONSTRUCTION IN SOIL

- ① - Live load - determined as per site conditions & AASHTO LRFD specifications
 - ② - Vertical Earth Load = $\gamma_s(H_g - H_w) + \gamma_b(H_w)$
 - ③ - Vertical Hydrostatic Pressure = $\gamma_w H_w$
 - ④ - Vertical Surcharge Load - determined as per site conditions (F_s)
 - ⑤ - Horizontal Hydrostatic Load: $a = \gamma_w H_w$ $b = \gamma_w(H_w - H_t)$
 - ⑥ - Horizontal Earth Load: $a = \gamma_s R_o (H_g - H_w) + \gamma_b R_o H_w$ $b = a + \gamma_b R_o H_t$
 - ⑦ - Horizontal Surcharge Load = $F_s R_o$
 - ⑧ - Vertical Hydrostatic Load (Buoyancy) = $\gamma_w (H_w + H_t)$
- Where:
 γ_s = dry unit weight of soil
 γ_b = buoyant unit weight of soil
 H_g = height of backfill over the tunnel
 H_w = height of water table over the tunnel
 H_t = height of the tunnel structure
 R_o = at rest lateral earth pressure coefficient
 F_s = magnitude of surcharges in units of Force/Area

Figure 9.7. Typical loads acting on cut and cover tunnel Bottom- up construction (C. Jeremy Hung et al 2009)

New Austrian Tunneling Method (NATM) or SEM

In NATM/SEM tunnels, a self-supporting arch within the surrounding ground is developed. The tunnel has typically dual lining as initial and final. Between these two linings typically water proofing and drainage system is provided. The cross-sections are usually curve-linear and sharp edges are avoided (Hung 2009). Usually the soil thickness above the NATM is around to have a minimum of one tunnel diameter. In shallow applications, multiple small excavations with intermediate temporary walls can allow to have 3 to 5 meters of soil thickness above the crown of the tunnel.



Description	Cross Section	Longitudinal Section	Photo
Intact Rock: <ul style="list-style-type: none"> Spot bolting Occasional sealing shotcrete Full face or top heading/bench excavation Round Length <ul style="list-style-type: none"> Top Heading: 8'-12" (2.5-3.7 m) Bench: Up to 16'-0" (4.9 m) Dimensions <ul style="list-style-type: none"> Height: 20'-0" (6 m) Width: 20'-0" (8.8 m) Example: Bergen Tunnels, NJ			
Stratified Rock: <ul style="list-style-type: none"> Systematic rock doweling Systematic shotcrete initial lining Top heading excavation Bench excavation follows distant Round Length <ul style="list-style-type: none"> Top Heading: 6'-6" (2 m) Bench: 6'-6" (2 m) Dimensions <ul style="list-style-type: none"> Height: 20'-6" (9 m) Width: 36'-0" (11 m) Example: Zederhaus, Austria			
Fractured Rock: <ul style="list-style-type: none"> Systematic rock doweling Systematic shotcrete initial lining Top heading excavation Bench excavation follows any time Round Length <ul style="list-style-type: none"> Top Heading: 7'-2" (2.2 m) Bench: 13'-0" (4.0 m) Dimensions <ul style="list-style-type: none"> Height: 28'-0" (8.5 m) Width: 36'-5" (11.1 m) Example: Devil's Slide Tunnels, CA			

Fig. Applications in Rock (Hung 2009)

Description	Cross Section	Longitudinal Section	Photo
Soft Ground – shallow cover: <ul style="list-style-type: none"> Systematic pre-support Systematic shotcrete initial lining support with early ring closure Top heading excavation (with temporary invert), bench and invert excavation Round Length <ul style="list-style-type: none"> Top Heading: I - 3'-3" (1 m) Top Heading: II - 6'-6" (2 m) Bench III/Invert IV - 6'-6" (2 m) Dimensions <ul style="list-style-type: none"> Height: 38'-0" (11.6 m) Width: 48'-0" (14.7 m) Example: Fort Canning Tunnel, Singapore			
Soft Ground – deep level: <ul style="list-style-type: none"> Systematic shotcrete support with early ring closure Top heading excavation closely followed by bench/invert excavation Round Length <ul style="list-style-type: none"> Top Heading: 3'-3" (1 m) Bench: 6'-6" (2 m) Dimensions <ul style="list-style-type: none"> Height: 20'-3" (6.3 m) Width: 20'-3" (6.3 m) Example: London Bridge Station, London, UK			

Fig. Applications in Soft Soil (Hung 2009)

Description	Cross Section	Longitudinal Section	Photo
<p>Soft Ground – deep level:</p> <ul style="list-style-type: none"> Systematic shotcrete support with early ring closure Sub-division into sidewall drifts Top heading excavation closely followed by bench and invert excavation Round Length <ul style="list-style-type: none"> Top Heading: 3'-2" (1 m) Bench: 6'-6" (2 m) Invert: 6'-6" (2 m) Dimensions <ul style="list-style-type: none"> Height: 30'-2" (9.2 m) Width: 37'-0" (11.3 m) <p>Example: London Bridge Station, London, UK</p>			

Fig. Applications in Soft Soil (Hung 2009)

TBM Tunnels

Analysis Types

Structural methods used to analyze TBM segmental linings must be able to indicate loads and deformations in accordance with the geologic and construction conditions and also represent the ground – lining interaction. There are various structural methods that satisfy these criteria. They include estimations based on empirical evidence, analytical solutions, and numerical simulations. General tendency for calculating the member forces of the TBM segmental lining is to perform numerical simulation. However, analytical methods are also commonly used to provide a collective check on the results. According to ITA – WG2, the member forces should be computed by using below mentioned methods:

- Elastic Equation Method
- Schulze and Duddeck Model
- Muir Wood Model
- Beam – Spring Method
- Finite Element Method

There is no unique solution in tunnel engineering. All of these methods have strengths and weaknesses. Also, each method mentioned above has some limitations that restrict the usage of them. For that reason, strengths, weaknesses, and limitations of the methods should be investigated in detail before selecting the proper method to be used in design.

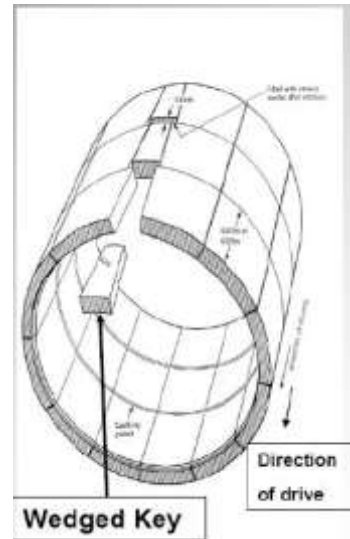


Figure 9.8.

Elastic Equation Method

The elastic equation method, also called as usual calculation method, is a simple method for calculating member forces of circular tunnels without a computer. This method is proposed by *Japanese Standard for Shield Tunnelling* and has been widely used in Japan. Key points of this method are provided in this section.

Load distribution model used for this method is shown in Figure 9.9. In the figure, P_0 is overload (surcharge); R_0 is the external radius of shield lining; R_c is the radius of middle line of shield lining; g is gravity of lining; P_{e1} and P_{w1} are, respectively, the vertical earth pressure and water pressure acted on the up side of shield lining. The lateral earth pressure and water pressure vary linearly and act on both sides of the shield lining. They are equal to q_{e1} and q_{w1} at the top of the shield lining, and q_{e2} and q_{w2} at the bottom of shield lining; P_{e2} and P_{w2} are respectively the vertical earth pressure and water pressure acted on the bottom side of shield lining; P_g is the vertical resistance of lining weight acted on the bottom side of shield lining.

For sandy clay, the earth pressure and water pressure are assumed to act on the lining separately. If the overburden thickness is two times larger than the external diameter D of shield lining ($h_0 \geq 2D$), an effective overburden thickness h_0 should be used and it can be determined by Terzaghi's formula

The distribution of horizontal earth resistance has a triangular shape and its application range is shown in Figure 9.9.

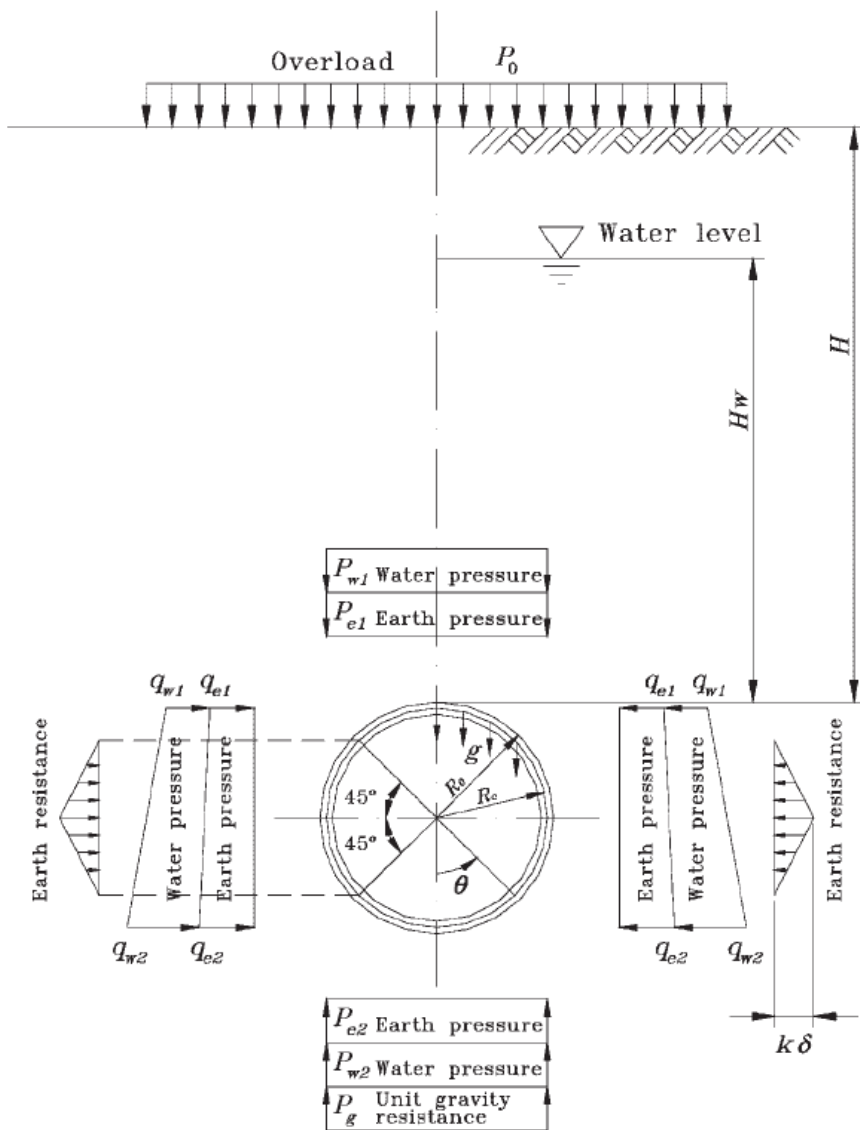


Figure 9.9. Load condition of Elastic Equation Method (*Japanese Standard for Shield Tunnelling*)

After having all parameters determined, the internal forces of the segmental lining can easily be computed. Elastic formulas for the calculation of member forces are given in Table 9.1.

Table 9.1. Equations of member forces for Elastic Equation Method (*Japanese Standard for Shield Tunnelling*)

Load	Bending Moment	Axial Force	Shear Force
Vertical Load (P = p _{e1} + p _{w1})	(1 - 2S2) * P * R _c ² / 4	S2 * R _c * P	-SC * R _c * P

Horizontal Load (Q = q _{e1} +q _{w1})	(1-2C2)*Q* R _c ² /4	C2*R _c *Q	-SC*R _c *Q
Horizontal Triangular Load (Q' = q _{e2} +q _{w2} - q _{e1} -q _{w1})	(6-3C-12C2+4C3)*Q'* R _c ² /48	(C+8C2-4C3)*Q'*R _c /16	(S+8SC-4SC2)*Q'*R _c /16
Soil Reaction (P _k = k _δ h)	$0 \leq \theta \leq \pi/4 : (0.2346-0.3536C)^* R_c^2 * k\delta$ $\pi/4 \leq \theta \leq \pi : (-0.3487+0.5S2+0.2357C3)^* R_c^2 * k\delta$	$0 \leq \theta \leq \pi/4 : 0.3536C^* R_c^* k\delta$ $\pi/4 \leq \theta \leq \pi : (-0.7071C+C2+0.7071S2C)^* R_c^* k\delta$	$0 \leq \theta \leq \pi/4 : 0.3536S^* R_c^* k\delta$ $\pi/4 \leq \theta \leq \pi : (SC-0.7071C2S)^* R_c^* k\delta$
Dead Load (P _g = π.g)	$0 \leq \theta \leq \pi/2 : (3/8\pi-\theta^*S-5/6C)^* R_c^2 * g$ $\pi/2 \leq \theta \leq \pi : [-\pi/8+(\pi-\theta)S-5/6C-1/2\pi*S2]^* R_c^2 * g$	$0 \leq \theta \leq \pi/2 : (\theta^*S-1/6C)^* R_c^* g$ $\pi/2 \leq \theta \leq \pi : (-\pi^*S+\theta^*S+\pi^*S2-1/6C)^* R_c^* g$	$0 \leq \theta \leq \pi/2 : (\theta^*C-1/6S)^* R_c^* g$ $\pi/2 \leq \theta \leq \pi : [-(\pi-\theta)^*C+\theta^*S+\pi^*SC-1/6S]^* R_c^* g$
Horizontal Deformation at Spring Line (δ _h)	$\delta_h = [(2P-Q')+\pi^*g]^* R_c^4 / [24^*(EI/h+0.045k^* R_c^4)]$		

θ= angle from crown, S= sin θ, S2= sin² θ, S3= sin³ θ, C= cos θ, C2= cos² θ, C3= cos³ θ. Segmental ring is composed of several segments which are connected by bolts or dowels. The deformation at these connection joints is larger than the one in a ring with uniform rigidity, because the rigidity of joints is less than the rigidity of segment section. Furthermore, the connections at the segment joints are generally staggered. However, this method assumes the segmental ring with uniform bending rigidity and can not represent the staggered geometry. Nevertheless, the solutions obtained by this method can be very practical and helpful for checking the results obtained by numerical methods. Also, this method is mostly used in preliminary design and cost estimation for a new tunnel project.

This method is more advantageous than other closed form solutions, because elastic equation method has a capability of calculating bending moment, axial force, and shear force of any point on the lining. However, other closed form solutions can only determine the bending moments and hoop forces at the point where relative maximum values occur.

Schulze and Duddeck Method

The thrust and bending moment in circular linings surrounded by an elastic medium can be determined by several closed form solutions such as Schulze and Duddeck Method. These closed form solutions deal only with tunneling models for soft ground and the some basic

assumptions are applied to derive a model such that the cross-section is circular, the material behavior of ground and lining is elastic, the active soil pressures on the lining are taken as equal to the primary stresses in the undisturbed ground, and there exists a bond between the lining and the ground for radial and tangential deformations .

The complete and closed solutions for the model intended for shallow tunnels ($H \leq 6R$) limited overburden is published by Schulze and Duddeck in 1964. Surrounding ground is represented by ground springs. Since tension springs may cause load reduction, bedding at the crown is omitted. The results of this study is given as direct design diagrams for bending moments, hoop forces, and radial displacements for those three points of the lining where relative maximum values occur. In this method, modulus of subgrade reaction (K_r) is a free parameter and the tangential stresses may be included in or omitted from the load parameters.

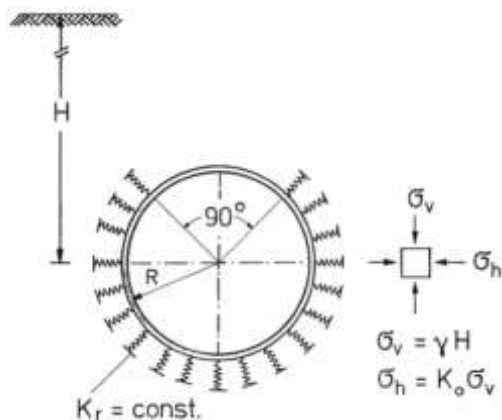


Figure 9.10. Bedded ring model without crown bedding

Muir Wood Method

Muir Wood Method is another closed form solution used to determine hoop forces, bending moments, and radial displacements. Like most closed form solutions, this model is based on the assumption that the ground is an infinite, elastic, homogeneous, and isotropic medium. Also, the basic assumptions for closed form solutions determined in the previous section are valid for this method.

Muir Wood model is based on plain strain continuum model shown in Figure 9.11. This method assumes that the circular lining deforms into an elliptical mode. The tangential ground stresses are included, but radial deformations due to the tangential stresses are omitted. Muir Wood proposed to take only 50% of the initial ground stresses into consideration that allows for some pre-decompression of the ground around the opening before the lining is placed. By reducing the lining stiffness by an amount equivalent to the effect of less rigid joints, the moments can be reduced.

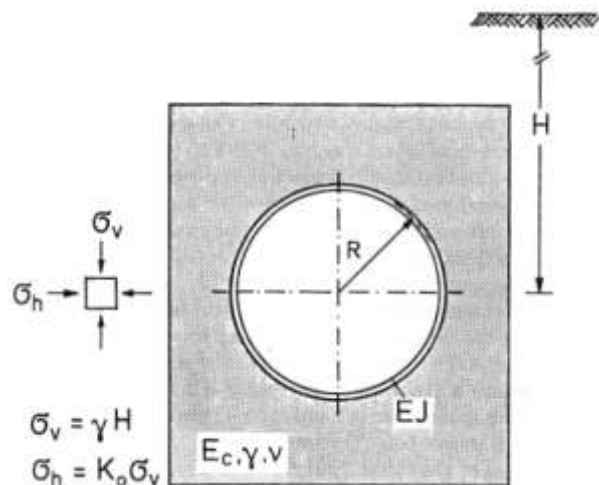


Figure 9.11. Plain strain continuum model

9.1. Beam – Spring Method

The Beam – Spring Method, also called as "Coefficient of Subgrade Reaction Method", is illustrated in Figure 9.12. In this method, the lining is generally represented by an arc, reduced to a polygon with fixed angles. Each piece of lining is supported by springs whose elasticity represents the ground reaction. In other words, the lining and ground are represented by a series of beams and springs respectively. It is assumed that the ground reaction is generated from the displacement of the lining proportionally to the deformation of ground. This assumption allows the consideration of the interaction between the segments and the surrounding ground.

In the applications of this method, the ground springs are commonly assumed to be effective in radial direction, but there are also exceptional examples assuming that the ground springs are also effective in the tangential direction. In order to produce conservative (safe) results, soil springs that act only in radial direction are used to represent the surrounding ground. This assumption means that frictionless sliding of the lining against the ground occurs.

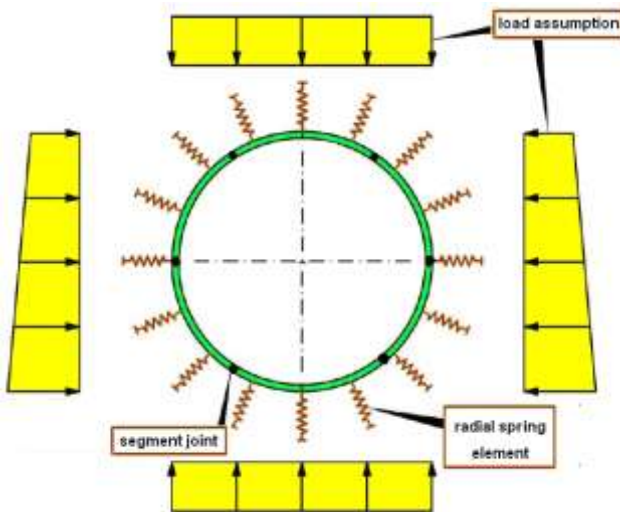


Figure 9.12. Model of Beam – Spring Method

Structural analysis with Beam – Spring Method is also based on the assumption that soil reaction forces are activated when the tunnel expands outward, but they are not activated when the tunnel contracts inward. For that reason, non-tension ground springs are used to represent the interaction between the lining and surrounding ground.

Segmental rings are generated by assembling several segments with bolts or dowels. These connection joints between the segments have a lower rigidity than main section of the segment. Therefore, the deformation of a segmental ring tends to be larger than a ring with uniform bending rigidity. At this point, evaluation of the decrease of rigidity at joints has an importance for calculating the member forces. For this purpose, various 2D approaches have been developed in order to evaluate the segment joints. In this sense, there exists several design models that assume the segmental ring as a solid ring with fully bending rigidity, solid ring with reduced bending rigidity, ring with multiple hinged joints, ring with rotational springs, and etc. These approaches are explained and discussed in Chapter 3.6.

The segments are assembled in a staggered pattern to compensate the decrease in the bending rigidity of the ring joint. Although 2D models are able to evaluate lining – ground interaction and the reduction of bending rigidity due to segment joints, they can not represent ring joints and the staggered arrangement of segments in adjoining rings. Unlike 2D models, the coupling of the adjacent rings and staggered arrangement of segments can be evaluated by 3D BSMs as illustrated in Figure 9.13.

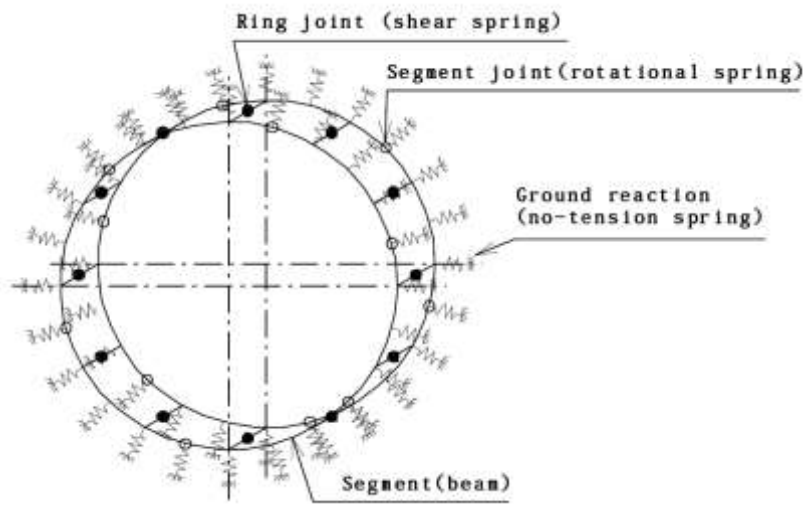


Figure 9.13. 3D Beam – Spring Model

As shown in Figure 9.13, this 3D model has an ability to evaluate the reduction of bending rigidity and splice effects of staggered geometry by using a model in which a segment is considered as a curved or straight beam, a segment joint as a rotational spring, and a ring joint as a shear spring. Like 2D model, ground reaction is represented by non-tension springs. In addition, minimum two or more rings are used in the 3D analysis in order to evaluate the coupling of rings, the effect of joint locations and combinations, and shear stresses on a ring joint.

Design procedure, design stages, loading types and conditions, and structural calculation used in the design of segmental linings are briefly discussed in Chapter 4.

Finite Element Method

Finite Element Method (FEM) which is illustrated in Figure 9.14 is one of the most widely used numerical methods in geomechanics. It is a continuum model but discontinuities can also be modeled individually. In FEM, the hosting ground is discretized into a limited number of smaller elements. These elements are connected at nodal points. The stress, strain, and deformation to be analyzed are caused by changing the original subsurface conditions. For instance, such change might be induced by tunneling process. The stresses and strains generated in one element effects the interconnected elements, and so forth [6].

The stress-strain relationships of the elements are modeled mathematically by creating a global stiffness matrix which relates the unknown quantities with known quantities. Then, this matrix is solved using standard matrix reduction techniques and the results are obtained. The equations to be solved are highly complicated, and as the number of the elements in the model increase, the calculation time and the storage capacity increase dramatically.

By means of FEM, complex underground conditions and tunnel characteristics can be analyzed. Furthermore, this method enables the simulation of complex constitutive laws, non-homogeneities, and the impact of advance and time dependent characteristics of the construction methods.

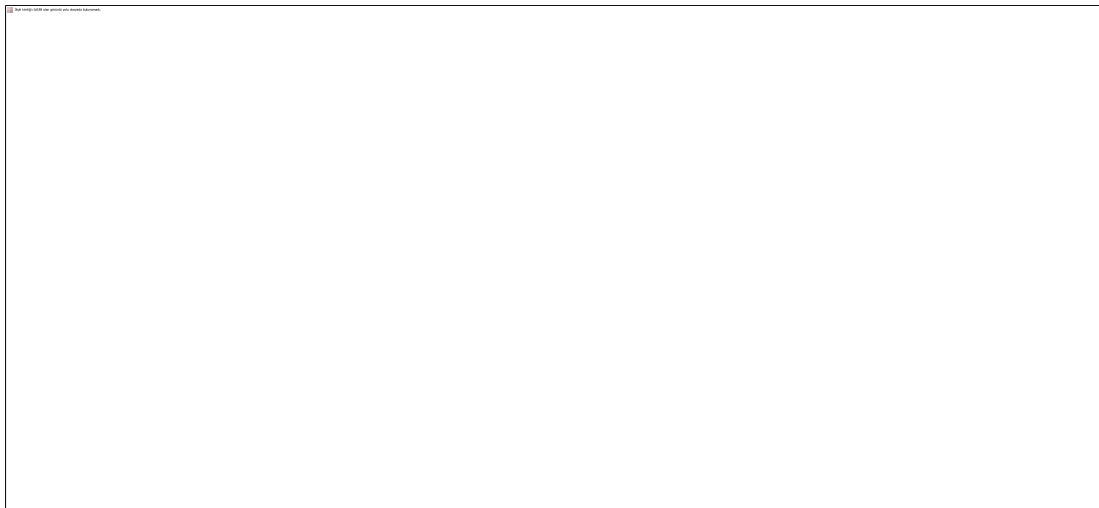


Figure 9.14. Finite element method for tunnel engineering

On the other hand, most FEM programs require more knowledge on program and computer than other methods do. Typically the output of the analysis is also complex and it becomes difficult to assess the results. Therefore, a post-processor may be utilized in order to overcome this difficulty.

Theoretical Approaches on Beam – Spring Method

Since Beam – Spring Method is the most effective and practical tool for the calculation of member forces of TBM segmental linings, several theoretical approaches have been developed in this field. The main determinant criteria in BSMs are the ground lining interaction and connection joints. For ground lining interaction, most approaches employ non-tension elastic ground springs. However, these approaches have different methods to evaluate connection joints. Therefore, these theoretical approaches can be classified by joint evaluations.

Selecting the proper structural model in order to calculate the member forces of TBM segmental linings should be done carefully, because it depends on several conditions, such as usage of tunnel, design loads, geometry and arrangement of segments, ground conditions, and required accuracy of analysis. Schematic drawings of structural models outlined by JSCE are illustrated in Figure 9.15.

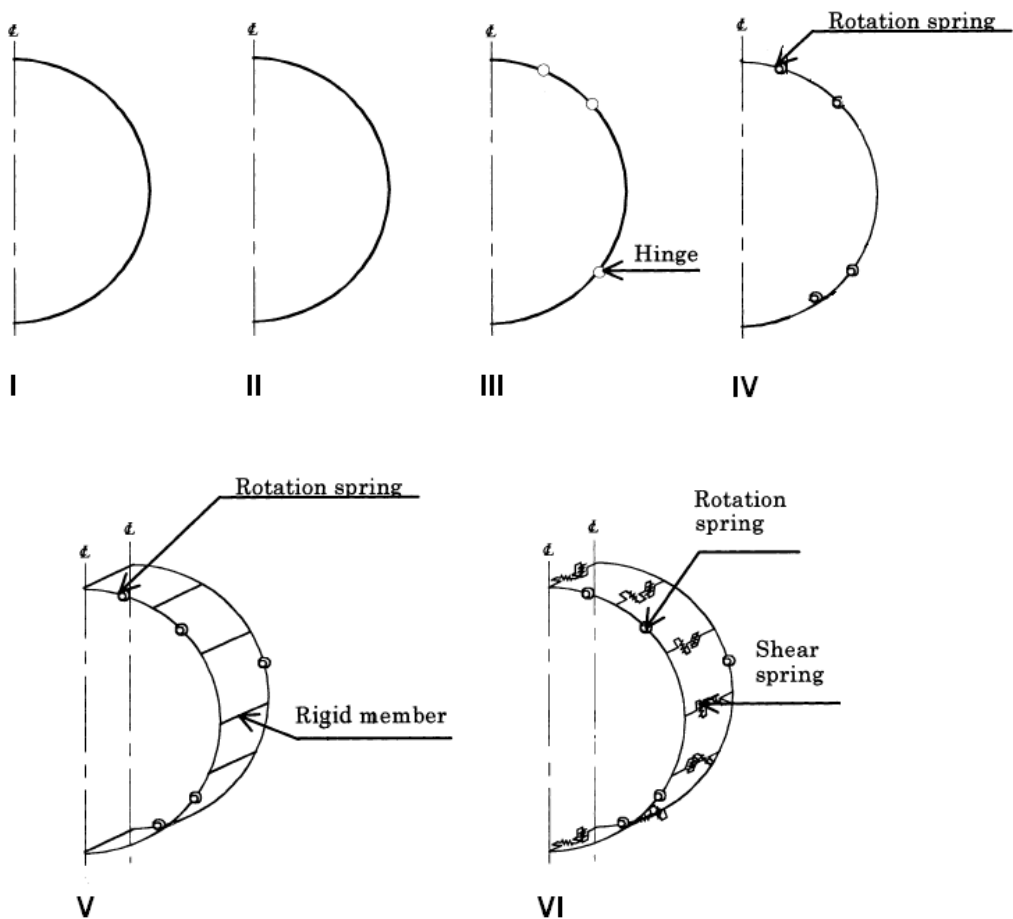


Figure 9.15. Structural design models for TBM segmental linings

Available structural models in the literature are summarized in Figure 9.15. 2D models (I-IV) are able to represent only segment joints by using reduced rigidity, hinges, or rotational springs. However, 3D models (V-VI) can simulate both segment joints and ring joints. In 3D models, segment joints are represented by rotational springs, and ring joints are modeled as rigid members or shear springs.

The common part of these BSMs is the ground – lining interaction. It is simulated by non-tension elastic ground springs in radial direction as shown in Figure 9.12 and Figure 9.13. The soil spring constant is calculated using the following theoretical formulas proposed by Muir Wood, in accordance with AFTES – WG7 Appendix 1 [28].

$$k = \frac{E}{(1 + \nu) \cdot R} \quad (9.1)$$

where, k : Modulus of subgrade reaction of the ground in the radial direction (kN/m^3),
 E : Modulus of deformation of ground (kN/m^2),
 ν : Poisson's ratio,

R : Outer radius of segment (m).

$$k_r = k \cdot A_t = k \cdot l_s \cdot w \quad (9.2)$$

where, k_r : Soil spring constant in the radial direction (kN/m),
 k : Modulus of subgrade reaction of the ground in the radial direction (kN/m³),
 A_t : Tributary area (m²),
 l_s : Distance between soil springs (m),
 w : Width of segment (m).

Structural models given in Figure 9.13 are sorted from the simplest one to the most complicated one, and also show the development of the approaches. After the conditions of tunnel project are denoted, structural calculations of segmental linings can be performed by a single model. In order to decide on the proper model, all models should be investigated.

In **Model I**, the segmental ring is assumed to be a ring with uniform bending rigidity. The decrease of rigidity at segment joints is ignored and a segmental ring is treated as a ring with uniform bending stiffness EI as a main section of a segment [24]. In other words, this model can be named as “solid ring with fully bending rigidity”. This is the simplest 2D model and can not evaluate the connection joints. Therefore, this model gives more conservative results than the others.

In **Model II**, the segmental ring is again assumed to be a ring with uniform bending rigidity, but bending rigidity is reduced in order to simulate the effects of segment joints. There are different approaches for the reduction of bending rigidity.

Bickel, Kuesel, and King have proposed a 2D model that simulates the segment joints by using reduced stiffness parameters. This model assumes that the stiffness (effective modulus of elasticity) of a segmental ring is half that of a monolithic ring and the moment of inertia of practical coffered precast segments ranges from 60 to 80% of that of solid sections with the same thickness. Due to reduced stiffness, this model is more flexible than Model I and expected to give less values for bending moment and hoop forces.

Furthermore, Koyama and Nishimura have recommended a model in a similar manner with the former model proposed by Bickel, Kuesel, and King. According to these Japanese researchers, the tunnel lining is assumed to be a continuous ring with a discounted rigidity by applying a reduction factor, η , to the bending rigidity (EI) of the tunnel lining. Koyama and Nishimura [31] suggested determining η by full ring structural testing. If experimental data are not available, the value of η can be assumed to be in the range of 0.6 – 1.0 for preliminary design analysis. For instance, a continuous monolithic ring beam having a constant effective rigidity ratio of $\eta= 0.8$ was used in the design of the Trans-Tokyo Bay Highway tunnel lining (Uchida 1992). The value of η adopted in the tunnel project was later verified by tests on a full-scale prototype segmental lining.

Muir wood investigated the effects of joints between the segments and proposed an easy to use empirical formula to estimate the effects of the longitudinal joints of rings in a calculation with a homogeneous rigid ring by reducing the bending stiffness of the lining. The effective moment of inertia, I_e , for a segmental tunnel ring with a number of equal segments can be expressed as follows.

$$I_e = I_j + \left(\frac{4}{n}\right)^2 \cdot I \quad I_e \leq I, n > 4 \quad (9.3)$$

where, I_e : The effective moment of inertia,
 I_j : The moment of inertia at the force transmission zone between the joints,
 I : The moment of inertia of the lining section,
 N : Number of segments (key segment not counted).

Muir Wood suggested that the existence of segment joints would not affect the rigidity of the lining for four or fewer lining segments. The earth pressure acting around a tunnel is assumed to be in an elliptical shape in this model. In order to obtain this elliptical shape for initial loading, sufficient overburden thickness is required. Therefore, Muir Wood model is more convenient for deep tunnels. This assumption may not be valid for shallow tunnels.

First two approaches given for **Model II** make some assumptions for the effect of segment joints. However, the effects of the number of segments are not considered. Although Muir Wood model takes into consideration the number of segments, it can not simulate joint orientation. According to numerical studies done by Hefny, Tan, and Macalevey , the values of moments induced in the lining are reduced by 8 times by orientating the joints with an angle of 45° . This shows that in addition to the number of segment joints, the orientation of joints also affects the member forces considerably. Since these effects may lead to large reduction in costs, they should be conceived.

Model III assumes the segmental ring as a ring having several hinges. This model is used in United Kingdom and Russia, where ground conditions are relatively good i.e. hard rock. In this model, segment joints are modeled as unfixed hinges. Afterwards, deformation is calculated and checked for safety. This model gives considerably less bending moments and leads to more economical design for the grounds in good condition. Since this method fairly depends on ground conditions, adequate study should be done in order to determine whether the model is suitable for the existing ground or not .

Model IV simulates not only the number of segment joints but also the joint orientation. Segment joints are modeled as rotational springs as illustrated in Figure 9.16a. The crucial point for this model is the calculation of rotational spring constant. For the behavior of rotational stiffness of longitudinal joints, worldwide accepted formulas proposed by Janssen based on the investigation of Leonhardt and Reimann for the resistance against rotation and bending of concrete hinges are used.

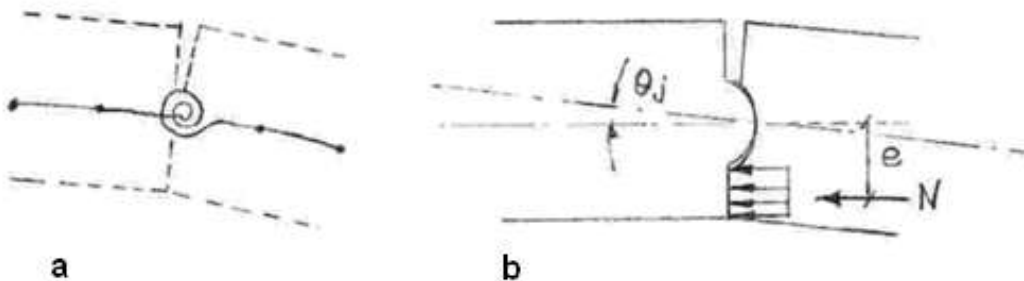


Figure 9.16. a) Rotational spring model, b) Stress distribution at the segment joint [37]

While developing the theoretical formula of Leonhardt and Reimann concerning concrete joints, the following assumptions are made on the basis of fundamental experimental results and observations concerning concrete joints.

- Tensile stress is not transmitted at joints.
- Compression stress has linear distribution.
- The deformation coefficient is constant, having the magnitude of E_0 , the initial connection elasticity coefficient in $\sigma = \epsilon = 0$.
- The scope of deformation in the acting direction of axial force is centered on the joint surface, and limited to the same scope as the width of the convex portion of the joint. Strain is distributed uniformly.

The theoretical formulas based on the above assumptions and the geometric relationships are developed as follows and shown in Figure 9.17.

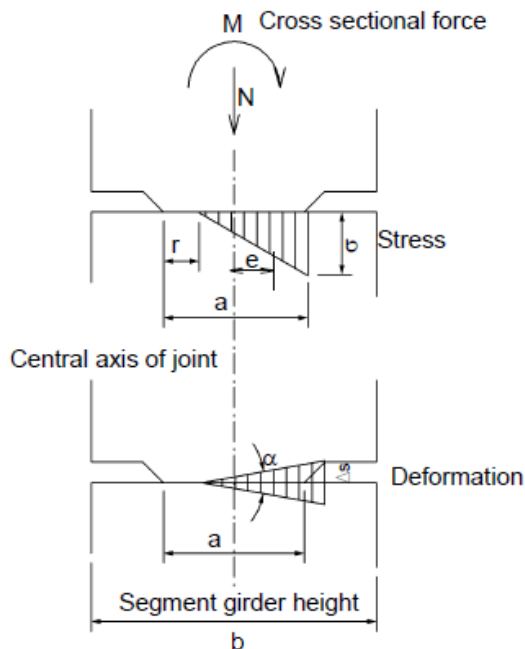


Figure 9.17. Stress and deformation in mortised portions

As long as the joint is fully compressed, the rotational stiffness is constant and could be described by the belowmentioned formula.

$$k_\theta = b \cdot \frac{E \cdot a^2}{12} \quad . \quad (9.4)$$

It depends only on the young's modulus E, the width of contact zone a, and the height of the segment b. If this bending moment exceeds the boundary bending moment

$(M_{bou} < N.b/6)$, the joint is gaping like a bird's mouth as shown in Figure 9.16b. From this point, the rotational stiffness depends on the normal forces N and the bending moment M . It can be determined by the following formula.

$$k_\theta = M / \alpha = \left(9 \cdot \frac{b \cdot a^2 \cdot E}{8} \right) \cdot m \cdot (1 - 2 \cdot m)^2 \quad (3.5)$$

where k_θ : Rotational spring constant of joint (kN.m/rad)

α : Rotational angle (rad)

M : Bending moment (kN.m)

M : Load eccentricity rate, $m = e/a = M / (N.a)$

N : Axial force (kN)

B : Contact zone (mortise) length (m)

A : Contact zone (mortise) width (m)

E : Young's modulus of concrete (kN/m²)

In order to employ this behavior, the above mentioned relationship between bending moment and rotational stiffness should be performed by non-linear rotational springs. Since rotational springs become extremely soft if the moment increases to more than about 80 % of the maximum moment, it is not necessary to define a yielding moment. Therefore, if only a linear rotational spring with the definition of a yielding moment is modeled, the simulation of behavior of segment joint seems to be very poor .

Model V, a 3D beam – spring model, is proposed by Koyama . This model simulates the segment joints as rotational spring like model IV and supposes a rigid connection between the rings by using rigid members. It is assumed that the displacement of the ring beam is equal to that of the neighboring ring beam at the joint. Therefore, no gap occurs due to the shear stress. However, relative displacement between the two neighboring rings occurs in the longitudinal direction, and is concentrated at the centerline of the segmental rings [39].

Model VI, also proposed by Koyama , is an advanced version of model V. Differently from Model V, connection between the rings is modeled as shear springs. Calculation of shear spring constant is a complex issue because it depends on many factors such as type of ring joint (flat, cam-and-pocket, tongue-and-groove), type of connectors (bolt, dowel), number, and orientation of connectors, loading on the ring, etc. Therefore, a general formula for determining the shear spring constant is not available. For that purpose, the compression characteristics of the shear strip are determined according to the relationship between the load and the displacement of materials used. This relation can be obtained by laboratory tests using actual joints. Figure 3.10 shows the relationship between deformation and the force acting on the shear strip during the application of shear force on the ring joint. Based on the figure, the shear spring constant (k_s) is calculated geometrically as follows:

$$k_s = \frac{F}{\delta} = \frac{F_n / \cos \theta}{\delta_n / \cos \theta} = \frac{F_n}{\delta_n} \quad (3.6)$$

where k_s : Shear spring constant in radial direction (kN/m),

F : Shear force acting on the joint (kN),

F_n : Vertical component of force on shear strip (kN),

δ : Total displacement of shear strip (m),

δ_n : Vertical component of compression displacement of the

shear strip (m).

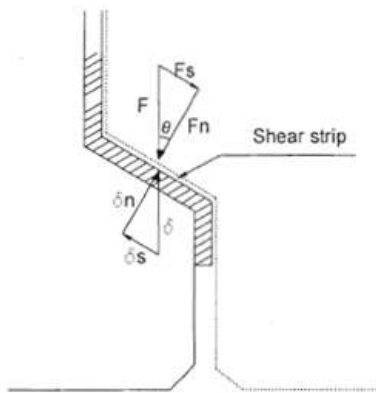


Figure 9.18. Forces acting on the ring joints and joint displacements

For the 3D analysis of segmental rings, the shear spring constant is generally obtained by laboratory tests or by experience of other comparable projects. However, if flat (plate) ring joints with plywood hardboards are used, the following formula for the shear stiffness of plywood can be used to determine shear spring constant [36].

$$k_s = \frac{G \cdot A}{d} \quad (9.7)$$

where k_s : Shear spring constant in radial direction (kN/m),
 G : Shear modulus of plywood (kN/m²),
 A : Area of hardboard (m²),
 D : Thickness of hardboard (m).

Among the models in scope, this model is the unique one that can simulate the interaction between adjacent rings. If spring constants are calculated properly, the most realistic results can be obtained with this model.

2D and 3D Analysis of TBM Segmental Linings

Tunneling is a 3D problem where structural behavior of tunnel in the longitudinal direction and the analysis of loads during and after the construction may play an important role in the design of tunnels. Numerical methods in tunnel engineering have been widely used with a steady growth since the early applications in the mid 1960's. This is most probably due to the fact that numerical methods are capable of simulating the excavation, construction, and service steps. In contrast with analytical solutions, these are the distinctive advantages for numerical methods [40].

Although 3D numerical analysis of tunnels can simulate the structural behavior of tunnel in the longitudinal direction and construction process, 2D numerical studies in tunneling are much more popular than the 3D analysis. 2D analyses assume plane-strain conditions for the lining and ground. This leads to avoiding three-dimensional effects. This type of simplifications made by performing 2D numerical analysis make the calculations easier and less time consuming, but they are not able to simulate 3D effects. In other words, 2D

numerical methods are suitable for some cases, but they are not as accurate as 3D models. For that reason, it is crucial to identify which situations are convenient for 2D or 3D analysis. Consequently, the aim of this study is to evaluate available analysis methods (analytical, 2D and 3D numerical) for TBM segmental lining and propose suitable type of analysis for certain situations.

Blom at al. investigated the stresses due to tunnel excavation by implementing 3D finite element model analyses for shield-driven Green Heart Tunnel. They have also compared the results obtained by 3D finite element analyses with analytical method (Schulze and Duddeck Model) and on-site measurements. This study showed that the results of 3D finite element model were so consistent with values obtained by on-site measurements, and 3D analysis simulated the stress distribution realistically. However, sectional forces predicted by analytical model did not fit well to on-site measurements. It can be concluded that 3D finite element models simulate the stresses and structural behavior of tunnels much more realistically than conventional methods.

Klappers at al. made a comparison between 3D Beam – Spring Method and 3D FEM analysis with shell elements. This comparison showed that the calculated sectional forces of both models were more or less the same, and also only deformations differed slightly. This means that 3D FEM calculations are not necessary for normal loading conditions. For special cases like openings in the lining, different loads on the rings or varying bedding conditions, 3D FEM modeling is needed to calculate internal forces and deformations. Mashimo and Ishumura [29] investigated loads acting on the shield tunnel lining by using 3D BSM. This study also revealed that 3D BSM gives realistic results if loading conditions and spring constants are calculated accurately.

Previous studies showed that 3D Beam – Spring Method is a useful tool in order to obtain sectional forces of TBM segmental linings. In this thesis study, an analytical method (elastic equation method), 2D beam – spring methods with different approaches and 3D beam – spring method will be evaluated and validity of methods for certain situations will be determined.

Results shall be presented

Section 10

Review Of Seismic Design Procedures For Cut And Cover Structures

Underground facilities, such as tunnels, are a crucial part of the transportation infrastructure. Due to their strategic importance, loss of functionality in an earthquake is not an acceptable performance criterion for tunnels. It is expected that tunnels can withstand the maximum credible earthquake without significant damage and loss of their function. While the structural performance of underground facilities during the past earthquakes were considerably better than the performance of bridges or above ground facilities (Dowding and Rozen 1978; Rowe 1992), significant structural damage has been reported during the 1971 San Fernando and 1995 Kobe earthquakes (C. Jeremy Hung et al 2009), see also Figure 10.1.



Figure 10.1. Reinforced concrete column failure observed in a cut-and-cover tunnel during 1995 Kobe Earthquake (C. Jeremy Hung et al 2009)

Seismic analyses and design procedures and guidelines are well established for bridges, and above ground structures. However, seismic design of underground facilities has received very little attention in the past. In fact, prior to 1960's, earthquake loading was not accounted for in the design process of underground structures (Wang 1993). Even today, there are very few, or no seismic design provisions for tunnels in most design codes.

Review of Seismic Analysis Procedures for Rectangular Tunnels

Analytical studies conducted in the last thirty years show that cut and cover tunnels are subjected to racking, axial and curvature deformations during a seismic event (Owen and Scholl 1981, Wang 1993). Figure illustrate these three deformation modes schematically.

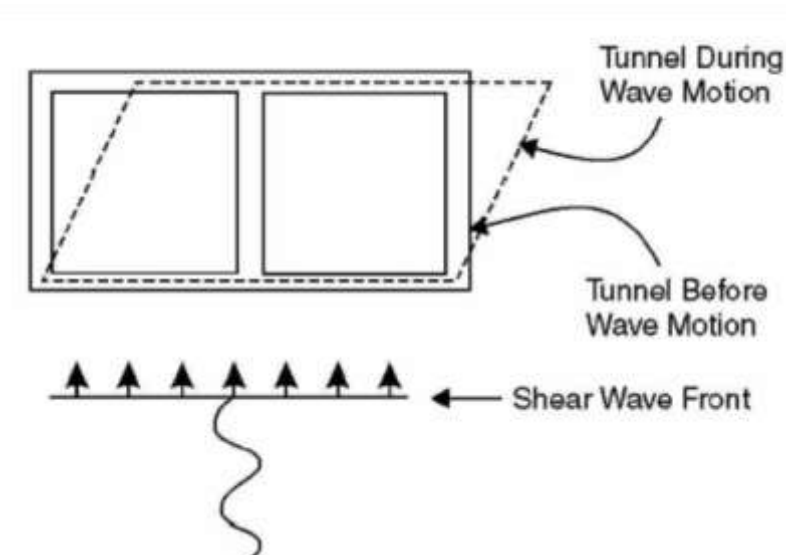
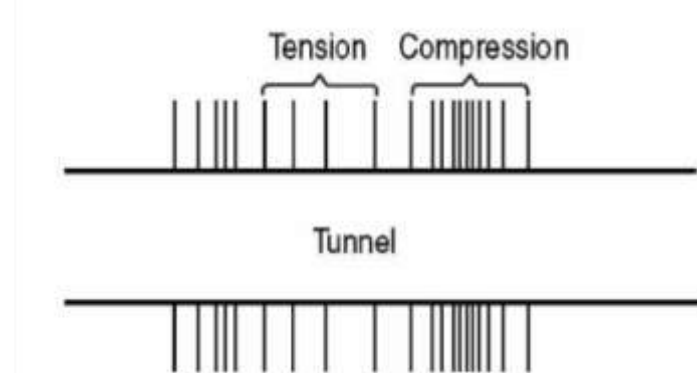


Figure 10.2. Racking deformation of a rectangular tunnel under vertically propagating shear waves (Wang 1993)



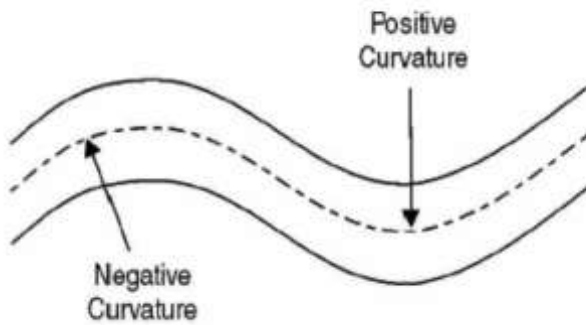


Figure 10.3. Axial and curvature deformation of tunnels under seismic loading (Owen and Scholl 1981)

As discussed in detail by Owen and Scholl (1981) and Wang (1993), the racking deformation caused by the vertically propagating shear waves is considered the most critical response of a rectangular cut and cover structure. Hence, different methods are proposed to determine the racking deformation of cut and cover structures.

These methods are categorized into three groups, namely:

- pseudo-static method
- free-field racking deformation method
- simplified tunnel-ground interaction method

These methods are explained in more details next.

Pseudo-static Methods

Pseudo-static methods, such as the Mononobe-Okabe method (Okabe 1926, Mononobe and Matsu 1929) or the procedure proposed by Wood (1973) are used to determine the dynamic earth pressure acting on the side walls of underground cut and cover structures (Anderson et al. 2008). The pseudo-static methods are usually based on the peak ground acceleration of the maximum creditable earthquake, and they ignore the frequency content of the ground motion.

The Mononobe-Okabe method, which was originally developed for seismic analysis of above ground yielding retaining walls, inherently assumes that the (above ground) retaining wall can tilt and/or move such that a Coulomb type soil wedge can form in the back-fill. Thus, the pseudo-static active earth pressure caused by the dynamic excitation is assumed to be due to the inertia force acting on the wedge. However, as discussed by Wang (1993), Hashash et al. (2001), and Hung et al. (2009), this assumption, that is, the tilting and/or moving wall, is not applicable for underground structures. During a seismic event, the cut and cover structure and the surrounding soil will move together, and a Coulomb type soil sliding wedge,

will not form. Consequently, the “Mononobe-Okabe” method will provide unrealistic results. The data and subsequent detailed analysis done by Ostadan (1997) have clearly shown that the seismic soil pressure is a result of the interaction between the soil and the structure during a seismic event. In fact, the deeper the tunnel embedment, the less realistic become calculated forces using the “Mononobe-Okabe” method. In fact, the effect of the structure's embedment and variation of the seismic forces with depth is not measurable in this method.

On the other hand, the analytical solution proposed by Wood (1973) is valid for non-yielding rigid buried walls. Although, the solution is based on dynamic modal analysis, in practice a horizontal pseudo-static body force is applied to the buried non-yielding rigid wall. Cut and cover tunnels are relatively flexible structures, and due to the rigid wall assumption, Wood method is not recommended for seismic design of such structures. In addition, this method does not include the wave propagation and amplification of the motion due to the geometry of the structure and soil properties.

Free-Field Racking Deformation Method

In the free-field racking deformation method, the stiffness of the underground structure is ignored, and the displacement demand of the underground structure subjected to a seismic event (that is racking demand) is assumed to be equal to the free-field deformation. Schematic presentation of this popular procedure, which is used in the design of San Francisco BART subway stations (Kuesel 1969) and Los Angles Metro project (Merritt 1991), is given in Figure 10.4

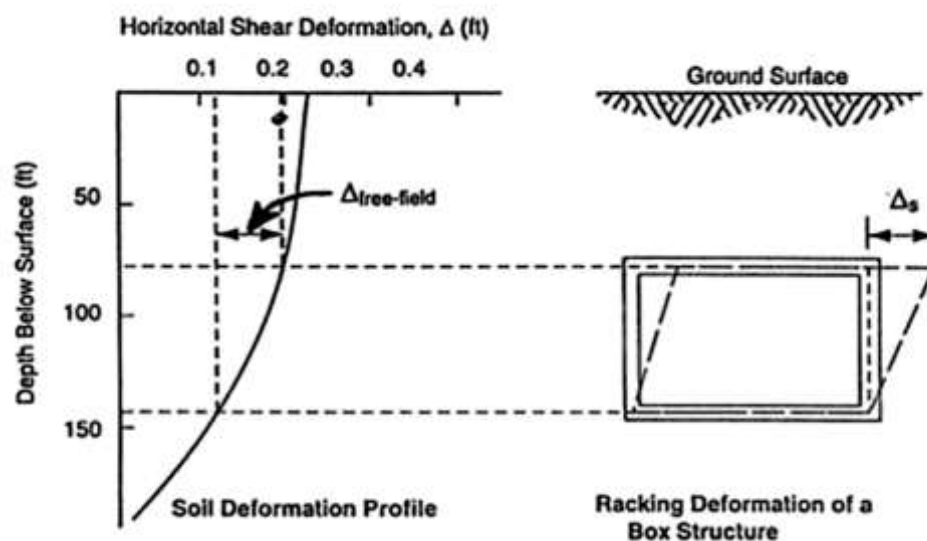


Figure 10.4. Schematic presentation of the free-field racking method (Wang 1993)

While the free-field racking deformation method is very attractive due to its simplicity, it will produce realistic results only if the flexibility of the underground structure is comparable with

the surrounding soil medium. However, the stiffness of a cut and cover tunnel located in soft soil can be much higher than the stiffness of the soil, such that it may deform less than the medium. In such cases, the free-field racking deformation method will produce very conservative demand estimates, as demonstrated by Wang (1993). This method is suitable for cases that the ground distortions are small.

Simplified Tunnel-Ground Interaction Analysis

Performing dynamic analysis on buried structures and tunnel are much more complicated compared to the above ground structures. Closed form solutions for tunnel-ground interaction are available for circular tunnels but due to the variable geometric characteristics of the cut and cover rectangular tunnels, these types of solutions are not available for cut and cover structures. Therefore, a simplified tunnel-ground interaction method will be a useful tool for engineers to overcome this problem.

Wang (1993), Penzien (2000), Nishioka and Unjoh (2003) proposed simplified tunnel-ground interaction curves to be used in the seismic analysis and design of cut and cover structures.

Wang (1993) conducted a series of finite element studies to study the dynamic response of cut and cover structures. In the finite element analyses, the soil medium and the structure are assumed to be (equivalent) linear elastic and no-slip between soil and concrete is assumed (Wang 1993). Based on the analyses, Wang (1993) reported that the seismic demand of a cut and cover structure was influenced by the relative stiffness of the underground structure with respect to the surrounding soil, structure geometry and embedment depth of the tunnel, in addition to the characteristics of the ground motion corresponding to the design earthquake.

Based on thirty-six dynamic finite element analyses, Wang (1993) concluded that the seismic racking demands in a cut and cover structure could be expressed as a function of flexibility ratio F_r , defined as (Wang 1993):

$$F_r = \frac{G_m W}{K_s H} \quad (10.1)$$

G_m : the average (equivalent or strain-compatible) shear modulus of the soil

K_s : the racking stiffness of the cut and cover structure

W : the width of the cut and cover structure

H : the height of the cut and cover structure

Based on the flexibility ratio calculated using equation (3-1), the racking coefficient is given as (Wang 1993):

$$R_r = \frac{\Delta_s}{\Delta_{ff}} = \frac{4(1-\nu_m)}{3-4\nu_m + F_r}$$

(10.2)

ν_m : the Poisson's ratio of the medium

Slip between the cut and cover tunnel and the soil medium were investigated later by Penzien (2000). Based on a series of finite element analyses, Penzien (2000) proposed a racking coefficient, which reads:

$$R_r = \frac{\Delta_s}{\Delta_{ff}} = \frac{4(1-\nu_m)F_r}{2.5 - 3\nu_m + F_r}$$

(10.3)

Figure compares the racking coefficient functions proposed by Wang (1993), and Penzien (2000). From Figure , it can be observed that the contribution of slip on the racking response is negligible. Furthermore, Figure shows that when the flexibility ratio is equal to unity, the racking coefficient is also equal to unity. In other words, when the soil stiffness equals to the structure stiffness, the racking deformation equals to the free-field deformation. When the flexibility ratio is less than unity, the free-field deformation is de-amplified, that is, the racking deformation is less than the free-field deformation. When the flexibility ratio is above unity (stiff soil, flexible tunnel) ground motion will amplify, such that the racking deformation is larger than the free-field deformation.

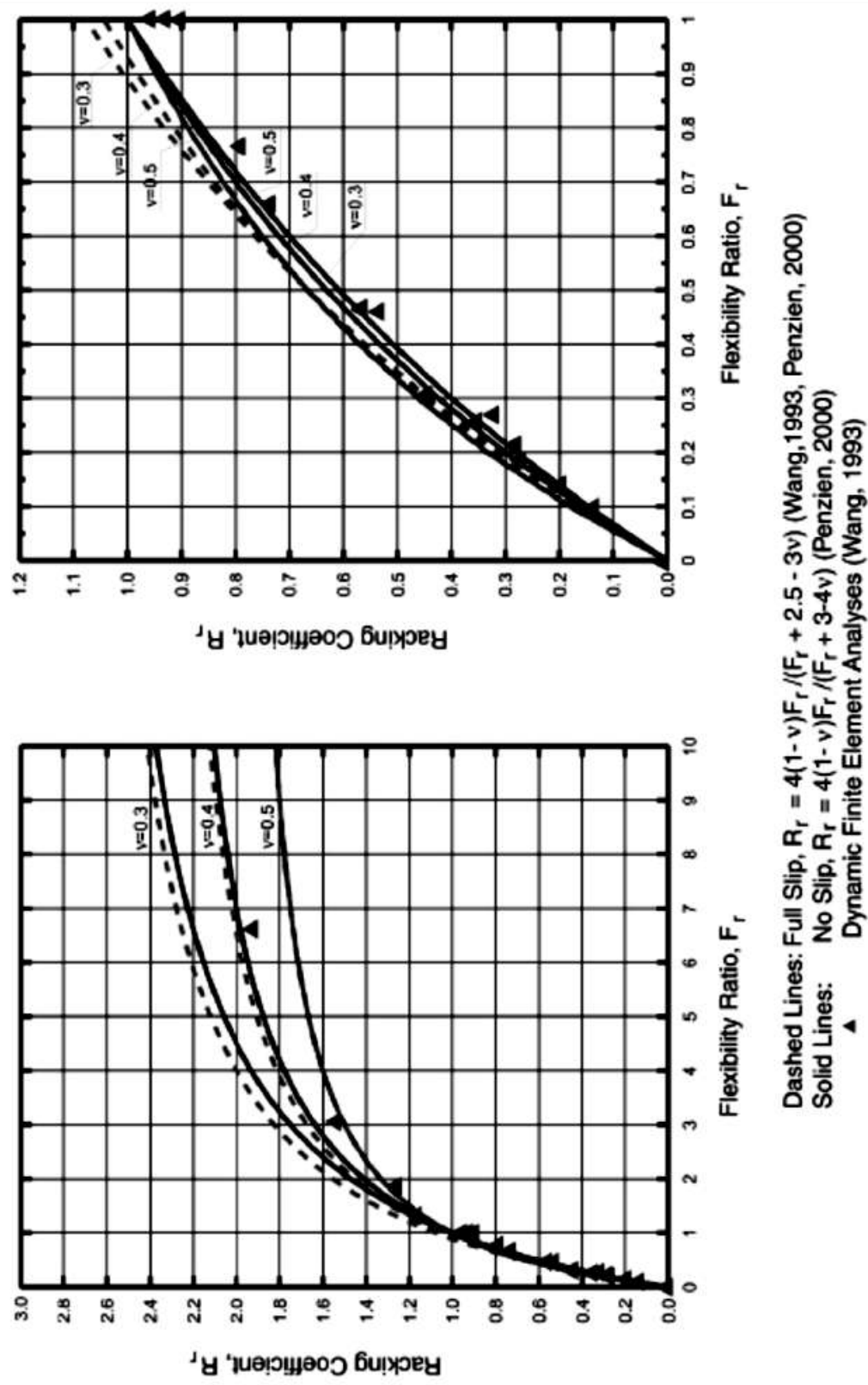


Figure 10.5. Racking coefficient for rectangular tunnels (C. Jeremy Hung et al 2009)

Structural Fire Resistance of Cut and Cover Tunnels

Introduction

Over the years many tunnel fires have been observed to result in economic loss, structural degradations and human loss. The first priority of action in a tunnel fire is mostly focused on life safety. The success of the rescue operations depend on keeping structural stability at high temperatures for a certain period of time.

In previous experimental researches, structural fire performance of circular linings such as TBM tunnel is investigated (Caner et al 2005, Caner and Boncu 2009). It shall also be noted that a variety of concrete structures or members have been extensively researched over the years investigating the structural stability, thickness of concrete cover, insulation materials and material degradation (Salse and Lin (1976), Elingwood and Shaver (1980), Huang et al (1999), Khoury (2002), Kodur and Sultan (2003), Shi et al (2004), Pichler et al (2006), Biondini and Nero (2011)). A very limited amount of research can be found in discussing the structural fire performance of cut and cover tunnels. It has been known that sagging of cut and cover tunnel roof at the positive moment region is possible during the fires as shown in Fig. 10.6 (Khoury (2003)). The maximum positive moment typically develops at the mid-span of the roof due to vertical loads carried by the roof.

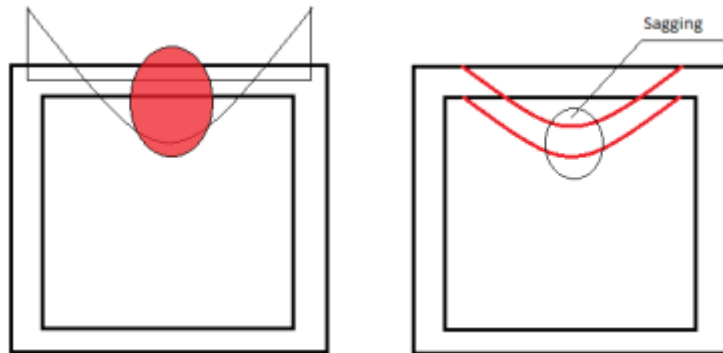


Figure 10.6. Sagging of Cut and Cover Tunnel Roof

The tension reinforcements at positive moment region of the roof need to be protected from adverse effects of high fire temperatures. Significant material degradation in tension steel induced by high temperatures can result in sagging of the roof. The concrete itself is known to be a poor thermal conductor, and in many structural designs, concrete cover can provide adequate fire protection for the reinforcement without use of additional protection layer (ACI 216 (2001), Shi et al (2004)). The main objective of this paper is to identify the structural condition of the positive moment region of tunnel lining concrete roof and to evaluate the load carrying capacity of the structural elements in the aftermath of a design fire scenario.

Test Segments

The internal loads determined for a standard rectangular shaped one cell railroad cut and cover tunnel has been used to design the test segments. Test segments have been designed per the requirements of the Turkish structural reinforced concrete code TS500 (2000). The design loads are taken to be similar to loads of backfill, lateral earth pressure

and self-weight taken from existing tunnel designs of Yedikule-Kazlıçeşme metro line in Marmaray Tube Crossing Project in Istanbul (Arsava 2011). Tested segment labels and characteristics are summarized in Table 10.1. The minimum required tension reinforcement is 5 Ø 12 bars. Some of the segments are allowed to have more than minimum reinforcement. Maximum measured compressive strength of concrete is given in Table 10.2.

Table 10.1. Segment Characteristics

Segment	Tested		Bottom Reinforcement	Condition	Tests	
	f_{ck} (MPa)	f_{yk} (MPa)			Fire	Static
Type BU-12	52.7	530	5Ø12	Unstressed	✓	✓
Type UU-12	61.8	520	3 Ø12, 2 Ø14	Unstressed		✓
Type BU-14	61.8	530	5Ø14	Unstressed	✓	✓
Type UU-14	57.6	520	5Ø14	Unstressed		✓
Type BS-12	61.4	530	5Ø12	Stressed	✓	✓
Type US-12	60.5	520	5Ø12	Stressed		✓
Type BS-14	61.6	530	5Ø14	Stressed	✓	✓
Type US-14	50.5	520	5Ø14	Stressed		✓

* The specimens are specified using the following formula: First letter indicates exposure to fire (B: Burnt, U: Unburnt). Second letter indicates stressed condition (S: Stressed, U: Unstressed). Last # indicates rebar size (12: Ø12, 14: Ø14). As an example: Type BU-12 indicates → Burnt, unstressed specimen with a rebar size Ø12.

Table 10.2. Comparison of Post-fire Compressive Strength of Concrete

Method	Compressive Strength of Concrete (MPa)			
	Type 1A-1	Type 2A-1	Type 1B-1	Type 2B-1
Arsava Pre-Fire Test	52.7	57.6	61.4	61.6
Arsava Post-Fire Test	43.0	N.A	48.1	N.A
ACI 216 (Analytical)	38.6	42.4	44.9	45.2
Eurocode 2 (Analytical)	47.6	52.0	55.4	55.7

Eight segments forming four pairs representing the characteristics of cut and cover tunnel roof have been manufactured in a precast concrete plant. The segments are casted using a similar mix-design adapted for bored and cut-and-cover tunnels of the Marmaray project in Istanbul (Arsava 2011). The typical concrete cover used in Turkish railroad tunnels of 60 mm is used at 1500 mm long segments having a cross-sectional depth of 600 and height of 400 mm as shown in Fig. 10.7. Out of these four types, two types have been internally pre-stressed to simulate the internal loads, axial load and moment, at the positive moment region of the tunnel roof determined from structural analysis with the design loads shown in Fig. 10.8. Only one segment out of each pair is tested under two hours of extreme design tunnel fire in the furnace. Following the furnace tests, all eight segments are tested to their flexure capacity.

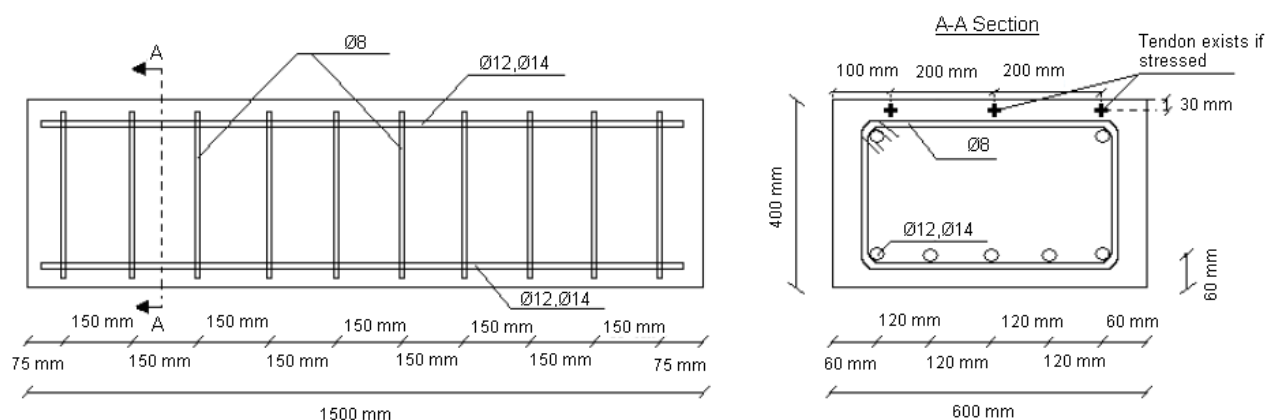


Figure 10.7. Segment Geometry and Reinforcement Details

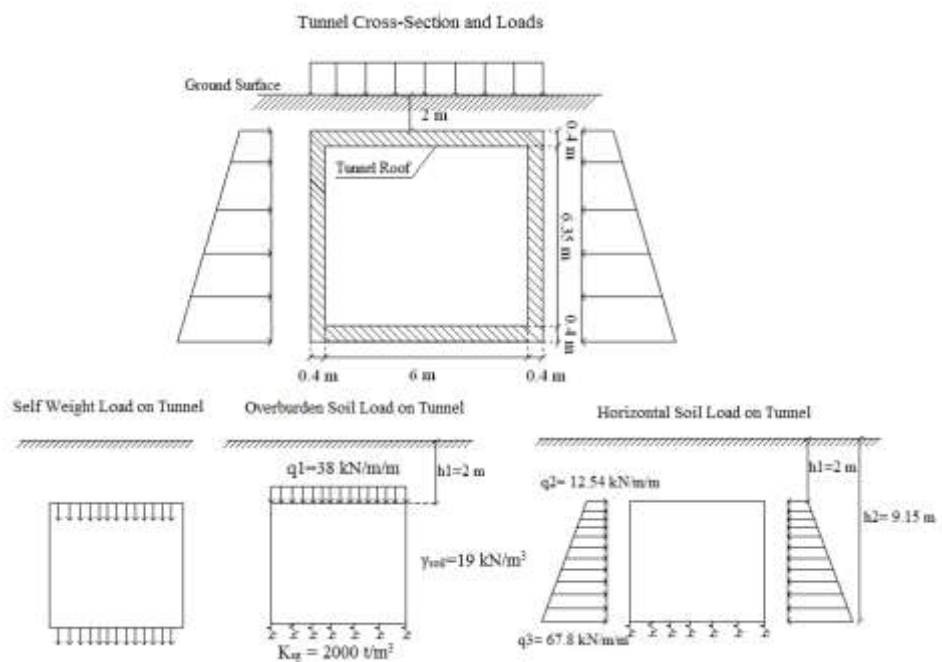


Figure 10.8. Cut and Cover Tunnel Loads

Prior to pouring the wet concrete into the formwork, the tendons are stressed and thermocouples are placed at the selected locations. For the stressed segments, three low-relaxation type prestressing tendons each having a net cross-sectional area of 127 mm² located at 30 mm depth from the top surface is stressed to 1350 MPa to develop the design axial load and moment. After the segment concrete is set, the tendons are cut. The eccentric axial tendon force develops a positive moment around the neutral axis of the cross-section.

Fire Tests

The furnace located in the Fluid Mechanics Laboratory of Mechanical Engineering Department at the Middle East Technical University is used for the fire testing of segments. The body of the furnace is of steel and inner surfaces are insulated with ceramic fiber and rock wool. The inner dimensions of the furnace are 1300 mm in width, 2500 mm in length and 1000 mm in height.

The industry standard for design fire duration is typically around 2 hours. The temperature in the furnace is controlled to be close to a fire temperature that can be generated by a 2 hour "Hydrocarbon" fire as shown in Fig. 10.9. To achieve the target fire curve, adjustments are made by shifting the location of inner compartment wall. The compartment steel wall is a rectangle shaped one with 20 mm thickness. In fire tests of stressed and unstressed specimens, tension faces of the segments are allowed to be touched by the flames of the burner. It shall be noted that the flame temperature is usually higher than the average temperature inside the furnace.

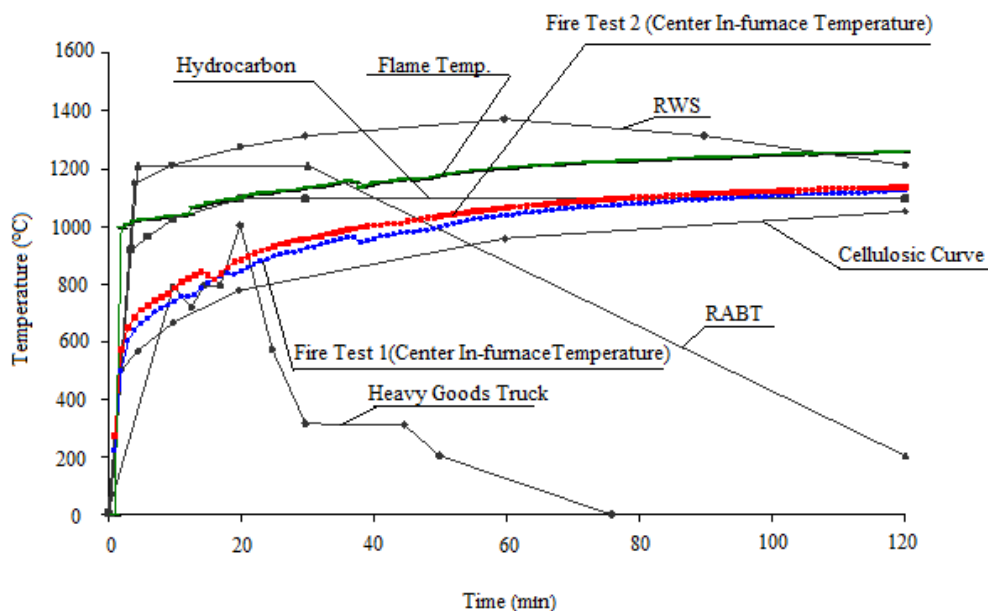


Figure 10.9. Temperature Curves - Tests

To measure the temperature distribution in the concrete, thermocouples are placed in segment Type BS-12 at 50, 100 and 150 mm away from tension surface of the segments in the construction phase of segment. Three other thermocouples are placed on top of

insulation (one close to center of furnace about 700 mm away from the mouth of the burner, one close to the burner to measure the flame temperature and one close to furnace edge) to monitor the in-furnace temperature during the fire test.

After 2 hours, the maximum temperature measured at 50 mm depth is observed to be 375°C. For the 100 mm depth, the maximum temperature measured is 255°C, and for 150 mm depth the maximum measurement show 100°C. The ACI 216 (2001) temperature penetration values for a less severe building fire design scenario at 50 mm, 100 mm and 150 mm depths are 400°C, 260°C and 160°C respectively. The differences in the temperature at the concrete layers close to hot surface are not that significant. The differences in results may occur due to differences in concrete mix design used in the current study and the ACI 216 (2001) study.

The temperatures measured in furnace on surface of concrete reached during fire tests are very close to "Hydrocarbon" curve limits and area under the temperature-time curve is very close to the one determined for "Hydrocarbon" curve (Fig. 10.9.). The average area under the furnace fire curves is around 125,026 min⁻¹°C and is about 2.6% less than the hydrocarbon fire curve area. The American Standard Testing Method (2000) suggests that for furnace fires if the area under the furnace temperature-time curve is close by 7.5% of the target area of the furnace temperature-time curve for a two-hour fire duration, the test is well controlled. The area under flame temperature – time curve is about 9.8% more than the hydrocarbon fire curve area.

Material Tests

The 150 x 150 x 150 mm cube samples casted at the precast concrete plant and 150 mm diameter core samples taken out from the burnt segments are tested under uniaxial compression to evaluate the unburnt and burnt strength of concrete. The suggested ACI 216 (2001) and Eurocode 2 (2007) material degradation models are compared to the test results (Table 10.2). ACI 216 (2001) recommendations for concrete compressive strength results in about 10% less than the degraded strengths measured in this study. The Eurocode 2 (2007) degradation model is over estimating the measured degraded compressive strength of the concrete by 10% to 25%.

To measure the changes between pre-fire and post-fire tensile strength of reinforcement bars tensile pull-out test is carried out. For this purpose, concrete cover on segment Type UU-12 and Type BS-14 is cleaned to expose the bars and two samples from each segment are taken out. ACI 216 (2001), Eurocode 2 (2007) and Shi et al (2004) degradation models are used in the evaluation of the results (Table 10.3). From investigation of the test results it is concluded that there is almost no difference between the post-fire and pre-fire tensile strength of reinforcement bars. The estimated temperature of 350°C at 60 mm depth in a 2 hour fire can result in 10% loss of material strength for tension reinforcement during the fire (ACI 216 (2001)).

Table 10.3. Comparison of Tensile Strength of Reinforcement

Method	Tensile Strength of Steel (MPa)	
	Yield Strength	Ultimate Strength
Arsava Pre-Fire Test	510	613
Arsava Post-Fire Test	535	640
ACI 216 at 120 th min (Analytical)	468	540
Eurocode 2 at 120 th min (Analytical)	497	573
Shi et al at 120 th min (Analytical)	420	485

To evaluate the chemical composition and crack patterns within the different depths of concrete, electron microscope are used to scan the samples that are extracted from 50, 100 and 200 mm depths of the cored sample of the test specimen Type BS-12 (Fig. 10.5). The samples are tried to be selected to in such a way that they contain both cement and aggregate to observe the quality of bonding between cement and aggregate. The electron microscope scanning results can be summarized as follows:

- Fire can develop internal cracking in the concrete at regions close to hot surface.
- The estimated temperature of 80 °C at 200 mm depth from the surface of specimen exposed to 2 hours fire indicates that, heat distribution does not lead to any chemical deformation at such depths.
- Specimens, which are taken at 50 mm and 100 mm depths, are in a more homogeneous form due to extreme heat effect. Hydration products are eliminated in these regions and the concrete is dehydrated. The calcium silicate hydrate gels, the main cementitious compound, and calcium hydroxide gels are more visible at 200 mm depth. The energy-dispersive X-ray spectrum at 50 mm and 200 mm depths indicates that the X-ray counts of gel material is much less at 50 mm depth.

In previous researches, it has been noted that higher moisture content can ignite explosive spalling during a fire (Caner et al, 2009). Moisture in the concrete can rapidly turn into steam at high temperatures and the steam pressure can produce explosive spalling especially for a concrete with high moisture content at the early stages of fire (Böncü, 2008). Therefore, moisture content, a measure for explosive spalling of concrete, need to be determined prior to fire testing.

High moisture content of a 2.7% of the volume is determined for the reference specimen Type US-14. It is observed that the moisture content of burnt samples have less than 1% of moisture content as expected. It has been known that the explosive spalling can occur in

concrete having more than 3% moisture content under high axial load levels that can develop more than 15 MPa compressive stress in concrete (Arsava 2011).

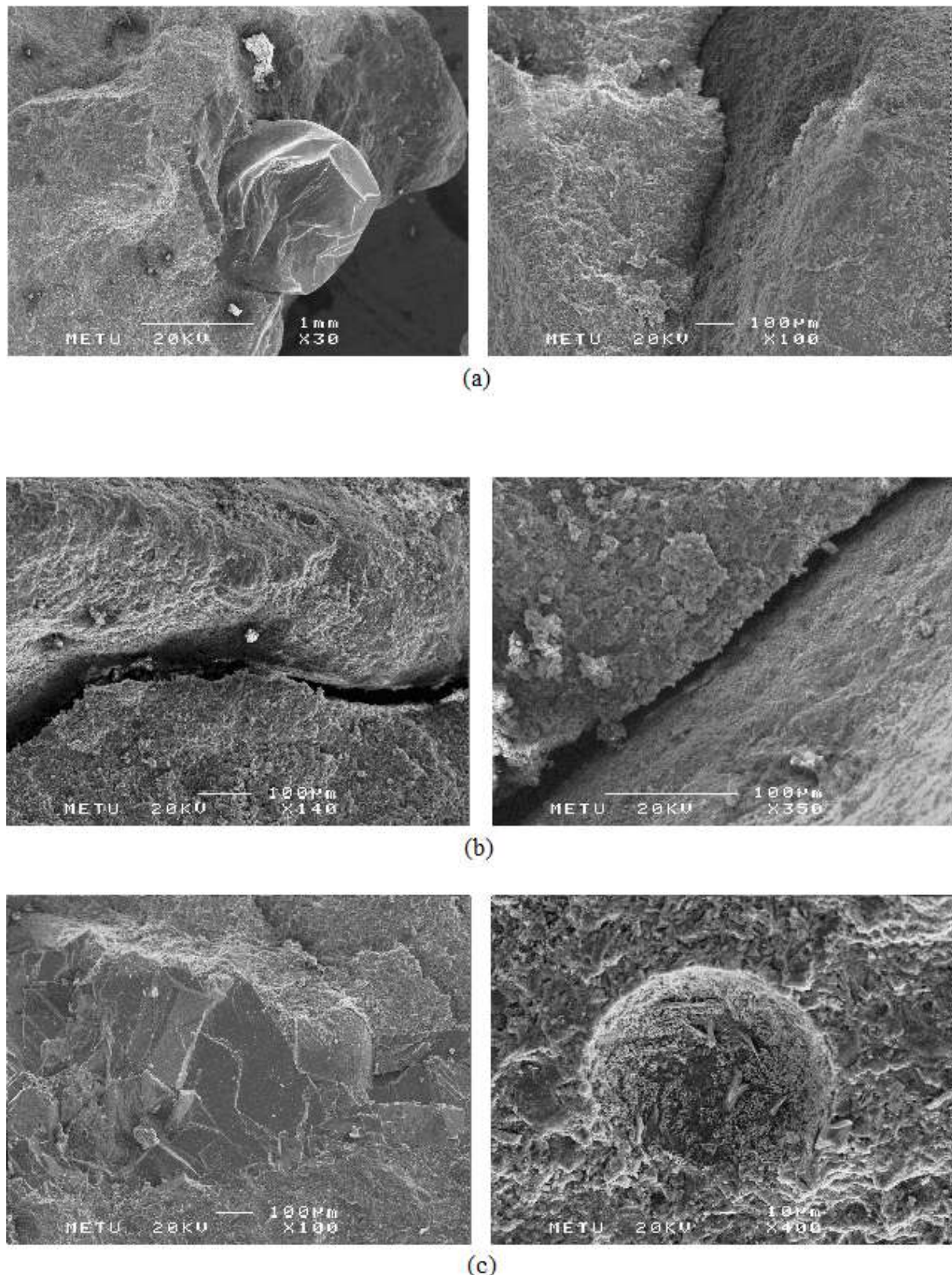


Figure 10.10. Electron Microscope Scans (a) 50 mm, (b) 100 mm and (c) 200 mm depth

In the test, it was observed that in the first 15 minutes minor amount of explosive type of spalling took place. It was further observed that the specimens have lost 40 to 60 mm of concrete layer at few spots where flames are touching after two hours of exposition to fire. It shall also be noted that some local regions of the surface exposed to more than 1100°C did not even spall.

Static Load Test

Following the fire furnace tests, segments are loaded by a point static load at their mid-span to evaluate the flexural capacity. The specimens are simply supported on the test apparatus and loads are measured with a load cell placed under the hydraulic jack. Displacement transducers are placed to measure the displacements, three at the center; two at the supports. Prior to tests, the load cells and displacement transducers are calibrated.

The loading frame has known to have a safe 500 kN loading capacity. Special short support columns are provided to support the beams ends. A steel type support in form of a hinge and a roller is places on top of the two support columns. The clear span length between centerline of supports is set to 1200 mm. The beams are not physically connected to the supports but they are in contact with steel supports by gravity forces. The pressure to the hydraulic cylinder is applied through a hand type pump. The speed of loading is manually increased. At every increment of 100 kN the test has been paused to detect the cracks on the segment.

It is observed that the difference between structural load carrying capacities of stressed and unstressed segments is not that significant as presented in Table 4. A typical load-deflection diagram is presented in Fig. 6. In stressed segments, the moment carrying capacity of the cross-section increases due to presence of initial compressive axial load induced by tendons. The tendons located close to top fiber of the beam induces an initial positive moment. At the failure stage, the increased moment capacity minus the initial positive moment results in a similar applied test moment as in the case of test of unburnt specimens. It is also observed that the difference of loss in applied load capacity between the burnt and unburnt specimens usually lies within 5% except one case. The reinforcement is placed in a safe concrete depth and is not affected from the fire related adverse material degradation in all cases. The segments having more than minimum required tension reinforcement carried more load compared to the ones having minimum required reinforcement as expected.

Table 10.4. Results of Tests and Analytical Methods

Specimen	Nominal Load Carrying Capacity (kN)			
	ACI 216	FireCap	LARSA	Test Results
Type BU-12	-	317	435	525
Type UU-12	368	384	447	525
Type BU-14	-	427	484	550
Type UU-14	435	456	517	575
Type BS-12	-	333	375	441
Type US-12	307	369	438	533
Type BS-14	-	441	495	582
Type US-14	423	467	517	599

* ACI 216 method recommends fire endurance in terms of hours for burnt segments rather than degraded capacity computation. Therefore the related cells are left blank for ACI 216.

To check the static loading test results, the cross-section analysis has been performed both by ACI 216 (2001) hand design check and FireCap program. The computational methods used in the FireCap program is described in detail in the study of Caner et al (2005) and Caner and Boncu (2009). FireCap program is basically a moment-axial load interaction program that takes into account the material degradation induced by thermal and time-dependent effects.

The ACI 216 (2001) method results in 30%, the FireCap solution results in 25% and LARSA analysis results in 15% of an average underestimation of load carrying capacity of the test results as presented in Table 4. The main reason in differences in results can be due to ignoring strain hardening of steel in analysis. As indicated in Table 3, the ultimate tensile strength of the steel is about 20% higher than its yield strength. For design purpose the 25% to 30% can be a reasonable safety factor to have in design. However for a better estimation of results, an advanced structural analysis such as the one described above might be used.

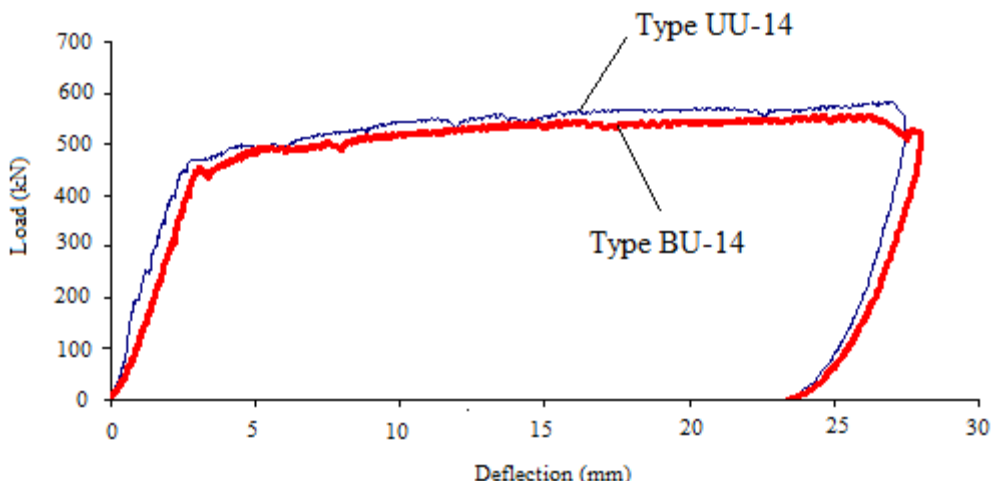


Fig. 10.11. Typical Load Deflection Diagram of Segments

Structural Fire Safety Evaluation

Cementitious materials and especially high strength, low permeability concrete can explosively spall at early stages of fire (Khoury 2002, Kutzniq 1999, Pichler et.al. 2006 and Tatnall 2002). Therefore, in a fire safety evaluation, explosive spalling of concrete shall be checked by investigating the concrete mix design and fire source since a suitable mix can eliminate or minimize explosive concrete spalling. (See Both et. al, (2003) for the various types of spalling in tunnel linings.)

Use of micro-polypropylene fibers, which melt during a fire, will increase the permeability of the concrete at temperatures above 130 °C, and will minimize or eliminate the explosive spalling by releasing steam (Khoury 2002, Kutzniq 1999, Pichler et.al. 2006 and Tatnall 2002). One of the disadvantages of the use of micro-polypropylene fibers in concrete mix design may be a reduction in the workability of the concrete (Caner et. al 2005). Alternatively, fire-proofing material can be used but it increases both cost of construction and maintenance cost. There are significant durability concerns on the long-term performance of the fire proofing materials (Martinola et. al 2007) since mortar based fire proofing materials may have cracking problems over the years.

The basic steps in a structural fire safety evaluation (Caner et.al. 2005) considering only gradual concrete spalling can be identified as follows:

- Divide lining section into layers at its thickness, t , and determine the temperature penetration into concrete using a heat-transfer analysis. In a heat-transfer analysis; the surrounding soil may also be modeled as a heat sink. Such analysis shall include temperature-dependent thermal properties of concrete such as thermal conductivity, specific heat and thermal expansion. These parameters are function of temperature, aggregate type and more generally composition of concrete mix design (Kodur and Sultan, 2003, ACI, 2001, and Flynn, 1999). An iterative method is used to satisfy convergence on thermal conductivity and specific heat at a certain temperature at an investigated layer. If a layer reaches its full material degradation at a high level temperature, the layer is expected to be spalled.

- Determine initial strains (thermal strains) at each stage of the fire due to temperature penetration into concrete. Sectional analysis with material degradation including spalling belongs to this step. Material strength of concrete and steel can be degraded at layers of concrete close to the face subjected to the fire (ACI 2001). Concrete subjected to 300 °C may lose about 10% of its strength during a fire and about 40% of its strength after cooling. The strength reduction in a concrete stressed to 40% of its initial strength capacity is less compared to an unstressed similar type of concrete at elevated temperatures. A rebar having a 420 MPa yield strength can lose its capacity by 20% at 600°C and by 80% at temperatures exceeding 800°C (ACI 2001). Initial strains at any layer can be determined from:

$$\varepsilon_{initial(T)i} = \begin{cases} \alpha_{it} T_i & \rightarrow T_i < T_m \\ 0 & \rightarrow T_i > T_m \end{cases}$$

(10.4)

where α_{it} is the temperature-dependent thermal expansion coefficient ($1/\text{°C}$) at a certain temperature T_i ($^{\circ}\text{C}$), and T_m is the temperature where material fully degrades. Stress at any layer can be determined from stress-strain diagram of the material at a certain temperature. Material degradation properties of concrete and steel at different temperatures can be found at ACI (2001). The force due to initial strains can be determined from:

$$F_{initial} = \sum \sigma_i (A_i)$$

(10.5)

where σ_i is the stress at a layer and A_i is the area of the same layer. The moment induced by initial thermal strains at the neutral axis of the section is:

$$M_{initial} = F_{initial} \cdot a$$

(10.6) (3)

where a is the moment arm between neutral axis of the section and the point of resultant compressive stress induced by thermal strains.

- Determine equilibrating (compatibility) strains. Cooler layers away from hot surface do not have tendency to expand as much as the layers close to the hot surface. Therefore, cooler layers will restrain the expansion of hot layers and result in equilibrating strains at the cross-section of a lining. Equilibrating forces at neutral axis of the section are:

$$\begin{aligned} F_{equilibrating} &= -F_{initial} \\ M_{equilibrating} &= -M_{initial} \end{aligned}$$

(10.7)

At an unloaded section, internal cracking can be expected since these layers can be subjected to stresses exceeding tensile strength of concrete. The cracking at internal layers can be detected from the following equation.

$$\varepsilon_{initial(T)i} + \varepsilon_{equilibrating(T)i} > \varepsilon_{tension}$$

(10.8)

where $\varepsilon_{equilibrating(T)i}$ is the strain induced by equilibrating forces and $\varepsilon_{tension}$ is the tensile strength of the concrete.

- Determine secondary strains. Entire structure shall be analyzed under existing and equilibrating loads. Secondary strains can be obtained from resulting forces of this analysis for a certain stage of fire. In such structural response analysis at global level, section and material properties shall be based on heat induced material degradation and concrete spalling at that stage. The soil stiffness surrounding the structure shall also be included in the analysis.
- Combine initial, equilibrating, secondary, and creep strains to determine the forces at any section of the lining. The total strain at any layer will be equal to:

$$\begin{aligned}\varepsilon_{total(T)i} &= \varepsilon_{initial(T)i} + \varepsilon_{equilibrating(T)i} + \varepsilon_{secondary(T)i} + \varepsilon_{o(T)i} \rightarrow \varepsilon_{total(T)i} < 0.011 \\ \varepsilon_{total(T)i} &= 0 \rightarrow \varepsilon_{total(T)i} > 0.011 \rightarrow \text{concrete spalled}\end{aligned}$$

(10.8)

where $\varepsilon_{secondary(T)i}$ is the strains induced by secondary forces and $\varepsilon_{o(T)i}$ is strains due to creep or stress relaxation. At high temperatures, concrete can develop 0.011 compressive crushing strain that will result in spalling per ACI (2001). Thermal strains are typically larger than creep strains as it can be seen from the related tables or figures of ACI (2001). Determine the demand forces from sectional analysis using strains obtained at this step.

- Compare the forces determined in the above step with the sectional capacity. Sectional capacity shall be based on material properties with degradation and concrete spalling.
- Repeat the above steps for each fire stage and cumulatively add the effects to each other for the fire stage in investigation. The factor of safety against failure is basically the capacity divided by the demand.

The analytical work described above cannot be used if a major explosive spalling of concrete is expected during a fire. In such a case for a new design concrete mix design can be improved to minimize this effect. In structural fire safety evaluation, a solid approach to detect major explosive spalling is to fire test the concrete as done in this research.

The global structural model of lining shall include lining-ground interaction. The lining in shape of a ring is modeled with beam elements and the ground is modeled with compression-only spring elements as shown in Figure 10.12. The stiffness of the spring elements is based on the subgrade reaction modulus of the surrounding soil. Similar bedding spring models for ground interaction can also be found at BTC (2004), Rombach (2004) and Caner et.al (2005).

In fire-safety evaluations, the following load combination is usually used.

$$1.0 \text{ DL} + 1.0 \text{ (HL+PL)} + 1.0 \text{ (FL(t))} = R_u(t) < \phi_r R_{nr}(t) \quad (10.9)$$

where DL is the dead load, HL is the hydrostatic load, PL is the earth pressure, FL(t) is the fire -induced structural load at the investigated time of the fire, ϕ_r is the resistance

factor (= 1.0 for extreme events per ACI (2001)) and $R_{nr}(t)$ is the reduced capacity due to material degradation at the investigated time of the fire.

Axial compressive forces are more significant than bending in design of circular tunnel linings. The time-dependent axial load capacity can be taken as:

$$P_n(t) = 0.60 \int f_{c_{ti}} A_{ti} dA \quad (10.10)$$

where $P_n(t)$ is the reduced axial load capacity, $f_{c_{ti}}$ is the reduced compressive strength of a concrete layer and A_{ti} is the reduced area of the corresponding layer at time t , of fire.

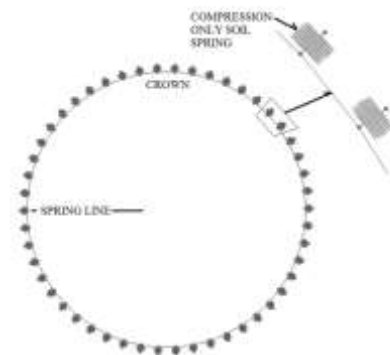
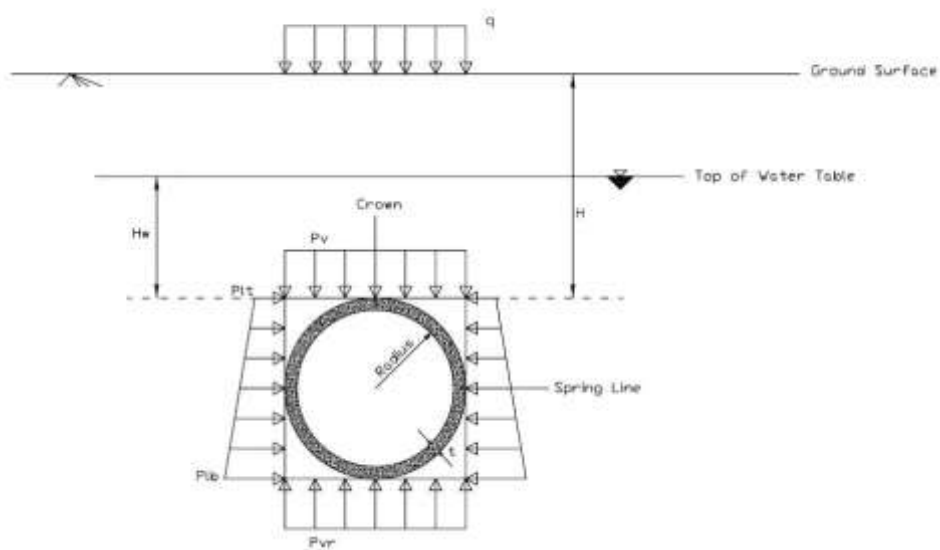
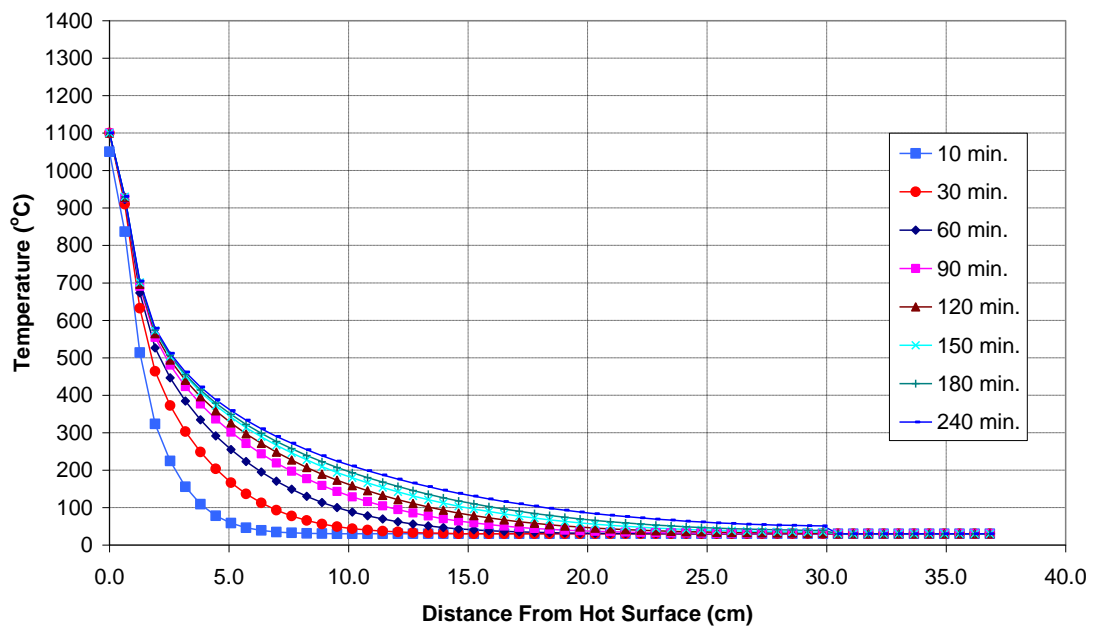
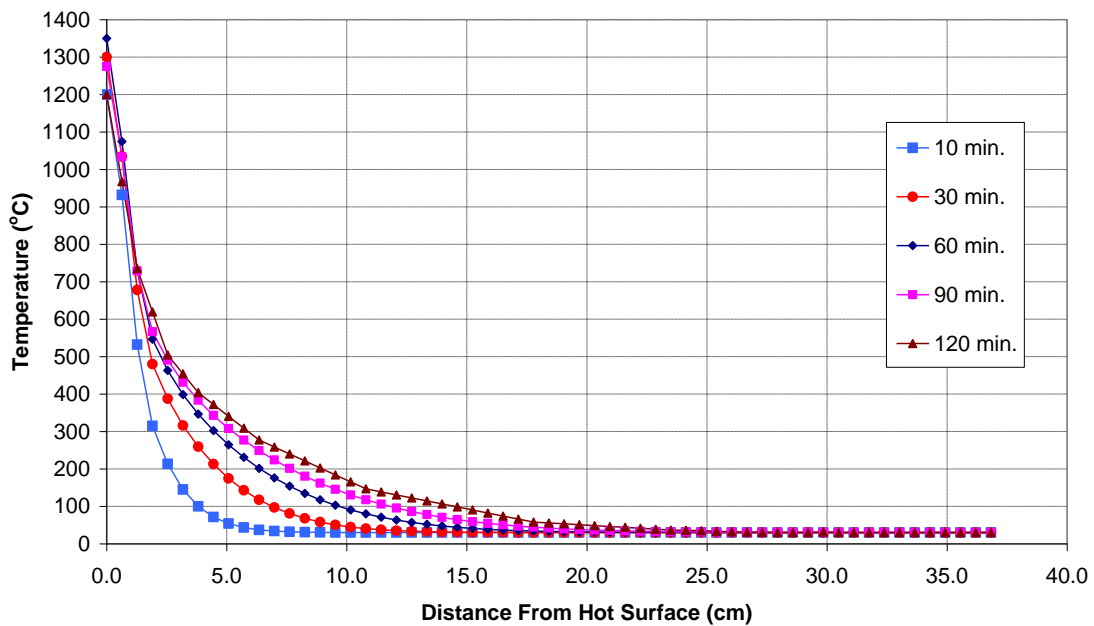


Figure 10.12. Beam-Spring Model





(a)



(b)

Figure 10.13. Temperature Penetration into Concrete Lining (a) Harmonized hydrocarbon fire for 4 hour rating, (b) Rijkswaterstaat hydrocarbon fire for 2 hour rating

Blast Design Philosophy

An explosion is a process by which a rapid release of energy generates a pressure wave of finite amplitude. The energy source can be anything that generates a violent reaction when initiated, such as chemical or nuclear materials, pressurized gases or electricity. The properties of air will cause the front of this pressure wave to steepen, as the front moves. The result is a shock front moving faster than the sound speed of the air ahead of it, with discontinuities in pressure, density, and particle velocity across the front.

As the blast wave propagates to greater distances from its source, its magnitude and velocity decreases until it propagates at the speed of sound. Theoretically, acoustical laws could then apply, but meteorological conditions tend to control its properties at long distances.

Figure 10.14 shows the movement of typical shock waves emerging from point "C". Waves marked with "I" points the incident waves and "R" points the reflective waves.

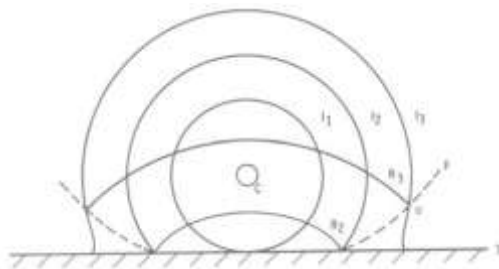
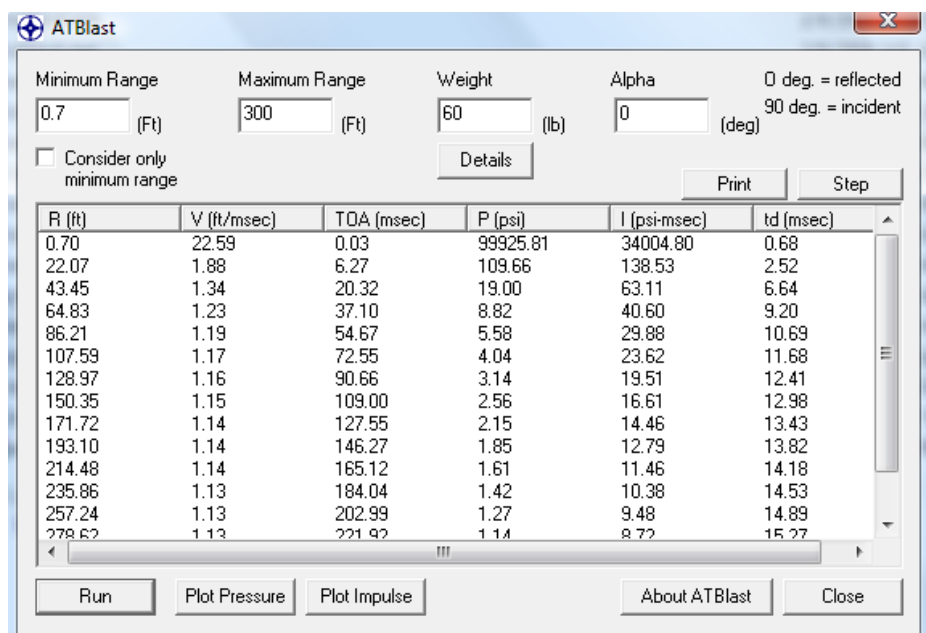
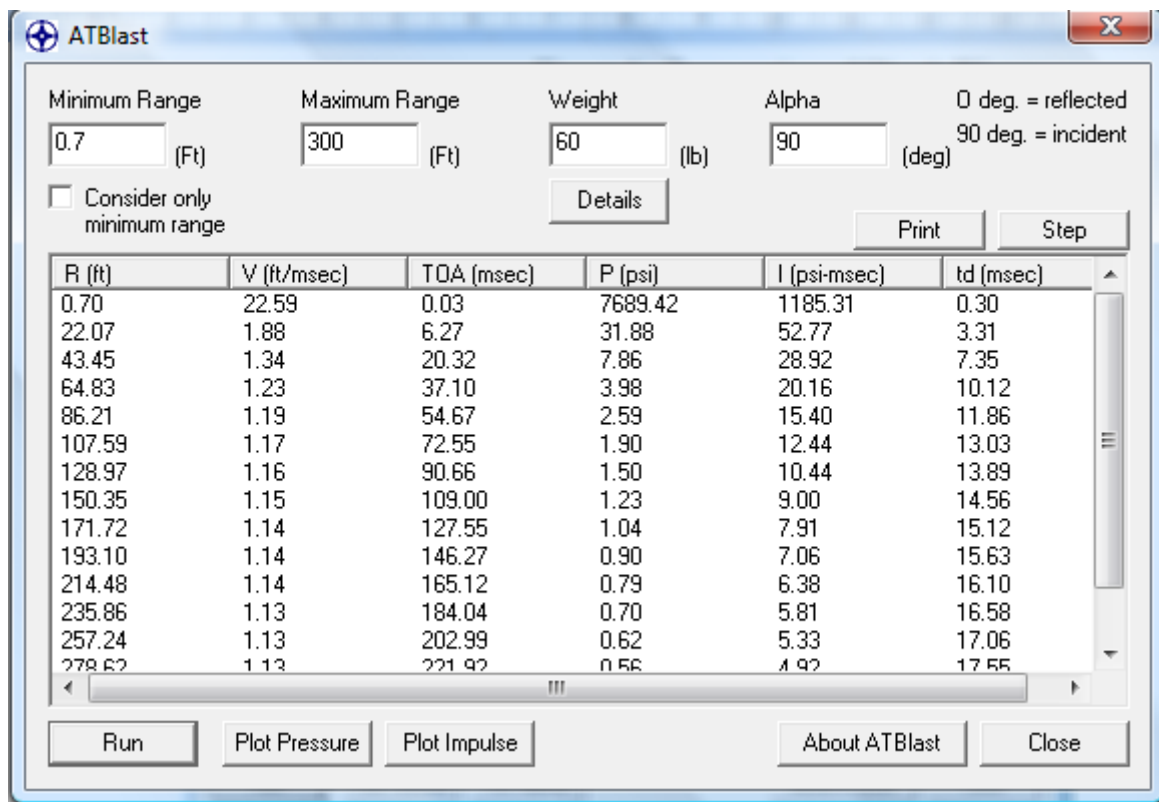


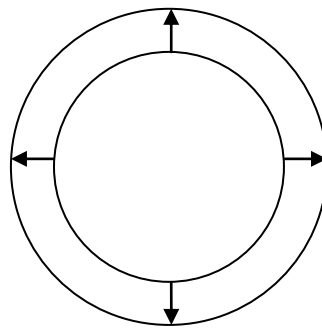
Figure 10.14. Propagation of Shock Waves



Reflected pressure due to an explosive that can be carried by a luggage



Incident pressure due to an explosive that can be carried by a luggage



Blast Pressure due to a small incident is taken as design value ($p=100 \text{ kN/m}^2$)

Typically in a blast design hardening of structural material shall be considered. For plastic protection, a protection element or layer is typically used to mitigate the effect of the blast to inner structures.

References:

- AASHTO (2010) "LRFD Bridge Design Specifications", 4th Edition, Washington DC.
- AASHTO (1996) "Standard Specifications for Highway Bridges", 16th Edition, Washington DC.
- Abdel Karim, A. M. (1995) "State of the Art Precast/Prestressed Spliced I-Girders", PCI Journal.
- AFTES – WG7, *Considerations on the Usual Methods of Tunnel Lining Design*, French Tunneling and Underground Engineering Association, Working Group No. 7 - Temporary Supports and Permanent Lining, 1993.
- American Concrete Institute (ACI). (2005). "Building code requirements for structural concrete," ACI318, Farmington Hills, Michigan.
- ASCE/SEI/SFPE 29-99 (2003). *Standard calculation methods for structural fire protection*, Reston, Virginia.
- American Concrete Institute (ACI) (2001). "Fire endurance of concrete elements", *ACI 2003 Manual of Concrete Practice, ACI216R-89*, Farmington Hills, Michigan.
- American Society of Testing and Materials (ASTM) (2010) . "Standard Test Methods for Fire Tests of Building Construction and Materials", *ASTM E 119*, Pennsylvania.
- Argınhan O. (2010) "Reliability Based Safety Level Evaluation of Turkish Type Precast Prestressed Concrete Bridge Girders Designed in Accordance with the Load and Resistance Factor Design Method", MS Thesis, METU, Ankara.
- Arsava, K. S. (2011). "Fire tests of cut and cover tunnel roof segments at positive moment region," *M.S. Thesis*, METU, Ankara
- Barker R. and Buckett J. A. (2007) "Design of Highway Bridges An LRFD Approach", Wiley Press
- Barr, P. J., Marc, O. E., and Stanton J. F. (2001) "Live-Load Distribution Factors in Prestressed Concrete Bridges", *Journal of Bridge Engineering*, 6(5), 298-306.
- Beard A. and Carvel R. (2005). *The handbook of tunnel fire safety*. Thomas Telford, London.
- Bickel, J.O., Kuesel, T.R., and King, E. H. (1997), *Tunnel Engineering Handbook*, 2nd Ed., Chapman & Hall, Inc., New York.
- Blom C.B.M., Horst E.J., Jovanovic P.S., *Three-Dimensional Structural Analyses of the Shield-Driven "Green Heart" Tunnel of the High-Speed Line South*, Tunneling and Underground Space Technology, Volume 14, No. 2, 1999
- Both C., Wolinsk G.M. and Breunese A.J (2003). "Spalling of concrete tunnel linings in fire.", *(Re)Claiming the Underground Space*, Sauver, Swets & Zeitlinger, Lisse, 227-231.
- British Tunnelling Society (BTC). (2004) *Tunnel lining design guide*, Thomas Telford, London.

- Biondini, F. and Nero A. (2011). "Cellular finite beam element for nonlinear analysis of concrete structures under fire". *J. Struct. Eng.*, 137(5), 543-558.
- Caner, A., and Boncu,A. (2009) "Structural fire safety of circular railroad tunnel linings," *J. Struct. Eng.*, 135(9), 1081-1092.
- Caner, A., Zlatanic, S. and Munfah, N. (2005) "Structural fire performance of concrete and shotcrete tunnel liners.", *J. Struct. Eng.*, 131(12), 1920-1925.
- Christopher G. G., and Therasa M. T. A (2004) "A Probabilistic Comparison of Presstress Loss Methods in Prestressed Concrete Beams Part 1&2" PCI Journal.
- Dowding, C.H., Rozen, A. Damage to rock tunnels from earthquake shaking. *J. Geotech. Eng. Div.*, ASCE 104 (GT2), pp.175-191, 1978.
- Duddeck H., Erdmann J., *Structural Design Models for Tunnels*, Universitat Braunschweig, Germany, 1982.
- EN 1991-2 (2003) "Eurocode 1: Actions on Structures-Part 2 Traffic Loads on Bridges", Brussels.
- Elingwood B. and Shaver, J. R. (1980) "Effect of fire on reinforced concrete members" *J. of the Structural Division*, 106(11), 2151-2166.
- Eurocode 2 (2007) "Design of concrete structures, Part 10: Structural fire design", CEN.
- Imam M. B., and Chryssanthopoulos, M. K. (2012), "Causes and Consequences of Metallic Bridge Failures", Structural Engineering International, IABSE, Switzerland.
- FHWA (2001) "LRFD for Highway Bridge Substructures", Washington DC.
- FHWA (2004) "Post-Tensioning Tendon Installation and Grouting Manual", Washington DC.
- Flynn, D. R. (1999). *Response of high performance concrete to fire conditions: review of thermal property data and measurement techniques*, NIST GCR 99-767, U.S. Department of Commerce Building and Fire Research Laboratory National Institute of Standards and Technology, Gaithersburg, Maryland.
- Gioda G., Swoboda G., *Developments and applications of the numerical analysis of tunnels in continuous media*, International Journal for Numerical and Analytical Methods in Geomechanics, Volume 23, 1999.
- Hefny A.M., Tan F.C., Macalevey N.F., *Numerical Study on the Behaviour of Jointed Tunnel Lining*, Journal of The Institution of Engineers, Volume 44, Issue 1, Singapore, 2004.
- Huang, Z., Burgess, I. W. and Plank, R. J. (1999). "Nonlinear analysis of reinforced concrete slabs subjected to fire" *ACI Struct J.* 96(1), 127-135.
- Hung, J. Monsees, J. Munfah N., and Wisniewski J. (2009) "Technical Manual for Design and Construction of Road Tunnels - Civil Elements", FHWA NHI-10-034.

ITA - WG2, *Guidelines for the Design of Shield Tunnel Lining*, International Tunnelling Association, Working Group No. 2 – Research, 2000.

Janssen P., *Tragverhalten von Tunnelausbauten mit Gelenktubbings*, Report No. 83-41, University of Braunschweig, Department of Civil Engineering, Institute for Structural Analysis, 1983.

JSCE, *Japanese Standard for Shield Tunnelling*, Japan Society of Civil Engineers, The third edition, Tokyo, 1996.

Khoury, G. A. (2002). "Passive protection against fire" *Tunnels and Tunneling International*, November , 40-42

Khoury, G. A. (2003). "Passive fire protection in tunnels" *Concrete*, 37(2) ,30-36.

Klappers C., Gruebl F., Ostermeier B., *Structural Analysis of Segmental Lining – Coupled Beam and Spring Analyses Versus 3D FEM Calculations with Shell Elements*, Tunneling and Underground Space Technology, Volume 21, Issues 3-4, 1999.

Kodur V. K. R., and Sultan, M. A. (2003) "Effect of temperature on thermal properties of high strength concrete", *J. Mater Civ. Eng.*, 15(2), 101-107.

Koyama Y., *Study on the Improvement of Design Method of Segments for Shield-Driven Tunnels*, RTRI Report: Special No. 33, 2000.

Koyama Y., *Present Status and Technology of Shield Tunneling Method in Japan*, Tunneling and Underground Space Technology, Volume 18, 2003.

Koyama Y., Nishimura T., *Design of Lining Segment of Shield Tunnel Using a Beam – Spring Model*, Quarterly Report of Railway Technical Research Institute, Volume: 39(1), Japan.

Kuesel, T.R., Earthquake Design Criteria for Subways, *J. Struct. Div.*, ASCE ST6, pp. 1213-1231, 1969.

Kun L. and Qilin Z. (2012) "Research for Calibration and Resistant Factors of LRFD Design of Steel Bridge in China", *J of Performance of Constr. Fac.* 26(2) , 212-219.

KGM (1982) "Yol Köprüleri için Teknik Şartname", Ankara.

LARSA (2010), *Quick start guide for version 7.01.69*, Melville, NY

Lee K.M., Ge X.W., *The Equivalence of a Jointed Shield-Driven Tunnel Lining to a Continuous Ring Structure*, Canadian Geotechnical Journal, Volume 38, No. 3, 2001.

Leonhard F., Reimann H., *Betongelenke*, Der Bauingenieur, Volume 41, 1966.

Leonhardt F. (1987) "Cable Stayed Bridges with Prestressed Concrete", PCI Journal.

Liu, C. (2002) "Reliability Validation of Multigirder Steel Bridges Designed by LRFD", 2002 Emerging Professionals Paper Competition, PBQD, Tampa, Florida.

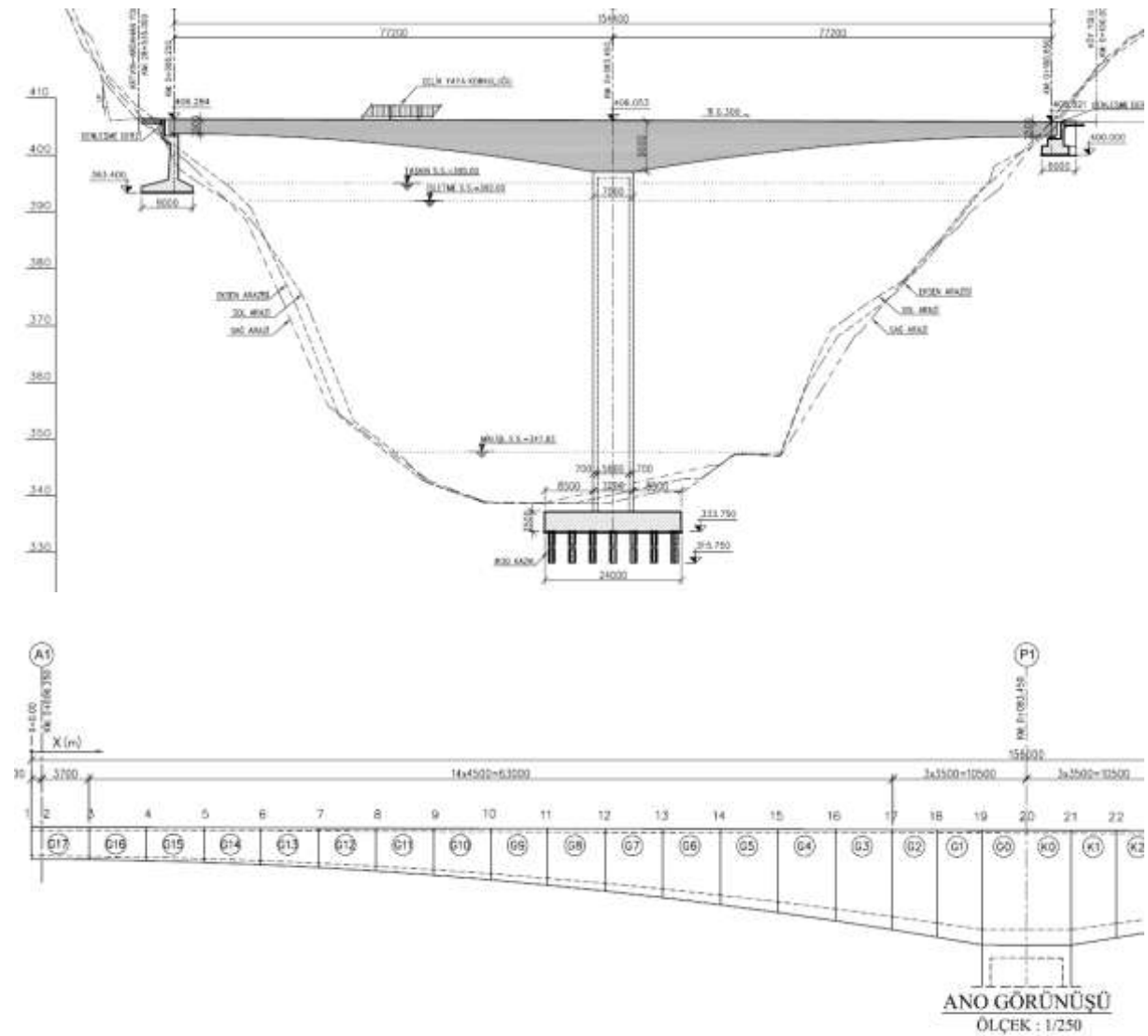
- Lucko G. and Garza J. M. D. (2003) "Constructability Considerations for Balanced Cantilever Construction", Practice Periodical on Structural Design and Construction, ASCE. 8(1), 47-56.
- Martinola, G., Bauml, M. F. and Walliser, A. (2007). "Numerical modeling of the long-term behavior of passive fire protection mortars applied on concrete tunnels.", *J. Mater. Civ. Eng.*, 19(6), 484-491.
- Mashimo H., Ishimura T., *Evaluation of the Load on a Shield Tunnel Lining in Gravel*, Public Works Research Institute, Independent Administrative Institution, Tsukuba, Japan, 2003.
- Merritt, J.L., Monsees, J.E., Hendron, A.J., Jr., Seismic design of underground structures, Proceedings of the 1985 Rapid Excavation Tunneling Conference, vol. 1, pp. 104-131, 1985.
- Mononobe, N., Matsuo, H., On The Determination of Earth Pressures During Earthquakes, Proceedings of World Engineering Congress, 1929.
- Moon S. Y. (2009) "Aesthetic Approach on Bridge Pier Design", IASDR.
- NCHRP498 (2003) "Design of Highway Bridges for Extreme Events", TRB, Washington DC.
- Okabe, S., General theory on earth pressure and seismic stability of retaining wall and dam, Journal of Japan Society of Civil Engineers, Vol. 12, No. 1, pp. 123-134, 1926.
- Okeil, A. M. (2006) "Allowable tensile stress for prestressed segmental concrete bridges", ACI Structural Journal, Vol. 103, No. 4.
- Owen, G.N., Scholl, R.E. Earthquake engineering of large underground structures. Report no. FHWA-RD-80-195. Federal Highway Administration and National Science Foundation, 1981.
- Penzien, J., Seismically induced raking of tunnel linings, *Earthquake Engineering and Structure Dynamics* 29, pp. 683-691, 2000.
- PCI (2004) "Design Handbook", 6th Edition, Illinois.
- PCI (2010) "PCI Bridge Design Manual", Illinois
- Pichler, C. Lackner R. and Mang H. A. (2006). "Safety assessment of concrete tunnel linings under fire load." *J. of Struct Eng.*, 132 (6), 961-969.
- Power, M., Rosidi, D., Kaneshiro, J. Seismic vulnerability of tunnels revisited. In: Ozedimir, L., (Ed.). Proceedings of the North American Tunneling Conference. Elsevier, Long Beach, CA, USA, 1998.
- PTI (2006) "Post-tensioning Manual, 6th Edition", Arizona
- Rignerth, J. (2000). "Simplified design of fire exposed concrete beams and columns – An evaluation of eurocode and swedish building code against advanced computer models.", *Department of Fire Safety Engineering*, Lund University, Sweden.

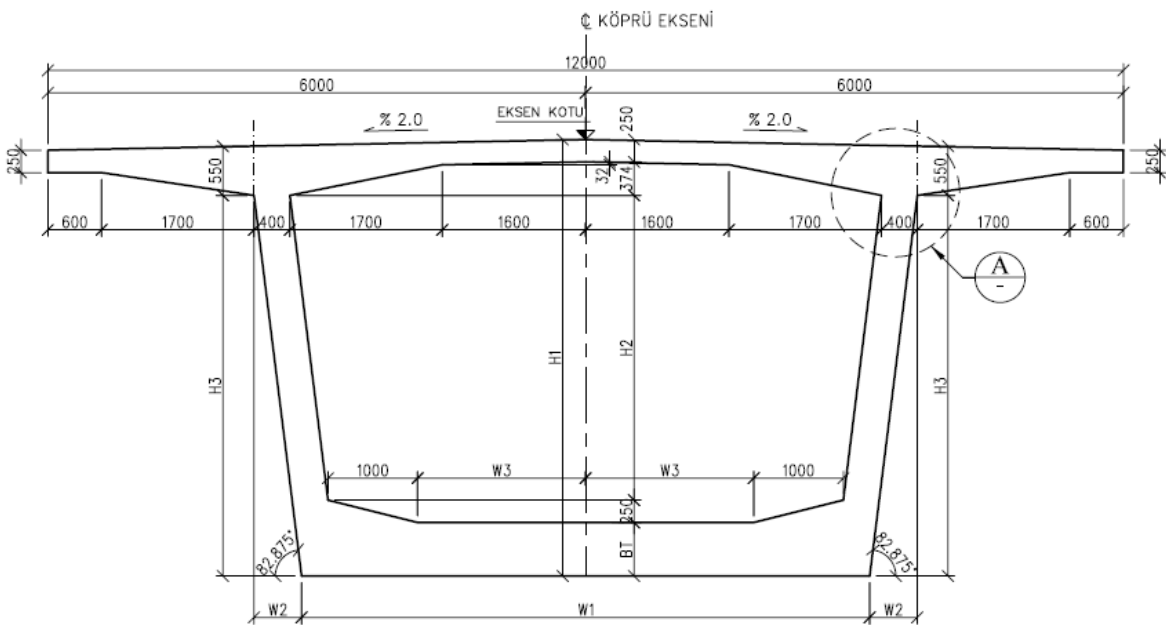
- Rombach, G. A. (2004). *Finite element design of concrete structures*. Thomas Telford, London.
- Salse, E. and Lin T. D. (1976). "Structural fire resistance of concrete" *J. of the Structural Division*, 102(1), 51-63.
- Shi X., Tan T. H., Tan K.H., and Guo Z. (2004) "Influence of concrete cover on fire resistance of reinforced concrete flexural members.", *J. Struct. Eng.*, 130(8), 1225-1232.
- Schulze H., Duddeck H., *Spannungen in Schildvorgetriebenen Tunneln*, Beton Stahlbetonb, Germany, 1964.
- Stevens, P.R. A review of the effects of earthquakes on underground mines. United States Geological Survey Open File Report 77-313. US Energy Research and Development Administration, Reston, VA, 1997.
- Tatnall, P. C. (2002). "Shotcrete in Fires: Effects of Fibers on Explosive Spalling", *Shotcrete*, www.shotcrete.org, American Shotcrete Association, Farmington Hills, Michigan, 10-12.
- Technical Manual for Design and Construction of Road Tunnels – Civil Elements. U.S. Department of Transportation, Federal Highway Administration, Publication No. FHWA-NH1-10-034, 2009.
- Turkish Standards (TS). (2000). "Requirements for design and construction of reinforced concrete structures", *TS500*, Bakanliklar, Ankara, Turkey.
- Wang, J. M., "The Distribution of Earthquake Damage to Underground Facilities during the 1976 Tangshan Earthquake," *Earthquake Spectra*, Vol. 1, No. 4, 1985.
- Wang J.J., *The Design Considerations for the Segmental Lining of the Hsuehshan Tunnel*, International Symposium on Design, Construction and Operation of Long Tunnels, Taiwan, 2005.
- Wang, J.-N. Seismic Design of Tunnels: A State-of-the-Art Approach, Monograph, monograph 7. Parsons, Brinckerhoff, Quade and Douglas Inc, New York, 1993.
- Wardhana K. and Hadipriono F. (2003) "Analysis of Recent Bridge Failures in the United States", *Journal of Performance of Constructuted Facilities*, ASCE, 17(3), 144-150.
- Wisniewski, D., Casas J. R., Henriques A. A. And Cruz P. J. (2009) "Probability-Based Assessment of Existing Concrete Bridges – Stochastic Resistance Models and Applications", *Structural Engineering International*, IABSE, Switzerland.
- Wood, J. H., "Earthquake-Induced Soil Pressures on Structures," Report No. EERL 73-05, California Institute of Technology, 1973.
- Wood M., *The Circular Tunnel in Elastic Ground*, Geotechnique, Volume 25, No. 1, 1975.

APPENDIX A. BALANCED CANTILEVER BRIDGE COMPUTER MODEL

Definition of the Bridge

The elevation and cross-sectional properties of the bridge are shown below. C40 concrete is used in the model.

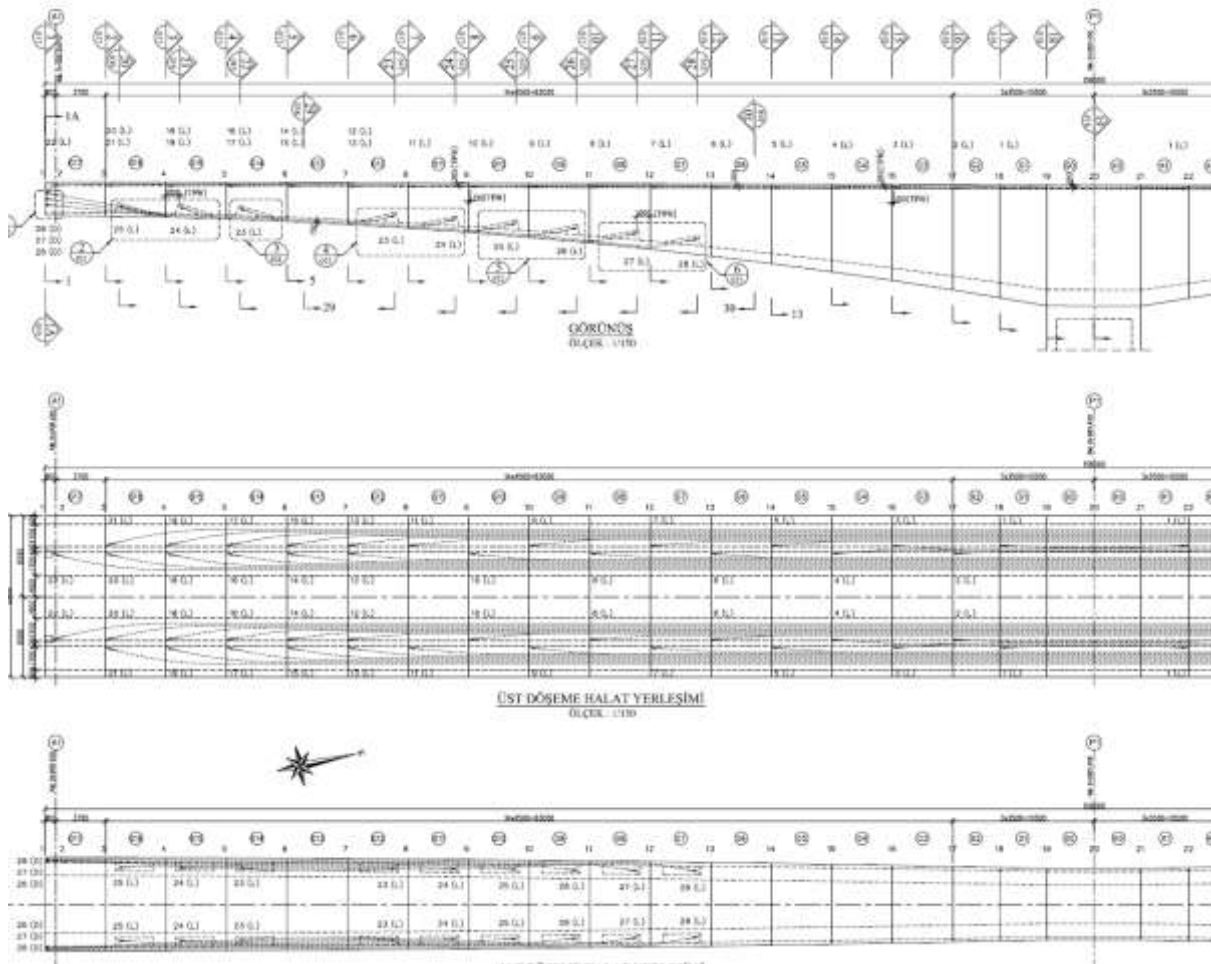




TİP EN KESİT

ÖLÇEK : 1/50

KUTU KİRİŞ GEOMETRİ TABLOSU														
Nokta No	Km.	m.	X (m)	Sol Dever (%)	Sağ Dever (%)	Eksen Kotu (m)	BT (mm)	H1 (mm)	H2 (mm)	H3 (mm)	W1 (mm)	W2 (mm)	W3 (mm)	
1	0+	5.450	0.00	-2.00	-2.00	406.226	250.0	2500.0	1376.0	1876.0	6931.0	234.5	2128.0	
2	A1	6.250	0.80	-2.00	-2.00	406.224	250.1	2500.7	1376.6	1876.7	6930.8	234.6	2127.9	
3		9.950	4.50	-2.00	-2.00	406.213	253.5	2523.7	1396.2	1899.7	6925.1	237.5	2125.5	
4		14.450	9.00	-2.00	-2.00	406.199	263.9	2594.9	1457.0	1970.9	6907.3	246.4	2117.9	
5		18.950	13.50	-2.00	-2.00	406.186	281.2	2713.4	1558.2	2089.4	6877.6	261.2	2105.2	
6		23.450	18.00	-2.00	-2.00	406.172	305.5	2879.4	1700.0	2255.4	6836.1	281.9	2087.5	
7		27.950	22.50	-2.00	-2.00	406.159	336.7	3092.9	1882.2	2468.9	6782.8	308.6	2064.7	
8		32.450	27.00	-2.00	-2.00	406.145	374.8	3353.7	2105.0	2729.7	6717.6	341.2	2036.9	
9		36.950	31.50	-2.00	-2.00	406.132	419.8	3662.0	2368.2	3038.0	6640.5	379.8	2004.0	
10		51.450	36.00	-2.00	-2.00	406.118	471.8	4017.8	2671.9	3393.8	6551.6	424.2	1966.0	
11		45.950	40.50	-2.00	-2.00	406.105	530.8	4420.9	3016.2	3796.9	6450.8	474.6	1923.0	
12		50.450	45.00	-2.00	-2.00	406.091	596.6	4871.5	3400.9	4247.5	6338.1	530.9	1874.9	
13		54.950	49.50	-2.00	-2.00	406.078	669.4	5369.5	3826.1	4745.5	6213.6	593.2	1821.7	
14		59.450	54.00	-2.00	-2.00	406.064	749.1	5915.0	4291.9	5291.0	6077.3	661.4	1763.5	
15		63.950	58.50	-2.00	-2.00	406.051	835.8	6507.9	4798.1	5883.9	5929.0	735.5	1700.2	
16		68.450	63.00	-2.00	-2.00	406.037	929.3	7148.2	5344.8	6524.2	5769.0	815.5	1631.9	
17		72.950	67.50	-2.00	-2.00	406.024	1029.9	7835.9	5932.0	7211.9	5597.0	901.5	1558.5	
18		76.450	71.00	-2.00	-2.00	406.013	1112.8	8403.6	6416.8	7779.6	5455.1	972.4	1497.9	
19		79.950	74.50	-2.00	-2.00	406.003	1200.0	9000.0	6926.0	8376.0	5306.0	1047.0	1434.3	
20	P1	83.450	78.00	-2.00	-2.00	405.992	1200.0	9000.0	6926.0	8376.0	5306.0	1047.0	1434.3	



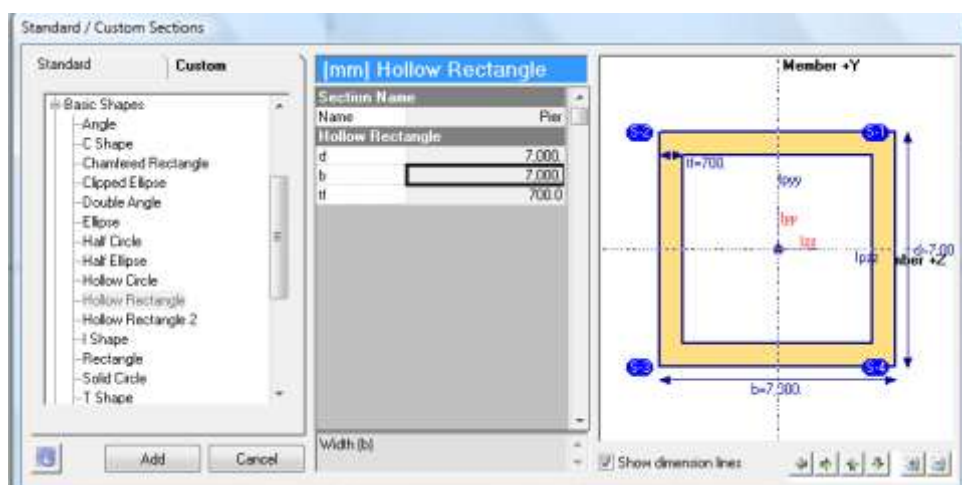
Defining Section Properties

Pier

Run the “Section Composer” (All Programs – LARSA 4D- Section Composer)

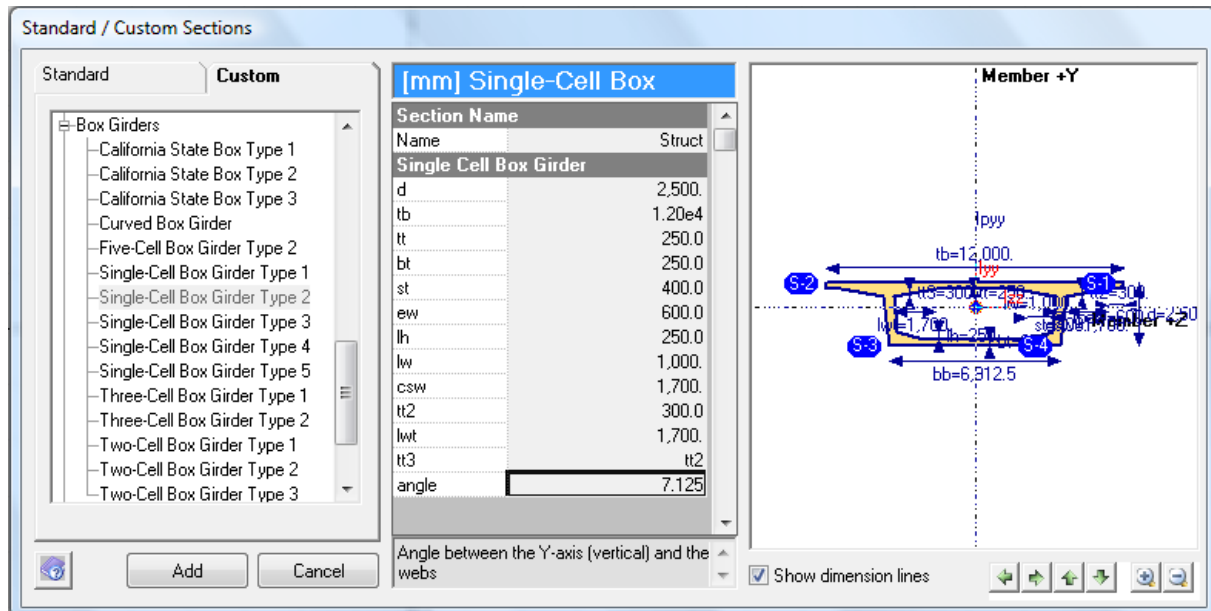
Goto “Section-Units” and change to “mm”

Goto “Shape – Insert Standard Shape- Custom-Basic Shapes- Hollow Rectangle”



Go to "Sections-Add New and Type SStructure"

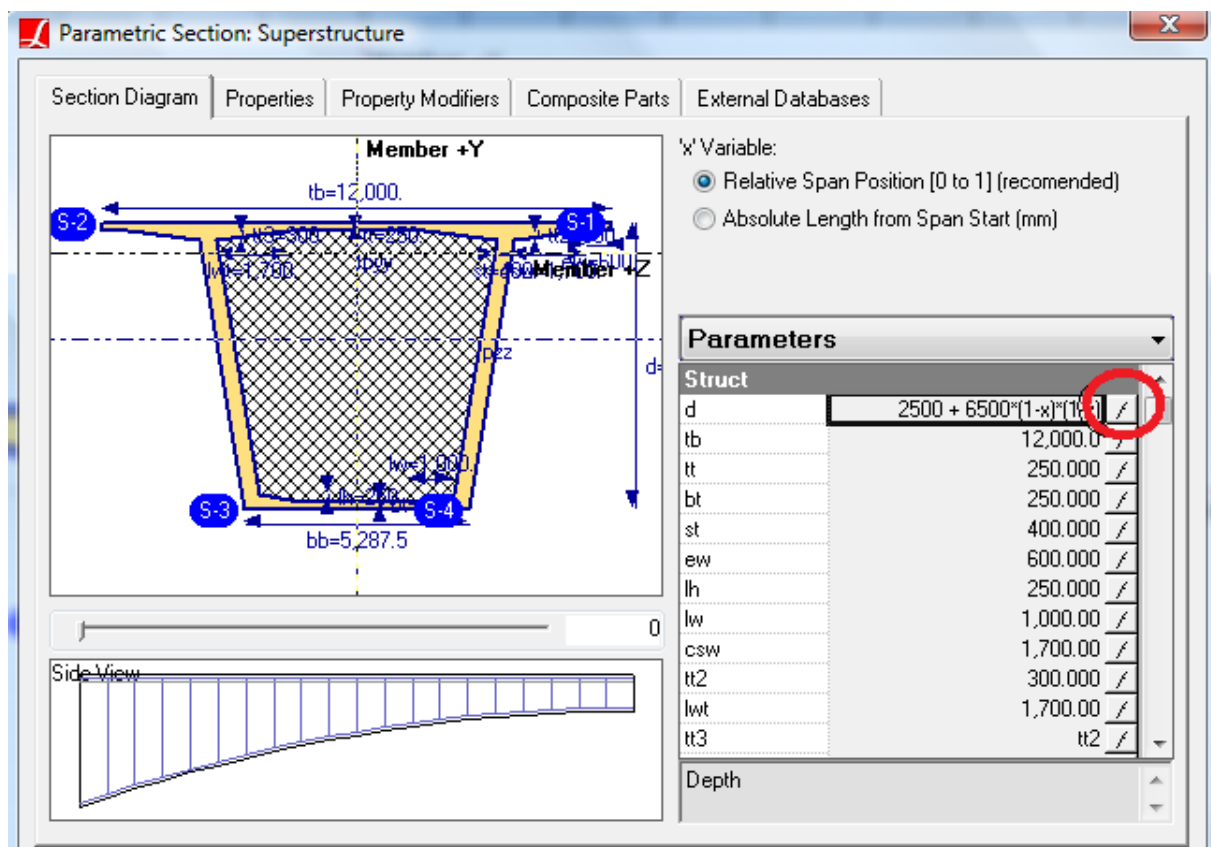
Go to "Shape-Insert Custom Shape-Box Girder-Single Box Type Girder 2"



Go to "Section-NonParametric Variation"

Click at the f of the d row as shown and write the following equation

$$2500 + 6500*(1-x)*(1-x)$$



Click at the f of the bt and type the following equation $1200 + x^* - 950$

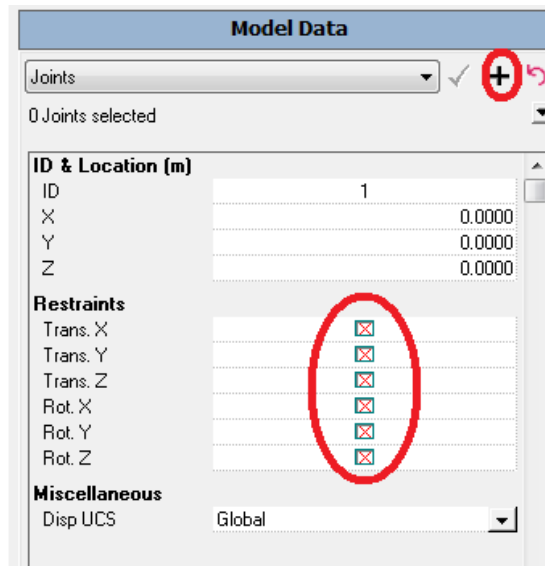
Click "Section – Move Section to Centroid of Section"

Save file as "ce767.lpsx"

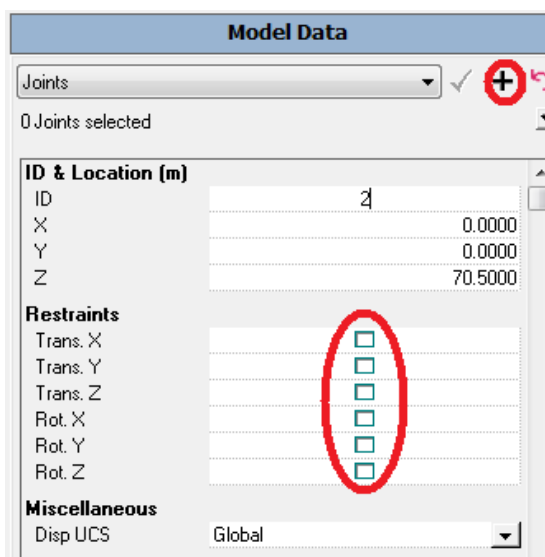
Open the LARSA software

Go to "Input-Units-Metric-Apply Conversion-Yes"

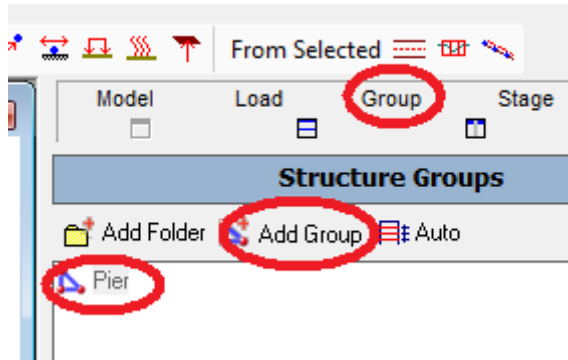
To define foundation joint, on the Model Data (at Right) click the "Restraints" as shown and press "+"



To define pier top joint change the above model data to:



Click “Group-Add Group-Rename Group 1 as Pier by right clicking on Group 1 and color it as you desire.



Drawing Members

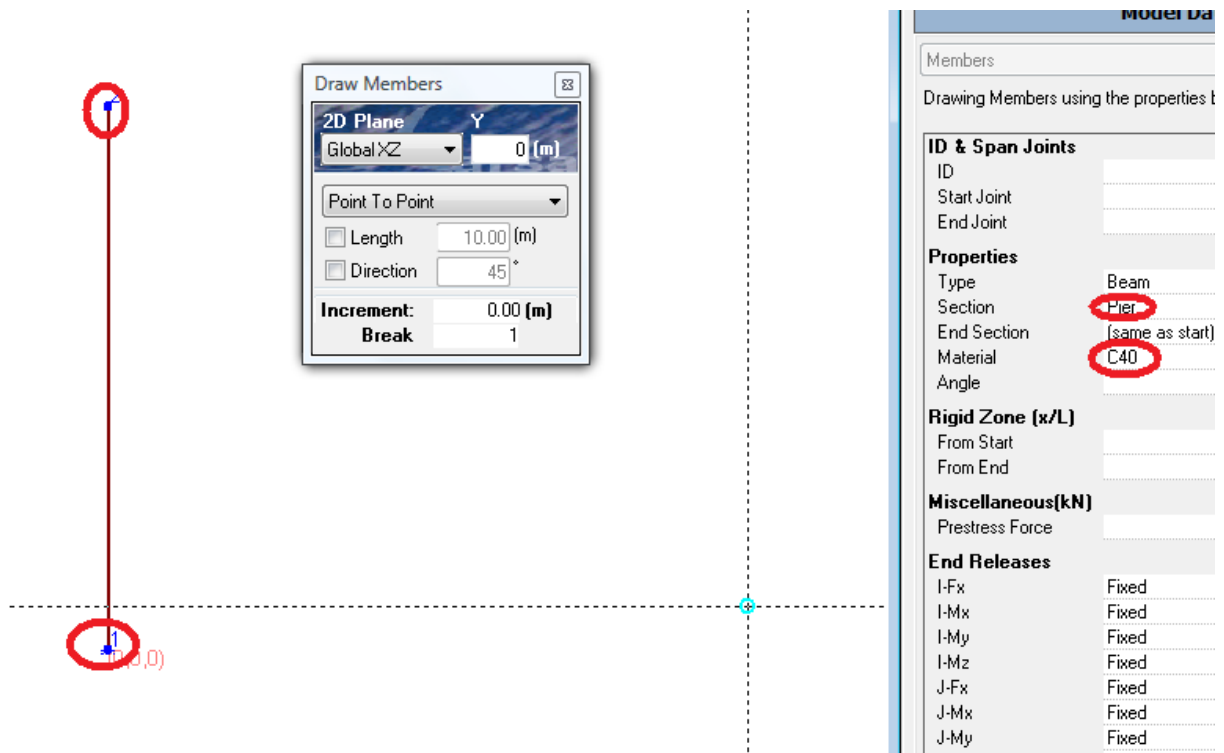
Go to “Input Data – Materials- Concrete-Concrete Turkish-C40”

Go to “Input – Connect Database- Connect User Database” and select CE767.ipsx

Go to “Draw-Geometry-Members”

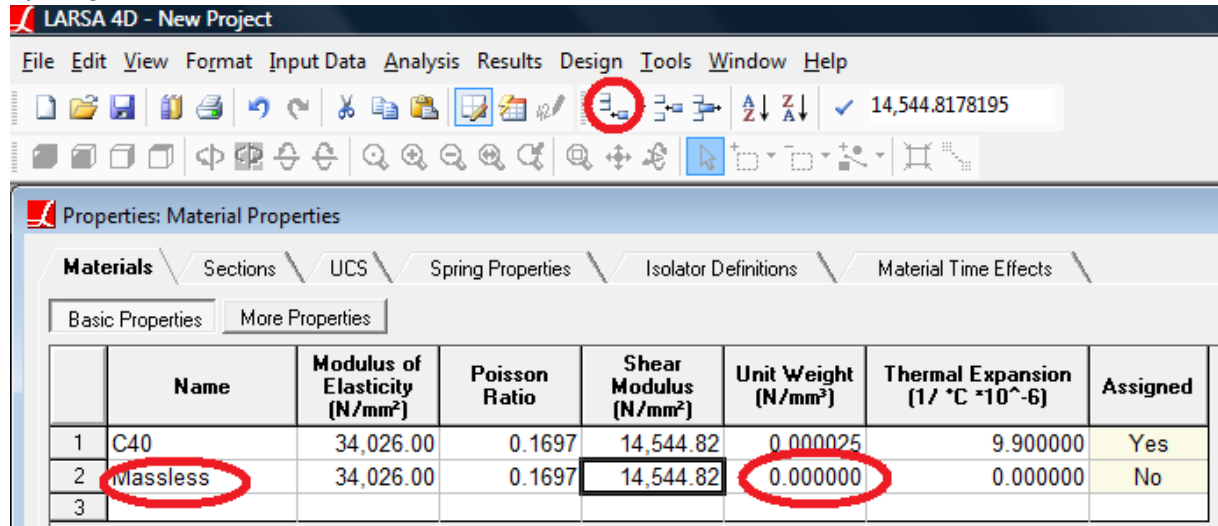
Change Section to Pier and Material to C40

Snap on node 1 and then to node 2 to draw the pier element

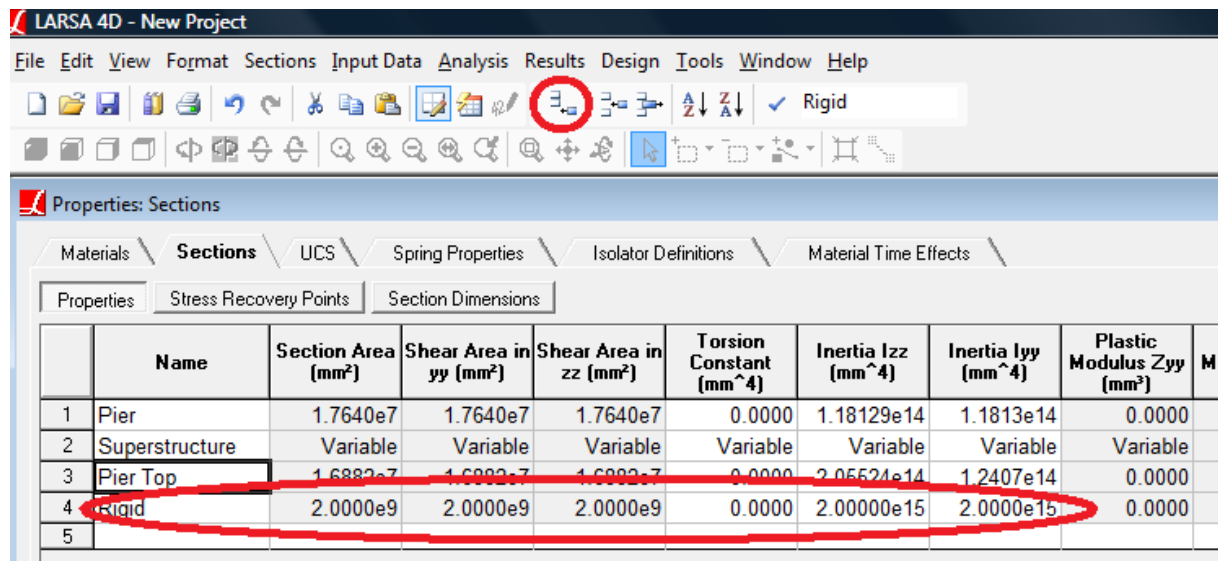


To define pier top element Go to “Input Data-Sections-Custom-Box Girders- Single Box Type Girder 2” enter the values as asked.

Define a massless material for rigid link to connect pier top to superstructure at its neutral axis go to “input data –properties –add rows” type “massless to the first column and values of the above row with 0 unit weight at the end. Change the unit weight of C40 to 0.000025 N/mm³.



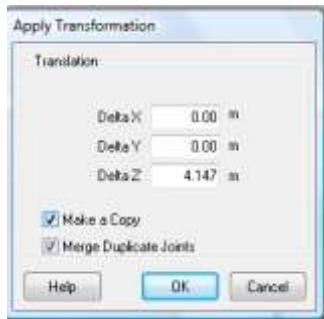
Add rigid link element properties – go to “Input data-properties – sections- add row” and type the following



Unselect all “Shift+F6”

Then press “F8” and drag Mouse from left to right so that node 2 will be in the selected box

To define the neutral axis of the superstructure, go to “modify-translate- delta z = 4.147 m and select make a copy. Go to “Draw-Geometry-Members” Change section to rigid and material to “massless”. Snap cursor on node 2 and then on node 3.



Unselect all "Shift+F6"

Then press "F8" and drag Mouse from left to right so that node 3 will be in the selected box
Modify-Translate x=73.5 m press make a copy - OK and then modify-translate x=-147m pres make a copy -OK.

Unselect all "Shift+F6"

Then press "F8" and drag Mouse from left to right so that node 3 will be in the selected box
Modify-Translate x=4 m press make a copy - OK and then modify-translate x=-8m press make a copy -OK. (slightly different from dwg)

To define the pier top element, go to "Draw-Members change section to Pier top material to C40 and angle to 90. Snap cursor on node 3 and then on node 6. Snap cursor on node 3 and then on node 7.

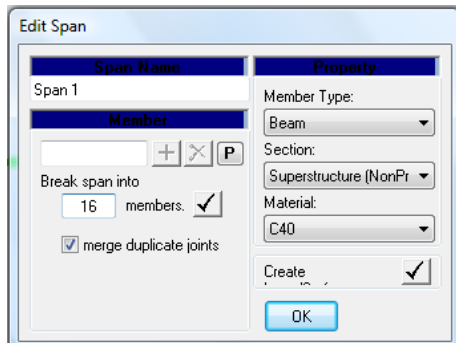
Unselect all "Shift+F6"

Click "Group-Add Group-Add Group. Rename Group 2 as Rigid and Group 3 as PierTop by right clicking for each Group and color it as you desire. Go to "Input Data-Geometry-Members Tab. At the Members Tab scroll to the far right and assign the group names as shown.

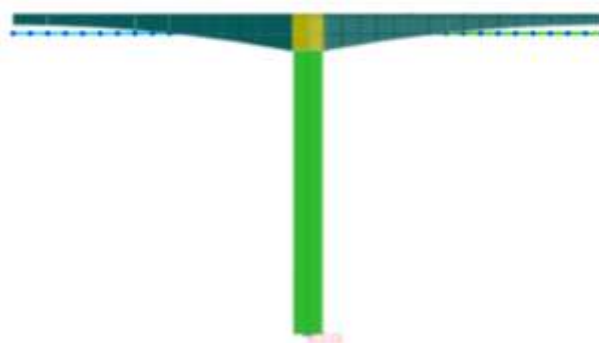
	Section at Start	Section at End	Material	Prestress Force (kN)	Length (m)	Rigid Zone from Start (x/L)	Rigid Zone from End (x/L)	Orientation Angle (deg)	Castig	Structure / Construction Group
1	Pier	same as sta	C40	0.0000	70.5000	0.0000	0.0000	0.0000	0	Pier
2	Rigid	same as sta	Massless	0.0000	4.1470	0.0000	0.0000	0.0000	0	Rigid
3	Pier Top	same as sta	C40	0.0000	4.0000	0.0000	0.0000	90.0000	0	PierTop
4	Pier Top	same as sta	C40	0.0000	4.0000	0.0000	0.0000	90.0000	0	PierTop
5										

To define the rest of the superstructure, go to "Draw-Members change section to superstructure and materials to C40 and angle to 90. Snap on node 6 and then on node 4. Snap on node 7 and then on node 5.

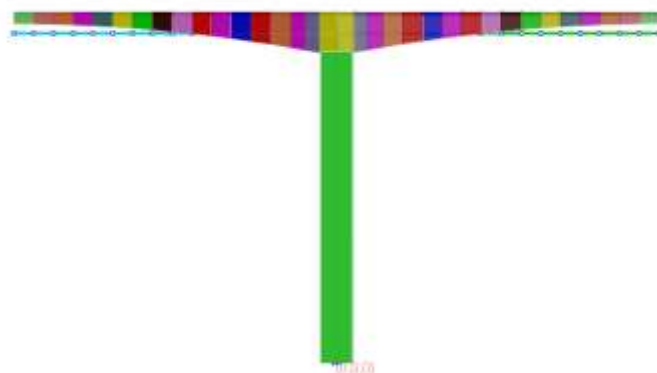
To define the other elements, go to draw – geometry – spans and click on the right span and type the following. First check Ok for break members and then click on create and click OK.



Generate Span 2 the same way. The model will look like as shown below.



Go to Input Data-Geometry-Joints to correct the coordinates as shown on the drawing. Later on group each pair of segment in a symmetric way.



Go to Properties-Material Time effects tab. Add two rows, first row name as concrete time and second row name as steel time. (default is CEB-FIP 90)

Go to Properties-Material and one additional row for post-tension as follows.

Properties: Material Properties							
Materials		Sections		UCS		Spring Properties	
Basic Properties		More Properties				Isolator Definitions	
	Name	Modulus of Elasticity [N/mm²]	Poisson Ratio	Shear Modulus [N/mm²]	Unit Weight [N/mm³]	Thermal Expansion [1/°C *10⁻⁶]	Assigned
1	C40	34,026.00	0.1697	14,544.82	0.000025	9.900000	Yes
2	Massless	34,026.00	0.1697	14,544.82	0.000000	0.000000	Yes
3	P/T	196,000.00	0.2000	81,666.67	0.000000	0.000000	No
4							

Click on More Properties and make the below changes

Properties: More Material Properties											
Materials		Sections		UCS		Spring Properties		Isolator Definitions		Material Time Effects	
Basic Properties		More Properties									
	Name	Yield Stress [N/mm²]	Post-yield to Initial Slope Ratio	Concrete Strength Specimen	Concrete fc28 or Steel Fu (N/mm²)	Concrete Cement Hardening Type	Tendon GUTS (N/mm²)	Material Time-Effect	Assigned		
1	C40	0.00	0.020	Cylinder	40.03	Normal	0.00 ConcreteTime	Yes			
2	Massless	0.00	0.020	Cylinder	0.00	Not Concrete	0.00 (NONE)	Yes			
3	P/T	0.00	0.020	Cylinder	0.00	Not Concrete	1,860.00 SteelTime	Yes			
4											

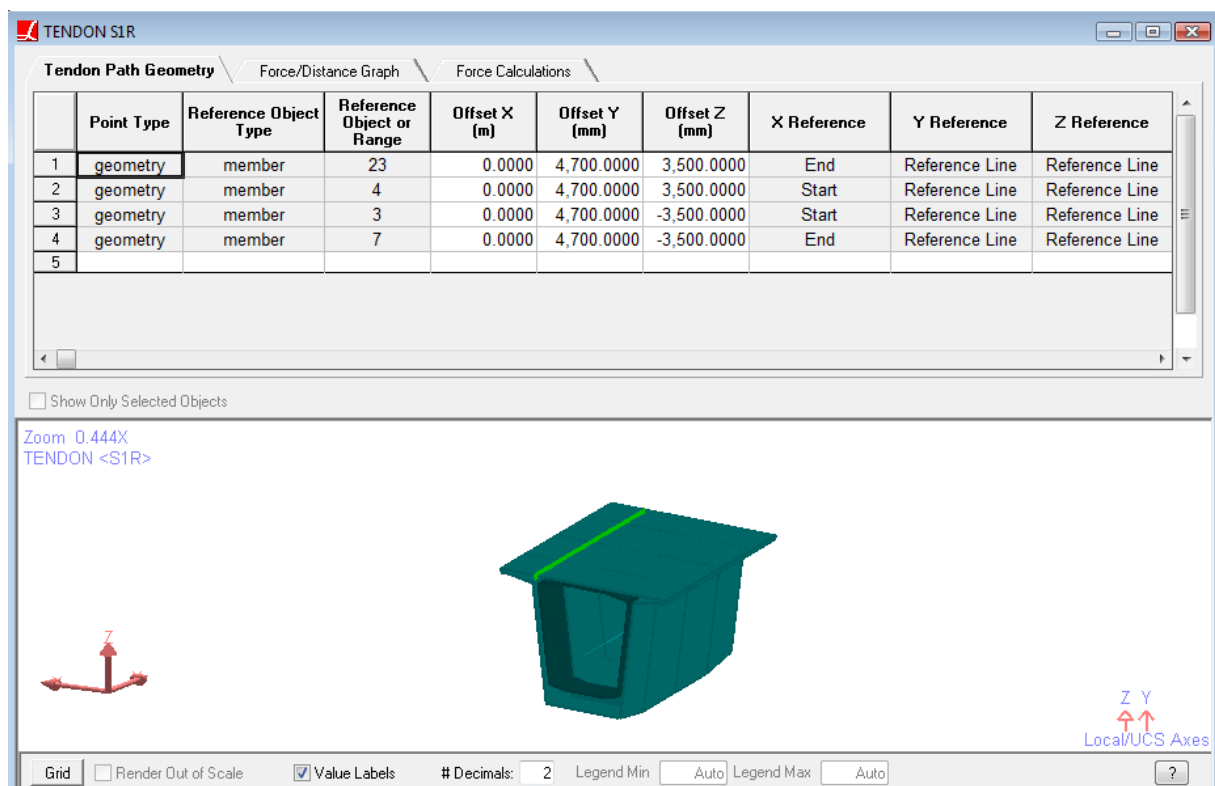
Tendons

Enter the following info found at input data- geometry- tendon by adding a row

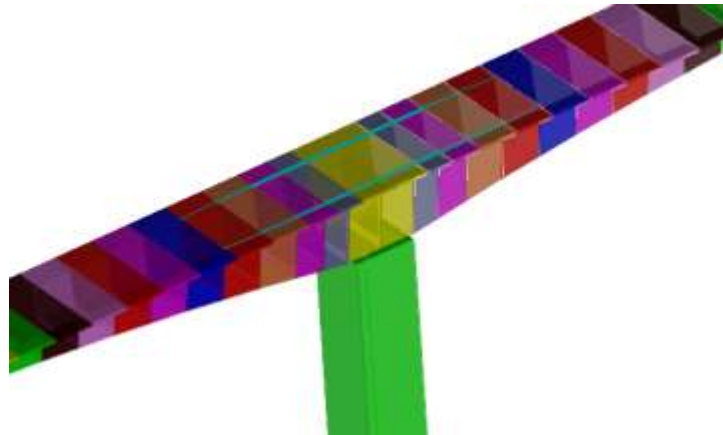
Geometry: Tendons									
Linear Two Node Springs Yield Surface Beam Elements Joints Members Plates Springs Mass Elements Isolators/Bearings Tendons Lanes/Surfaces Bricks									
	Tendon Name	Design Group	Material	Exposure	Strand Area (per strand) (mm²)	# of Strands	Jacking Force @ Start (kN)	Jacking Force @ End (kN)	Jacking End
1	S1R	(none)	P/T	Post-Ten	140.0000	19	3,627.1349	3,627.1349	Start then End

Geometry: Tendons										
Linear Two Node Springs Yield Surface Beam Elements Joints Members Plates Springs Mass Elements Isolators/Bearings Tendons Lanes/Surfaces Bricks										
	Jacking End	Anchor Set (mm)	Wobble Coefficient (per m)	Curvature Friction Coefficient	Peak Stress Ratio - Ends	Peak Stress Ratio - Interior	Elongation After Pull 1	Elongation After Pull 2	Elongation @ Left of Stationary	Elongation @ Right of Stationary
1	Start then End	9.0000	0.0000007	0.2500	0.7000	0.7000	0.0000	0.0000	0.0000	0.0000
2										

On S1R right click and go to path spreadsheet and type the following



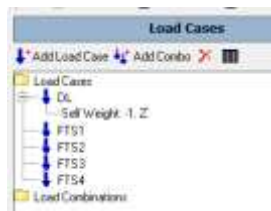
And repeat the same procedure for each tendon layout. In this example, the construction stage analysis will be conducted till erection of Segment 15 (the one before last one). The solution can be solved as 2-D problem and Y-translation can be taken to be off.



Adding Loads and Construction Stages

Enter 5 load cases as follows. Right click on the first one to activate the gravity loads.

Assume the traveler form is 90 tons including the dynamic forces. Apply joint loads of 90 tons at each joint corresponding to form traveler. (Double click on the rest of the load cases and at each load case and enter two joint forces)



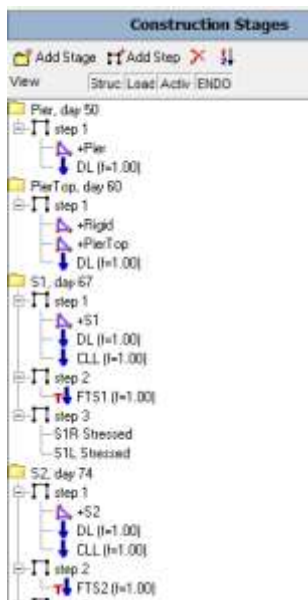
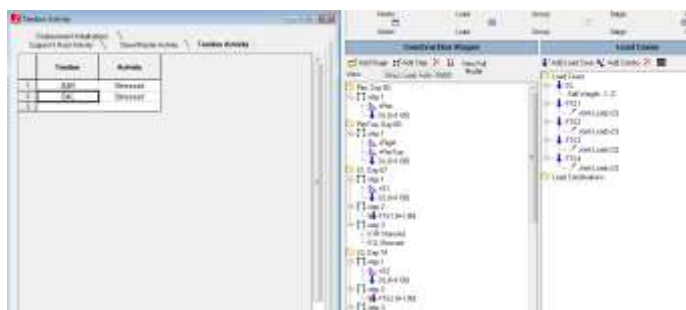
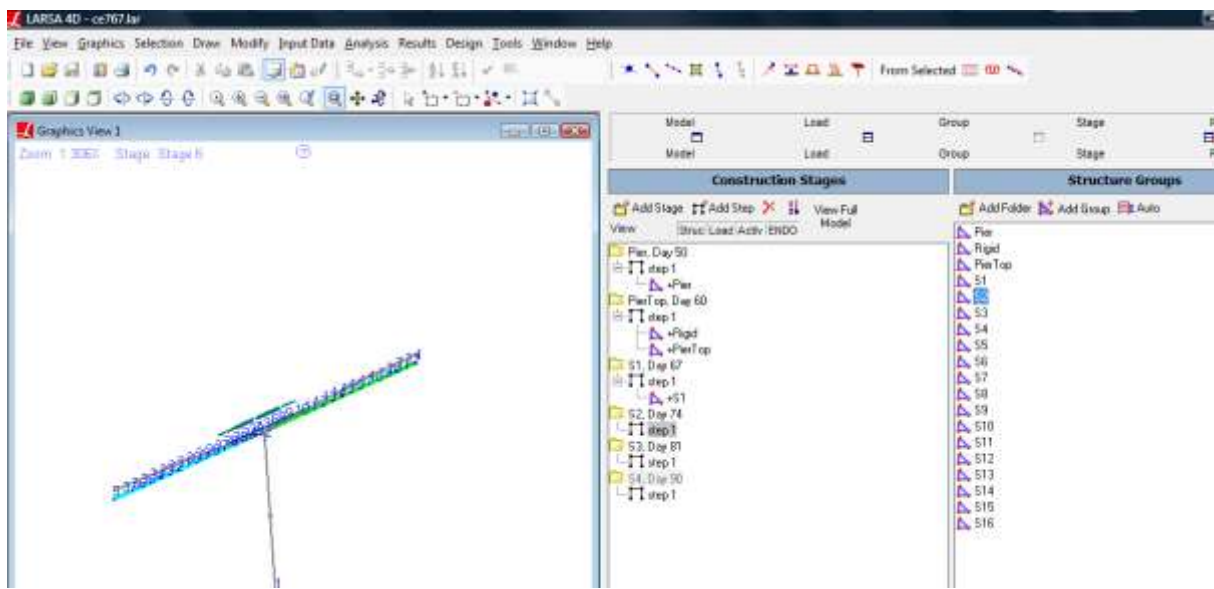
Joint	X-Force (kN)	Y-Force (kN)	Z-Force (kN)	X-Moment (kN-m)	Y-Moment (kN-m)	Z-Moment (kN-m)
1	0.0000	0.0000	-900.0000	0.0000	0.0000	0.0000
2	0.0000	0.0000	-900.0000	0.0000	0.0000	0.0000
3						

Assume 7 day cycle for construction of the segments. Develop the following scheme by dragging the necessary items to the stage module as follows.

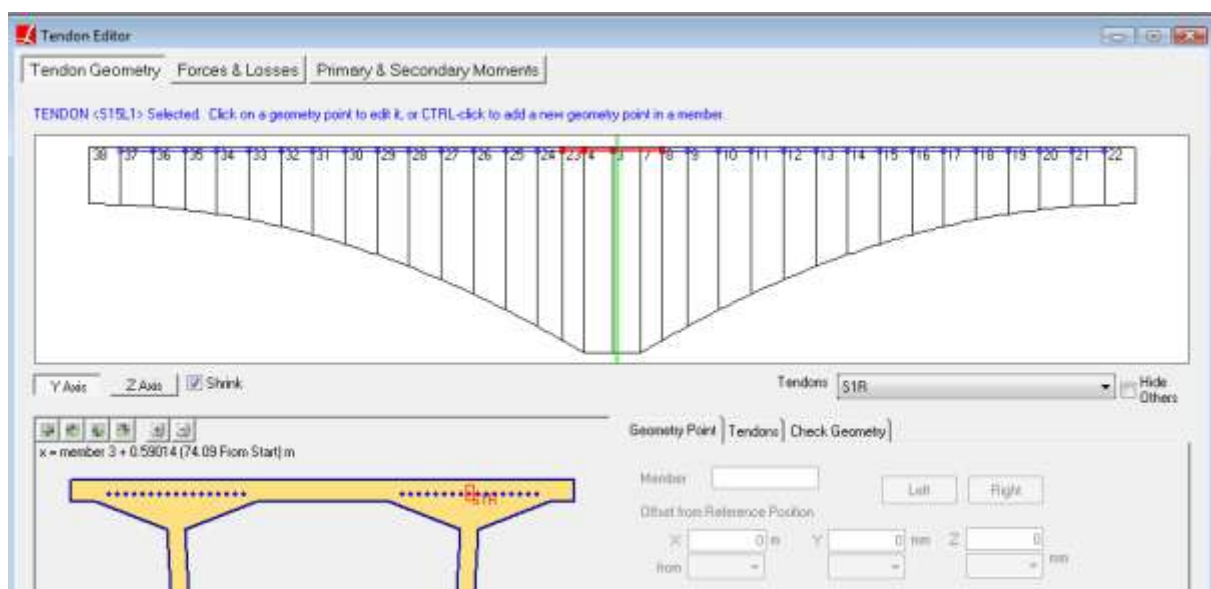
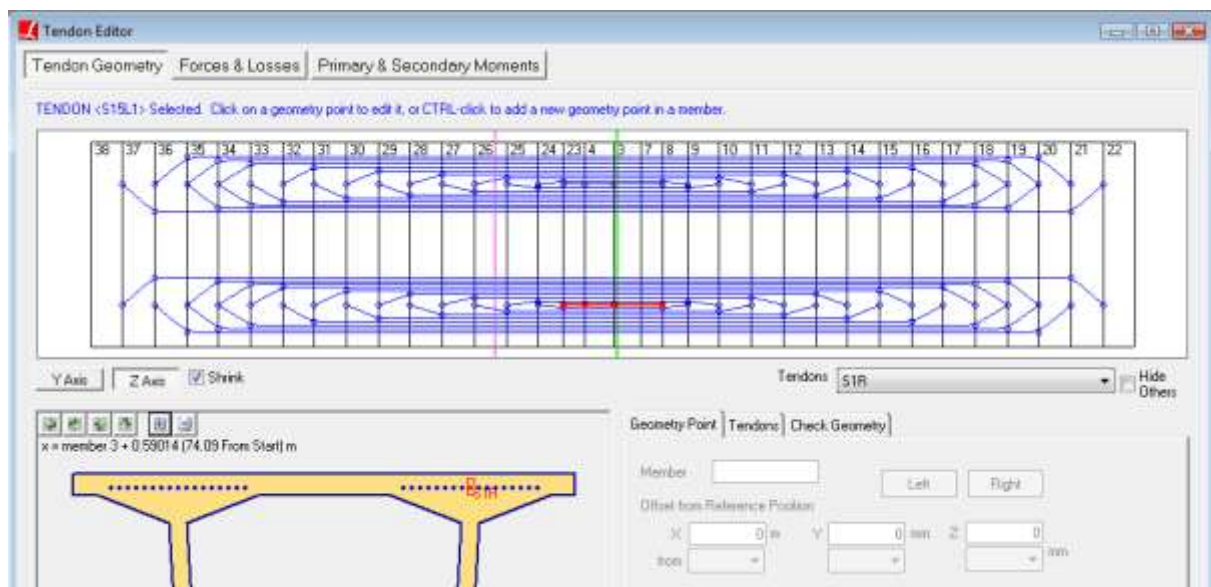
Load Combo: DC+CLL+DIFF+CE+IE+CR+SH

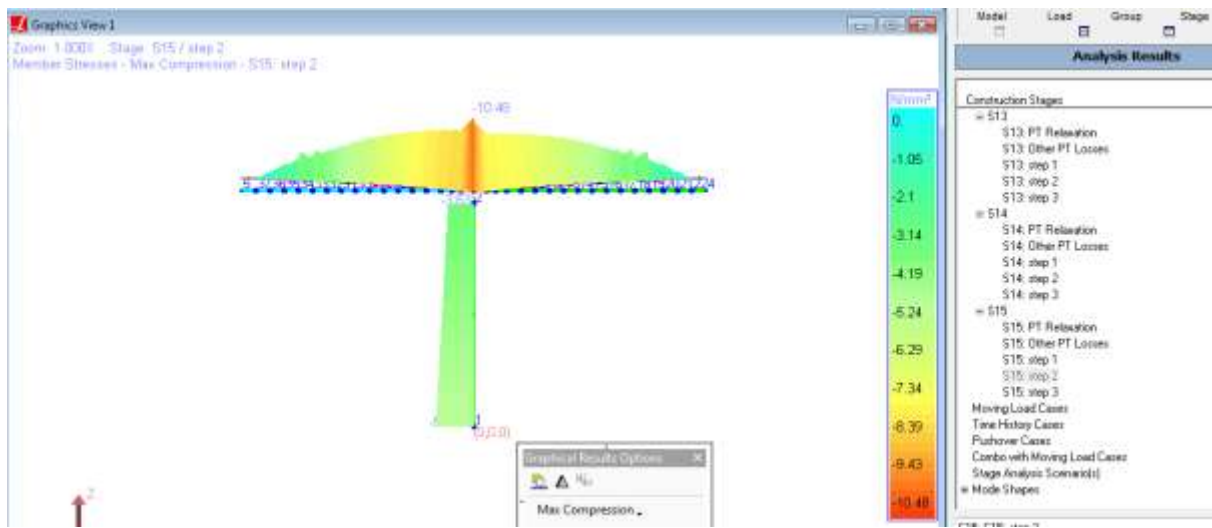
The form traveler load is applied as temporary load at step 2 and post-tensioning is applied at step 3.

The post-tensioning can be applied as lump sum in the middle of the top slab if wanted instead of two ducts located at their original position.

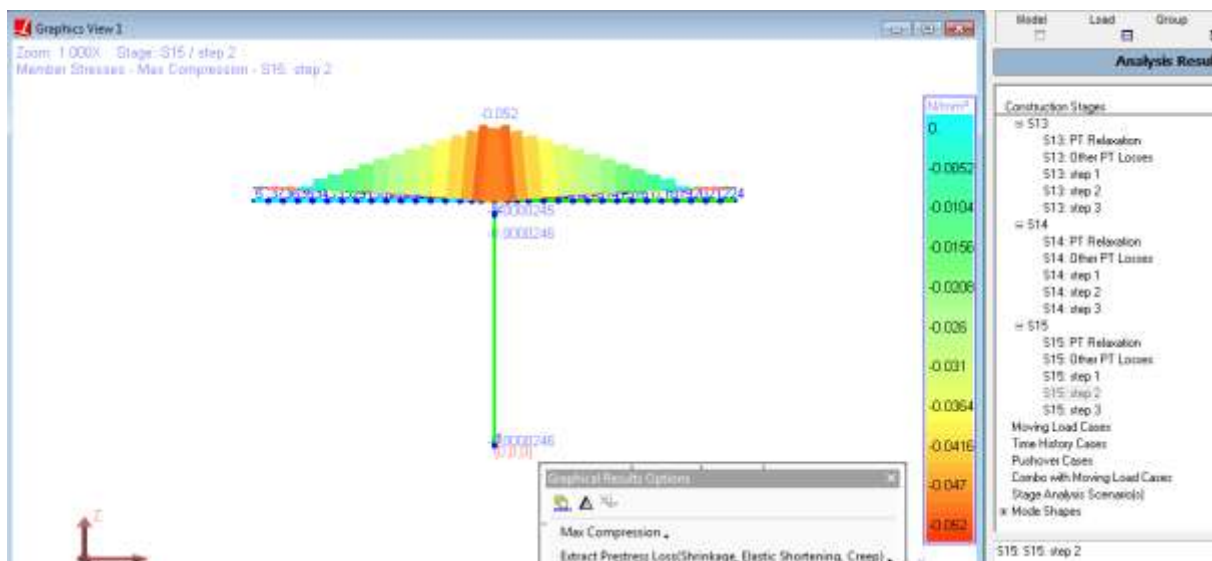


Tendon Editor Tendon Layout





Cumulative



Time Dependent Stresses (167 days)

